

# Sheffield Hallam University

*Optical effects in Langmuir-Blodgett films of novel organic materials.*

OMAR, Ozma.

Available from the Sheffield Hallam University Research Archive (SHURA) at:

<http://shura.shu.ac.uk/20143/>

## A Sheffield Hallam University thesis

This thesis is protected by copyright which belongs to the author.

The content must not be changed in any way or sold commercially in any format or medium without the formal permission of the author.

When referring to this work, full bibliographic details including the author, title, awarding institution and date of the thesis must be given.

Please visit <http://shura.shu.ac.uk/20143/> and <http://shura.shu.ac.uk/information.html> for further details about copyright and re-use permissions.

LEARNING CENTRE  
CITY CAMPUS, POND STREET,  
SHEFFIELD, S1 1WB.

101 585 618 7



**REFERENCE**

ProQuest Number: 10697450

All rights reserved

INFORMATION TO ALL USERS

The quality of this reproduction is dependent upon the quality of the copy submitted.

In the unlikely event that the author did not send a complete manuscript and there are missing pages, these will be noted. Also, if material had to be removed, a note will indicate the deletion.



ProQuest 10697450

Published by ProQuest LLC (2017). Copyright of the Dissertation is held by the Author.

All rights reserved.

This work is protected against unauthorized copying under Title 17, United States Code  
Microform Edition © ProQuest LLC.

ProQuest LLC.  
789 East Eisenhower Parkway  
P.O. Box 1346  
Ann Arbor, MI 48106 – 1346

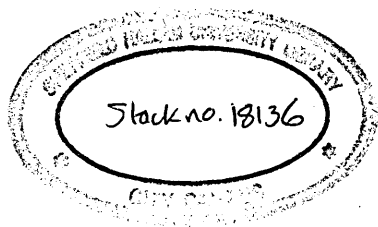
**OPTICAL EFFECTS IN LANGMUIR-BLODGETT FILMS  
OF NOVEL ORGANIC MATERIALS**

**OZMA OMAR**

A thesis submitted in partial fulfilment of the requirements of Sheffield Hallam  
University for the degree of Doctor of Philosophy

September 1998

School of Engineering  
Sheffield Hallam University  
Sheffield, England



# DECLARATION

I hereby declare that this thesis is entirely my own work and that it has not been submitted as an exercise for a degree at any other University

A handwritten signature in blue ink, appearing to read 'Ozma Omar', is centered on the page.

Ozma Omar

## Acknowledgements

I would like to offer a big thanks to my Director of Studies, Professor Asim Ray for his unwavering support and guidance both in and out of the lab. I am particularly grateful for his advice during my long and arduous writing up period. I would also like to thank my supervisor, Professor Fary Ghassemlooy for his help during my time spent in the research group. I am very grateful to Dr Aseel Hassan and Dr Alexey Nabok for many hours of fruitful discussion. Thanks for always making the time to answer my many questions and maintaining a sense of humour!

I also offer thanks to Professor Mike Cook, Dr Frank Davis, Professor Geoff Ashwell, Dr Ziad-Ali-Adib, Dr Tim Richardson for provision of materials and help with measurements.

Lots of thanks go to everyone in the research lab for making my PhD a humorous as well as a learning experience. Firstly, Rob, who provided me with (healthy, low fat) sustenance, a place to stay every weekend and other such things. Many, many thanks to Dr and Mr Crosbie for the provision of years of fun. That's quite a formal thank-you to two people better know as San-a-Tree and Sandor the Hungarian Sailor. A cheers to all those who've come and gone in the research lab, particularly Uwe, Andy and Rob I. Also, a big thanks to Luigi (has anyone seen him recently?)

A huge thank-you to Rashmi (aka CLBS) for about 14 years of fun and antics. I'm grateful for your support during my writing up period and giggling along with me. Where is there a carrier bag when you need one? Thanks to Shehla for always being available for a chat for as long as I can remember.

Finally, I am grateful to my family for the support they have given me throughout all my educational years. Thanks Mum and Dad for listening, helping and always providing. Thank-you Ali for being everything I wanted from a little brother and a friend (a monkey). Thanks to Nargis Khala for always being there for us.

## Abstract

The high level of molecular control makes the Langmuir-Blodgett (LB) technique an appealing method of film deposition. The uniform nature of the films produced allows convenient investigation of intermolecular interactions and provides information pertaining to the orientation of molecules within films.

LB films of two amphiphilic materials with contrasting molecular structures have been deposited. AmPc5 (a metal-free phthalocyanine (pc)) is a two-dimensional, cyclic molecule, whereas AmAz1 (a resorcinol calixarene) possesses a three-dimensional basket-type structure. The amphiphilic nature of both molecules is as a result of functional side-chains.

The AmPc5 spreading solution was prepared by dissolving in trichloroethane to a concentration of 0.1 mg/ml. After spreading 500-600  $\mu$ l, the resulting Langmuir film was found to have a critical pressure of 28 mN/m and an area per molecule of 1.61 nm<sup>2</sup> on the water surface. Monolayer deposition onto glass substrates enabled spectroscopic examination of the films and comparison to solution spectra. The solution spectrum shows the split Q-band absorption peaks at 700 nm and 733 nm characteristic of metal-free pc's. The LB film spectrum shows a broadening of both peaks and a red shift of the 733 nm peak, and a blue shift of the 700 nm peak. The 700 nm peak is suppressed as a result of the stack-like packing structure of AmPc5. Absorption spectra of floating AmPc5 monolayers imply that the material does not assume the monomer state at any stage of compression. This is characteristic of rigid molecules that induce order within the floating monolayer.

The refractive indices (n) and extinction coefficients (k) were determined across the visible wavelength range. Both the n and k values are shown to increase with monolayer thickness, although the n value tends towards a steady value of 2.1.

Deposition onto gold coated glass substrates enabled surface plasmon resonance analysis and determination of n and k at specific film thickness'. The n was found to increase with film thickness, tending towards a steady state value of 2.0. This is in excellent agreement with spectroscopic analysis.

Absorption spectra measured using polarised light show AmPc5 exhibits dichroism. The calculations indicate that the pc ring lies almost perpendicular to the substrate.

AmAz1 was dissolved in chloroform to a concentration of 0.5 mg/ml with 10% ethanol to aid solubility. The optimum solution spreading quantity required to form a floating monolayer was found to be between 50 and 100  $\mu$ l. The film was shown to have a critical pressure of 30 mN/m and an area per molecule of 1.86 nm<sup>2</sup> on the water surface. Both LB film and solution spectra show a single absorbance peak at 454 nm which is due to transitions in the azo functional side chains.

Calculation of n and k shows that they tend towards steady values of 1.5 and 2.0, respectively. The n obtained via surface plasmon resonance analysis shows a steady state value of 1.43 on silver coated glass and 1.35 on gold coated glass. This suggests a different type of packing structure on all three substrates. The lack of dichroism exhibited by AmAz1 indicates the formation of in-plane amorphous films.

AmAz1 was deposited in alternating layers with tricosenoic acid. The structure was confirmed by X-ray diffraction studies and investigated using second harmonic generation. The second harmonic signal was shown to be proportional to the square of the number of bilayers.

# Contents

<b>Chapter 1</b>	<b>Introduction</b>	<b>1</b>
1.1	Molecular Structure	1
1.2	Applications of Langmuir-Blodgett Films	3
1.3	Thesis Outline	10
<b>Chapter 2</b>	<b>Optical Investigation Techniques</b>	<b>14</b>
2.1	Surface Plasmon Resonance	19
2.1.1	Characterisation	19
2.1.2	Sensing Devices	22
2.1.3	Biological Applications	24
2.2	Visible Spectroscopy	26
2.3	Second Harmonic Generation	29
2.3.1	Langmuir-Blodgett Films	32
<b>Chapter 3</b>	<b>Review of Materials</b>	<b>34</b>
3.1	Phthalocyanine and its Derivatives	34
3.1.1	Introduction	34
3.1.2	Structural Characterizations	35
3.1.3	Optical Data Recording	38
3.1.4	Non linear Applications	40
3.1.5	Gas Sensing	42
3.1.6	Medical Applications	44
3.2	Calixarene and its Derivatives	46

3.2.1 Introduction	46	
3.2.2 Structure	47	
3.2.3 Non-linear Effects	49	
3.2.4 Sensing Properties	51	
<b>Chapter 4</b>	<b>Thin Film Deposition</b>	<b>58</b>
4.1 Concepts of Langmuir-Blodgett Films		58
4.1.1 Introduction		58
4.1.2 Amphiphilic Materials		59
4.1.3 Langmuir Films		60
4.1.4 Langmuir-Blodgett Films		62
4.1.5 The Langmuir-Blodgett Trough		64
4.2 Langmuir-Blodgett Film Deposition		67
4.2.1 The Langmuir-Blodgett Trough		67
4.2.2 Materials Preparation		68
4.2.3 Formation of Langmuir Films		69
4.2.3.1 AmPc5		69
4.2.3.2 AmAz1		74
4.2.4 Langmuir-Blodgett Film Deposition		77
4.2.4.1 AmPc5 Molecules		78
4.2.4.2 AmAz1 Molecules		78
4.2.5 Substrates Preparation		79
4.2.5.1 Glass Substrates		79
4.2.5.2 Gold Coated Glass Substrates		80
4.2.5.3 Silver Coated Glass Substrates		80

4.3 Recent Developments in the Langmuir-Blodgett Technique	81
<b>Chapter 5</b>	<b>85</b>
<b>Optical and Structural Characterisation</b>	
5.1 Spectroscopic Measurements	85
5.1.1 Absorption Spectra	89
5.1.1.1 AmPc5 Absorption Spectra Analysis	89
5.1.1.2 Azobenzene Absorption Analysis	100
5.1.2 Reflectance Spectra	102
5.1.2.1 Refractive Index and Extinction Coefficient Calculation for AmPc5	105
5.1.3 Absorption of Polarised Light	109
5.1.3.1 Dichroism in AmPc5	113
5.1.3.2 Dichroism in AmAz1	120
5.2 Surface Plasmon Resonance Measurements	123
5.2.1 Surface Plasmon Excitation	123
5.2.2 Experimental Set-up	127
5.2.3 Surface Plasmon Excitation in a Three Boundary System	131
5.2.4 Determination of film thickness and optical constants	134
5.2.5 Surface Plasmon Resonance in AmPc5	134
5.2.6 Surface plasmon resonance in AmAz1	148
5.3 Alternate Layer Structure	160
5.3.1 X-Ray Diffraction Analysis	160
5.3.2 Second Harmonic Generation Measurements	161
5.4 Scanning Electron Microscopy	165

<b>Chapter 6</b>	<b>Conclusion</b>	<b>168</b>
6.1	Suggestions for Further Work	176
	<b>References</b>	<b>179</b>

### **Appendix I**

Omar, O et al, Optical characterisation of amphiphilic, metal-free, non-peripheral phthalocyanine in Langmuir-Blodgett films, *SPIE*, Vol 2852, 1996

### **Appendix II**

Omar, O et al, Resorcinol calixarenes (resorcarennes); Langmuir-Blodgett films and optical properties, *Journal of Supramolecular Science*, 1997

### **Appendix III**

Langmuir-Blodgett Trough and Substrate Cleaning Procedures

### **Appendix IV**

Nabok, A et al, Inclusion phenomena in mixed floating layers containing phthalocyanines, *Thin Solid Films*, 1998

### **Appendix V**

Ray, A K et al, An interpretation of the structure of Langmuir-Blodgett films of octa-substituted metal-free phthalocyanine molecules from optical spectra, *Philosophical Magazine B*, Vol 78, 1998

### **Appendix VI**

Second Harmonic Generation Experimental Setup (Ashwell, G J et al, The highest observed second harmonic intensity from a multilayered Langmuir-Blodgett film structure, *SPIE*, Vol 1361, 1990)

# Chapter 1 Introduction

Consideration of organic materials at a molecular level via Langmuir-Blodgett deposition has led to ramifications in a number of fields. Research advancements in fields such as molecular electronics, non-linear optics and biological systems are dependent upon the determination of optical and physical constants of the materials suitable for practical applications.

As the next stage from pure research, consumer demand for increasing device complexity coupled with further miniaturisation is indirectly driving applied research in material development.

In this research the optical effects of two structurally different materials have been investigated; a calixarene and phthalocyanine with functional side chains.

## 1.1 Molecular Structure

Calixarenes and phthalocyanines are similar in that they are both thermally and chemically stable compounds. Structurally, phthalocyanine is a two-dimensional macrocyclic molecule, whereas a calixarene molecule has a three-dimensional basket-type structure.

The phthalocyanine molecule studied is an octa-substituted, metal free, non-peripheral phthalocyanine, 1,4-di(4-hydroxybutyl)-8,11,15,18,22,25-iso-pentylphthalocyanine (AmPc5), synthesised at the University of East Anglia (Figure 1-1). The synthesis of compounds of the same family are given by Cook et al (Cook et al 1994) with an initial study due to Omar et al (Omar et al 1996) (Appendix I).

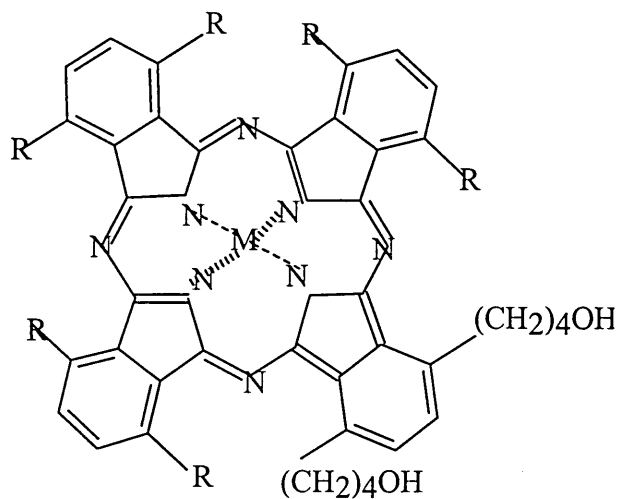


**Figure 1-1 Structure of A40 where  $R=C_5H_{11}$  and  $M=H_2$**

The calixarene in study is an amphiphilic azobenzene substituted calix(4)resorcinarene (AmAz1) synthesised by Dr F Davis (Omar et al 1997, Appendix II) at the University of Sheffield (Figure 1-2). The CPK model is pictorially represented in Figure 1-3.

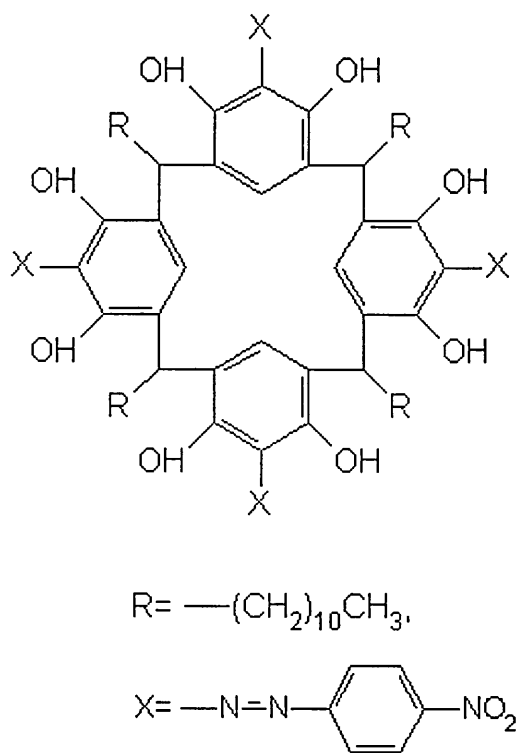


**Figure 1-2 Chemical structure of AmAz1**

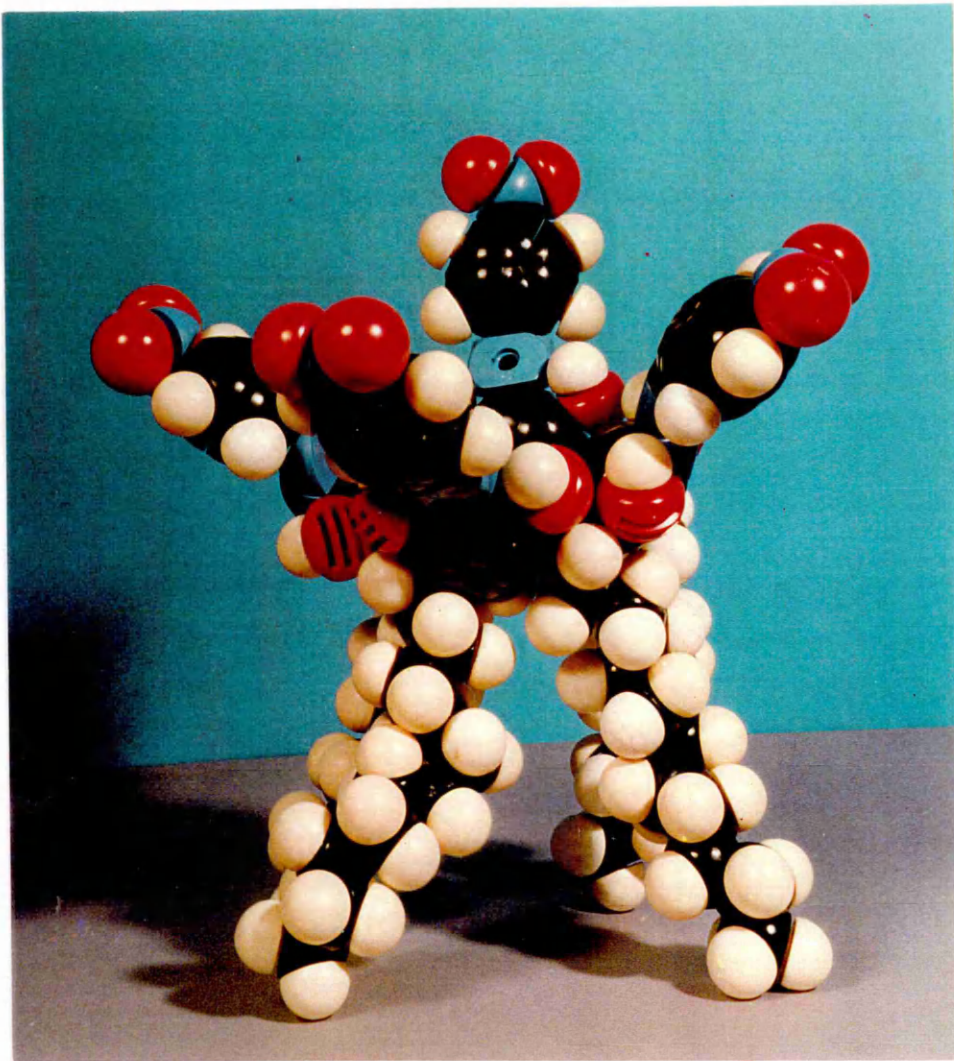


**Figure 1-3 CPK model AmAz1**

The materials have been deposited as Langmuir-Blodgett films and the electronic structure studied spectroscopically, via surface plasmon resonance, second harmonic generation and scanning electron microscopy. These experiments have enabled the determination of some optical constants and an understanding of the molecular orientation in Langmuir-Blodgett films.

### 1.2 Applications of Langmuir-Blodgett Films

Langmuir-Blodgett films are currently being studied in fundamental and applied research. Fundamental research involves the use of Langmuir and Langmuir-Blodgett

films for investigation into electronic conduction and optical excitation processes. Applied research is centred in areas of industrial and commercial exploitation. Appealing aspects of Langmuir-Blodgett films are the degree of molecular control, the ability to produce very thin films and the unique way in which they may react with their environment. The film structure enables convenient investigation of intermolecular interactions and provides information pertaining to the orientation of molecules within films.

The study of fluorescence from mixed monolayers of dye molecules and fatty acids is one example (Kuhn 1983). In Figure 1-4 the compound X absorbs in UV and fluoresces in blue, whereas compound Y absorbs blue and fluoresces in yellow.

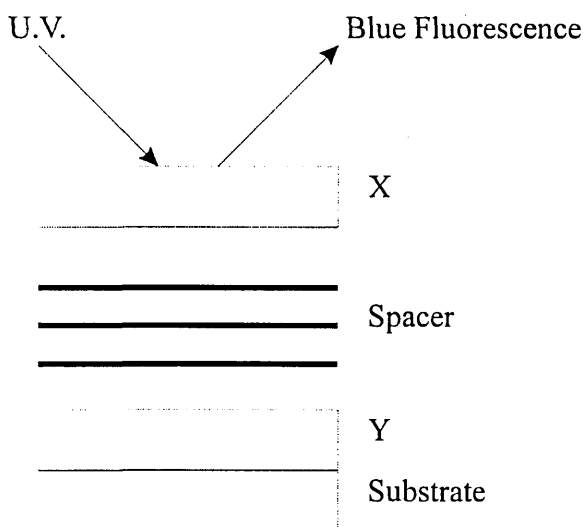


**Figure 1-4 Mixed layer fluorescence (Kuhn 1983)**

With a thick spacer compound X fluoresces with no effect from Y. With a thinner spacer layer below a certain threshold, the excitation energy of X is transferred to Y via quantum mechanical tunnelling. As a result compound Y fluoresces in yellow.

Conducting Langmuir-Blodgett films of docosylpyridinium<sup>+</sup>TCNQ<sup>-</sup> can be produced by oxidation using iodine vapours (Barraud 1985) by ion exchange in the subphase.

There are numerous applications of Langmuir-Blodgett films in biological systems, where the films can be used as protective coatings (Fuchs et al 1991), biological membrane analogues (Petty 1987) or sensing materials in biosensors (Garland, P B 1996).

Artificial implants that come into contact with body fluids have to be biocompatible. When biocompatibility is reduced there is usually an interaction of proteins with the surface of the artificial implant. A Langmuir-Blodgett coating on the surface of the mechanism allows the surface charge densities, surface potential, the degree of hydrophilicity and the functional groups of the surface to be adjusted to prevent surface reactions (Fuchs et al 1991).

There is a resemblance of many monomolecular Langmuir-Blodgett materials to naturally occurring cell membranes (Okhi et al 1976). Hence a Langmuir-Blodgett bilayer may be a suitable model for a cell membrane enabling study of specific biological processes.

Langmuir-Blodgett films can be used in applications that exploit their mechanical properties or in molecular electronics. The mechanical properties of barium stearate Langmuir-Blodgett films as a lubricant for magnetic tapes have been studied (Seto et al 1985). Seven monolayers deposited onto the tape has resulted in a reduction of the friction coefficient by a factor of four. Although difficulties may be encountered with the mechanical stability of the films.

Incorporation of Langmuir-Blodgett films into electronic devices has led to the emergence of molecular electronics as an area of research, where the properties of the films can be considered on a bulk or molecular scale. The bulk properties of the layers can be used in electrical or optoelectrical devices, whereas the molecules themselves can be used in molecular scale electronics. It is envisioned that the molecules may become

the smallest addressable component in a high-density organic memory system (Geddes et al 1995).

Electroluminescence is the emission of radiation when an electric field is applied across a suitable material. This effect was first observed in Langmuir-Blodgett films in 1984 (Roberts 1984). The films consisted of a substituted anthracene derivative which emitted in the blue region of the visible spectrum. A three layer heterostructure containing an active Langmuir-Blodgett emitting layer sandwiched between charge transport layers has been developed (Era et al 1992). The area of electroluminescence is important for the development of flat panel colour displays. The metal/insulator/semiconductor (MIS) heterostructure can be used for other applications such as photovoltaic cells where the power output is optimised using the Langmuir-Blodgett layers (Petty 1987) and field effect transistors.

Device miniaturisation and hence the demand to decrease the size of components in a computing system, has led to research into molecular electronic devices. In order to realise this miniaturisation devices of submicrometre dimensions need to be incorporated in integrated circuits (Ray et al 1992). Junctions have been created which show rectifying behaviour due to the unidirectional behaviour of current flow through D- $\sigma$ -A or D- $\pi$ -A molecules. It has been shown that metal/Langmuir-Blodgett/metal (MIM) structures can be constructed into molecular rectifiers by deposition of the film onto a metal coated substrate, with evaporation of the counterelectrode (Geddes et al 1995). The  $I$ - $V$  characteristics of the materials measured were found to be similar in form to those of a conventional semiconductor p-n junction, although the currents supported were significantly lower. A similar study was performed on substituted phthalocyanines deposited in Z-type structure onto ITO glass showing a similar rectifying effect (Liu et al 1995 (b)).

The ability of certain Langmuir-Blodgett materials to deposit in Z or X-type structures leads to their suitability for second harmonic generation measurements. Molecules that possess a highly conjugated, delocalized  $\pi$  electron system with electron donating or accepting groups can be more easily polarised in one direction than another. When these molecules interact with the electric field of a powerful laser beam, the electric dipoles of the molecules are set into non-linear oscillation. As a result some photons are emitted that have a different frequency to the input laser frequency. This effect has been studied on zwitterionic compounds (Ashwell et al 1990). The same effect can be observed for materials deposited in alternating layers (see section 5.3). The main application for such materials can be found in electro-optic switching.

The surface potentials of alternating layer structures of stearic acid (A) and stearylamine (B) have been measured (Tredgold et al 1992) as a function of the number of deposited bilayers. For deposition ABAB... the surface potential increases linearly with film thickness, reaching a plateau of 700 mV at about 5 monolayers. For BABA... structure the surface potential is of a different sign forming a smooth sinusoidal curve with respect to thickness.

A structure containing an insulator ( $\omega$ -tricosenoic acid) and photoactive phthalocyanine dimers deposited in alternate layers has been developed (Scott et al 1994). When an electric field is applied across these multilayers in a direction parallel to the dipping direction, electron transfer takes place in the phthalocyanine dimers in the monolayer plane. These electrons undergo interplane tunnelling in the phthalocyanine multilayers but are blocked when they reach the insulating layer. Hence electron transfer is controlled in a direction parallel to dipping direction which can be extended to create electronic blocks that can be turned on or off by an electric field.

It is also possible to arrange an alternating structure of two different types of molecules in the same monolayer, as shown in Figure 1-5. Under normal conditions the Langmuir-

Blodgett technique is not able to control the positioning of different types of molecules in the same monolayer. Attempts at such deposition usually result in randomly distributed domains of both species. Two different types of molecules, A and B, that interact with each other to form a molecular unit  $A^-B^+$  have been designed (Maack et al 1994).

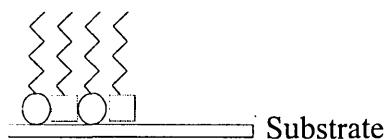


**Figure 1-5 Two different types of molecules in a single Langmuir-Blodgett monolayer**

In this case A was dimyristoyl phosphatidic acid (DMPA) and B was N[p(octyl phenylazo) pheny-loxy eicosyl pyridinium bromide], where A was shorter than B. This provided a large volume for the azo-benzene moiety to undergo cis-trans isomerisation where DMPA was used as the spacer layer. This type of molecular packing has applications in optical data storage. Mixed monolayers were used to enhance second harmonic generation by using an amphiphilic ion as a spacer to prevent aggregation of hemicyanine dyes (Ashwell et al 1992).

Langmuir-Blodgett based sensors cover a wide range of applications where the films themselves respond in some way to an external stimulus. Pyroelectric detection involves the sensing of temperature changes by the absorption of incident infrared photons. The pyroelectric material possesses a temperature dependant spontaneous polarisation (Richardson et al 1994). This effect occurs in alternate layer Langmuir-Blodgett films through the ionic interactions between headgroups of acid and base molecules in adjacent monolayers. This forms an ionic dipole parallel to dipping direction in the multilayers. The design of the molecules and length of the spacers are used to enhance

the effect which is studied using a metal/Langmuir-Blodgett (insulator)/metal device (Figure 1-6) connected to a current measuring system. The current through the device is monitored whilst the system is repeatedly heated and cooled.

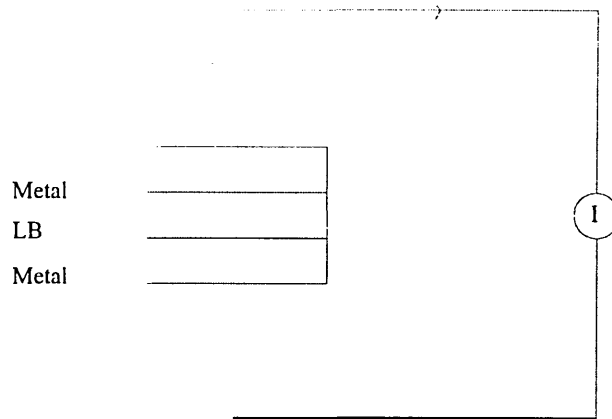


**Figure 1-6 Metal-insulator-metal sandwich structure used to study the pyroelectric effect**

Over the past two decades there has been widespread academic and commercial interest in the invention and development of biosensors. These developments were not only in biomedical research, but also in healthcare diagnostics, the food industry and environmental monitoring. These applications have been discussed in section 2.1.

Some of the possible applications of Langmuir-Blodgett films are summarised below in Table 1-1.

Application/Effect	Details	Author
Lubricant	Magnetic tape	Seto et al 1985
Biological membrane	Artificial membrane as a biological model	Petty 1987
Second harmonic generation	Electro-optic switching	Ashwell et al 1990
Biological protective coatings	Artificial implants	Fuchs et al 1991
Electroluminescence	Flat panel colour displays	Era et al 1992
Pyroelectric effect	Temperature sensor	Richardson et al 1994
Molecular rectifier	Rectifying circuits	Geddes et al 1995 Liu et al 1995 (b)
Biosensor	e.g. biotin-streptavidin system	Garland, P B 1996

**Table 1-1 Some possible applications of Langmuir-Blodgett films**

### 1.3 Thesis Outline

The thesis is organised into six chapters. Chapter 2 provides a review of optical investigation techniques with an emphasis on the techniques applied in the current research. The use of the surface plasmon resonance technique has been reviewed with emphasis on applications in material characterisation, sensing and biological applications. It can be argued that the use of the technique in material characterisation research directly results in commercial applications in fields such as optical gas sensing (Abdelghani et al 1997) and immunosensing (Gizeli et al 1996). Visible spectroscopy applications are found to provide a method for determination of suitability for applications and finally second harmonic generation is studied generally and with a focus on Langmuir-Blodgett films.

Chapter 3 provides a review of theoretical and practical applications regarding phthalocyanine and calixarene and their derivatives. Structural reviews of both materials are presented with the remaining chapter concentrating on applications specific to each material. The remaining section covering phthalocyanine provides reviews on applications in optical data recording, optically non-linear effects and gas sensing. Medical applications of phthalocyanine have been documented recently in growing numbers, particularly due to the potential application in cancer treatment.

Calixarene derivatives with appropriate substitutions can become donor-acceptor aromatics (such as AmAz1). When deposited in a non-centrosymmetric structure, second harmonic effects can be studied. Applications of this type are presented in the second section of Chapter 3. The basket structure of calixarenes makes them the obvious choice as sensing materials. This is reflected in the vast array of publications in the field of calixarene guest-host complexation reviewed in this section.

Both materials studied in the present research have been deposited using the Langmuir-Blodgett technique. In Chapter 4 the experimental technique, analysis and recent developments are presented. Both materials are deposited onto two substrates, each requiring slightly different deposition characteristics. Deposition onto glass substrates is performed for spectroscopic analysis while gold and silver coated glass substrates are used for surface plasmon resonance measurements.

In the second section of Chapter 4, recent developments of the Langmuir-Blodgett technique are presented. The nature of Langmuir-Blodgett deposition results in relatively easy attainment of molecular organisation along the z-axis (i.e. from molecule to molecule across the layers). The organisation can be achieved through z, x or y-type deposition. Organisation along the x or y axes (i.e. in each molecular layer) is generally outside the capabilities of the technique, but can be achieved to an extent by molecular

manipulation or equipment modification. Developments in this area are considered in the supramolecular architecture section.

The optical effects studied using AmAz1 and AmPc5 are presented in Chapter 5 along with the analysis of results and discussion. The structural characterisation of the alternate layer structure containing AmAz1 and tricosenoic acid are also presented and discussed. In addition a brief account of the theoretical processes behind each study is provided.

Spectroscopic data in solution form, Langmuir-Blodgett film form and Langmuir film form are studied in terms of absorbance peaks and the electronic transitions responsible. The absorbance spectra for AmPc5 provides more detail than the AmAz1 spectra. AmPc5 absorbs in the visible region, where absorption arising in solution and solid form differ in characteristic resulting in different spectra. Spectroscopic data were used to calculate refractive index and extinction coefficient for each film thickness considered. Dichroic effects, if any, can be observed from absorbance spectra measured using p-polarised light. Where the material displays dichroism, the molecular orientation within the film can be calculated.

In the second section of Chapter 5, surface plasmon resonance measurements performed on both materials are presented. The experimental set-up and justification of metal coating is presented along with the ideal metal thickness in order to achieve optimum resonance. The differences between the materials are indicated in this section, where AmPc5 is considered an absorbing material and AmAz1 a non-absorbing one at the He-Ne laser wavelength.

The change in shape of AmPc5 curves and the featureless shape of AmAz1 curves are explained in terms of the surface plasma damping mechanisms at work in each material. Fitting of the resonance curves provides values for refractive index, extinction coefficient and film thickness for each sample. The dependence of refractive index on

thickness when considering films of molecular thickness is illustrated in the results obtained. The results obtained from this method can be compared to those obtained using spectroscopic techniques.

X-ray diffraction studies of the alternate layer film confirm the structure, and so the second harmonic generation measurements performed are considered in the next section. The results indicate the non-linear optical activity of AmAz1 when deposited in an alternating structure. The calixarene molecule of study, AmAz1, contains azobenzene groups on the sidechains. The nitrogen molecules on the chain provide the molecule with a conjugated  $\pi$ -electron system. The highly deformable nature of these delocalised electrons results in the ability to provide an optically non-linear effect. Deposition of these molecules in the standard Langmuir-Blodgett style is expected to cancel out the microscopic non-linearity. The macroscopic centrosymmetric structure inhibits second order non-linear effects. Deposition of the molecules in a non-centrosymmetric fashion satisfies both the macroscopic and microscopic non-linear optical requirements. This structure can be achieved by alternate layer deposition in which a different molecule is deposited in each layer. For the current research, tricosenoic acid was selected as the alternating molecule due to its ease of deposition and transparency in the UV/VIS region. The molecule does not contain any factors that may interfere or enhance the second harmonic signal generated by the calixarene molecule.

Scanning electron microscopy of the phthalocyanine molecule, AmPc5, provided a comparison of the surface homogeneity of a thin and thick Langmuir-Blodgett film sample. This molecule has potential applications in optical data recording where the surface behaviour of films is fundamental to design.

A comparison of the optical constants of both materials obtained via spectroscopic and surface plasmon resonance methods is presented in Chapter 6.

## Chapter 2      Optical Investigation Techniques

The investigation of materials by optical methods facilitates a molecular level understanding of their behaviour and hence practical applications. Study of the absorption spectra of an octa-substituted phthalocyanine has enabled an understanding of the physical behaviour of a hybrid phthalocyanine/silicon field-effect transistor sensor for NO<sub>2</sub> (Barker et al 1996).

Optical techniques such as surface plasmon resonance are used in this study as a characterisation tool, but are increasingly being used in the field of optical transduction. A variety of optical transducers have been reviewed by (Brecht et al 1997) that have particular applications in bioanalytics. These are presented according to principle in Table 2-1.

Classification	Transducer	Principle
Extrinsic fibre optics	Optodes	Reflectance, fluorescence
Intrinsic fibre sensors	Fibre	<ul style="list-style-type: none"> <li>• Fluorescence</li> <li>• Total internal reflection fluorescence</li> <li>• Attenuated total reflection</li> <li>• Fibre surface plasmon resonance</li> </ul>
	D-shaped	Interferometer
Waveguides	Stripe (waveguide)	<ul style="list-style-type: none"> <li>• Intrinsic effect</li> <li>• Young interferometer</li> <li>• Mach-Zehnder interferometer</li> </ul>
	Slab (film) waveguide	<ul style="list-style-type: none"> <li>• TE/TM differential mode interferometer</li> <li>• Mode coupling 3 x 3</li> <li>• Prism coupler</li> <li>• Grating coupler</li> <li>• Bidiffractive grating</li> <li>• Chirped waveguides</li> <li>• Input/output coupler on Mach-Zehnder chip</li> </ul>
	Surface plasmon resonance	<ul style="list-style-type: none"> <li>• Monochromatic, resolving the angle</li> <li>• Spectral</li> <li>• Waveguide-based SPR</li> </ul>
Reflectometry	Reflectometric interference spectroscopy	
	Ellipsometry	

**Table 2-1 Optical transducer principles**

An interesting study highlights the importance of characterising thin films by the use of more than one technique (Arndt et al 1984). Seven laboratories were invited to take part in the study, where each group received films of two different thicknesses of  $\text{Sc}_2\text{O}_3$  and Rh and the samples were prepared in a single deposition run. The aim of the study was to demonstrate that, even for nominally the same films, careful experimenters would obtain different values of optical constants and film thickness depending on the method used and the model assumed for the films. The results obtained from each research group are shown in Table 2-2 for  $\text{Sc}_2\text{O}_3$  and Table 2-3 for Rh.

Institution	1	2	3	4	5	6	7
Thickness							
$t_1$ (nm)	224.5	228.2	217.6	219.0	225.0	221.2	219.4
$t_2$ (nm)	452.5	462.6	447.8	447.4	450.0	450.3	449.6
n (600 nm)							
for $t_1$ (nm)	1.84	1.82	1.87	1.85	1.84	1.84	1.83
for $t_2$ (nm)	1.86	1.82	1.85	1.84	1.87	1.84	1.85

**Table 2-2 Table showing values of n and t for  $\text{Sc}_2\text{O}_3$  for comparison (Arndt et al 1984)**

Institution	1		2		4		5		6		7	
Thickness												
t <sub>1</sub> (nm)	14.2		15.5		17.2		12.0		16.9		17.0	
t <sub>2</sub> (nm)	27.1		31.6		30.1		27.5		31.7		—	
At 600 nm	n	k	n	k	n	k	n	k	n	k	n	k
for t <sub>1</sub> (nm)	2.95	3.65	2.92	3.54	2.46	3.40	3.30	3.90	2.55	3.35	3.15	3.03
for t <sub>2</sub> (nm)	2.62	3.75	2.92	3.54	2.23	3.59	3.30	3.40	2.55	3.35	—	—

**Table 2-3 Table showing values of n, k and t for Rh for comparison (Arndt et al 1984)**

The tables show there to be distinct variations in values of refractive index and thickness obtained in each laboratory.

The participating institutes and methods employed are listed in Table 2-4.

Institute	Method
1 Michelson Laboratory California, USA	R, T and t
2 University of New Orleans Louisiana, USA	Reflection ellipsometry
3 Centre d'Etudes des Couches Minces Marseille, France	Wide-Band Spectrophotometric
4 Optical Coating Laboratory Inc California, USA	Modified Valeev Turning Point
5 Vought Corporation Texas, USA	Algebraic Inversion
6 National Research Council of Canada Ontario, Canada	Inverse Synthesis
7 Optical Sciences Centre Arizona, USA	Envelope

**Table 2-4 Table showing institutes participating in study along with experimental method employed**

Whilst the accuracy of techniques may have advanced in the fourteen years since the research was published, the basic differences in geometry and environmental conditions from laboratory to laboratory have remained. The experiments were performed on thermally evaporated films, although it can be argued that deposition conditions for Langmuir-Blodgett films may also vary.

The materials studied in the present research have been characterised by the use of the surface plasmon resonance technique and spectroscopic methods, thus enabling

comparison between the material optical constants obtained from two different techniques.

## **2.1 Surface Plasmon Resonance**

The surface sensitivity of the surface plasmon resonance technique has led to its exploitation in a diverse range of applications, both commercial (Melendez et al 1997) and experimental (Swalen 1986). Experimentally, the technique can be used to characterise a material according to its refractive index at monolayer thicknesses when studying Langmuir-Blodgett films. Once the refractive index of the material has been determined, it can be used within surface plasmon resonance or other optical applications such as waveguiding.

### **2.1.1 Characterisation**

The surface plasmon resonance technique is used as a characterisation tool to study thin biomolecular films and thin organic films. The optical parameters of a self-assembled lipid bilayer (egg phosphatidylcholine) have been obtained by deposition on a silver layer using the Kretschmann configuration (Salamon et al 1994). Surface plasmon resonance spectroscopy enables a dynamic study of the lipid which replaces the previous static view obtained using electron microscopy. The entire measurement apparatus was positioned on top of water, where the silver surface came into contact with the water. The lipid was deposited onto the silver surface forming a bilayer membrane. This influenced the plasmon wave which was excited using a He-Ne laser source. The reflectivity curves obtained were analysed using a least squares procedure, producing values of 1.63, 0.15 and 7.2 nm for refractive index, extinction coefficient and film thickness at saturation. The study further indicated a homogeneous lipid

covering of the silver film as a single resonance minimum was observed for a given concentration demonstrating parameters similar to Langmuir-Blodgett films.

When considering materials as optical storage media it is essential to determine the extinction coefficient. To capture laser light effectively, dyes are needed with high extinction coefficients at the output wavelength of the laser in use (Kuder 1986). The surface plasmon resonance technique can be used as a tool to determine optical storage material suitability.

A qualitative, visual characterisation technique has been employed to obtain images of Langmuir-Blodgett monolayers (Morgan et al 1994). A description of the three-dimensional, image reconstruction of thin films is given. The method uses reflected light intensity from a metal/dielectric interface, as in the Kretschmann configuration. The light passes through a lens and into a CCD camera, allowing processing of the image by a computer. This produces a two-dimensional image, where the gold layer appears black and the monolayers as lighter shades of grey with increasing thickness. The monolayer thicknesses were determined by fitting to Fresnel's equations, with a further polynomial fitting procedure used to determine thickness in terms of reflection, thus allowing conversion of the two-dimensional image into a three-dimensional image. The technique can also be used to quantitatively study particular defects known as striations (or ridges) (Merle et al 1992). These striations occur in regions of a Langmuir-Blodgett film that have a thickness greater than the rest of the film. The defects extend parallel to the water meniscus during deposition and are represented in surface plasmon resonance reflectivity curves by a second minima. The second minima occurs at a greater angle of incidence than the first. Comparison of the experimental curves to theoretical data shows the striations to be exactly one bilayer thicker than the rest of the film.

The idea that surface plasmon excitation can result in enhanced photoresponsive signals in some photoelectric devices has been examined by using an organic solar cell mounted on a glass prism in the Kretschmann configuration (Hayashi et al 1991). The current-voltage characteristics were measured using an Ar<sup>+</sup>-ion laser as a source under normal conditions and during surface plasmon resonance. The conversion efficiency of the copper phthalocyanine cell was found to be enhanced by a factor of 7 during surface plasmon resonance. The *I-V* curves obtained under conditions of resonance exhibit behaviour observed when the incident power is increased, although the power was actually kept constant. The enhancement is believed to have arisen from the increase in light absorption and photocarrier generation in the copper phthalocyanine layer upon surface plasmon resonance.

The simplicity of the Kretschmann configuration has made the technique one of the most commonly used methods of surface plasmon resonance measurement. However, the method is slow and has a relatively low angular resolution (Lenferink et al 1991). Another approach is to apply a focused light beam to the metal interface and to use a diode array to detect the angular dependant reflectance (Ivarsson et al 1990). The method is used in refractive index determination of analytes, where a single pixel in the diode array corresponds to approximately  $10^{-3}$  refractive index units. A low analyte concentration can lead to a surface plasmon resonance response as low as  $10^{-5}$  refractive index units which encroaches upon the limitations of the technique. In an improvement to this technique a vibrating mirror is used to obtain an angle scan of about 4 degrees, where the reflectance is measured as a function of time (Lenferink et al 1991). Cylindrical optics are used to keep the incident laser spot stationary and thus eliminate disturbances due to surface irregularities.

### 2.1.2 Sensing Devices

The determination of refractive index based upon surface plasmon resonance phenomenon can be employed as a process control or monitoring tool in chemical, environmental and biological applications.

A low cost, miniaturised and integrated surface plasmon resonance chemical sensor has been developed which is able to detect concentration changes in ethylene glycol to the order of one part in  $10^4$  (Melendez et al 1997). The system uses a near-infrared LED as the light source that is coupled into a plastic prism, with sputtered gold as the exciton layer. The system has displayed adequate sensitivity, stability and reproducibility and hence is manufacturable.

In an earlier work (Melendez et al 1996) a sensor that is able to sense refractive index variations in alcohol solutions is described. All sensor components were die mounted and wire bonded onto a miniature platform using standard semiconductor based optoelectronic manufacturing techniques. The sensor was then encapsulated, to provide packaging as well as a surface for the mounting of optics. This provided a miniature, portable sensor.

This set-up differs from a surface plasmon resonance based integrated optical sensor (Homola et al 1997) where a planar waveguide and a thin metal overlayer act as a sensing element. The guided mode of the waveguide excites a surface plasmon at the interface between the metal and a sensed medium. The evanescent nature of the surface plasmon results in a damping of the waveguide mode. As the coupling strength depends on the refractive index of the sensed medium, small variations in the refractive index of the sensed medium may produce large changes in the attenuation of the waveguide mode. It was demonstrated that variations in the refractive index of the sensed medium as small as  $2 \times 10^{-5}$  may be resolved.

Optical fibres can also be used to construct gas sensors (Abdelghani et al 1997) where a silver film is deposited onto the silica core of an optical fibre. The silver film was protected from oxidation by self-assembled monolayers of long-chain alkanethiols. A beam of light from a laser diode source is directed into the fibre at variable angles of incidence using a rotation stage. An angle of incidence of  $12^\circ$  is selected that shows the greatest variation in transmitted optical power for a given refractive index variation (i.e. maximum sensitivity). Upon exposure to the sensing gases, the light transmitted through the fibre is found to increase in power. It has been shown that halogenated hydrocarbons can be detected to a limit of 0.3% with the response and desorption time less than 2 minutes.

A glass-silver-Teflon-air multilayer structure has been investigated (Podgorsek et al 1997) for applications in aromatic hydrocarbon vapour sensing. Vapours such as benzene, toluene and xylene can be produced from evaporation of oil products or accidental thermal decomposition of polymers. Changes in the refractive index of Teflon due to the adsorption of these vapours leads to shifts in the surface plasmon resonance curves. The curves consist of the leaky mode resonances of the Teflon film as well as surface plasmon resonances. A fitting procedure yields the thickness and refractive index of the deposited films and changes in the refractive index due to vapour adsorption. The dynamic response of the sensor was determined by measuring the reflectivity at a fixed angle of incidence whilst the vapour penetrated the Teflon. The measurements show that the time constants for the diffusion process depend on the size of the diffusing molecule. This shows that the sensor can be used for selective detection of mixed vapour atmospheres.

A sensor system capable of remote on-site and real-time determination of chlorinated hydrocarbons (CHC) in water has been developed (Jakusch et al 1997). Whilst not directly utilising the surface plasmon resonance technique, the system is based upon the

presence of evanescent waves in optical fibres, where the fibres act as both signal carriers and sensing elements. An ethylene/propylene coated sensing fibre is calibrated and used as the sensing head with a FTIR spectrometer and detector. The system was immersed in water, with the spectra showing a marked increase in absorbance after 10 minute enrichment, yielding a detection limit for tetrachloroethylene of 300 ppb.

### **2.1.3 Biological Applications**

The idea that molecular engineering can be considered as a counterpart of molecular biology suggests that complex artificial systems can be constructed using co-operating molecules (Kuhn 1983). The Langmuir-Blodgett technique allows construction of such artificial organised aggregates (organizates), whilst the surface plasmon resonance technique can be used to study these organizates and their related effects (Kuhn 1983). Optical immunosensors can be used to directly monitor the binding of an antibody to its specific antigen based upon surface plasmon resonance reflectivity curves (Gizeli et al 1996). Adsorption of monoclonal mouse and polyclonal sheep to a gold surface and the subsequent changes in reflectivity have enabled the kinetics of the binding events to be studied (Geddes et al 1994).

An optical rig for the detection of proteins in solution has been described in detail (Lofas et al 1991). The sensor chip consists of gold coated glass slide onto which a coupling matrix has been bound. Light is focused onto the glass slide of the sensor chip whilst a flow channel detection cell containing the protein is passed over the matrix side. The interaction between the matrix and analyte causes shifts in the surface plasmon resonance curve. The sensor chip contained several parallel flow cells and sensing areas enabling simultaneous measurement. The coupling reactions are monitored in real-time, as the angle of incidence is kept fixed and the resonance signal is measured. Any

increase in signal implies a change in coupling reaction. All steps in covalent coupling and regeneration of the sensor surface can be studied in this way.

A technique for protein detection has been developed for detecting the presence of a specific oligosaccharide sequence on a glycoprotein (Hutchinson 1994). In this automated method the signal measurements are made in situ before and after the oligosaccharide binds to the glycoprotein.

The E-coli virus, which has obtained much media coverage recently, was studied using surface plasmon resonance (Schuster et al 1993). The research involved the assembly of a complex of four protein components believed to be involved in the production of the virus at the sensor surface. A direct interaction between the proteins was identified as the factor that modulated the light coupling.

Some processes involving DNA have been measured by existing technologies (Garland, P B 1996), but the kinetics of DNA synthesis have not. The use of surface plasmon resonance technology for the measurement of various DNA dependent processes has been described (Nilsson et al 1995). It involves the change in mass at a sensor surface with covalently attached DNA in response to activity of the DNA in question.

A review of the surface plasmon resonance technique and its applications to biomaterial processes has been reported which summarises surface characterisation studies and biomaterial sensing (Davies 1994). Attention is also drawn to a limitation of the technique concerning low molecular weight analytes. The smaller the molecule in detection, the smaller the change in surface plasmon resonance angle. One method to overcome this problem requires linking the molecule to another molecule with a high refractive index. This, however, labels the molecule and may cause changes in its behaviour.

## 2.2 Visible Spectroscopy

The use of electronic spectroscopy for the characterisation of molecular assemblies has become a well established technique (Cook 1993). Polarised optical spectroscopy is now used routinely for assessing films deposited by the Langmuir-Blodgett technique, and infrared methods are finding an increasing use as well. These optical methods have been used extensively to study substituted phthalocyanines and their preferred packing in Langmuir-Blodgett films. An understanding of the preferred packing has enabled chemists to synthesise a variety of substituents providing the chain length required for certain packing types.

Visible absorption spectra of certain amphiphilic dyes have been studied (Lehmann et al 1997) enabling a determination of the suitability of the materials in optical pH sensing. For dyes to be suitable for optical sensing applications their absorption or fluorescence should be compatible with cheap and small light sources and photodetectors. They must also be photostable and not prone to leaching from the optical fibres or waveguides used as support. Lehmann et al have shown that the acidochromic hydroxystilbazolium dyes show an absorption maxima in the range 500 to 700 nm. These wavelengths are compatible with light emitting diodes and diode lasers. The development of cheap and small sensor devices becomes feasible by making the molecular engineering of pH indicator dyes with appropriate physical properties.

Visible absorption spectra are also studied purely for molecular characterisation purposes. Spectra of an octa-substituted phthalocyanine spin coated onto glass substrates have been studied (Barker et al 1996). The spectra reveal the characteristic phthalocyanine absorption region for solids, referred to as the Q-band. This provides evidence of molecular ordering. The band envelope is very similar to that observed for crystals of the same compound and Langmuir-Blodgett films of a close analogue.

The optical properties of mixed cyanine dye crystals were investigated (Bliznyuk et al 1993) in order to understand their structure. The absorption spectra of monolayers of the material exhibited two pronounced peaks ascribed to the monomer and a smaller band between the two ascribed to the monomer. It was suggested that this spectra corresponded to the Davydov split (Davydov 1962) for a crystal with two differently orientated molecules. This study enabled an understanding of the formation of two-dimensional crystals to be obtained.

A spectral study of mixtures of *p*-terphenyl (TP) and stearic acid (SA) deposited in Langmuir-Blodgett films has been conducted (Dutta et al 1994). Normalised absorption spectra of TP in ethanol-water solution at room temperature reveal a single structureless band with a maximum at 276 nm. Langmuir-Blodgett films of TP and SA show 2 distinct bands, corresponding to 2 states, which may have arisen due to organisation of the TP molecules in Langmuir-Blodgett films. The absorption spectra of TP in an ethanol-water mixture follows a similar pattern to the TP Langmuir-Blodgett film spectra. The researchers suggest this is as a result of aggregation providing some form of order.

Spectroscopic measurements have been used to study the effects of voltage cycling and annealing of MoOPc films (James et al 1992). The absorption spectra of the untreated material shows the characteristic Davydov peaks (Davydov 1962). Material annealing, where the films are heat treated for 2 and 24 hours, results in a reduction of absorption intensity for both heat times, where the components of Davydov splitting are gradually smoothed by longer period of heating. The position of the absorption bands does not appear to appreciably change. When the film is cycled ten times through a voltage of  $\pm 1.5V$ , the Davidov split peaks disappear, and the Q-band is blue-shifted. The spectra obtained from a heat treated film cycled through a voltage of  $\pm 1.5V$  ten times, shows

the resultant absorption when the effect of annealing is superimposed on that of voltage cycling.

Highly polarised molecules were often used for depositing Langmuir-Blodgett films due to their suitability and relative ease of deposition (Ogawa et al 1989 and Vandevyver et al 1992). Molecules that undergo strong polar interactions exhibit less dichroism than unpolarised molecules (Ruaudel-Teixier 1996). It was suggested that amphiphilic molecules need a high mobility to organise themselves into planar oriented columns. This cannot be achieved when the molecules are able to undergo polar interactions within the monolayer of other layers.

In the last two decades there has been an increased interest in the dichroic measurement of substituted phthalocyanines deposited in Langmuir-Blodgett films (Capelletti et al 1995, Liang et al 1997, Yan et al 1992) following from the work of Yoneyama (Yoneyama et al 1986). The polarised UV-VIS absorption spectra of a metal-substituted phthalocyanine (CuPcBC) have been measured with a view to providing information of the material suitability as an electrical gas sensor (Rella et al 1996). The average orientation of the phthalocyanine macrocycles was determined from the knowledge of dichroic ratios, using the method described by Yoneyama (Yoneyama et al 1986). The statistical results indicate that on the average, the molecules are orientated with their edges on the substrate.

The spectroscopic behaviour of 2,9,16,23- tetra- tert- butyltetrabenzotriazaporphine (TBTAPC), a particular phthalocyanine derivative, has been studied in Langmuir-Blodgett films when co-deposited with stearic acid (Fu et al 1994). The absorption spectra of varying mixtures of TBTAPC and stearic acid were obtained, where the spectra show a higher absorbance per layer for a vertically ordered monolayer than for horizontally ordered monolayers. When the phthalocyanine derivative is deposited in a vertically orientated fashion, a greater surface concentration is achieved than when

deposition is horizontal. This occurs due to the two-dimensional disc-like structure of the molecule.

The dichroic measurements confirm that vertically ordered Langmuir-Blodgett films with a preference of facing one direction will display dichroism. The horizontally orientated molecules do not produce a dichroic effect. The dichroic effect observed is shown to be reproducible and seen with other similar films.

Polarised light absorption spectra is used to determine the packing of 2-octadecylthio-1,4-benzoquinone multilayers deposited in Langmuir-Blodgett films (Bjornholm et al 1993 (b)). The comparison of the film spectra to solution spectra reveals the presence of two peaks in the Langmuir-Blodgett films which are not present in solution. As these peaks are not dependent on the number of layers or on the presence of the film on both or only one side of the substrate, they must be due to intermolecular interactions between the close packed head groups and not due to interference phenomena. The maximum absorption was found when light was polarised along the dipping direction indicating that the films are partially aligned along the dipping direction.

### **2.3 Second Harmonic Generation**

The interest in non-linear optics, particularly second order effects, is due to the investigation of new phenomena as well as the potential applications in new technology (Prasad 1991). As the non-linear optical effects are often purely electronic in nature, response times can be extremely short. Devices using third order non-linear optical processes are relatively undeveloped as compared to second order devices, as observation of third order effects requires much more powerful laser sources (Truong et al 1994). The research presented in this thesis in Section 5.3.2 measures the second harmonic signal from Langmuir-Blodgett films of the study materials, thus enabling material suitability for optically non-linear applications to be determined.

Devices based on non-linear optical effects can be classified according to those that utilise frequency conversion (high frequency) and those that exhibit refractive index modulation (low frequency). Refractive index modulation of a material occurs in the presence of an electric field and is usually referred to as the Pockels effect. The second harmonic generation is considered as a high frequency effect displaying frequency conversion.

In the last decade there has been a growth in the field of information technology with a concurrent demand for higher density data storage. Data capacities of compact discs are limited to the spot size to which an infra-red laser can be focused to retrieve data. The theoretical limiting resolution of a lens ( $R$ ) is defined as the ability of the laser to distinguish between two objects. The resolution gives the minimum distance between objects and is proportional to the laser wavelength ( $\lambda$ ) as shown below,

$$R = \frac{0.61\lambda}{n \sin i} \quad 2.1$$

where  $n$  = refractive index of the film

$i$  = angle of incidence

Doubling the value of the wavelength of the laser source, results in doubling the value of  $R$  and hence quadrupling the maximum storage density available. This can be achieved using a blue or UV wavelength laser (Prasad 1991).

Blue light can be generated using the second order non-linear response of a material to frequency double light produced by an IR laser, providing the advantage that existing, inexpensive compact laser diodes can be used.

Molecules with a high second order non-linear coefficient often pack in a centrosymmetric structure (Willock 1993), so rendering the crystal inactive. An electrostatic model is presented to predict the crystal structure of such non-linear optical molecules. A crystal structure prediction program, where crystal structures obtained from x-ray diffraction patterns has been used as the starting point. Their program provides an advantage over previous programs as the electrostatic interactions between highly polarised molecules in close proximity is taken into consideration.

When determining the second order optical susceptibility of a polymer ( $\chi^{(2)}$ ) (Herold et al 1995) have used the Pockels effect and compared the value obtained to that previously measured using second harmonic generation. The  $\chi^{(2)}$  value calculated using the Pockels effect was  $7 \times 10^{-11}$  m/V, which was found to be in excellent agreement with the value of  $6.5 \times 10^{-11}$  m/V obtained from second harmonic generation. The values for  $\chi^{(3)}$  were found to differ significantly when measured using the Kerr effect and compared to third harmonic generation.

In a recent study (Aktsipetrov et al 1998) second harmonic generation is suggested as a non-linear optical non-destructive readout of thin film based optical memories. The photoinduced, electroinduced and magnetoinduced variations in the materials in question used for recording information were easily distinguished by the second harmonic generation readout. In addition, the radiation source used for the excitation of the second harmonic signal was shown not to disturb the recorded memory.

The diversity of the applications of second harmonic generation is demonstrated in the use of the technique in cancer research (Lenz 1994). In vivo studies on rats ears were performed using a Nd-YAG laser to irradiate the ears resulting in an emission of green light. The quadratic dependence on irradiation intensity revealed the presence of second harmonic generation. The technique enabled larger tumours to be treatable.

### 2.3.1 Langmuir-Blodgett Films

The second harmonic signal in this study has been obtained using Langmuir-Blodgett films. Films of AmAz1 and tricosenoic acid were deposited in alternating layers in order to overcome the problem of symmetry of deposition.

Ruthenium(II)-bipyridine complex and ammonium amphiphiles have been deposited in alternate layer Langmuir-Blodgett films and irradiated with a Nd-YAG laser to exhibit second harmonic generation (Sakaguchi et al 1994). The films were exposed to a UV pulsed laser which reduced the second harmonic signal by half. After excitation by the UV pulses the second harmonic intensity reverted to that before excitation without any loss. This reversible modulation was attributed to a reduction in the molecular hyperpolarisability of the ruthenium complex in the excited state.

In a later study of Langmuir-Blodgett deposited hemicyanine molecules (Xu et al 1997), pulsed exposure to UV reorients the molecules with their chromophore axes along the direction of the UV beam. Annealing of the films lead to randomisation of the molecules.

The stability of alternating layers of an electron acceptor (octadecylthiobenzoquinone) and donor (7-(N-octadecylaminomethyl)-8-16-dioxidibenzo(f,g)perylene) has been measured with respect to time by measuring the second harmonic intensity (Bjornholm et al 1993 (a)). With a 10 layer sample stored in darkness, the second harmonic activity degrades by approximately 25% over a period of 15 days. Upon irradiation with green light, the signal rapidly decreases with a loss of the red colour of the films. By heating the films to 80°C, the red colour is regenerated but not the second harmonic signal. This suggests that a photochemical oxidation of the donor has lead to the decrease in signal.

The molecular arrangement in heat treated Langmuir-Blodgett films was shown to become more non-centrosymmetric with heat treatment time (Miyamoto et al 1992). The second harmonic intensity was measured from film samples after heat treatment and

was found to be greater for films that had undergone longer heat treatment. The change in molecular structure was confirmed by UV-VIS spectra and x-ray diffraction.

Second harmonic generation is commonly used to determine  $\chi^{(2)}$  for Langmuir-Blodgett films of various materials for characterisation purposes (Liu et al 1996, Zhou et al 1997 (b), Yokoyama et al 1997, Garland, N L et al 1997). The second harmonic generation technique has been studied extensively by the research group based at Cranfield University when determining  $\chi^{(2)}$  for materials such as a bis-chromophore zinc complex (Zhou et al 1997 (b)); a squaraine (Ashwell et al 1998 (a)); a squaraine with donor groups (Ashwell et al 1998 (c)); a transparent dye (Ashwell et al 1998 (b)).

The second harmonic signal observed from a material is also dependant upon the environment. The effect of a gas environment has been studied by (Zhao et al 1995), leading to the conclusion that non-linear optical materials can be used as chemical sensors, or that it may be possible to modulate the behaviour of a film by variation of the gas environment.

## **Chapter 3      Review of Materials**

The research reported in this thesis has focused on the optical properties of AmPc5 and AmAz1 (see Chapter 1 for molecular structures). AmPc5 is an asymmetrical, octa-substituted, metal free phthalocyanine possessing the characteristic two-dimensional disc like structure of phthalocyanine and its derivatives. The AmAz1 molecule is a resorcinol calixarene possessing the basket-type structure characteristic of calixarenes. Molecules from both families have shown potential in device applications and it was the purpose of this study to determine the optical parameters of these molecules for future applications.

In this chapter reviews are presented of literature published on the characterisation and application potential of certain phthalocyanine and calixarene derivatives.

### **3.1 Phthalocyanine and its Derivatives**

#### **3.1.1 Introduction**

After the accidental discovery of phthalocyanine at the start of this century they were used as blue-green pigments, following which the basic chemistry of the molecule was established (Law 1993). This work was initiated by Linstead and co-workers in 1934 who originated the term phthalocyanine with reference to this class of organic material (Gould 1996). Commercial production of various phthalocyanines began in this period and as a result the number of phthalocyanine derivatives now documented is immense (Cook 1993). In general, phthalocyanines exhibit great stability towards heat, acids and bases. Combinations of these properties and ease of manufacture has led to their extensive use as pigments for inks and textiles (Archibald et al 1997), colourants in paints and plastics, dyes for clothes and colour photography (Cook 1993). Over seventy

different metals have been incorporated into the centre of the phthalocyanine ring system as well as hydrogen which results in a metal free phthalocyanine. Substituents added onto the ring system expands the range of known and potential phthalocyanines enormously, where the substituents can be located on a peripheral or non-peripheral site. This means that the chemical and physical properties of phthalocyanine can be tailored over a very wide range by desired chemical modification ie. molecular engineering (Nalwa et al 1995).

They exhibit intense absorption in the red and their appearance in the solid state ranges from dark blue to metallic bronze to green. Phthalocyanines exhibit polymorphism as the intermolecular forces between phthalocyanine molecules are relatively weak. Copper phthalocyanine, for example, has 5 different polymorphs with each crystalline structure possessing characteristic solid state absorption spectra and x-ray diffraction patterns (Law 1993).

The phthalocyanine in the present is metal free with substituents on non-peripheral sites. These substituents provide the molecule with its amphiphilic nature. Deposition of stable Langmuir-Blodgett films of metal free phthalocyanines is shown for the first time by (Baker et al 1983 (a)). Here Langmuir-Blodgett films of a peripherally substituted and unsubstituted phthalocyanine have been deposited.

The architectural flexibility of phthalocyanine has lead to a sizeable number of potential and realised applications that exploit the properties of each molecule type.

### **3.1.2 Structural Characterisations**

In order to successfully incorporate phthalocyanine molecules into working devices it is important to build uniform, well ordered and relatively defect-free films. Polarised optical absorption is commonly used to determine the presence of a preferred orientation

of phthalocyanine molecules (Granito et al 1996, Capelletti et al 1995, Liang et al 1997).

Langmuir-Blodgett films of a particular phthalocyanine derivative have been structurally and morphologically studied (Manno et al 1996). Films of up to 80 monolayers were deposited and the refractive index and extinction coefficient at normal incidence were determined (Heavens 1964). The molecular orientation was determined (Yoneyama et al 1986), and it was found that the average orientation of films deposited from toluene solution was not normal to the substrate, whereas the orientation for films deposited from ethyl acetate solution was normal to the substrate. These findings stressed the active role of the spreading solvent in determining the structure of the Langmuir-Blodgett films. Observations by transmission electron microscopy reveal small ordered domains in a matrix exhibiting short range order.

Multilayered films composed of copper phthalocyanine and naphthalene tetracarboxylic dianhydride have been fabricated using organic molecular beam deposition (Imanishi et al 1994). Analyses of the resulting films has revealed a layer by layer structure of the multilayers. Construction of such a superlattice structure may facilitate the containment of excitation within one kind of molecular layer or induction of charge transfer at the interfaces between layers. These results point towards the possibility of future photonics devices.

The technique of surface plasmon resonance has been used to characterise films of phthalocyanine deposited by spin coating (Vukusic et al 1992). Various thicknesses of these films were deposited by variation of the substrate rotation speed and the surface plasmon resonance curves were measured. The curves were fitted according to theoretical reflectivity curves and the thicknesses were determined. The results indicated a near linear relationship between spin speed of the substrate and the inverse of the deposited thickness of phthalocyanine. The structural properties of 3 different

phthalocyanine deposited using spin coating and the Langmuir-Blodgett method were compared by deposition onto glass substrates (Bryant et al 1994). The study showed that film deposited using the Langmuir-Blodgett method had higher degree of ordering, whereas the spin coating method provided a more convenient method of film forming.

In a recent publication (Ruau-del-Teixier 1996) the pressure-area isotherms and linear dichroism measurements of a number of symmetrical tetra-functionalised phthalocyanines have been reported. Substitutions were performed on the parent tetracarboxyphthalocyanine. From the measurements taken it was clear that the length and linearity of the chains was important for the stability of the Langmuir film and the quality of the Langmuir-Blodgett films. It was found that a six-carbon linear chain was the minimum length needed to obtain good quality Langmuir-Blodgett films.

The molecule with four-carbon chain was found to be untransferrable from floating monolayer to substrate. It was suggested that hydrogen bonds were formed between the molecules within the floating monolayer preventing the transfer despite the formation of a stable monolayer.

The nature of the substituents was found to have a profound effect on solubility but not on monolayer organisation and the phthalocyanine ring was found to lie perpendicular to the plane of the substrate in all cases.

The planar anisotropy was found to improve after thermal annealing at 553 K as revealed by dichroic measurements taken before and after annealing.

A spectroscopic characterisation of a substituted phthalocyanine reveals that average orientation of the molecules deposited in Langmuir-Blodgett films is dependant upon the spreading solution and type of substrate (Pasimeni et al 1996). Molecular orientation was probed using polarised UV/VIS absorption spectra where films deposited from ethyl acetate were shown to have a lower dichroic ratio than those deposited from toluene.

The phthalocyanine studied in the present research is structurally related to the family of amphiphilic, octa-substituted phthalocyanine derivatives previously studied (Cook et al 1994). The film forming properties and molecular packing of 20 different molecules belonging to two families; alkoxy phthalocyanines and alkyl phthalocyanines have already been reported. The alkyl phthalocyanines formed better monolayers that exhibited improved deposition behaviour as compared to the alkoxy phthalocyanines. They were also shown to form more highly ordered films through x-ray diffraction and spectroscopic measurements. The molecular packing was found to be dependant upon the length of the hydrophobic chain, with the shortest chain derivative (C<sub>6</sub>) differing from the others (C<sub>7</sub> to C<sub>10</sub>). The metallated phthalocyanine molecules for both groups showed consistently better behaviour than the metal free derivatives. This study has shown that a change in the length of the alkyl chains provides a means of controlling the type of molecular packing within the Langmuir-Blodgett films. Further molecular characterisation studies on these octa-substituted phthalocyanines have been performed (Nabok et al 1997), (Cook 1994) and (Poynter et al 1994).

### **3.1.3 Optical Data Recording**

Phthalocyanine derivatives are considered excellent materials for use in optical data recording applications as they display thermal stability and resistance to oxidation and moisture (Tao et al 1994). Optical properties of phthalocyanines and organic materials in general can be adjusted to an appropriate laser wavelength by modification of the molecular structure and the materials can be fabricated at low cost with reliable coating techniques (Gu et al 1995). Recording in phthalocyanine films is effected by a change of state of the material by vaporisation, sublimation or other physical deformation by a high density beam. This has an effect on the reflectance and/or optical absorbance of the films and hence the change can be read back. Reading is usually performed by

measuring variations in the intensity of reflected light from a low power laser (Kuder 1986).

The write-once-read-many characteristics of vanadyl based phthalocyanine derivatives have been studied (Gu et al 1995). Different substituent and metallic ions were originally selected for the phthalocyanine ring, and the absorption bands of thin films of the compounds were matched with the wavelengths of semiconductor lasers. It was found that the absorption regions of the vanadyl phthalocyanine derivatives were between 580 and 850 nm. Vanadyl phthalocyanine was found to be a suitable recording material as the morphology of the recording layer before and after laser irradiation indicated a sharp contrast. An accelerated ageing study of the thin films showed satisfactory performance with regards to its lifetime for practical applications.

In a similar study the write-once-read-many characteristics of copper phthalocyanine have been measured where exposure to a low power He-Ne laser initiated a relatively large reflectivity change (Chen et al 1994).

Experimental writing and erasing data obtained from tetra-neopentoxo phthalocyanine zinc (TNPPcZn) is presented (Tao et al 1994). The phthalocyanine undergoes similar phase changes under laser energy or heat treatment. With increasing laser power the material transforms from disordered monomer to ordered dimer and then to ordered monomer. These structural changes are accompanied by a reduction in reflectance for the first structural change followed by an increase in reflectance for the second transformation. It is suggested that the writing and erasing is caused by the phase transformation between the disordered monomer and ordered monomer.

### **3.1.4 Non linear Applications**

Nonlinear optical characterisation of materials enables their suitability for applications such as optical communication, data storage (Liu et al 1995 (a)), optical computing (Liu

et al 1995 (a)), dynamic holography, harmonic generators, frequency mixing and optical switching to be determined (Nalwa et al 1995).

In a third order nonlinear optical study, the relationship between molecular structure and third order optical nonlinearity of certain metallophthalocyanines has been established (Nalwa et al 1995). The third order nonlinear optical susceptibility ( $\chi^{(3)}$ ) of phthalocyanine containing central metal atoms oxovanadium, copper, nickel, iron and cobalt and with various peripheral substitutes were measured using the third harmonic generation technique and compared for the first time. The results indicate that the  $\chi^{(3)}$  value of metallophthalocyanines is associated with the metal atom substitution. Although the variation is not very dramatic, the oxovanadium cation is the most effective. It is suggested that the axial oxygen group plays a major role in the molecular arrangement, leading to a relatively large value for  $\chi^{(3)}$ .

When studying the effect of substituents, unsubstituted oxovanadium phthalocyanine has the largest  $\chi^{(3)}$  value, and as peripheral groups are substituted, its magnitude decreases significantly. This may be as the substitution adversely affects the molecular stacking resulting in reduced molecular interactions.

The opposite effect was displayed by copper and nickel phthalocyanine, where the substituted values were found to be slightly larger than the unsubstituted. It was thought that the magnitude of optical nonlinearity was related to the induced polarisability in the phthalocyanine ring by an individual substituent.

It is also suggested that there may be some correlation between  $\chi^{(3)}$  and the photoconductivity, as materials that show large third order optical nonlinearities also exhibit high photoconductivity.

Third harmonic generation measurements performed on evaporated thin films of chlorogallium and fluoro-aluminium phthalocyanines is presented (Ho et al 1987). The

measurements produced a value for  $\chi^{(3)}$  attributed to the preferred structure of cofacial stacking as opposed to the slip-stacked structure.

The measurement of  $\chi^{(3)}$  values for octa-substituted metallophthalocyanines deposited in Langmuir-Blodgett films has been performed (Diaz-Garcia et al 1996). Metal-free, copper, nickel and cobalt phthalocyanines were deposited in order to analyse the possible influence of the molecular arrangement in the nonlinear response. The  $\chi^{(3)}$  values which would correspond to films deposited in an unordered fashion with the same thickness and optical density as the Langmuir-Blodgett films were calculated and compared to those obtained from measurement of the Langmuir-Blodgett films in the study. It was found that the calculated  $\chi^{(3)}$  value was one order of magnitude larger than that measured, suggesting that the particular molecular arrangement achieved in these films decreased the nonlinear response.

The study of second harmonic generation in phthalocyanine derivatives has been limited due to their inactivity at this level. In order to observe second order macroscopic nonlinearity, it is necessary to have an intramolecular charge transfer molecule and a noncentrosymmetric film structure. These can be realised by chemical modification of phthalocyanine molecules and z (or x) type deposition or deposition in alternating layers.

An asymmetrically substituted phthalocyanine has been modified by attachment of a donor and acceptor group to its peripheral ring, thus creating intramolecular charge transfer through the  $\pi$ -conjugated system (Liu et al 1995 (a)). No second harmonic signal was measured from the layers deposited in a z-type structure, and hence an alternating film structure was used. The Langmuir-Blodgett films displayed a nearly quadratic dependence of second harmonic intensity on the number of bilayers. The tilt angle of the phthalocyanine molecules was maintained during the deposition process

through comparison of the pressure-area isotherm and calculated molecular size from CPK modelling.

In a later publication by the same author (Liu et al 1996), the second harmonic generation from Langmuir-Blodgett films of an asymmetrically substituted metallophthalocyanine are reported. In this contrasting study, the Langmuir-Blodgett films deposited in a z-type structure exhibited a much better result than films deposited in an alternating structure. Examination of the relationship of the second harmonic intensity versus the number of bilayers reveals that the z-type structure displays a nearly quadratic dependence of second harmonic intensity on the number of layers. The same relationship as observed for alternating layer structures is not quadratic. These results indicate that z-type deposition occurred equally well for each layer and that the orientation within each layer remained constant.

### **3.1.5 Gas Sensing**

The gas sensing applications of certain phthalocyanines and some other molecules using surface plasmon resonance are illustrated in Section 2.1.2. In this section the use of phthalocyanines in gas sensors is discussed in general terms. The increasing use of phthalocyanines in the research of gas sensors has arisen due to the highly stable nature of the phthalocyanine molecule and the ease of molecular manipulation during synthesis.

Since the first demonstration of a copper phthalocyanine as a conductometric  $\text{NO}_x$  gas sensors, many phthalocyanine derivatives have been applied in the use of  $\text{SO}_2$ , and ammonia (Roberts 1984). Typically when determining electrical gas sensor properties, Langmuir-Blodgett films are deposited onto a substrate with pre-deposited interdigitated platinum electrodes, and exposed to pulses of low concentrations of gases with mixed

air (Cook 1996). The electrical conductivity of the films is then shown to change in the presence of gas to be detected.

Such a method has been used to study the response of a copper phthalocyanine to  $\text{NO}_2$  (Travis et al 1995). The research demonstrates the suitability of the material as a “single shot” disposable sensor that satisfies the current regulations for occupational hazards. The material was tested by mounting the sample in a gas cell whilst maintaining a constant gas flow rate and varying the concentration of  $\text{NO}_2$  by mixing different quantities of the gas with clean, dry air. A constant voltage was placed across the sample, and the current through the sample was monitored for different concentrations of  $\text{NO}_2$ . For concentrations ranging from 1 to 5 ppm of  $\text{NO}_2$  the conductivity was found to increase with concentration. For each level of concentration, the conductivity was shown to vary exponentially with time for exposure and recovery to exposure. The results show that the recovery time constants are longer than the response time constants which lead to gradual degradation of reproducibility for repeated  $\text{NO}_2$  air mixtures. This points to the material suitability for use as disposable sensors.

In a similar study, a different copper phthalocyanine derivative deposited in Langmuir-Blodgett films was shown to possess reversible  $\text{NO}_2$  gas sensitive properties at 443 K (Rella et al 1996). Two gold contacts were used to measure the electrical resistance as a result of  $\text{NO}_2$  adsorption on the surface of the Langmuir-Blodgett films. The resistance was shown to drop upon injection of  $\text{NO}_2$  gas. The study shows this adsorption process to be reversible at a temperature of 443 K, but only partially reversible at room temperature. This factor may lead to difficulties when considering the material for use in practical gas sensing devices. The gas sensing properties of the same material (Cu(II)-tetrakis-(3,3-dimethylbutoxycarbonyl)phthalocyanine) have been reported by the University of Lecce in more recent publications (Rella et al 1997(a),(b),(c),(d)). The dynamic response characteristics of electrical conductance to different  $\text{NO}_2$

concentrations are presented (Rella et al 1997 (c)) as well as the material response to NO<sub>2</sub> gas when deposited in alternating Langmuir-Blodgett films (Rella et al 1997 (d)) and 1:1 mixtures (Rella et al 1997 (b)) with a similar copper phthalocyanine derivative. The response characteristics of the mixture was also studied for exposure to NO (Rella et al 1997 (a)).

The NO<sub>2</sub> gas sensing properties of a number of metallophthalocyanines have been investigated by stacking the materials in Langmuir-Blodgett films onto a quartz crystal microbalance (Kim et al 1997). The results show different sensing properties for each type of central metal atom. The sensing properties for the metals considered were found to be in the following order,

cobalt > lead > metal-free > copper

where cobalt possessed the highest sensitivity.

A gadolinium phthalocyanine is studied for its application in the sensing of approximately 10 ppm of chlorine gas (Richardson et al 1997). The optical absorbance spectra for the phthalocyanine shows an absorbance band at 690 nm which decreases upon exposure to chlorine, with the addition of a new peak at 734 nm. The Langmuir-Blodgett film is shown to recover almost completely (>95%) upon switching off the chlorine supply. It is suggested that the spectral changes observed are indicative of oxidation of the phthalocyanine complex by chlorine.

### **3.1.6 Medical Applications**

Sulphonated chloroaluminium phthalocyanines have been investigated for their use as photosensitisers of singlet oxygen in photodynamic therapy (PDT). PDT is a process that uses light to activate otherwise relatively inert photosensitisers that produce oxygen which causes cell injury.

This effect can be used as a potential method of treating certain types of cancer where a tumour cell selectively absorbs a sensitiser. Upon irradiation of the malignant area, the sensitiser promotes the generation of singlet oxygen which destroys the tumour (Rosenthal 1989).

The same technique, again utilising sulphonated chloroaluminium phthalocyanine, has been demonstrated to inhibit allograft rejection in rats and is being developed for use in vascular bioprotheses in humans (LaMuraglia et al 1995). In the treatment of coronary disease, vascular grafts can be rejected by the human body and the study has shown that PDT can destroy the cells responsible. The sulphonated chloroaluminium phthalocyanine is administered intravenously prior to graft implantation and then irradiated by an argon pumped dye laser at 675nm, the wavelength of photoactivation.

The research performed on phthalocyanines for their use in PDT as treatments for cancer is extensive (Kudrevich et al 1997, Witjes et al 1997, Separovic et al 1997). The most frequently used material previously for PDT, a haemotoporphyrin derivative left the patient sensitive to sunlight for several weeks after treatment (Bown 1993).

Apart from cancer treatments, phthalocyanines have been used in PDT for blood sterilisation applications (Allen et al 1995). The usual methods of sterilisation are shown to be harsh and unsuitable for blood products and the researchers have evaluated a series of sulfophthalocyanines with Ga, Al and Zn central metal atoms as photosensitizers. The results showed anti-viral activity was greatest with Zn as the central metal atom and greater amphiphilicity of the molecule enhanced photodynamic activity.

In addition to PDT, the use of phthalocyanine in the design of polymeric drug carriers has been reported, where the biological properties of the system have been evaluated (Kopecek et al 1997) and cobalt phthalocyanine has been applied in the development of a glucose biosensor (Gilmartin et al 1995).

## 3.2 Calixarene and its Derivatives

### 3.2.1 Introduction

The term calixarene was borne out of a need for a more succinct and descriptive name to describe this class of molecules. The cyclic tetrameric structure was first postulated by Zinke in 1952 who referred to the molecules as 'Mehrkernmethylenephenolverbindungen' (Gutsche 1989). Study of the CPK model of calixarene (Figure 1.3) reveals a similarity between the molecular shape and a Greek vase called a calix crater. The name is derived from the word calix and arene, which indicates the presence of aryl residues in the macrocyclic array. The reference to calixarenes as molecular baskets is owed to their ability to form complexes with a range of chemical species. The cavity size can be engineered at a molecular level to enable incorporation of different guest molecules (ArnaudNeu et al 1997), hence opening a range of calixarene applications in gas sensing, non-linear optics and ion extraction. The application of a calixarene derivative utilising the physical properties of the material rather than the ability to incorporate guest molecules has been reported (Fujita et al 1996). The derivative was tested as a high resolution negative resist under an electron beam lithographic process. A 10 nm resolution was achieved with little side roughness and high durability indicating suitability for nanoscale device processes. The research group based at the NEC Corporation, Japan have recently reported the application of the material in nanoscale MOSFET's (Kawaura et al 1998). The fabricated device exhibited normal transistor characteristics even in the 32 nm gate length regime at room temperature. In a recent report, similar negative photoresist properties have been reported for a calix(4)resorcinarene derivative (Nakayama et al 1997).

The very high thermal stability (typically, melting points > 273 K) of calixarenes has been used to study the pyroelectric effect in two calix(8)arene molecules with inserted

carboxyl and amino groups in each molecule (Richardson et al 1995). The molecules were deposited in alternating Langmuir-Blodgett films to enable study of the temperature dependant electric polarisation. FTIR spectra of an alternate layer sample reveal two carbonyl peaks that suggest partial proton transfer and lead to a large dipole moment. Current measurement is demonstrated to be dependant upon temperature which confirms the pyroelectric nature of the material. The variation of the pyroelectric response is found to differ according to the structure of the pendant hydrophobic chains (McCartney et al 1997).

The molecule studied in the present research is a resorcinol derived calixarene (calix(4)resorcinarene) with attached azobenzene groups (Figure 1.2).

### **3.2.2 Structure**

Investigation of the structure of the calixarene derivative is a necessary precursor to exploring the possibility of application in devices and the study of physical effects. An optical characterisation of AmAz1 deposited in Langmuir-Blodgett films has been published (Omar et al 1997). The refractive index and extinction coefficient obtained from surface plasmon resonance curves are given here.

Spontaneous multilayering of unsubstituted calix-4-resorcinarene by Van der Waals interdigitation and hydrogen bonding alternation has been reported (Davis et al 1995). The multilayering was observed to be extensive and rapid from bulk solution into ordered films. The hydrocarbon chains in the calixarene structure particularly favour such multilayering, with deep layer to layer interdigitation of the chains. The multilayers were deposited from a number of solvents where the extent of deposition is dependent upon the hydrogen bonding ability of the solvent. Hence, the greatest deposition was observed from hexane and the least from propane and ethanol. As the infra-red C-H frequency stretch intensity is dependant upon the calix-4-resorcinarene

concentration, a higher intensity was observed from hexane, implying a greater number of monolayers (44) and rapid multilayering. The C-H stretch frequency was shifted to a higher frequency for the molecule which was consistent with the idea of interdigitation in the multilayer. Data obtained from X-ray and neutron reflectivity experiments further support the theory of alkyl chain interdigitation.

These spontaneously assembled multilayers were compared with Langmuir-Blodgett films of the same material in a later publication (Davis et al 1996 (a)), further verifying the interdigitation of the bilayers.

The multilayers were shown to form from hexane solution, where ethanol and propanone were shown to reverse deposition of hexane deposited films. The dispersion of the multilayer was prevented by terminating the alkyl chains of the molecule with vinyl groups and irradiating with UV light (Davis et al 1996 (b)). The irradiation had the effect of cross-linking the chain, resulting in stability of the multilayer and resistance to dispersal.

Composite polyaniline/calixarene derivative Langmuir-Blodgett films have been prepared and studied in floating monolayer form (Lavrik et al 1996), where they have been shown to form stable monolayers. The pressure-area isotherms of mixtures varying from 0% to 100% by weight of calixarene derivative were recorded and compared. For 60% and greater calixarene weight the pressure-area isotherms were similar to those of pure calixarene. It has been suggested that the mixture sits on the water surface with the polyaniline molecules beneath the calixarene molecules, partially incorporated in between their polar fragments. The mixture is then deposited as Langmuir-Blodgett films onto substrates in the same formation. The average thickness per monolayer was found to be 1.6 nm from ellipsometric measurements. The correlation has been demonstrated as the height of the calixarene molecule is about 1.1 nm and that of polyaniline is 0.5 nm. Scanning tunnelling microscopy images reveal a homogeneous

distribution of calixarene molecules and proper molecular mixing over the scan area as formation of a nanoporous structure is apparent.

The structures of composite Langmuir-Blodgett films from mixtures of fullerene and various calixarenes were investigated by (Kazantseva et al 1997). Study of the Langmuir floating monolayer behaviour, ellipsometric and UV-VIS spectroscopic data of Langmuir-Blodgett films, followed by scanning electron microscope and scanning tunnelling microscope images, pointed towards production of good quality Langmuir-Blodgett films. It was found that calix(8)arene produced perfect films where fullerene was contained in the matrix in a non-aggregated form as a result of the formation of calix(8)arene and fullerene inclusion complex.

### **3.2.3 Non-linear Effects**

The observation of non-linear effects in molecular structures is conditional to the presence of a non-centrosymmetric build and dependant upon the strength of molecular donor groups (Prasad 1991). Calixarenes possessing the crown (or cone) conformation (Gutsche 1989) with the appropriate substitutions are examples of donor-acceptor aromatics which are locked in a non-centrosymmetric arrangement (Morley et al 1997). These molecules may possess a large dipole moment and hence large molecular hyperpolarisability. When considering poled polymer films, the molecules need a large dipole moment to be orientated by a strong electric field near the glass transition temperature. This results in the retention of a non-centrosymmetric structure upon cooling. It is suggested that the poling process can also be applied to calixarenes possessing large molecular hyperpolarisabilities. The hyperpolarisabilities of a series of calixarenes were measured and were found to be dependant upon the orientation of the donor substituent. An increase in calixarene ring size was found to have a small effect on the electronic properties. Molecular structures that enabled conjugation between the

lone pair electrons and  $\pi$ -electron systems of the aromatic rings showed the greatest non-linearity.

Second harmonic generation has been used as an optical method of imaging nanometre thick calixarene derivative self assembled films (Smilowitz et al 1997). The method was developed as the second harmonic signal is highly sensitive to the physical orientation of molecules at interfaces and hence can be used as a non-linear optical microscope. The technique uses a component of the second order nonlinear optical susceptibility which arises due to the symmetry breaking at the surface of the film. Provided that the molecule has a non-centrosymmetric structure, the bulk of the material can be in a centrosymmetric formation and the second harmonic signal will still be observable. Self assembled monolayers of the calixarene were patterned using a layer of photoresist spun onto the film. The samples was irradiated with UV light and then developed to generate a pattern. The uncovered sections of the film were etched and after removal of the remaining resist the patterned monolayer remained. Upon irradiation with the Nd/YAG source, light is generated in the patterned regions and is observed. It is suggested this method is applicable in the study of buried interfaces as well as surfaces.

In a theoretical study the geometries and second order nonlinear optical properties of four conformations of donor-acceptor substituted calix(4)arenes were investigated (Brouyere et al 1997). Attention is drawn to the four  $\pi$ -conjugated electron systems in each of the molecules and the effect of changing the relative orientations of the systems on the second order optical response. The four molecular conformations of the calixarene derivate were in the cone, partial cone 1,2 alternate and 1,3 alternate conformations, (nomenclature adopted from Gutsche 1989), where the molecular hyperpolarisability was found to decrease in the same order. In general terms this decrease can be attributed to a decreasing pattern of  $\pi$ -electron conjugation. In an earlier publication (Kelderman et al 1993) the variation in structure due to the number and

relative positions of the donor and/or acceptor  $\pi$ -conjugated units was discussed. The non-linear optical properties of the molecules are found to be stable.

### 3.2.4 Sensing Properties

The sensing properties of calixarene and its derivatives have been applied in the areas of metal ion complex formation (Thuery et al 1997, Davis et al 1996 (c)), solvent vapour detection (Dickert et al 1997) and organic pollutant detection in water (Lucklum et al 1996). As the difference between an efficient sensing agent and an ineffective one has been very difficult to predict on a molecular basis, most materials are tested on an *ad hoc* basis (Diamond et al 1996).

Complexation can take place inside the calixarene cavity and/or in between molecules with solid state and solution systems. This is due to the flexible nature of substituents that can bend inwards to fill the cavity. The flexibility can also result in intramolecular complexation which prevents external guest molecules from entering the cavity (Gutsche 1989). The strength with which the guest molecule is held by the calixarene also varies within the series of molecules.

A recent review describes the discovery that certain tetramic calixarene derivatives possess significant affinity for alkali metal salts, namely sodium (Diamond et al 1996). Initial screening experiments carried out with liquid membrane sensors confirmed that excellent sensors for sodium could be produced. These results provided an obvious commercial application for the sodium sensors in the clinical analysis of sodium in body fluids. The technique can also be applied to the analysis of sodium levels in mineral water samples. Studies on lifetime expectancy and reliability have shown that the sensors can be used for months at a time, with the analysis of several thousand blood samples.

Manipulation of the cavity size of the calixarene has enabled potassium selectivity. A calix(4)arene substructure in which two of the four bridging methylene units are expanded by additional oxygen atoms has resulted in a cavity size larger than a normal tetramer. Early measurements indicate an inferior selectivity to that of a well known potassium sensor (Diamond et al 1996).

A calix(4)arene derivative was developed for use in the sensing of ammonia gas by the optical evanescent wave technique (Grady et al 1997). The compound belongs to a family of chromogenic calixarenes which display a dramatic change in absorption upon complexation with lithium (and to a lesser extent with sodium and potassium) in the presence of an appropriate base. A shift in the absorbance maximum from 380 to 520 nm is observed upon lithium complexation in the presence of tridodecylamine, with no shift in the absence of the base.

A membrane coated optical fibre configuration was used in a mass flow controller to enable spectroscopic measurement of various ammonia gas concentrations. The absorbance was found to increase with gaseous ammonia level, where the sensitivity was variable depending upon the metal in use (sensitivity found to be  $\text{Li} > \text{Na} > \text{K}$ ).

As ammonia is recognised as one of the primary irritants to humans, its detection in clinical, environmental and industrial processes is essential. A threshold limit of 25 ppm in air for human exposure has been recommended, where the sensor under investigation was shown to perform to 10 ppm.

The sensor response time was demonstrated to be of the order of a few minutes, whereas the recovery time was found to be up to 1 hour. Obviously, this factor must be addressed before the sensor can be developed for commercial applications.

Calix(6)arene derivatives have been found to be caesium selective. X-ray diffraction studies confirm that the cavities are more open than the sodium selective tetramers

(Diamond et al 1996). This allows removal of caesium from highly salted radioactive waste (Ungaro et al 1996).

Research into the use of calixarenes as uranophiles has been performed and followed by the issue of patents in the name of Shinkai and co-workers (Gutsche 1989). The investigation is concerned with the possibility of uranium extraction from seawater, where the uranium is strongly complexed with carbon dioxide. Tetramic sulfonated calix(4)arenes were shown to complex with uranium on a small scale when compared to calix(5)arenes and calix(6)arenes. It was suggested that the uranium ion was able to fit the larger cavity size of the calix (5) and calix (6) molecules better than the calix(4) molecule.

A similar idea is applied to the separation of radioactive waste from aqueous waste streams (Dasaradhi et al 1997). The research was focused on the removal of actinides such as plutonium (IV) from soil and process waste streams in the presence of more abundant and competing metal ions such as iron (III) and aluminium (III). The technique is receiving attention due to stringent regulatory limits that stipulate substances such as plutonium and americium must be removed from waste streams prior to discharge to ultra low levels. The technique is also applicable to actinide removal from contaminated soil and water.

Three calix(4)arene derivatives were selected for extraction (a tetrahydroxamic derivative; its analogues and a tetracarboxylic acid derivative), where their rigid skeletons provided a degree of molecular preorganization. The molecules were tested for their ability to extract thorium (IV), iron (III), uranium (VI) and copper (II) into chloroform from aqueous solution at various pH values. Thorium (IV) was selected for the study as it is known as a surrogate for plutonium (IV). All three molecules were shown to extract thorium and iron to a similar level, with increasing effectiveness with an increase of pH (from 2 to 4). The primary hydroxamate was shown to be the most

effective extractant at pH 2 for both ions, with the carboxylic derivative the least effective. Extraction of uranium was also measured and shown to increase with pH over a greater range (from 2 to 7). Once again, the primary hydroxamate is most efficient and is shown to extract nearly 100% of the uranium at a Ph of 4. Both other derivatives achieve this status approaching a pH of 7. Derivative behaviour for copper extraction followed the same pattern between pH 2 and 6, except the carboxylic derivative displayed very little ability to extract copper into chlorine.

Competitive metal ion extraction of thorium and iron was performed for all three derivatives, where all three were shown to selectively extract iron over thorium. The results indicate selective extraction of thorium using the three calixarene derivatives is only possible by increasing the pH.

A tetrapodal calixarene derivative similar to the molecule studied in the present research has been studied for selective adsorption (Adams et al 1994). The tetrapodal nature of the molecule was designed to enable the calix(4)resorcinarene to anchor onto a gold surface and produce a self assembled monolayer. A low contact angle of the order of  $28^\circ$  confirms the formation of a hydrophilic surface. It can therefore be concluded that the molecule forms the basket structure in preference to other formations.

An adsorption study revealed that simple ions were not adsorbed, whilst polar compounds were readily adsorbed. The adsorption was easily reversed for glutaric acid and poly(vinyl pyrrolidone) by washing with pure water for several hours, but was not the case for the polyhydroxy compounds (glucoronolactone, gluconic acid and vitamin C). The hydrogen bonding to the rim of the calix(4)resorcinarene bowls was thought to be the reason. It is not possible to remove vitamin C even in the presence molecules shown to bind strongly to calix(4)resorcinarenes. This implies the possibility of covalent binding. An attempt to prepare the calix(4)resorcinarene/Vitamin C adduct from

solution was unsuccessful. This was possibly due to the bowl to bowl packing of the resorcinarene molecules.

The adsorbing properties of calix(4)resorcinarenes (referred to as calix(4)resorcinolarenes) Langmuir-Blodgett films have been investigated (Nabok et al 1995). Three types of the calix(4)resorcinarene molecule was prepared, each possessing a different substituted carbon chain length of 3, 7 and 15. The crown structure of the calix ring was confirmed by nuclear magnetic spectroscopy while additional molecular rigidity was provided by the hydrogen bonds between the OH groups of the calix ring. Water and a mixture of aromatics (benzene, toluene and aniline) were used as adsorbates in the study, where measurements were taken using the quartz crystal balance method. The mass changes caused by adsorption were compared for differing monolayer thicknesses and plotted in the form mass change 'v' number of monolayers. The results indicate that adsorption for both water and aromatics increases linearly with film thickness. However, the aromatics are shown to be adsorbed to a greater level than water, where the curves for change in mass after water adsorption and without adsorbate are almost parallel. This indicates that adsorption of water occurs in the top monolayer or at the Langmuir-Blodgett film surface. A steeper curves is obtained for adsorption of aromatics, showing that adsorption occurs in the whole Langmuir-Blodgett film bulk. Ellipsometric data of the flow of benzene with time show a strong peak at the moment of benzene injection followed by signal relaxation to a steady state, and a sharp signal decrease after injection of pure atmosphere. This pattern is shown to take place in decreasing intensities for decreasing benzene concentrations. The ellipsometric data confirm a swelling mechanism in the adsorption of aromatics and also fast adsorption and desorption processes.

The adsorption abilities of tetrapodal and non-tetrapodal calix(4)resorcinarene derivatives have been compared by use of the quartz crystal microbalance (QCM) and

surface acoustic wave (SAW) techniques (Dickert et al 1997). The derivatives have been tested with respect to their chemical sensing capabilities in coatings on mass-sensitive devices. Two methods of detection have been used as SAW requires ultra thin layers for surface detection and in contrast QCM resonators require bulky microporous coatings with high vapour permeability. These techniques are capable of providing low cost gas monitoring equipment.

The molecular structure of calix(4)resorcinarene was engineered to create different calix cavities and variable spacers as well as the synthesis of tetrapodal molecules. Three families of molecules were synthesised from the basic molecule. Family 1 was made up of four molecules 1a, 1b (tetrapodal), 1c and 1d where the hydrocarbon chains were of length 1, 9, 7 and 11, consecutively. Family 2 consisted of 2a, 2b (tetrapodal) and 2c with hydrocarbon chain lengths of 1, 9 and 7, consecutively with four quinoxalines substituted on the periphery of the calix ring. The last group, family 3 was made up of a single molecule (3, tetrapodal) with only three quinoxalines and one position left unsubstituted and a hydrocarbon chain length of 11.

The sensitivity of molecules 1b, 2a, 2b, 2c and 3 to some solvents were compared by the degree of filling at an analyte concentration of 1000 ppm. Molecule 3 was shown to have the highest sensitivity to almost all solvents; the partially open structure leaves a molecular entrance resulting in fast kinetics of inclusion and desorption of guest molecules. 2c exhibits a better affinity to dichloromethane as the hydrocarbon chains form a second smaller cavity that engulfs dichloromethane but is too small for other larger molecules.

Host molecules 1b and 3 have eight and two hydroxyl groups, respectively, they are able to form hydrogen bonds and hence show an affinity for solvents such as butanol and pyridine. Hydrogen bonding shows a superior strength of interaction and in the case of

pyridine, the filling factor indicates the binding of more than one analyte molecule per host 1b and 3.

The conductometric gas sensing properties of phosphorylated calix(4)resorcinarene (CA) and polyaniline (PA) alternating Langmuir-Blodgett films were measured (Lavrik et al 1996). The materials were selected for their ability to form a nanoporous structure with a high electrical conductivity. The research is based on the premise that the conductivity of conjugated polymers depends on the protonating and oxidising processes and consequently may be influenced by various gases.

Initially, the insulating films are doped with HCl which causes a prompt, significant increase in conductivity, displaying a dependence on the CA percentage. 60% CA shows a lower conductivity than 20% CA, although the latter shows a much lower retained conductivity and hence can be doped reversibly. The conductivity of the doped CA (20%)-PA films is shown to decrease on exposure to ammonia, whilst for CA (60%)-PA, the conductivity increases upon exposure to hydrochloric acid. In addition, CA (60%)-PA films when exposed to certain hydrophobic amines show a decrease in relative conductivity by two orders of magnitude greater than in the films of pure PA. This is believed to be due to the molecular recognition ability of CA's.

A role reversal for a calix(4)resorcinarene with azobenzene groups is examined, where the calix molecules are adsorbed into the surface of colloidal silica particles (Ueda et al 1997). Upon irradiation with UV light, the azobenzene groups underwent photoisomerization, resulting in the formation of porous precipitates. Subsequent visible light irradiation regenerated a dispersed state for the silica particles. Hence the technique enables photocontrol of the reversible alternation between dispersed and aggregated states of the silica particles.

## Chapter 4      Thin Film Deposition

Ultra-thin films of organic materials can be deposited using various techniques such as Langmuir-Blodgett (Petty 1996), spin coating (Herold et al 1995), sol-gel (Jones 1989) and simple vacuum evaporation (Baran et al 1995). The molecular precision of Langmuir-Blodgett deposition provides advantages over other techniques both in characterisation of novel materials and device development. The technique allows the deposition of an amphiphilic floating monolayer onto a solid substrate using dipping mechanisms in a Langmuir-Blodgett trough. The materials can be deposited onto a variety of substrates depending upon the required characterisation or application.

### 4.1 Concepts of Langmuir-Blodgett Films

#### 4.1.1 Introduction

The idea that oil spreads on water is not a recent development. In ancient Babylonia (18C B. C.) the observation of the spread of oil on water, used as a fortune-telling method, was documented on clay tablets (Tabor 1980).

In 1774, the American statesman Benjamin Franklin performed his famous ‘teaspoon of oil’ experiment on Clapham Common pond, the results of which were reported in the Royal Society (Franklin 1774). On a windy day in London he poured some oil onto the pond and watched it quickly spread out over the surface, producing an instant calm. These findings were not studied quantitatively until the 1880’s when Lord Rayleigh succeeded in estimating that oil films were between 10 and 20 nm thick (Rayleigh 1890). The earliest form of Langmuir-Blodgett trough was designed by Agnes Pockels in 1891, consisting of a water basin and a strip of tin (Pockels 1892) which enabled Rayleigh to calculate the thickness of a monolayer of castor oil to be 1 nm.

These early experiments laid the foundations for Irving Langmuir to develop the apparatus used by Pockels and to perform his definitive measurements on monolayers (Langmuir 1917). He concluded that fatty acids were orientated with their polar groups into the water and hydrocarbon chains directed nearly vertically from the water surface. Work performed by Langmuir with Katherine Blodgett in 1935 resulted in the first sequential monolayer transfer from a water surface to a solid (Blodgett 1935). These films became known as Langmuir-Blodgett films and were not further studied until the 1960's when Hans Kuhn studied the spectroscopic properties of organised monolayers. Current research in the field is not limited to the study of fatty acids as materials can be designed at a molecular level to possess hydrophobic and hydrophilic components.

#### 4.1.2 Amphiphilic Materials

The formation of high quality Langmuir-Blodgett films is dependant upon the amphiphatic balance of the molecules as the material must be able to form a stable monolayer at the air/water interface. Each molecule consists of a hydrophilic head and a hydrophobic tail end (Figure 4-1).

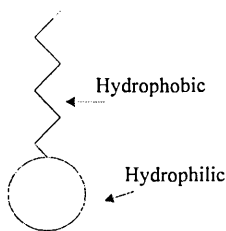


**Figure 4-1 Schematic of an amphiphilic molecule**

The hydrophilic head usually consists of a polar COOH group which is attracted to a polar media such as water. The hydrophobic tail consists of a hydrocarbon chain that displays insolubility in water. In order to form an insoluble monolayer the hydrophobic

and hydrophilic parts of the molecule must balance. With no polar group on the molecule, no monolayer is formed on the water surface with the material floating as lenses without spreading (Petty 1987). With a short tail group the molecule can dissolve into the water. The length of the hydrocarbon chain required depends on the polarity of the molecule.

The material is introduced onto the water surface by firstly dissolving the solid in a volatile solvent and then applying dropwise to the cleaned water surface of the Langmuir-Blodgett trough. The solvent evaporates as the solution spreads over the entire surface, distributing the molecules over the entire surface area available. This distribution is disordered but with each molecule oriented on the surface with the head of the molecule next to the water and the tail pointing away. The solvent must not react chemically with the water or material and possess the necessary properties to dissolve the material in a suitable concentration (0.1-1 mg/ml). It must also evaporate from the water surface within a reasonable time. Typical amphiphilic molecules are fatty acids, such as stearic acid,  $C_{16}H_{32}COOH$ . The 16  $CH_2$  groups form the hydrophobic tail end whilst the  $COOH$  group forms the hydrophilic head.

#### **4.1.3 Langmuir Films**

Once the solvent has completely evaporated the molecules can be compressed by sweeping a barrier over the surface of the water. The compression of the floating monolayer passes through phase transformations that can be viewed on a pressure-area isotherm (Figure 4-2).

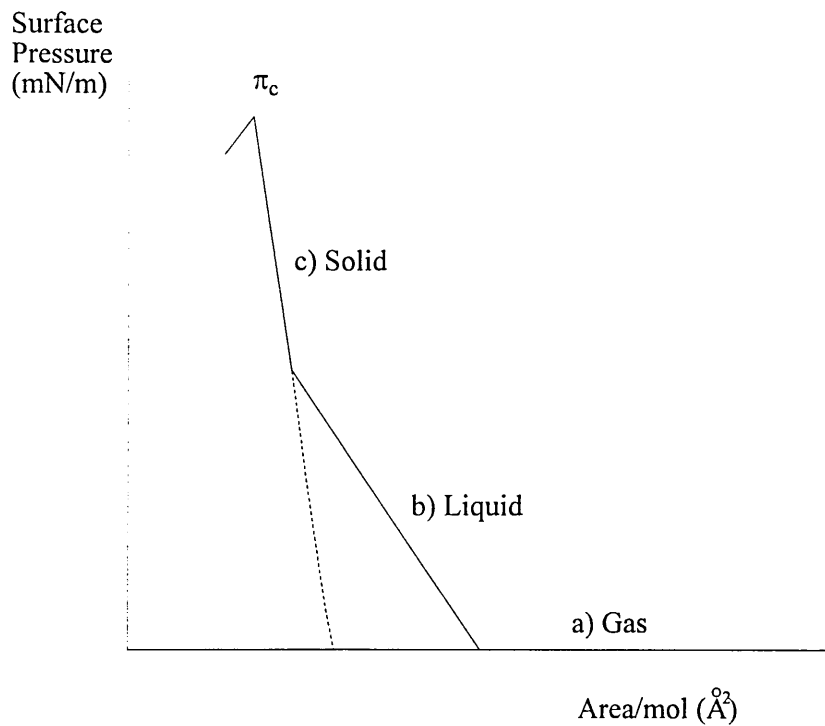


**Figure 4-2 Generic pressure-area isotherm**

The resulting pressure-area isotherm shows the decrease in trough area as a function of increase in surface pressure. The surface pressure is defined as the difference between the surface tension of pure water and film covered surface (Petty 1996). Study of the isotherm can reveal many monolayer characteristics. The isotherm produced can be seen to consist of three distinct phases, which are known as the 2-dimensional solid, liquid and gas phases (Ulman 1991). Initially, when no pressure is applied to the monolayer, the molecules behave as a 2-dimensional gas (line (a) in Figure 4-2). On compression, some ordering of the film takes place (line (b) in Figure 4-2) and forms the 2-dimensional liquid phase. Further compression forces the molecules into a more ordered state and so into the 2-dimensional solid phase (line (c) in Figure 4-2). The floating monolayer can be repeatedly compressed and decompressed through the 2-dimensional solid, liquid and gas phases producing a similar shape of isotherm. A slight change in the slope of the isotherm is sometimes visible due to hysteresis effects in the monolayer. These hysteresis effects can be reduced or eliminated by compressing and

decompressing the monolayer (performing an isocycle) several times. This has the effect of annealing the film and improving the quality. At this stage the monolayer obeys Hooke's law upon repeated compression and decompression. If the monolayer is compressed still further, eventually the critical pressure  $\pi_c$  is reached; the point at which the pressure exerted upon the film is too much and the film collapses. Beyond  $\pi_c$  the compression is irreversible with the monolayer no longer possessing a monomolecular form or obeying Hooke's law. Extrapolation of the solid phase line (line (c)) to zero pressure on the Molecular Area axis gives the area occupied by one molecule at zero pressure on the water surface. This provides information of the packing of the floating monolayer.

#### **4.1.4 Langmuir-Blodgett Films**

The Langmuir-Blodgett films are formed monolayer by monolayer onto a suitably treated solid substrate by dipping through the monolayer floating on the water surface maintained at a particular pressure. The value of  $\pi_c$  determines the pressure at which the substrate dipping should take place. A safe pressure well below  $\pi_c$ , but in the solid region of the isotherm is usually chosen. The floating monomolecular layer is transferred onto the substrate as shown in Figure 4-3. The substrates used must be extremely smooth and ultrasonically cleaned in the first instance. They are then chemically treated so as to be hydrophobic or hydrophilic on the surface. Deposition onto a hydrophobic surface begins on the downward motion of the substrate as shown in Figure 4-3.

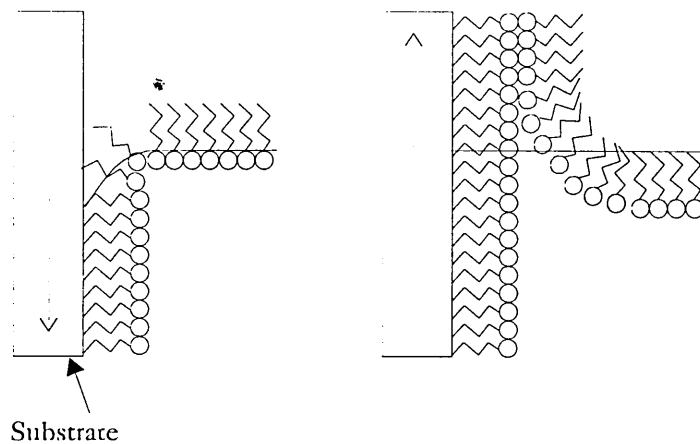


**Figure 4-3 Transfer mechanism of floating Langmuir monolayer to substrate surface**

It can be seen that the hydrophobic tail groups are bound to the substrate with the remainder of the molecule normal to the substrate plane. The second monolayer is deposited by an upward motion of the substrate through the subphase. In this case the hydrophilic head group of the floating monolayer is attracted to the hydrophilic group of the deposited monolayer. Subsequent monolayers are deposited in the same way until the desired film thickness is achieved. Deposition onto a hydrophilically treated substrate begins with a first upward stroke, with following film transfers taking place in the same way. The resulting structure is known as a Y-type structure (Figure 4-4 (b)).

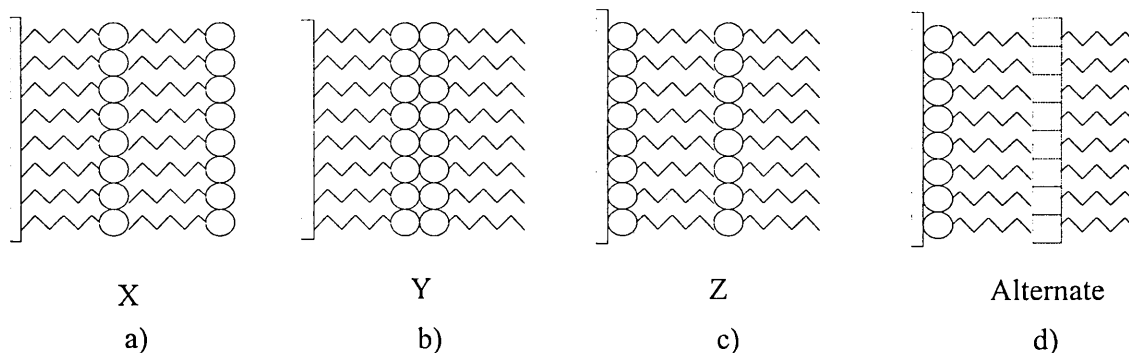


**Figure 4-4 Schematic comparison of Langmuir-Blodgett film deposition types**

Some materials deposit on the up or down strokes only, resulting in Z-type or X-type structures, respectively (Figure 4-4 (a) and (c)). An alternate layer Langmuir-Blodgett trough (Section 4.1.5) enables deposition of two different type of material similar to the Y-type structure (Figure 4-4 (d)). The monolayers are deposited alternately with each monolayer occupying its own separate space in the trough.

The efficiency of deposition of each layer is estimated by monitoring the transfer ratios. The transfer ratios are simply an estimate of the amount of material transferred from the subphase to the substrate. This is expressed as a ratio,

$$TR = \frac{\text{area of monolayer removed from subphase}}{\text{area of coated substrate}} \quad 4.1$$

where  $TR$  is the transfer ratio.

The ratio is expressed as a percentage and ideally should be 100%, but in practice it is possible to achieve transfer ratios widely differing from 100%, whilst obtaining successfully coated substrates. These variations may arise from inaccurate determination of the trough or substrate area. The transfer may also be more successful in one direction of motion than the other and hence consistent transfer ratios are a better indication of film quality.

#### **4.1.5 The Langmuir-Blodgett Trough**

All Langmuir-Blodgett troughs are designed to allow the containment of an aqueous subphase and mechanisms to enable surface pressure measurement of a floating monolayer and subsequent deposition onto a substrate. The subphase is usually ultra-pure deionised water where the behaviour of the floating monolayer depends on the pH and temperature of the water. Certain ions can be introduced into the water which allow

further control over monolayer behaviour. The water is contained in the trough area which can be circular or rectangular and is usually made of polytetrafluoroethylene (PTFE). PTFE is an inert, robust material that is highly hydrophobic. A review of Langmuir-Blodgett troughs is given in Grunfeld (1993).

A moveable barrier, (also made of PTFE) travelling at a given speed is used to confine the floating monolayer in a well defined surface area (Figure 4-5).

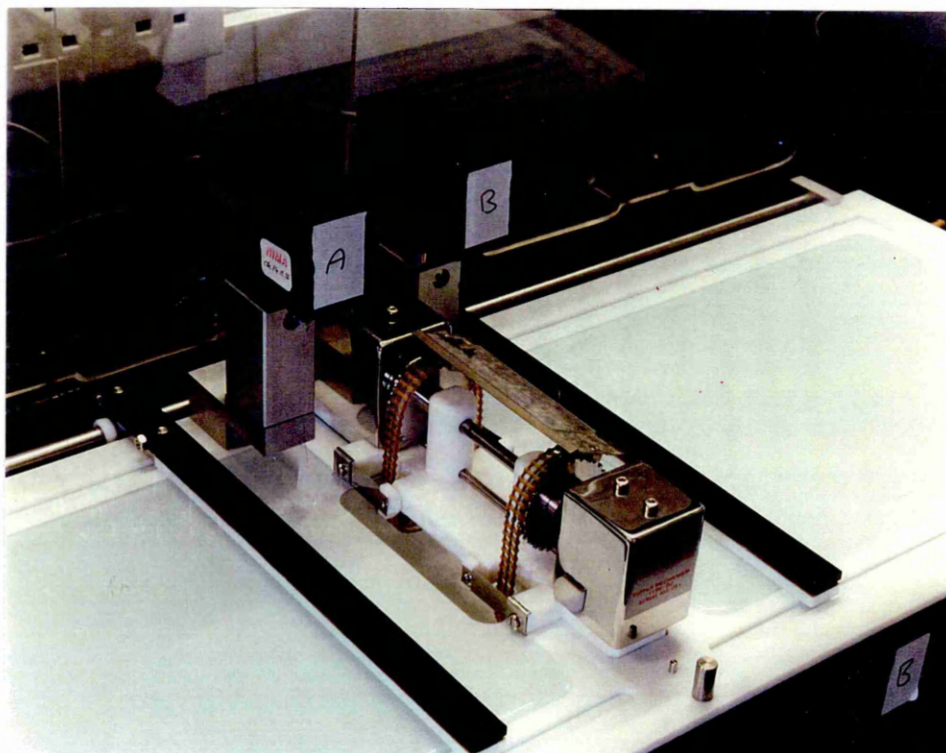


**Figure 4-5 Photograph of the Langmuir-Blodgett trough used in experiments**

As this barrier moves further into the trough, the surface area decreases and the surface pressure increases. This increase is monitored by a pressure sensor consisting of a Wilhelmy plate arrangement. The Wilhelmy plate is simply a strip of filter paper which is pulled down into the bulk of the subphase by the surface tension of the water. The plate is suspended from a very sensitive microbalance by a thin wire. The pressure sensor actually measures the difference in the surface tension between clean water and that of floating monolayer on water. This difference gives the surface pressure which is

the quantity stated in all experiments. The dimensions of the Wilhelmy plate are irrelevant for surface pressure measurement as the balance is set to zero prior to compression. For practical reasons the plate has dimensions of approximately 2x1 cm.

The movement of the substrate through the subphase is controlled by a motor driven micrometer that allows smooth movement at a constant speed of the order of mm per minute.

The devices can be manually controlled, or more commonly by a PC (Figure 4-6).



**Figure 4-6 The Langmuir-Blodgett trough and the PC control unit**

The computer software is used to plot the pressure-area isotherms produced, where surface pressure is measured in mN/m and the reduction in trough surface area is measured in cm<sup>2</sup>. If the relative molecular mass and the volume of the material spread on the water surface are known, then the area occupied per molecule at a given pressure can be calculated.

An alternate layer trough works using the same methods with two moveable barriers. Each barrier compresses two independent surface areas that share a common subphase. The substrate is rotated downwards through the first subphase and upwards through the second.

## **4.2 Langmuir-Blodgett Film Deposition**

This section covers the preparation and deposition in thin films of both materials on different substrates.

### **4.2.1 The Langmuir-Blodgett Trough**

The Langmuir-Blodgett trough used is a two compartment Nima Technology 622 with a linear dipping mechanism housed in a nominal Class 100 clean room. The trough is enclosed in a transparent, sealed cupboard to eliminate the effect of constant air flow present in the clean room. Air flow over the Langmuir film can cause ripples and hence disruption of the monolayer. The trough and cupboard are mounted on an optical bench to reduce the effect of vibrations which would further disrupt the monolayer. The trough has been used in alternate layer mode with both compartments and single layer mode using one compartment only. The alternate layer dipper mechanism has been used to deposit alternating layers of both materials. The conventional dipper has been used to deposit monolayers of one material only.

To perform successful deposition a thorough set of cleaning procedures must be followed, as detailed in Appendix III.

After cleaning the trough is filled with deionised water and the subphase is checked for cleanliness by producing a pressure area isotherm. If the surface of the subphase is dust

free, the pressure-area isotherm produced will show no increase in pressure. This method for checking subphase cleanliness was used each time the trough was used.

The speed of the barriers is measured in  $\text{cm}^2/\text{min}$ . This corresponds to a decrease in the surface area of the trough in a given time. For cleaning purposes this was set to 500 or  $250 \text{ cm}^2/\text{min}$  and for monolayer study at  $100 \text{ cm}^2/\text{min}$ .

The measurement of surface pressure is taken in  $\text{mN/m}$  using the Wilhelmy plate as set in International Standard ISO 304.

The speed of both dipping mechanisms is measured in  $\text{mm/min}$  with the deposition area pre-definable when using the trough in single material mode. This also enables film deposition in a step structure. When using the trough in alternate layer mode deposition takes place over the entire area of the substrate.

#### **4.2.2 The Materials Preparation**

Both AmPc5 and AmAz1 were stored in sealed containers in the dark to eliminate any effects induced by light or air. Solutions were prepared by initially dissolving mixtures in ultrasonically cleaned flasks and then placed in the ultra sonic bath for approximately 15 minutes to improve homogeneity. Once prepared the solutions were kept refrigerated in darkened containers until use to reduce solvent evaporation. Both solutions kept extremely well and could be used weeks after preparation.

Trichloroethane was recommended as the solvent for use with AmPc5, with the solution to be made to a concentration of  $0.1 \text{ mg/ml}$ .

AmAz1 was dissolved in chloroform to a concentration of  $0.5 \text{ mg/ml}$  with 10% ethanol to aid solubility. Absence of ethanol in solution resulted in very poor solubility even after continued ultrasonic treatment.

### **4.2.3 Formation of Langmuir Films**

The solutions were spread onto the surface of the water using a 50 $\mu$ l or 100 $\mu$ l syringe. The syringes were thoroughly cleaned and rinsed in the material solvent before use. The syringe was held a few mm above the surface of the water and the solution was poured drop by drop onto the subphase (at room temperature, pH = 5.5). Each drop was allowed to evaporate before the next was applied. The optimum amount of spreading solution was found by referring to the pressure area isotherms produced. A period of drying between 5 and 30 minutes was allowed for each monolayer prior to compression, in order to let any residual solvent evaporate.

Testing the stability of the monolayer is extremely important as it gives an indication of the suitability of the material for Langmuir monolayer production and the effectiveness of the dipping procedure. The monolayer is compressed to the target pressure and held at this value for about 1 hour. The pressure and area of the monolayer are monitored as a function of time. If the decrease in the area of the monolayer is small over this time, then the film is considered stable and this demonstrates the suitability of the pressure selected as the dipping pressure.

Another important test is the observation of any hysteresis effects in the pressure-area isotherm. The monolayer is compressed to the target pressure and then expanded to 0 mN/m where the isotherm shows the hysteresis taking place. If repetition of the isocycle reduces the effect then the film is said to be annealed.

#### **4.2.3.1 AmPc5**

Experimental trials of film deposition proved successful when a quantity between 500  $\mu$ l and 600  $\mu$ l was spread on the water surface producing a Langmuir monolayer. The very low concentration of AmPc5 indicated that long solvent evaporation times should be allowed. The trials indicated that the monolayer should be left on the water surface

for a time period of approximately 30 minutes before compression. Shorter time periods were found to produce unrepeatable and inaccurate pressure-area isotherms. Longer evaporation times were found to have no effect on the shape of the isotherms.

Upon compression an isotherm was produced showing a hysteresis effect. Further compression and decompression had the effect of annealing the monolayer and producing an isotherm with less hysteresis. This can be seen in Figure 4-7 where two isocycles have been performed. The training of the monolayer involved compression to 25 mN/m and decompression to 0 mN/m. The decrease in the slope of the isotherm at about 28 mN/m indicates the critical pressure,  $\pi_c$  where the monolayer collapses. The sudden increase in surface pressure almost immediately after collapse of the film is unusual. It is possible that at this point the monolayer forms a bilayer on the water surface. A Langmuir-Blodgett film deposition pressure of 25 mN/m was selected and so the stability of the monolayer was tested at this pressure. The decrease in surface area over a time period of an hour with the monolayer held at the deposition pressure was found to be negligible, demonstrating the suitability of the material for this film deposition technique.

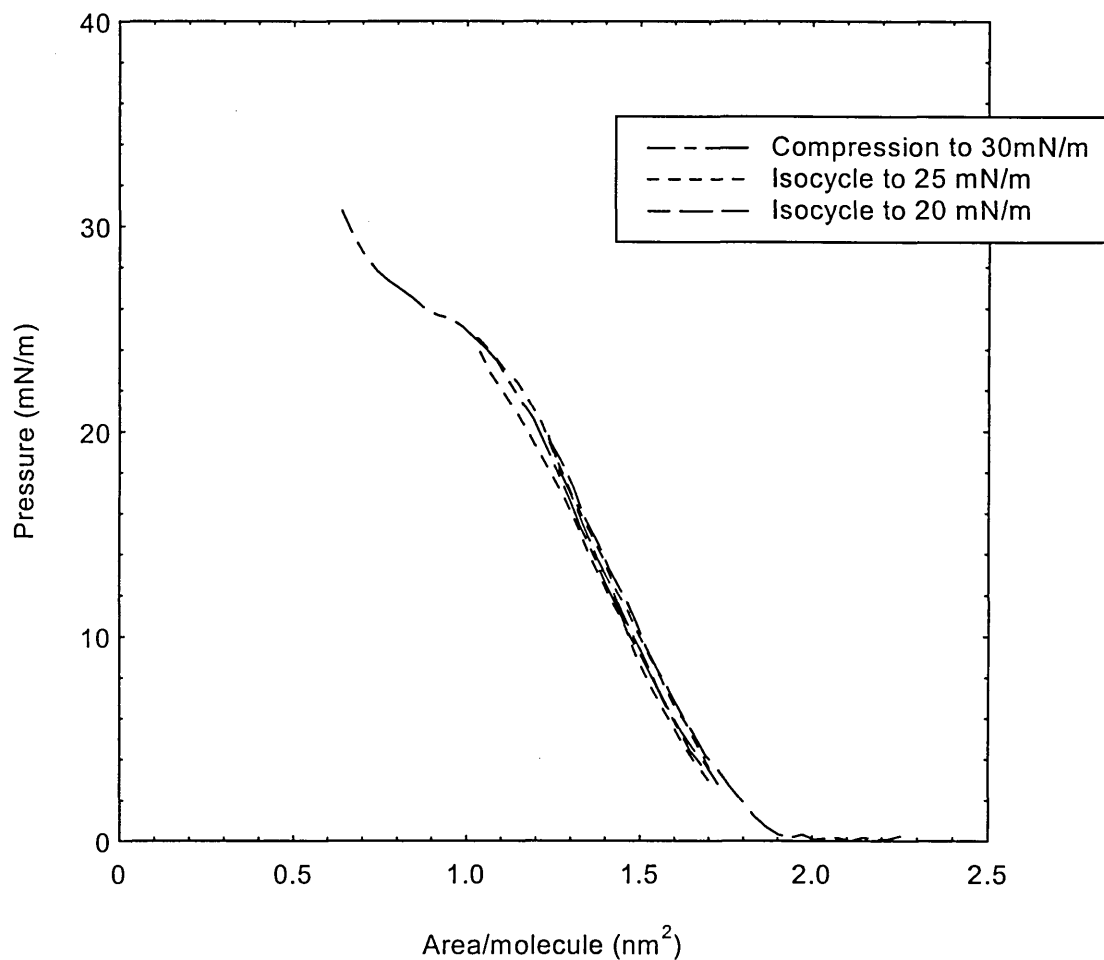


**Figure 4-7 Pressure-area isotherm of AmPc5 showing 2 isocycles and film collapse**

The isotherm obtained before annealing and the isotherm produced after isocycle repetition is shown in Figure 4-8. Extrapolation of the linear region of the isotherm produced after annealing to the x-axis gives a value of  $1.61 \text{ nm}^2$  for the area per molecule on the water subphase.

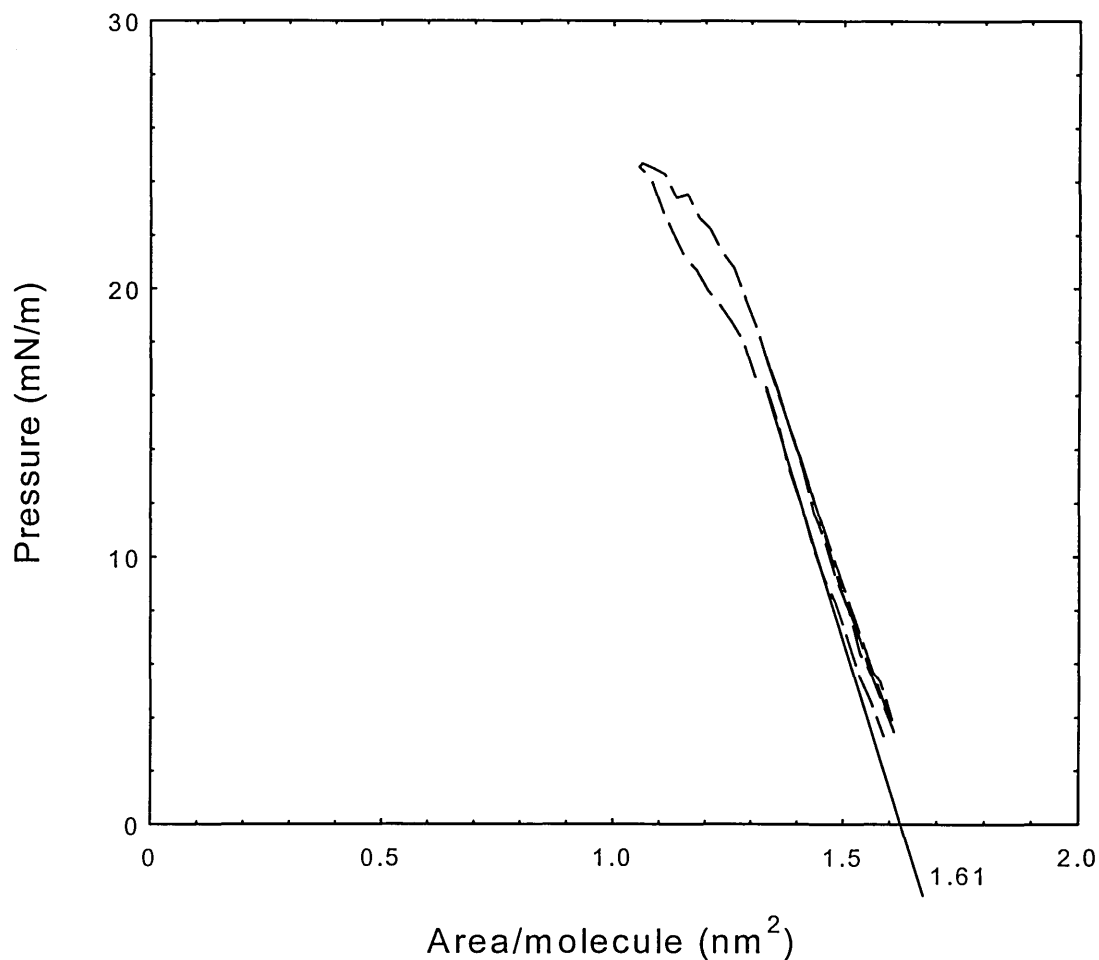


**Figure 4-8 Pressure area isotherm produced before and after annealing of the monolayer**

Study of the chemical structure of AmPc5 in Chapter 1 suggests that when the material is introduced onto the water surface the molecules orient themselves with the hydrophilic  $(\text{CH}_2)_4\text{OH}$  groups onto the subphase and the hydrocarbon groups  $\text{C}_5\text{H}_{11}$  pointing upwards away from the water surface. Figure 4-9 depicts a simple geometrical model for the AmPc5 molecule which is considered to be a rectangular box with the dimensions  $l_1$ ,  $l_2$ , and  $h$  occupying an area  $A$  on the water surface,

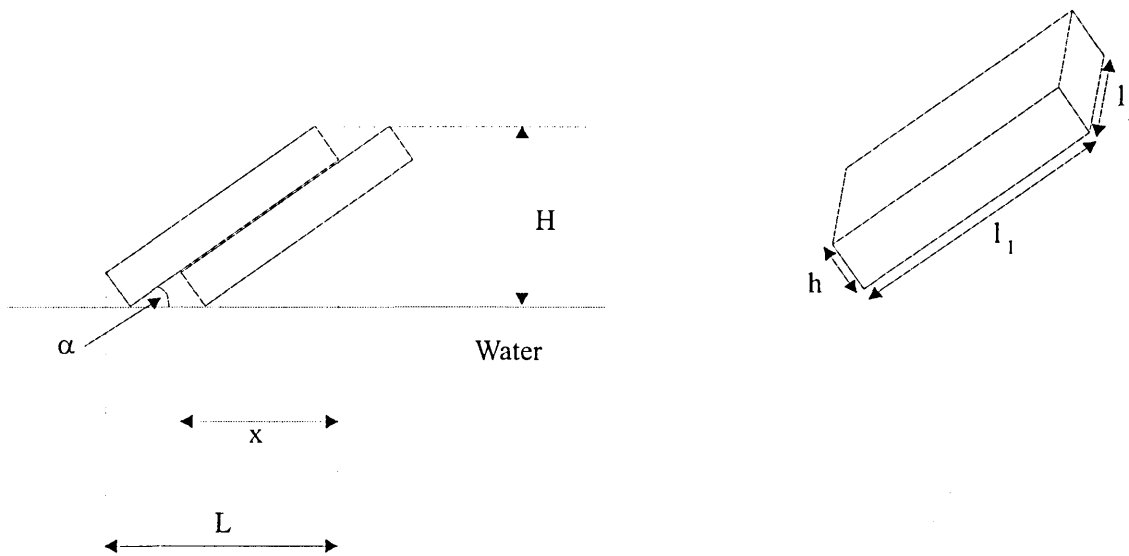


**Figure 4-9 Schematic of the AmPc5 molecular box model**

The molecular tilt angle on the surface of the water can be expressed as (Nabok et al 1998, Appendix IV),

$$\alpha = \sin^{-1}\left(\frac{l_2 h}{A}\right) \quad 4.2$$

and the monolayer thickness,  $H$  as,

$$H = l_1 \sin \alpha + h \cos \alpha \quad 4.3$$

The lengths of phthalocyanine molecules ( $l_1$ ) from the same family with differing chain lengths are given in (Cook et al 1994). These lengths correspond to the maximum length from the OH groups to the fully extended alkyl chains. The widths of the molecules ( $l_2$ ) corresponding to fully extended alkyl chains are given in (Poynter et al 1994). From this data the molecular dimension ( $l_1$  and  $l_2$ ) of AmPc5 can be assumed (Table 4-1) and  $A$ ,  $\alpha^\circ$  and  $H$  can be calculated using equations 4.2 and 4.3.

Material	$l_1$ (nm)	$l_2$ (nm)	$A$ (nm <sup>2</sup> )	$\alpha^\circ$	$H$ (nm)
C <sub>5</sub> H <sub>11</sub> (AmPc5)	2.25	2.5	1.61	44.33	1.89

**Table 4-1 Molecular dimensions of peripherally substituted phthalocyanine**

#### 4.2.3.2 AmAz1

After spreading between 50 and 100  $\mu$ l of solution an evaporation time of 5-10 minutes was allowed for AmAz1, as the concentration used was relatively high. The pressure-area isotherm produced is shown in Figure 4-10 with obvious hysteresis. The graph shows 3 isocycles with the first showing the largest hysteresis effect.

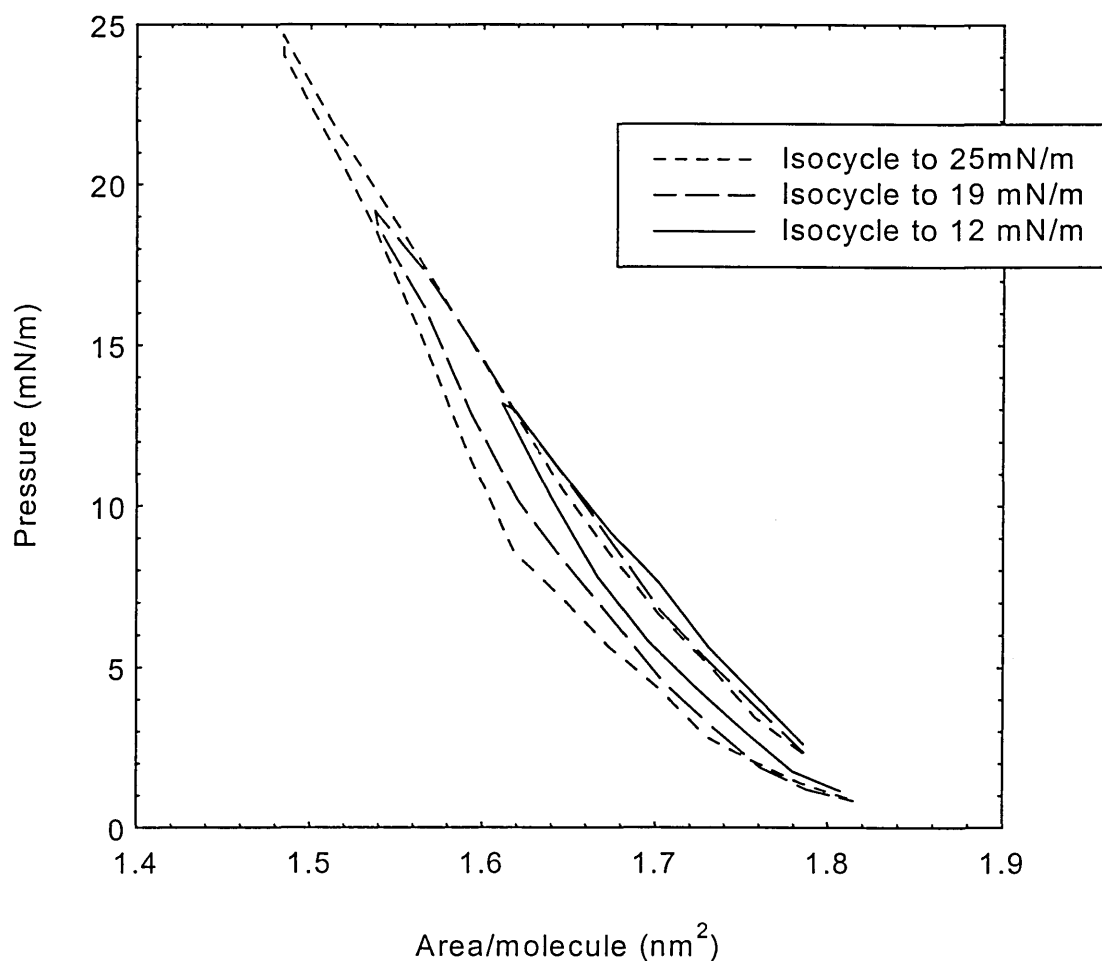


**Figure 4-10 Pressure-area isotherm of AmAz1 exhibiting hysteresis**

Upon monolayer training the hysteresis is reduced resulting in a reproducible isotherm. Figure 4-11 shows such an isotherm. The area per molecule was derived from the pressure-area isotherm by extrapolating the linear section of the graph to pressure = 0 mN/m, and a value of about 1.86 nm<sup>2</sup> was obtained. After study of the isotherm the film was found to collapse above 30 mN/m and hence a film deposition pressure of 25 mN/m was selected. The monolayer was held at the deposition pressure for a period of an hour with very little decrease in surface area observed. This indicates a stable monolayer.

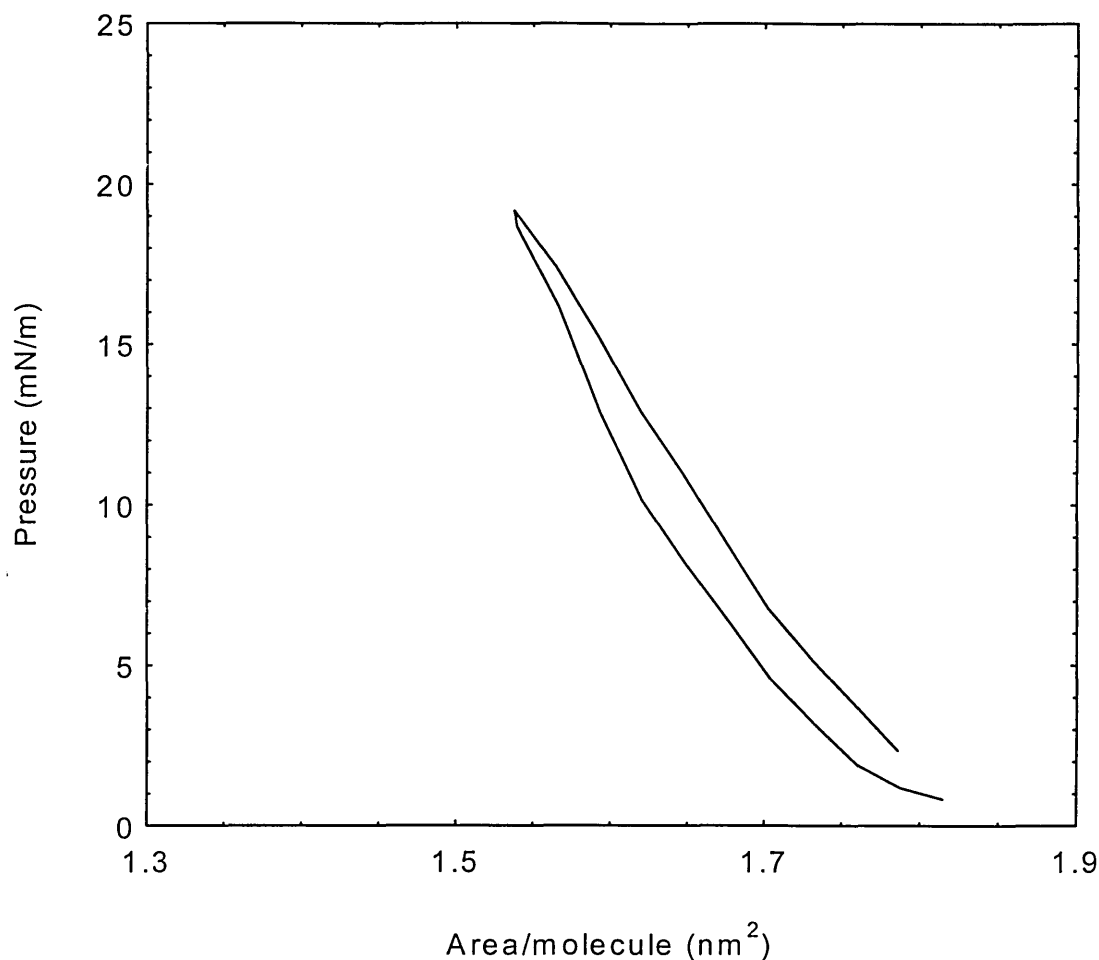


**Figure 4-11 Pressure-area isotherm of AmAz1**

Unlike phthalocyanines, the calixarenes cannot be assumed to occupy a rectangular box shaped area. Study of the 3-dimensional (CPK model) molecular structure of AmAz1 (Chapter 1) shows the familiar basket style shape of the calixarenes. For AmAz1 it is possible to say that the hydrocarbon chains ( $R_{11}H_{22}$ ) form the hydrophobic part of the molecule, whereas the polar azobenzene groups form the hydrophilic part of the molecule. Hence, the molecule lies on the water surface with azobenzene groups towards the water surface and the hydrocarbon groups pointing away. The area per molecule actually gives the area occupied by the four azobenzene groups. Due to the high symmetry of the AmAz1 molecule it is fair to assume that each molecule is positioned perpendicular to the water surface with all four azobenzene legs equally

spaced under conditions of zero surface pressure. As the barrier begins compression, one side of the molecule has a greater force exerted upon it than the other. This results in the azobenzene legs occupying unequal and non-uniform areas. As the monolayer is relaxed, the legs assume their original stable positions. This phenomenon is observed in the hysteresis effects in the pressure-area isotherm (Figure 4-10). The hysteresis effect may also be as a result of different types of two-dimensional packing during monolayer phase change. Upon training one would expect the azobenzene groups to become equally spaced under compression, and this is observed in the reduction of the hysteresis effect.

#### **4.2.4 Langmuir-Blodgett Film Deposition**

All film deposition took place at room temperature and with a water subphase with a pH of 5.5. The pH of the subphase was maintained during experiments by regular replacement of the water subphase. The deposition of the first layer is of the utmost importance as this predetermines the manner in which the subsequent layers are deposited. If the initial monolayer is deposited in a homogenous and uniform manner, then subsequent depositions are more likely to be successful.

The monolayer is compressed to the target pressure selected for the material in question before dipping commences. The substrate is placed in its holder and positioned for coating over the desired surface area. The speed of floating monolayer compression, film deposition and possible monolayer drying time are determined through experimentation for each material and substrate. The deposition is monitored by observing the pressure-area isotherm and transfer ratios. The pressure-area isotherm shows a gradual decrease in trough area at the deposition pressure. For deposition of thick films the material on the water surface is replenished as necessary.

Certain substrates cannot be treated hydrophobic in the usual manner and must be used in their natural form. Gold and silver coated glass substrates are intrinsically slightly hydrophilic and so the deposition parameters are determined individually.

#### **4.2.4.1 AmPc5 Molecules**

The first layer of phthalocyanine is deposited onto a hydrophobically treated glass substrate on the down stroke with the dipper travelling at 20 mm/min, with the Langmuir-Blodgett trough set in single layer mode. Deposition attempts made on hydrophilic substrates were found to be unsuccessful. The movement of the meniscus of the subphase with substrate movement provides an indication of the effectiveness of deposition. As the substrate passes down through the subphase and the first layer is deposited, the meniscus can be seen to curve downwards. The second layer is deposited on the up stroke, as the substrate is passed up through the water/air interface, forcing the meniscus to curve upwards. This procedure is repeated until the desired number of monolayers has been deposited. Deposition onto a hydrophilic substrate would result in movement of the meniscus in the opposite direction with immersion of the substrate in the subphase prior to film spreading. It was found that a drying after each bilayer deposition did not improve film homogeneity and thus was not included in succeeding sample preparation. It was found that transfer took place fairly consistently on both the up and down strokes, implying that standard Y-type deposition was taking place (Figure 4-4). Deposition onto gold substrates was found to take place effectively at 25 mN/m with 10 minutes drying time between each bilayer.

#### **4.2.4.2 AmAz1 Molecules**

As with deposition of AmPc5, AmAz1 was found to deposit effectively onto hydrophobically treated substrates only. The trough was used in single layer mode with

a dipping speed of 20 mm/min for glass substrates and 15 mm/min onto metallic substrates. The consistent transfer ratio implied Y-type deposition onto the substrates.

AmAz1 was deposited in combination with tricosenoic acid in alternating Langmuir-Blodgett layers. Tricosenoic acid was dissolved in chloroform to 0.5 mg/ml concentration and allowed 5 minutes evaporation time prior to compression. A target pressure of 30 mN/m was selected after study of the isotherm with deposition onto hydrophobic glass substrates. Tricosenoic acid was chosen as a spacer layer for AmAz1 due to its ease of deposition. The Langmuir-Blodgett films produced possess a non-centrosymmetric structure with the azobenzene chromophores acting in a single direction. These samples were prepared for second harmonic generation measurements. For both materials it was found that varying the substrates had an effect on the dipping parameters. It was found necessary to decrease the target pressure and dipping speed when depositing onto metallic substrates.

#### **4.2.5 Substrate Preparation**

The substrates used were varied according to the experimental requirements for each characterisation. The substrate cleanliness is a crucial factor when working at a molecular level and so in each case the surfaces were treated in as clean an environment as possible.

##### **4.2.5.1 Glass Substrates**

The glass substrates used were 0.8-1.0 mm thickness BDH microscope glass slides. All slides and flasks used to contain solutions were cleaned according to the procedure in Appendix III.

Once cleaned, the hydrophobic substrate was prepared by soaking the slide in a solution of dimethyldichlorosilane for about 30 minutes. This was found to render the substrate

suitably hydrophobic. The slide was then washed in a solution of tetrahydrofuran before washing in deionised water, as the water was found to react with the dimethyldichlorosilane solution producing an unsuitable surface layer.

The samples deposited onto glass slides, with varying thicknesses, were used for spectroscopic analysis and scanning electron microscope measurements. Glass substrates for alternate layer deposition were prepared in the same way.

#### **4.2.5.2 Gold Coated Glass Substrates**

The gold substrates were prepared under vacuum by evaporation of 99.9% pure gold onto glass slides. The glass slides were cleaned according to the above procedure and then treated with dimethyldichlorosilane solution to render them hydrophobic. The surface of glass is hydrophilic in nature and it was found that the gold layer did not adhere to the surface strongly. The gold coated onto hydrophobic glass was found to be much more durable. Once coated, the gold substrates are hydrophilic in nature. Although once removed from high vacuum the slides became less hydrophilic as the gold adsorbs hydrocarbons present in the air.

The evaporation procedure was conducted at a pressure of  $10^{-5}$  torr where the thickness of gold was monitored using an oscillating quartz crystal thickness measuring device. The gold substrates were used for surface plasmon resonance experiments where the optimum gold thickness for surface plasmon excitation was found to be around 400 Å. Hence this was the standard of thickness aimed for in all evaporation.

#### **4.2.5.3 Silver Coated Glass Substrates**

The silver substrates were prepared under high vacuum using the above defined method with 99.99% pure silver. Once prepared the samples were used as soon as possible as silver has a tendency to tarnish over time.

### 4.3 Recent Developments in the Langmuir-Blodgett Technique

The bulk properties of a Langmuir-Blodgett film and the resulting device fabrication are highly dependant on the ordering of molecules in a supermolecular structure. It is essential to control the alignment along the x, y and z directions to obtain maximum activity in devices, where x, y and z are defined in Figure 4-12. Control in the one-dimensional array, the two-dimensional plane and the three-dimensional network must be realised.

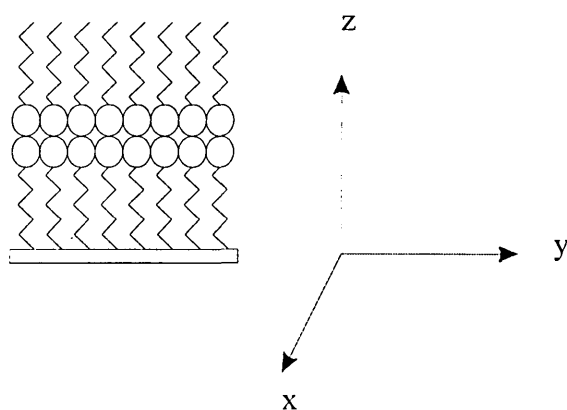


**Figure 4-12 X, y and z directions with respect to film deposition direction**

Organisation along the z-axis is easily attained by the type of deposition involved, whether it be Z, X, Y-type or alternate layer structures. Rigid molecules such as the phthalocyanines and more recently polycyclic aromatic quinones (Eckhardt et al 1994) induce order in the floating monolayers and subsequently in Langmuir-Blodgett films. The main drawback of these materials is that they can be more difficult to transfer onto substrates than classical aliphatic compounds and even fracture on transfer.

In-plane organisation along one direction whether that be along the x-axis or y-axis is outside the direct capabilities of the Langmuir-Blodgett technique, but can be achieved by molecular manipulation or equipment modification prior to deposition. Molecular

alignment in the Langmuir film in a given direction can be provided by using an oriented support. Oriented PTFE can be used to orient polymers or liquid crystals (Pichler et al 1993, Araya et al 1986), but with limited results.

Experiments have been performed by (Schwiegk et al 1992) on the orientation of several rigid rod polymers. The polymers have been engineered to contain aliphatic chains to provide solubility and the rigid rods consist of two or more monomers. The rods float on the water subphase with no definite arrangement but when transferred onto solid substrates orientate themselves along the dipping direction. The orientation is forced by hydrodynamic forces due to the flow conditions between the film and the substrate. The molecularly defined rods give the film its solid form whilst the aliphatic chains create a liquid-like state. As a result the films behave as a solid with regards to their mechanical properties and liquid with regards to the optical properties.

Order in the shape of columns can be encouraged by the use of symmetrical molecules such as phthalocyanines (Ruaudel-Tiexier 1996) and penta-alkynylbenzene (Janietz et al 1994) with chemically attached side substituents.

Two-dimensional order where molecules are oriented in-plane along x and y can now be achieved using a number of strategies. When the head and tail of an amphiphilic molecule have the same cross-sectional area, compression of the Langmuir layer produces a close packed arrangement. With complex compounds this ordering is not obvious and the molecules are gathered in the plane with no long range order. Domains are usually present in the Langmuir and Langmuir-Blodgett films which restricts physical properties such as electronic and magnetic effects. One method used to overcome this effect was described as a 'paving stone strategy' (Lefevre et al 1993). Molecules such as porphins or porphyrazines are designed to lie flat on the water surface and are able to couple in two mutually perpendicular directions by a solid state reaction. Another approach used streptavidin and biotin (Ahlers et al 1989). Streptavidin

is dissolved in the subphase beneath a Langmuir film of biotin-derived lipid where each streptavidin molecule attaches itself to the lipid forming the two-dimensional array.

Three-dimensional networks can be formed by control of the chemistry and location of all the molecules involved. If the molecules in one monolayer are functionalised at one end so that they interlock with the layer above via a chemical reaction, many applications can be found. One such application is explained in the Introduction (Chapter 1).

The ability to tailor position and interlocking of molecules allows the development of designed arrays for active biological and electrical mechanisms.

A comparative study of stearic acid and manganese stearate films obtained by Langmuir-Blodgett and vacuum deposition methods has been performed (Baran et al 1995). The IR spectra for both forms of stearic acid were found to correspond to a monoclinic crystalline structure. The band of the C=O stretching vibration in a Langmuir-Blodgett film of one monolayer is weaker and broader than in vacuum deposited film where the effect is attributed to the interaction of the polar C=O with Si-OH and Si-O groups on the silicon substrate. Similarly, the CH<sub>2</sub> bands are broadened in Langmuir-Blodgett films which is a result of rotational restriction of the methylene chains.

Vacuum deposited manganese stearate was found to decompose on heating producing disordered stearone (C<sub>17</sub>H<sub>35</sub>)<sub>2</sub>CO on the substrate, with an increase of order with increasing thickness. The stearone molecule was shown to exhibit a difference in orientation with respect to substrate. In thin Langmuir-Blodgett films the C=O band is broadened as in the case of stearic acid. The CH<sub>2</sub> bands exhibit narrowing as the films grow thicker up to about 30 monolayers which indicates a gradual freezing of the molecular rotational motion. These bands are still broader than in vacuum deposited films which points towards a greater ordering in vacuum deposited films than in similar

Langmuir-Blodgett films. Scanning electron microscope studies show that whilst the vacuum deposited films of both materials have a higher level of ordering, this is at the cost of morphology and homogeneity as compared to Langmuir-Blodgett films.

## Chapter 5      Optical and Structural Characterisation

The optical and spectroscopic measurements performed on AmPc5 and AmAz1 are presented in this chapter along with the structural characterisation of alternate layers of AmAz1. The techniques used for observing films and molecular behaviour in solution have enabled optical characterisation of the materials in solid monolayer, floating monolayer and monomer form.

### 5.1 Spectroscopic Measurements

The molecular processes associated with each region of the electromagnetic spectrum are very different and depend on the associated energy change, as detailed below in Table 5-1 (Halliday 1988);

Radiation Type	N.M.R	E.S.R	Microwave	Infra-red	Visible and U-V	X-ray	$\gamma$ -ray
Wavelength range	10m	100cm	1cm	100 $\mu$ m	1 $\mu$ m	10nm	100pm
Change of molecular process	spin	spin	orientation	configuration	electron distribution	electron distribution	nuclear configuration

**Table 5-1 Electronic processes in the electromagnetic spectrum**

The lower energy processes of microwave and infra-red display rotational and vibrational changes of the molecules, respectively. The ultra-violet and visible region of the spectrum is associated with a change in the distribution of electrons. This change arises from the excitation of a valence electron by an incident photon from a lower to higher energy level. The wavelength of the absorption is a measure of the separation of the energy levels of the orbitals concerned. The probability that a transition will take

place is dependant upon the area and shape of the chromophore, as well as the proximity to other chromophores. The greater the surface area of the chromophore the more likely absorption is to take place which corresponds to a greater absorption intensity. The shape of the chromophore will be determined by the molecular structure and resulting electronic configuration.

For example, if we consider the case of ethylene (Figure 5.1) the s and p orbitals of each of the carbon atoms can form three  $sp^2$  orbitals. This is possible as the ground state electronic configuration of carbon is  $1s^2 2s^2 2p^2$  and the single 2s orbital and three 2p orbitals combine to form planar trigonal orbitals (Pope 1982). The bonds formed from these orbitals to the hydrogen atoms and other carbon atom are known as  $\sigma$ -bonds. An isolated ethylene molecule forms an unconjugated  $\pi$ -bond between the carbon atoms as shown in Figure 5-1.

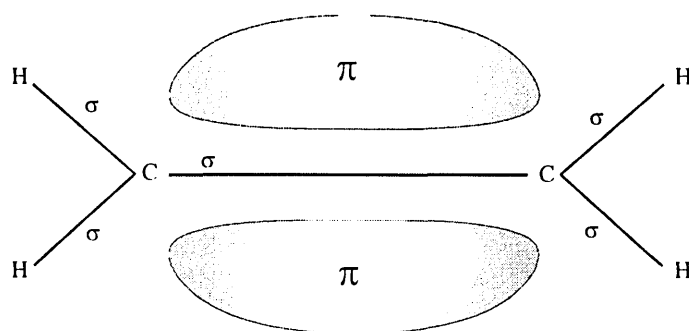


**Figure 5-1 Unconjugated  $\pi$ -bond between carbon atoms of an isolated ethylene molecule**

Most of the unconjugated chromophores give rise to high energy and hence low wavelength absorption, as shown in Table 5-2 (Williams 1966).

Chromophore	Transition	$\lambda_{\max}$ ( $\mu\text{m}$ )
$\sigma$ -bonded C—C and C—H	$\sigma \rightarrow \sigma^*$	~ 150
Lone pair electrons —O—	$n \rightarrow \sigma^*$	~ 185
—N<	$n \rightarrow \sigma^*$	~ 195
—S—	$n \rightarrow \sigma^*$	~ 195
>C=O	$n \rightarrow \pi^*$	~ 300
>C=O	$n \rightarrow \sigma^*$	~ 190
$\pi$ -bonded >C=C< (isolated)	$\pi \rightarrow \pi^*$	~ 190

**Table 5-2 Table showing the electronic processes and wavelengths associated with each chromophore**

When the molecular orbitals of two isolated double bonds are brought close together they will eventually overlap and become conjugated. Historically such bonds are denoted by alternating single and double bonds, although physically the electrons are delocalised over the molecule in a  $\pi$ -cloud. The energy level of the highest occupied orbital is raised and that of the lowest unoccupied orbital is lowered, as shown in Figure 5-2.

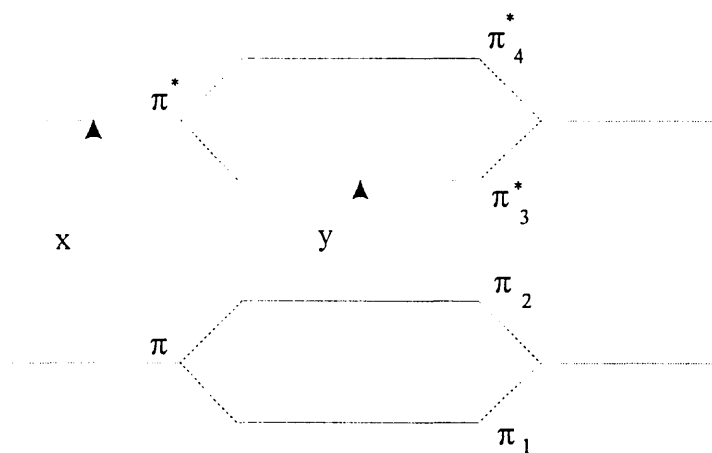


**Figure 5-2 Energy level separation in a  $\pi$ -conjugated system**

The transition x corresponds to the  $\pi \rightarrow \pi^*$  transition in an isolated carbon double bond, whereas the transition y,  $\pi_2 \rightarrow \pi_3^*$  represents absorption in a conjugated double bond. Hence, conjugation results in a reduction of energy level separation. When considering longer conjugated systems the separation of energy levels is further reduced with increasing chromophore area.

For this work it is essential to study the electron distribution surrounding the benzene ring (Figure 5-3) (Pope 1982). The  $\pi$ -bond in this case establishes a delocalised electron cloud above and below the plane of carbon atoms with no electron distribution in the centre of the ring. This electronic distribution gives the benzene ring an enhanced stability. Molecules with large numbers of conjugated systems will result in very low energy separations between  $\pi \rightarrow \pi^*$  and absorption occurring in the visible part of the spectrum.

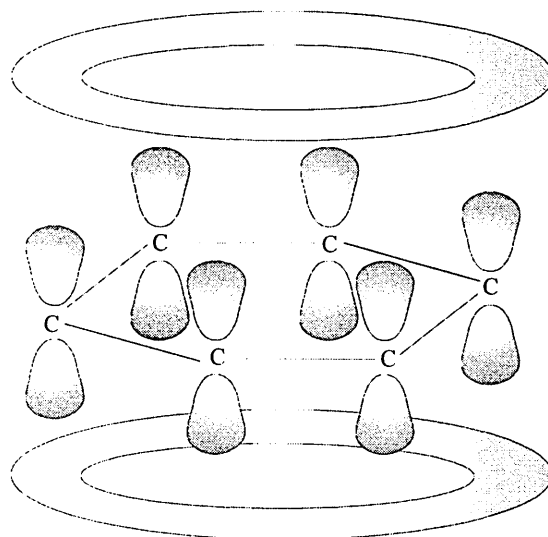


**Figure 5-3 Electron distribution surrounding the benzene ring**

### 5.1.1 Absorption Spectra

When light is incident upon a surface it can be transmitted, absorbed or reflected with all three processes equalling unity according to the law of conservation of energy. The transmission of light ( $I$ ) through a substance is governed by Beer's Law (Williams 1966),

$$I = I_0 \exp(-\alpha d) \quad 5.1$$

where  $I_0$  is the incident light intensity,  $\alpha$  is the absorption coefficient and  $d$  is the film or cell thickness. The transmittance ( $T$ ) of the film ( $I/I_0$ ) is measured using a double beam Unicam UV\VIS spectrometer, and so the absorption coefficient  $\alpha$  can be expressed as,

$$\alpha = -\frac{\ln T}{d} = \log_{10} \frac{A}{d} \quad 5.2$$

where  $A$  is the absorbance of the film expressed as  $\log_{10}$ .

#### 5.1.1.1 AmPc5 Absorption Spectra Analysis

The absorbance of 58 Langmuir-Blodgett monolayers of AmPc5 transposed on the monomer solution spectra for comparison is shown in Figure 5-4.

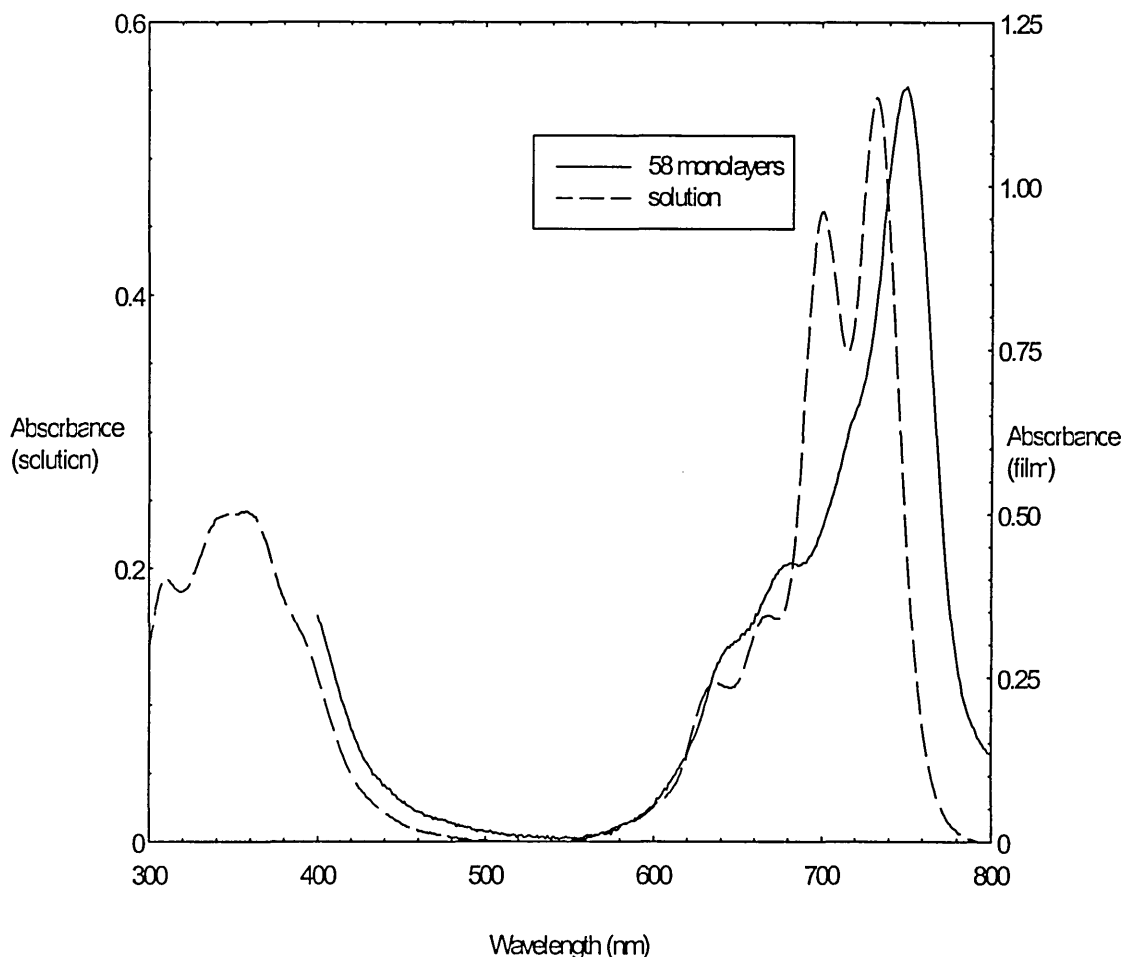


**Figure 5-4 Absorption spectra of AmPc5 in 58 monolayers Langmuir-Blodgett films and in solution of 0.1mg/ml TCE**

The absorbance minimum between 500-546 nm is characteristic of the phthalocyanines and accounts for the blue-green colour of AmPc5. Inspection of the solution spectra at lower wavelengths reveals an absorbance maximum at 350 nm with a shoulder at 308 nm. These peaks can be attributed to the B band which is normally more intense in the ultra-violet region of the spectra (Cook 1993). Study of the solution spectra in the visible region reveals two absorption peaks at 700 nm 733 nm, with the latter being of greater intensity than the former. These lower energy absorption occur in the red region of the spectrum and are referred to as the Q absorption band. Both the B and Q bands in the solution spectra are split. This phenomenon can be explained by comparison of the

metal-free phthalocyanine, AmPc5, to that of a metallated phthalocyanine, MPc (Gu et al 1995). The Q and B bands arising from MPc solution spectra appear as a single absorption with the band wavelength exhibiting sensitivity to the central metal atom. These differences in absorption arise from the differing molecular symmetries.

Metal free phthalocyanines have a lower order of symmetry than metallated phthalocyanines. The band splitting is more apparent in the Q band than the B band mainly because the Q band is well separated from other bands. Conventionally, the lower energy peak (red-shifted) is referred to as the  $Q_x$  peak and the higher energy peak (blue-shifted) as  $Q_y$ . The lower intensity bands observed to the left of the Q band are vibronic in nature (Cook 1993).

Absorption in the Q band arises from  $\pi \rightarrow \pi^*$  transition with the molecular orbital symmetries differing according to the symmetry of the molecule itself. Metallated phthalocyanines possessing the  $D_{4h}$  structure have the LUMO (lowest unoccupied molecular orbital) levels with symmetry  $e_g$  and HOMO (highest occupied molecular orbital) with symmetry  $a_{1u}$ . For a metal free phthalocyanine the lower symmetry  $D_{2h}$  leads to a more complex set of orbitals. The HOMO is of the same symmetry as a metallated phthalocyanine whereas the two LUMO's are of  $b_{2g}$  and  $b_{3g}$  symmetry, which correspond with the  $Q_x$  and  $Q_y$  components, respectively. Hence the transition for a metallated phthalocyanine is  $a_{1u} \rightarrow e_g$  and for a metal free phthalocyanine are  $a_u \rightarrow b_{2g}$  and  $a_u \rightarrow b_{3g}$  as shown in Figure 5-5.

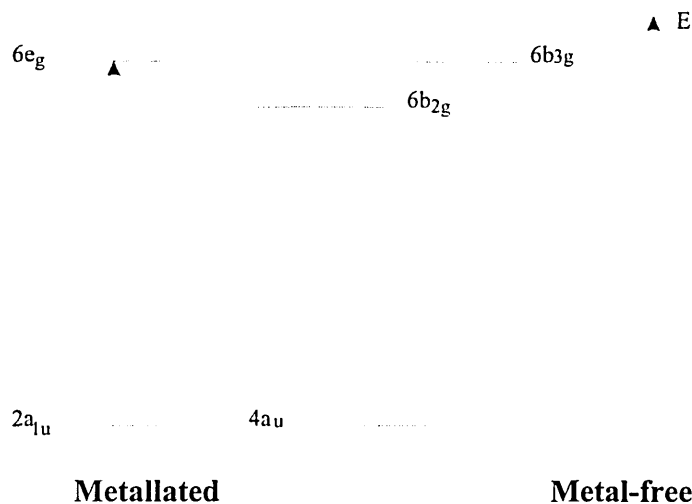


**Figure 5-5 Energy levels for metallated and metal-free phthalocyanines**

Similarly the B band absorption can also be regarded as a  $\pi \rightarrow \pi^*$  transition from  $a_{2u} \rightarrow e_g$  for metallated phthalocyanines and  $7b_{1u} \rightarrow 6b_{2g}$  and  $7b_{1u} \rightarrow 6b_{3g}$  for metal free phthalocyanines (Orti et al 1990). These absorption are not as clearly visible as in the Q band as they are buried in the absorption produced by transitions of comparable energy and the resulting broadening.

Study of the absorption spectra of AmPc5 in Langmuir-Blodgett films reveals a change in the spectral shape. When compared with solution spectra a visual inspection suggests that the  $Q_x$  peak is broadened and shifted further towards the red, whereas the  $Q_y$  peak has either dramatically reduced in intensity or disappeared altogether. In order to gain an understanding of this spectral change it is necessary to compare the spectra produced by phthalocyanines from the same family. The metal free, non-peripheral, octa-substituted phthalocyanines synthesised at the University of East Anglia (Poynter et al, 94 and Hibberd, 96) follow a similar spectroscopic pattern. The  $Q_x$  and  $Q_y$  bands produced by the monomer in solution are individually split into two bands which appear to the red and blue of the original peak. This behaviour can be explained by study of the planar molecular order ie. the order within each monolayer. Assuming the phthalocyanine rings

deposit almost perpendicular to the substrate, a suggested plan view of the sample is shown in Figure 5-6.

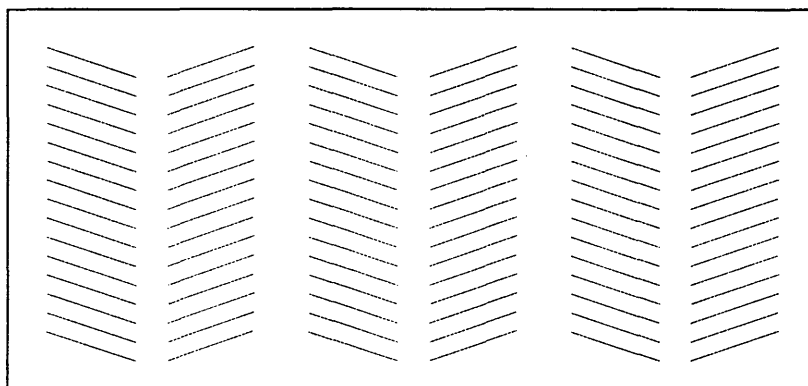


**Figure 5-6 Molecular plan view of the phthalocyanine herring-bone array**

This type of molecular pattern is commonly known as a ‘herring-bone array’ (Poynter et al 1994) and the direction of wavelength shift can be predicted using Kasha’s dimer model (Kasha 1976). In the model a dimer consists of 2 molecules that have been brought close together but are not actually chemically bonded and hence are referred to as physical dimers. The presence of the dimer causes a splitting of the monomer energy level accompanied by an energy shift relative to the monomer as shown in Figure 5-7.

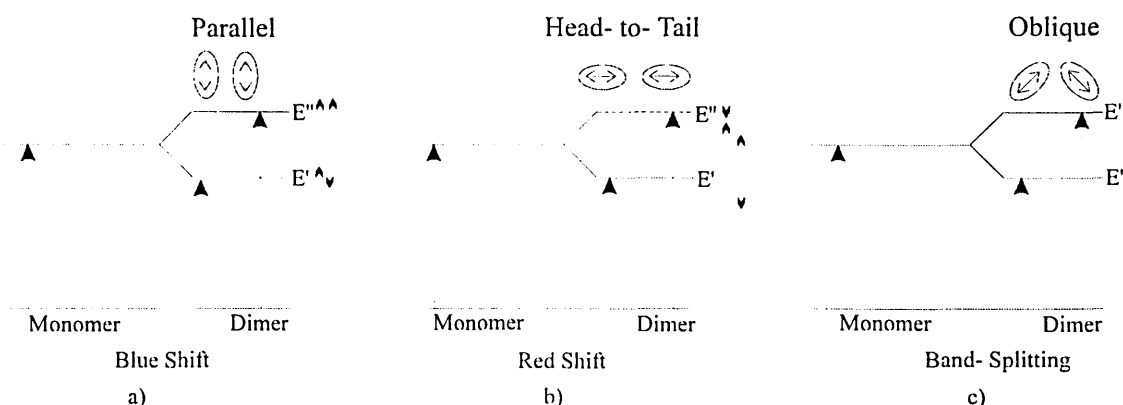


**Figure 5-7 Differences in energy level separations of phthalocyanine physical dimers**

From the herring-bone structure in Figure 5-6 it can be seen that the translationally non-equivalent planar molecular geometry resembles that of case (c) in Figure 5-7, resulting in a splitting of the band with shifts to the red and blue.

The shorter carbon chain length of AmPc5 ( $C_5$ ) compared to that of previous molecules ( $C_6$ ,  $C_8$ ,  $C_{10}$ ) results in a structure that is not of the herring-bone form, but with greater resemblance to a stack-like structure (Figure 5-8).

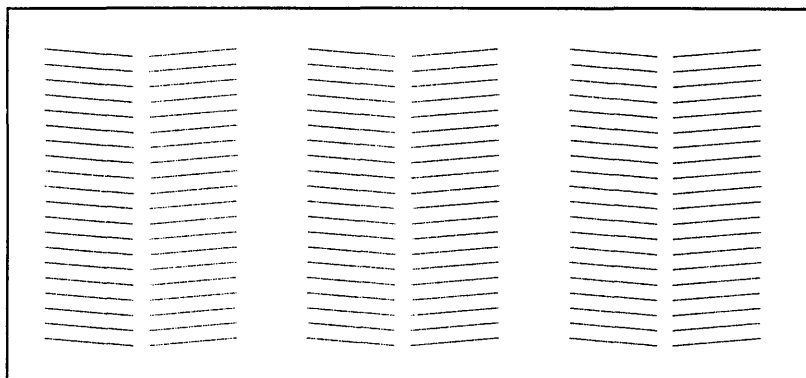


**Figure 5-8 Stack like structure for shorter carbon chains phthalocyanines**

This type of packing can be compared to case (b) in Figure 5-7 with some contribution from case (c). It is experimentally observed in Figure 5-4 that the splitting of the  $Q_y$  band is suppressed which can be explained by forbidden transition dipole in case (b) of Figure 5-7.

Application of the Davydov theory to AmPc5 involving decomposition of the Q band into the Gaussian/Lorentzian components was undertaken using the following equation (Ray et al 1998, see Appendix V);

$$\tan^2\left(\frac{\alpha}{2}\right) = \frac{A_1 + A_4}{A_2 + A_3} \quad 5.3$$

where  $A_1$ -  $A_4$  are the integral intensities of the respective bands.  $A_1$  and  $A_2$  correspond to the blue and red shifted peaks of  $Q_x$ , respectively and  $A_4$  and  $A_3$  correspond to the blue and red shifted peaks of  $Q_y$ , respectively.

The value of angle  $\alpha$  ( $55.4^\circ$ ) calculated for AmPc5 using the above equation is found to be inconsistent with other values of  $\alpha$  and contradictory to the assumed molecular order. This is due to the predominance of the stack-like structure as opposed to the herring-bone structure. It is therefore suggested that it is not possible to quantitatively apply the Davydov splitting theory for such shorter carbon chain phthalocyanines.

The absorption spectra for different thicknesses of AmPc5 Langmuir-Blodgett films are found to follow the same pattern ( Figure 5-9 ) and hence the absorbance at 740 nm is found to increase linearly with monolayer thickness ( Figure 5-10).

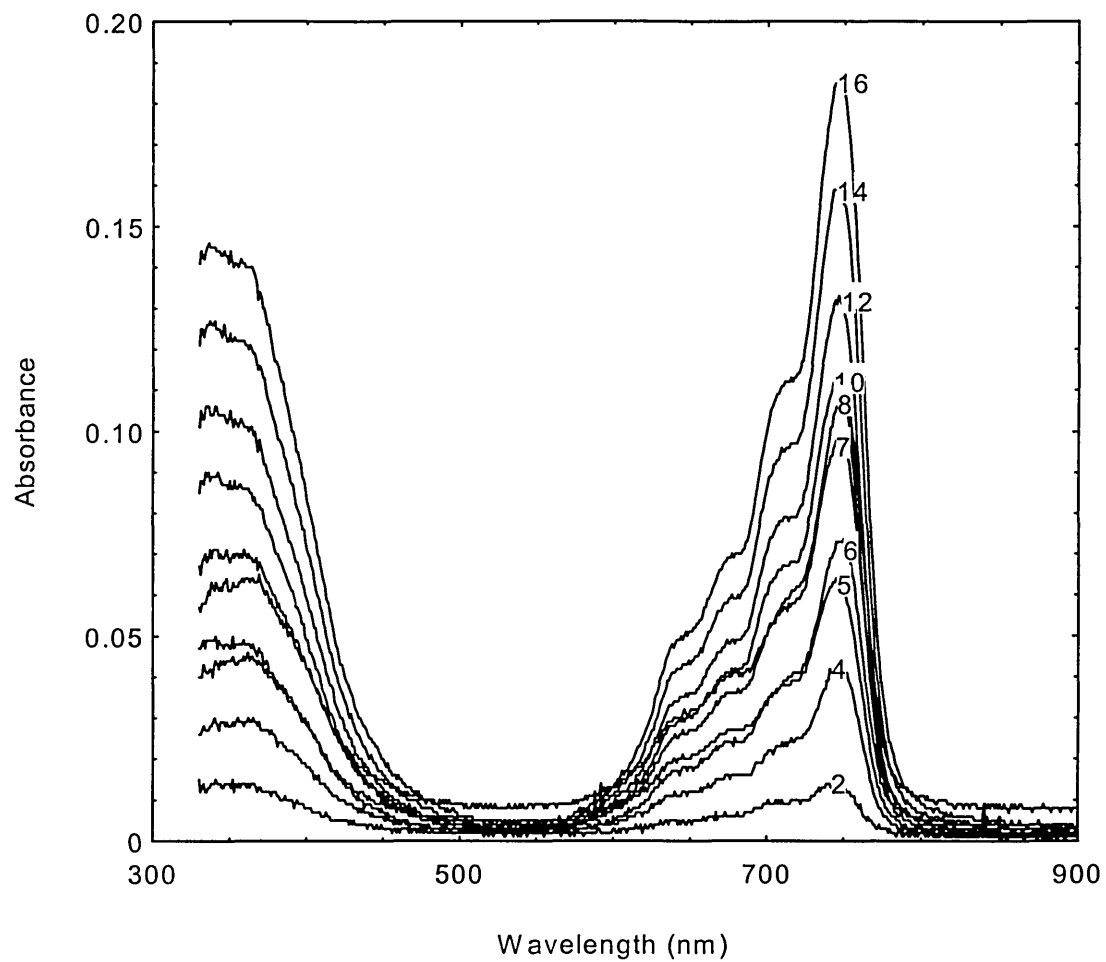


**Figure 5-9 Absorbance spectra of increasing numbers of Langmuir-Blodgett films of AmPc5**

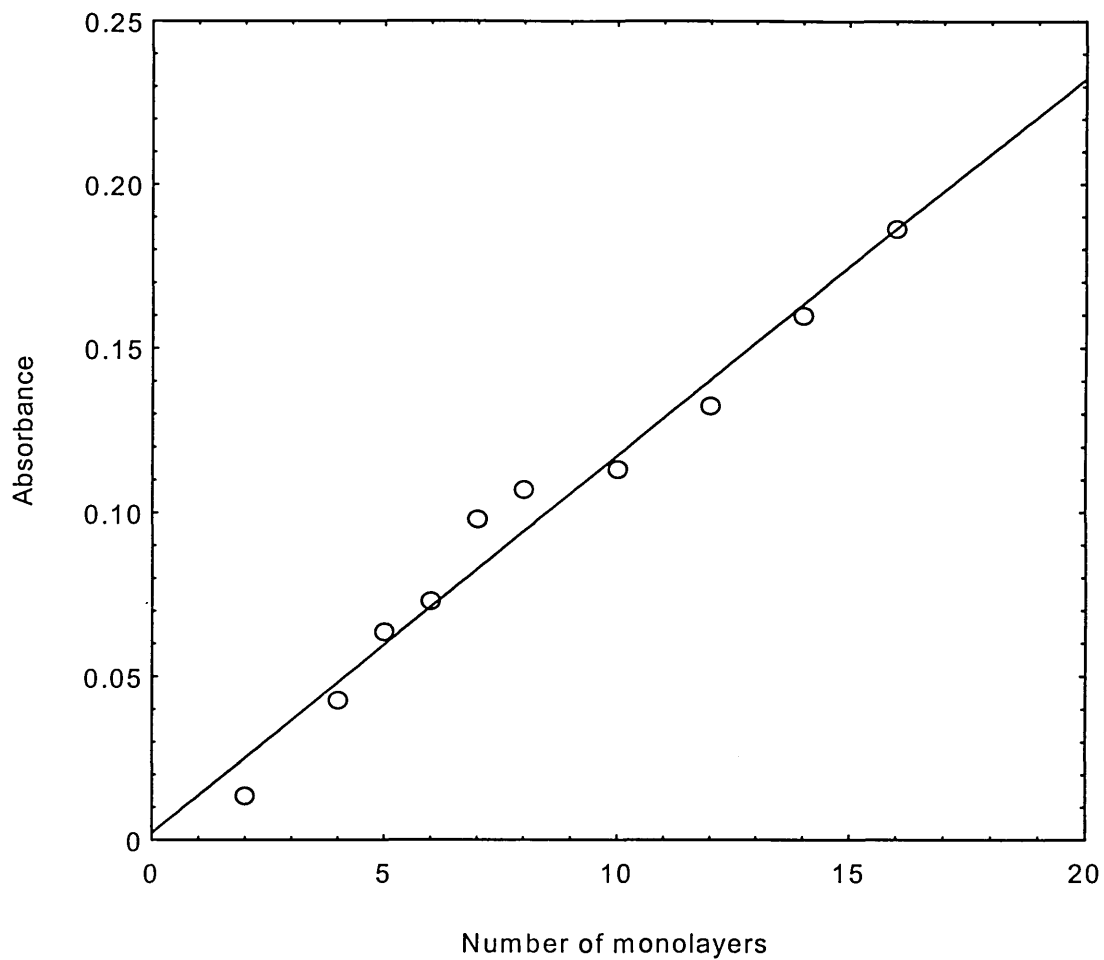


**Figure 5-10 Graph showing relationship between absorbance and increase in number of monolayers at  $\lambda_{\max}$**

The absorption coefficient for the AmPc5 films is calculated using equation 5.2, yielding the results shown in Figure 5-11. Clearly the wavelength dependence of the absorption coefficient mimics the absorbance spectrum.

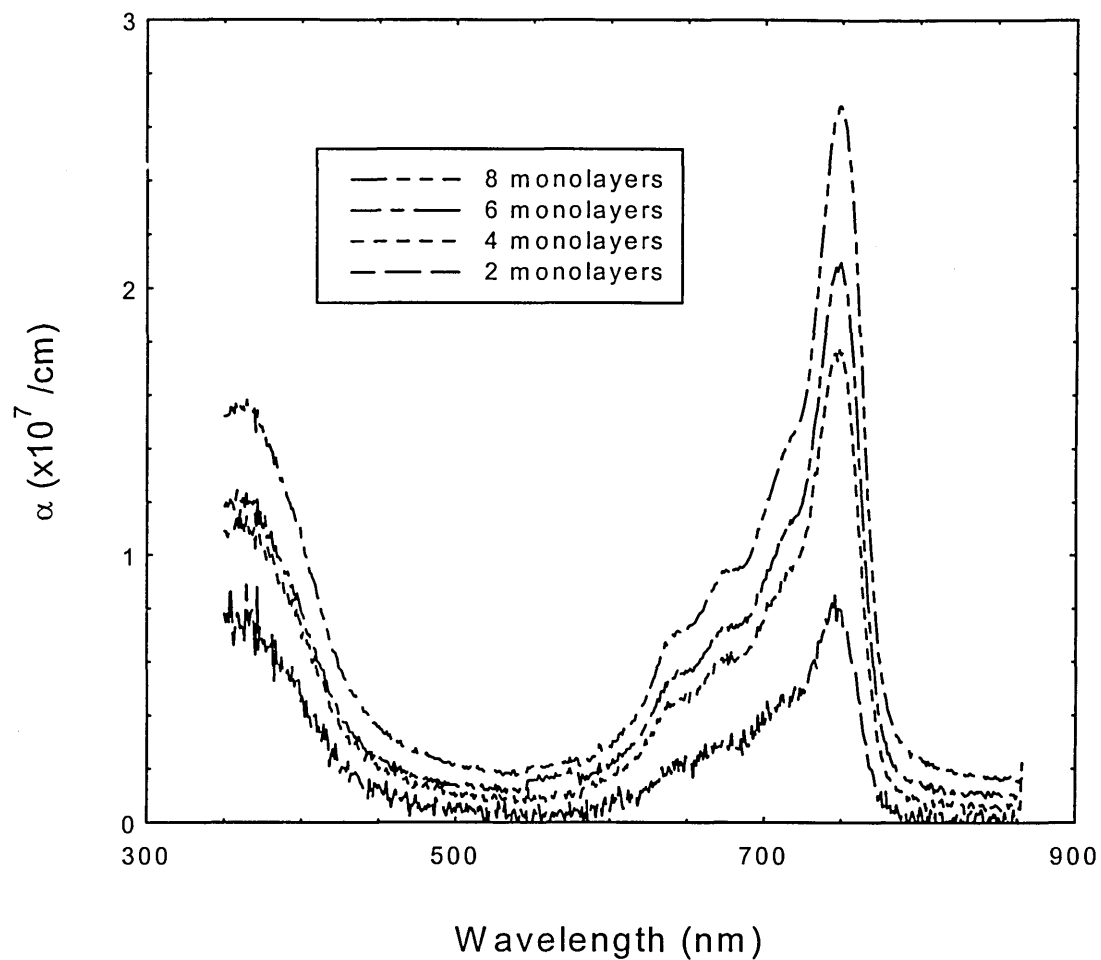


**Figure 5-11 Wavelength dependence of the absorption coefficient of differing monolayers of AmPc5**

The absorbance spectra of floating layers of pure AmPc5 measured at different surface pressures are given in Figure 5-12. The spectra appear noisy as a result of the liquid subphase movement.

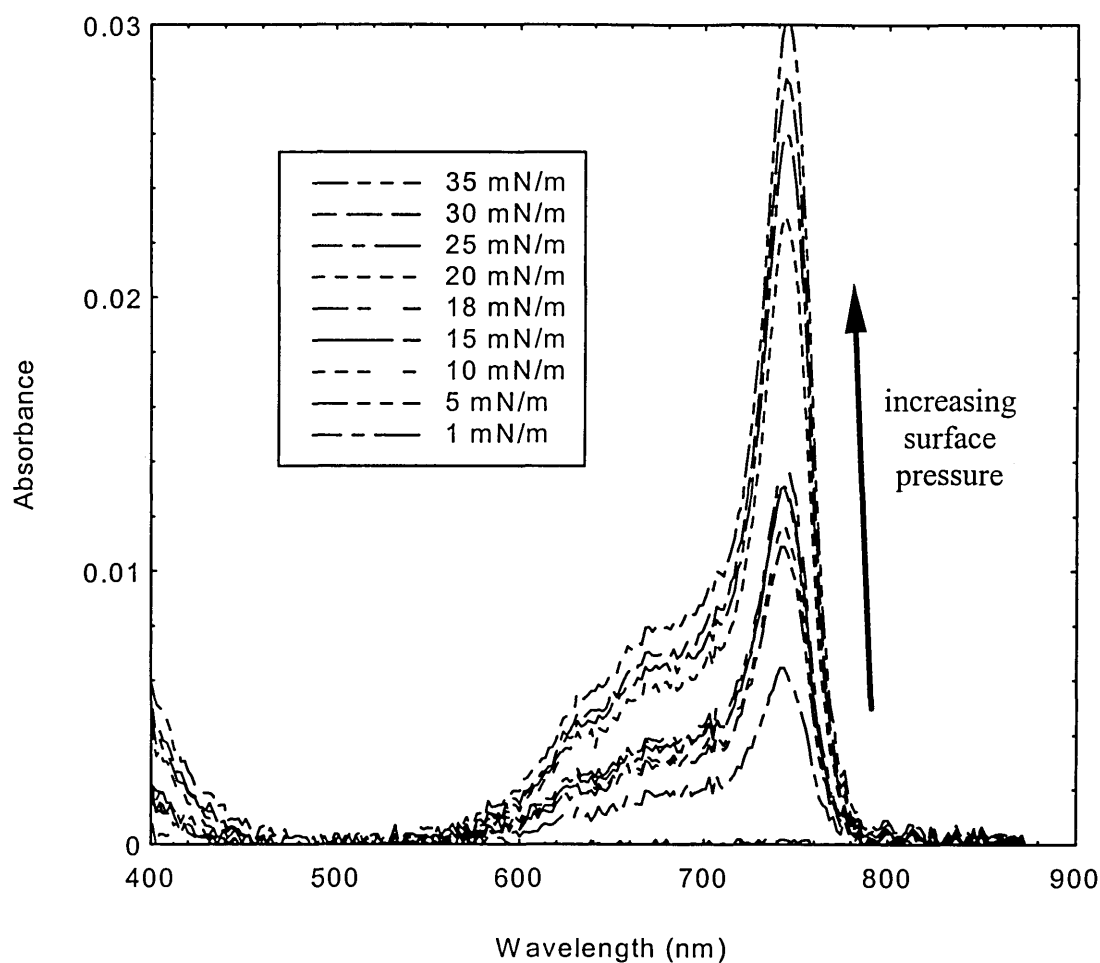


**Figure 5-12 Floating monolayer absorbance spectra for AmPc5 at various surface pressures**

The spectra of the monolayer taken at low pressures are of particular interest as they should display the properties of the floating layer in its two-dimensional gas and liquid phase. Study of the spectrum taken at 1mN/m, where the monolayer is expected to be in the gas phase, reveals a pattern attributable to the solid phase of the phthalocyanine. A similar pattern is observed for the spectrum measured at 10mN/m, corresponding to the two-dimensional liquid phase. These spectra imply that the phthalocyanine does not assume the monomer state at any stage of compression as a floating layer and that the solid phase is formed very soon after the spread of solution. This behaviour is characteristic of rigid molecules that induce order as the floating monolayer. This can make transfer onto substrates more difficult than with classical aliphatic molecules as the transfer itself can induce fracture. The absorbance intensity at the peak wavelength

is shown to increase with increasing surface pressure. This indicates more tightly packed molecules under monolayer compression.

### 5.1.1.2 Azobenzene Absorption Analysis

The absorption spectra of 72 monolayers of AmAz1 in Langmuir-Blodgett films and the spectra of 0.5mg/ml of AmAz1 dissolved in chloroform are shown in Figure 5-13.

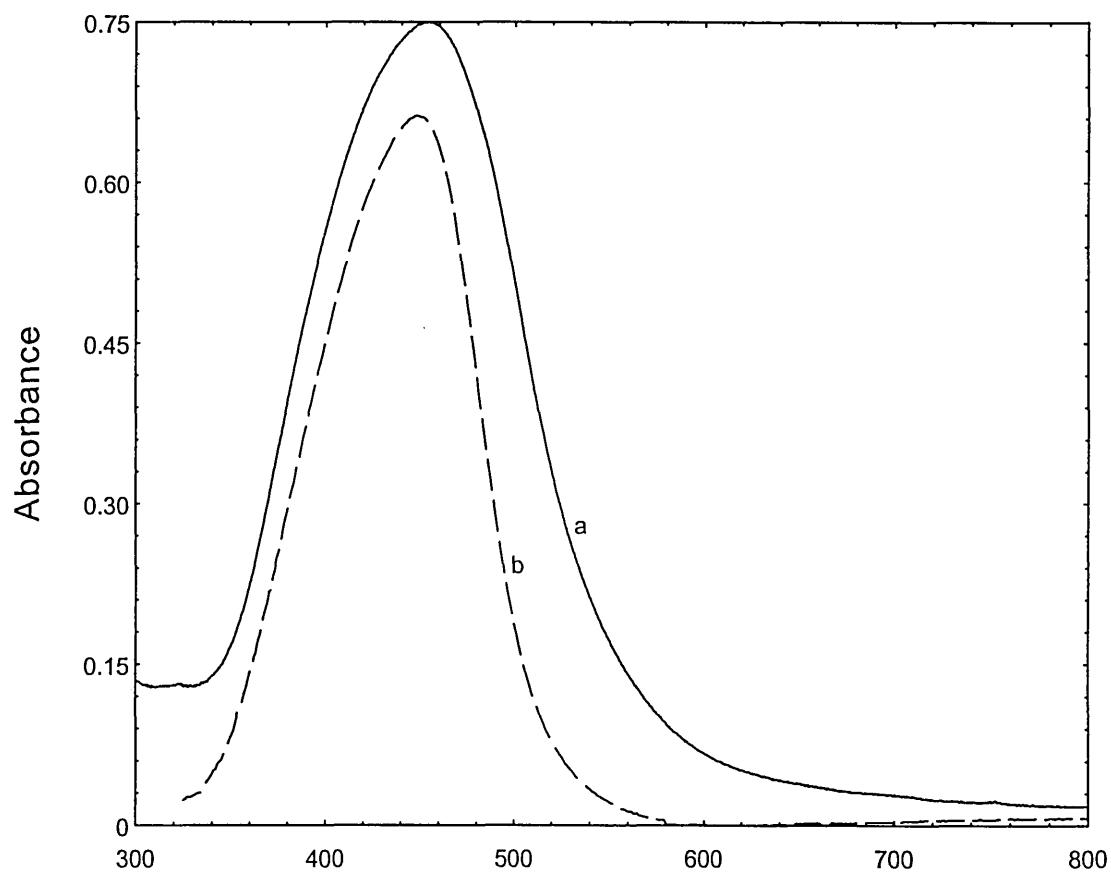


**Figure 5-13 Absorbance spectra of 78 monolayers of AmAz1 in Langmuir-Blodgett films (a) and in 0.5 mg/ml of chloroform (b)**

In comparison to AmPc5, this is a relatively featureless absorbance spectrum with a single, broad peak observed at 454 nm. The calixarene basket of the molecule is

transparent in the visible region of the spectrum (Gutsche 1989), so the absorbance peak for AmAz1 is due to electronic transitions in the azo part of the molecule. The conjugated system in this part of the molecule gives rise to  $\pi \rightarrow \pi^*$  transitions (Labarthe et al 1996).

The material is found to deposit uniformly with increasing thickness ( Figure 5-14 ) as indicated by Figure 5-15.

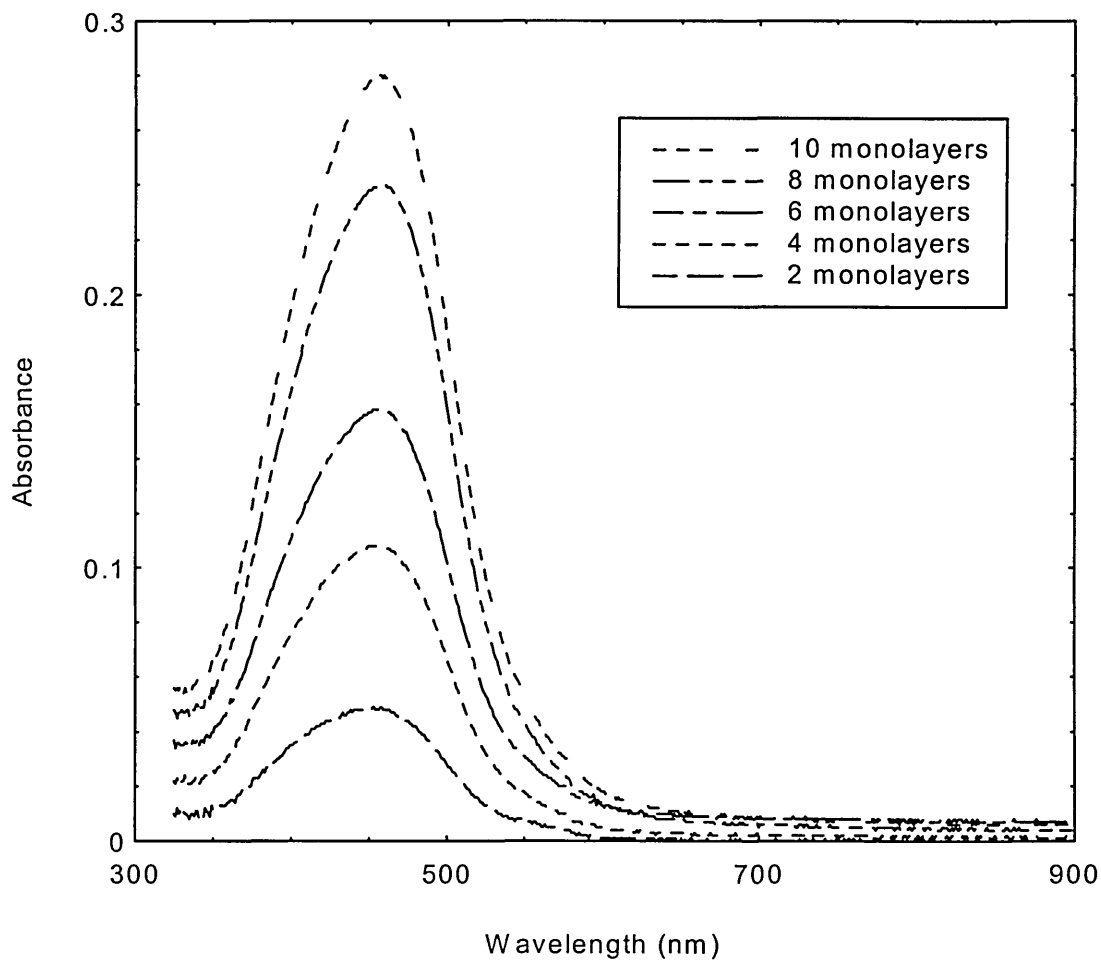


**Figure 5-14 Absorbance spectra of increasing numbers of monolayers of AmAz1**

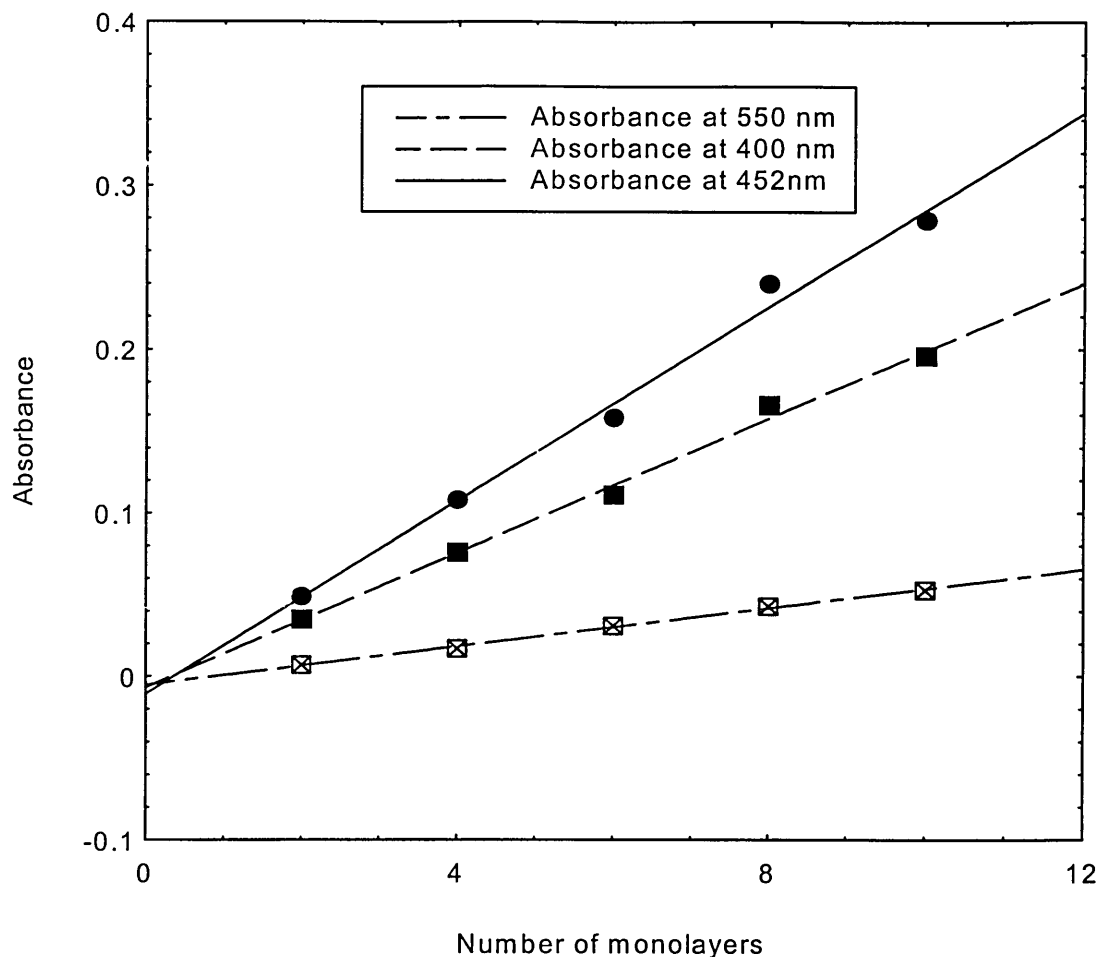


**Figure 5-15 Relationship between increasing numbers of monolayers with absorbance of AmAz1**

### 5.1.2 Reflectance Spectra

The amount of light reflected from a surface, particularly in very thin films, is dependant upon the structure of the film. Like transmittance, but unlike absorbance, reflectance ( $R$ ) is a physically measurable quantity normally stated as a percentage in the form;

$$R = \frac{R_D}{I_0} \quad 5.4$$

where  $R_D$  is the detected reflectivity and  $I_0$  is the incident light intensity.

Initially, if we consider the general case of reflection at a boundary between two media (Figure 5-16) there will be a transmitted (and/or absorbed) and reflected component of the incident light.

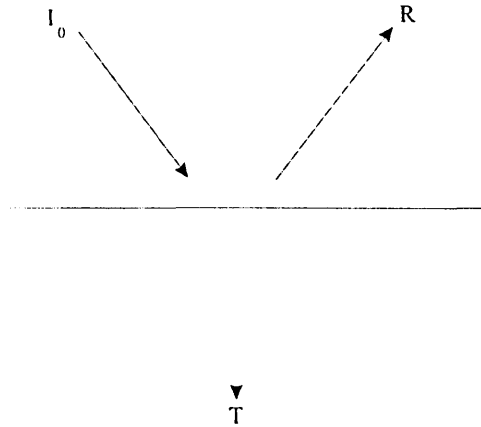


**Figure 5-16 Reflection at a boundary between two media**

For this model the absorbing medium is assumed to be thick which allows multiple reflections within the medium to be neglected. In the optical domain a thick film is assumed to have a thickness of the order of optical wavelengths and lateral dimensions large compared with the wavelength of light.

For the case of light of normal incidence the above assumptions lead to the following expression for refractive index ( $n$ ) and extinction coefficient ( $k$ ) (Fowles 1975);

$$R = \frac{(1-n)^2 + k^2}{(1+n)^2 + k^2} \quad 5.5$$

When considering Langmuir-Blodgett films of a few monolayers the above assumptions do not hold as the films are much thinner (2-20nm) than the wavelength of light and so multiple reflections within the film and from the substrate cannot be neglected.

For an absorbing film on a transparent substrate (Figure 5-17)

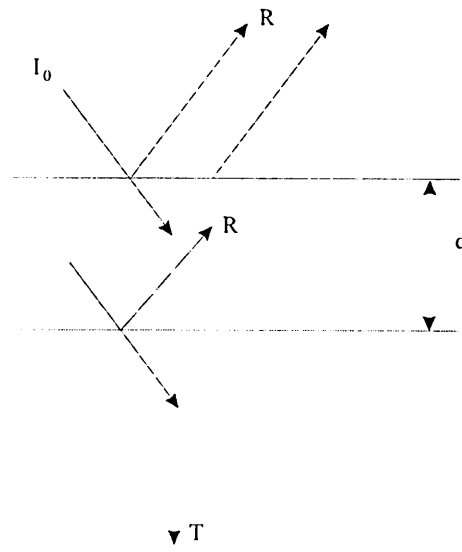


**Figure 5-17 Multiple reflections at a boundary of an absorbing film and a transparent substrate**

with light at normal incidence the reflectance and transmittance can be expressed in the following form (Heavens 1964);

$$R = \frac{A \cosh(\alpha) + B \sinh(\alpha) - C \cos \beta + D \sin \beta}{E \cosh(\alpha) + F \sinh(\alpha) - G \cos \beta + H \sin \beta} \quad 5.6$$

$$T = \frac{8n_s n_0 (n^2 + k^2)}{E \cosh(\alpha) + F \sinh(\alpha) - G \cos \beta + H \sin \beta} \quad 5.7$$

where,

$$\begin{aligned} A &= (n^2 + k^2 + n_0^2)(n^2 + k^2 + n_s^2) - 4n^2 n_0 n_s \\ B &= 2n[n_s(n^2 + k^2 + n_0^2) - n_0(n^2 + k^2 + n_s^2)] \\ C &= (n^2 + k^2 - n_0^2)(n^2 + k^2 - n_s^2) + 4k^2 n_0 n_s \\ D &= 2k[n_s(n^2 + k^2 - n_0^2) - n_0(n^2 + k^2 - n_s^2)] \\ E &= (n^2 + k^2 + n_0^2)(n^2 + k^2 + n_s^2) + 4n^2 n_0 n_s \\ F &= 2n[n_s(n^2 + k^2 + n_0^2) + n_0(n^2 + k^2 + n_s^2)] \\ G &= (n^2 + k^2 - n_0^2)(n^2 + k^2 - n_s^2) - 4k^2 n_0 n_s \\ H &= 2k[n_s(n^2 + k^2 - n_0^2) + n_0(n^2 + k^2 - n_s^2)] \end{aligned}$$

and  $n_0$  is the refractive index of air,  $n_s$  is the refractive index of the glass substrate,  $n$  is the refractive index of the film,  $k$  is the extinction coefficient of the film,  $\alpha=4\pi kd/\lambda$ ,  $\beta=4\pi nd/\lambda$  and  $d$  is the thickness of the film.

The extinction coefficient  $\alpha$  is related to absorbance ( $A$ ) by:

$$\alpha = \frac{\log A}{d} \quad 5.8$$

where  $d$  is the film thickness.

The above equations allow calculation of  $n$  across a wavelength range upon measurement of  $R$  or  $T$  and determination of  $k$  and  $d$ .

#### **5.1.2.1 Refractive Index and Extinction Coefficient Calculation for AmPc5**

Determination of the extinction coefficient of 2, 4, 6, and 8 monolayers of AmPc5 yields the graph in Figure 5-18 across the 300 to 900 nm wavelength range.

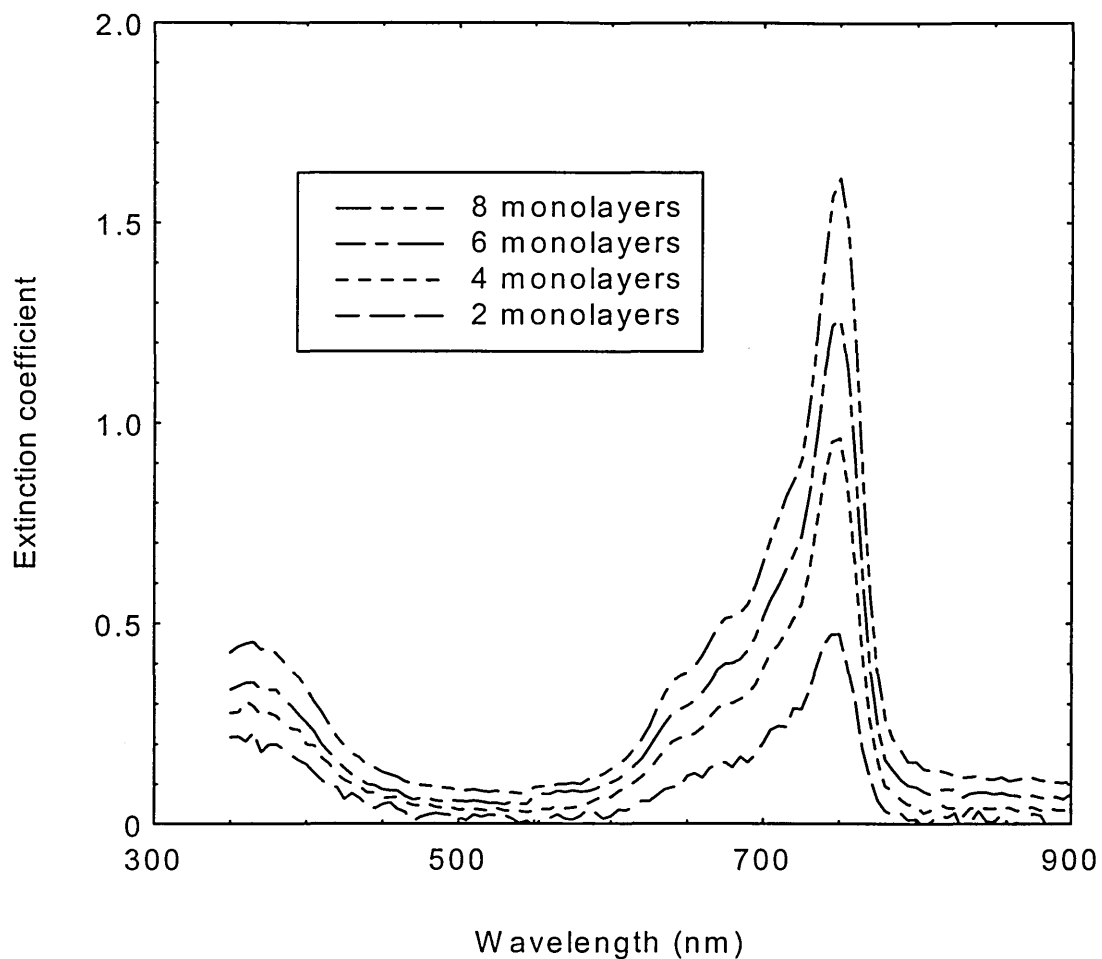


**Figure 5-18 Extinction coefficient values of 2, 4, 6, and 8 monolayers of AmPc5 across the visible spectrum region**

The extinction coefficient values vary across the visible spectral region in a manner similar to absorbance as predicted by equation 5.8. The values are shown to increase linearly with monolayer thickness.

The refractive index across the same wavelength range can be calculated using equation 5.7, producing the graph shown in Figure 5-19.

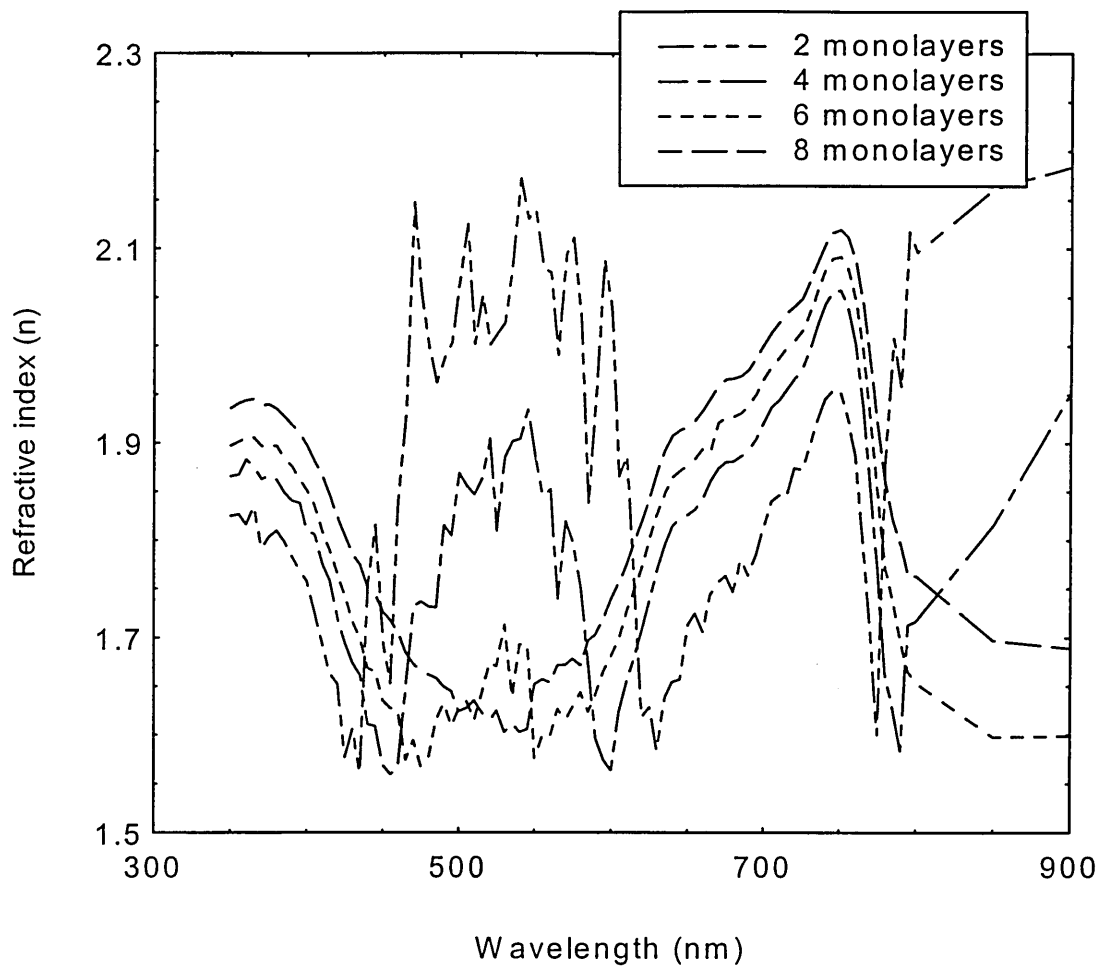


**Figure 5-19 Refractive index of 2, 4, 6, and 8 monolayers of AmPc5 in Langmuir-Blodgett films**

The refractive index is seen to vary considerably across the 300 to 900 nm range, with the absorbance minimum region from approximately 500 to 546 nm increasing dramatically with thickness. This region of the refractive index profile is also highly susceptible to noise arising from the relatively high transmission values, and so an accurate refractive index value cannot be given in this range. The refractive index values between approximately 550 and 800 nm are far more stable, allowing accurate values to be determined. The increase in refractive index with increasing monolayer thickness appears to be a non-linear relationship and is covered in more detail in section 5.2.4.

### 5.1.2.2 Refractive Index and Extinction Coefficient Calculation for AmAz1

The extinction coefficient for 2, 4, 6, and 8 monolayers of AmAz1 in Langmuir-Blodgett films is calculated using equation 5.8 producing the graph in Figure 5-20. The extinction coefficient values do not increase with film thickness, but tend towards a values of approximately 1.5.

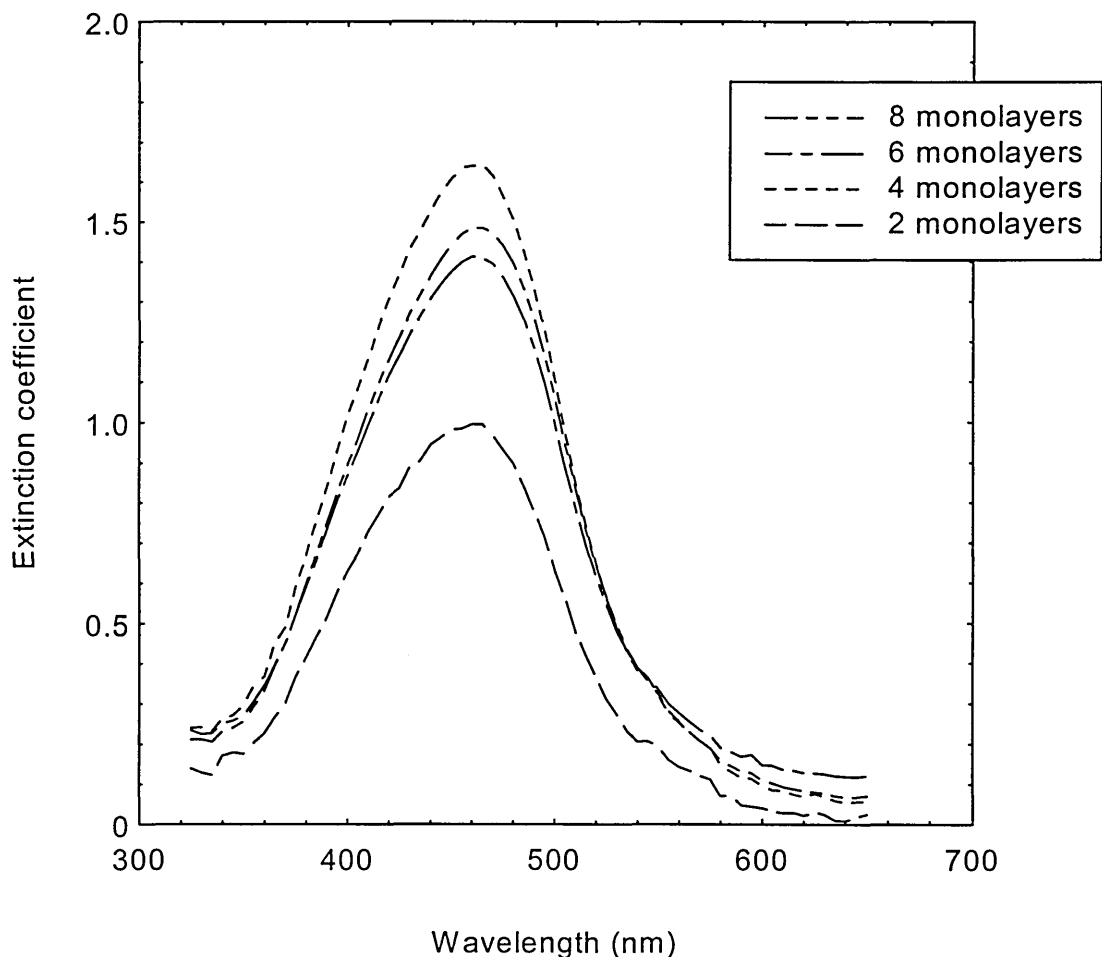


**Figure 5-20 Extinction coefficient of 2, 4, 6 and 8 Langmuir-Blodgett monolayers of AmAz1**

The refractive indices of the various film thicknesses of AmAz1 are calculated from transmission data and are shown in Figure 5-21.

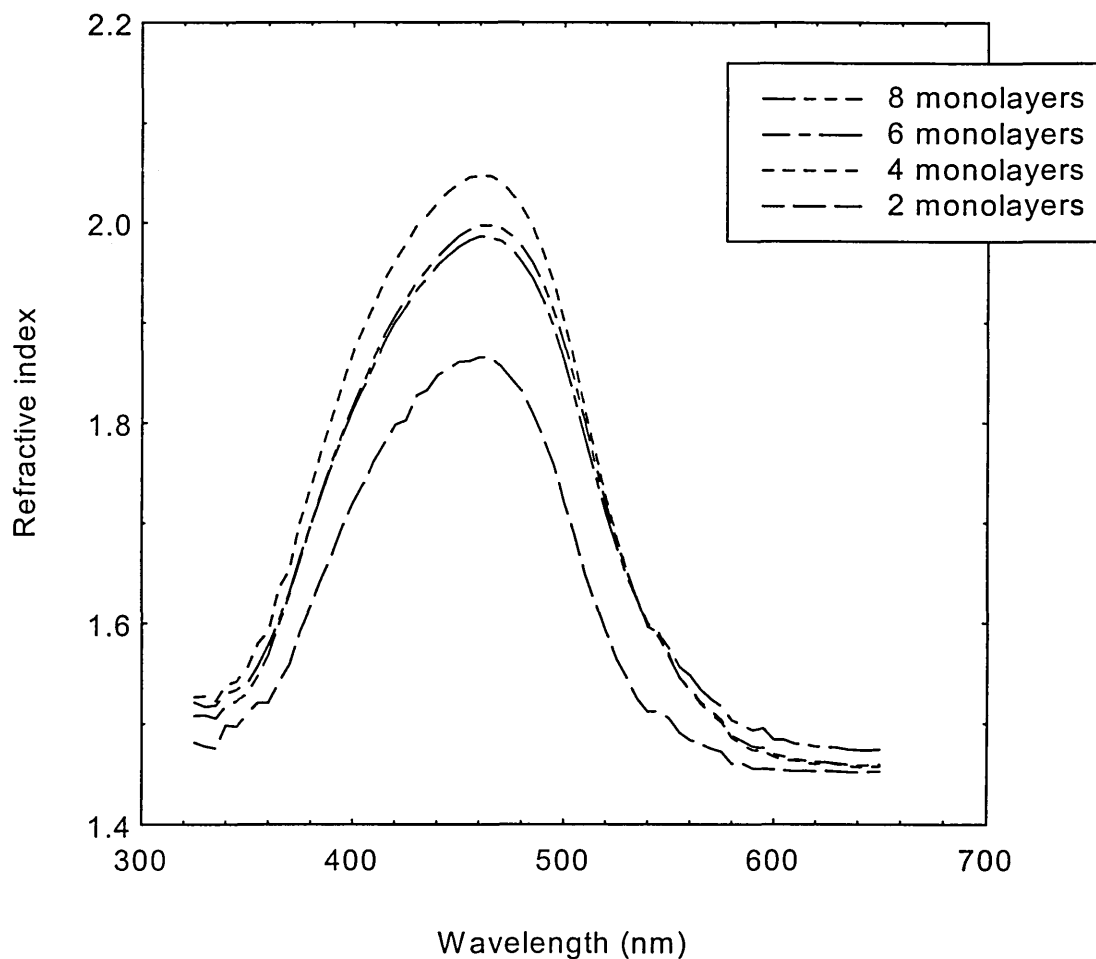


**Figure 5-21 Refractive index of 2, 4, 6 and 8 Langmuir-Blodgett monolayers of AmAz1**

Similarly, the refractive index values do not increase with film thickness but also tend towards a values of approximately 2.0.

### 5.1.3 Absorption of Polarised Light

Light can be considered to be transverse waves since it consists of oscillating electric (E) and magnetic (B) fields perpendicular to each other and also mutually perpendicular to the direction of propagation, (x). The oscillating E and B fields in sound and compression waves are along the direction of propagation of the wave and are known as longitudinal waves. Transverse waves have the ability to be polarised as the plane or planes of oscillation of E do not affect the direction of propagation. Most

electromagnetic radiation detectors are sensitive to the electric field, so when studying polarisation it is the E field vector that is considered.

Unpolarised light is made up of independent wave trains whose E fields oscillate in many different planes (Figure 5-22).

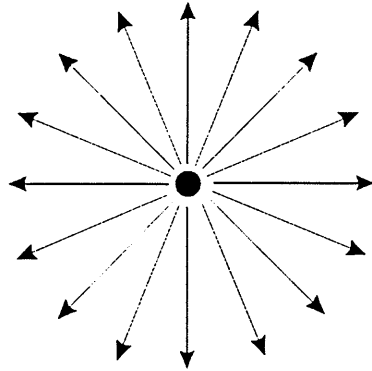


**Figure 5-22 Oscillating E fields of unpolarised light**

So it can be said that unpolarised light is made up of randomly orientated, rapidly fluctuating, polarised light. If the E vector always oscillates in the same plane with constant amplitude, then the light is termed plane-polarised (or linearly polarised). In Figure 5-23 the E field oscillates exclusively in the yz plane, whilst the B field oscillates in the zx plane. If it were possible to see the electric vector at the oncoming beam it would be seen to be oscillating along a fixed line, up and down. If the E vector were to maintain a constant magnitude but rotate about the x-axis, the wave would no longer be plane-polarised, but circularly polarised. If the E vector were also to change in magnitude, the wave would become elliptically polarised (Halliday 1989).

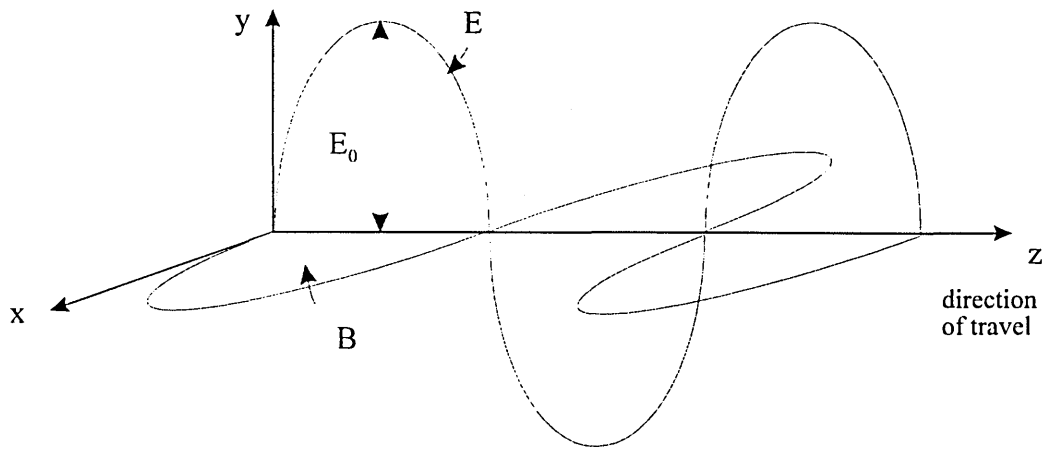


**Figure 5-23 Oscillating E fields of polarised light**

It is possible to produce plane-polarised light from unpolarised light by using the commercially available product of Polaroid developed by Edwin Land. The material used displays anisotropic optical absorption, resulting in one component of polarisation being more strongly absorbed than another. A light wave with an E vector parallel to the transmission axis of the polariser will be transmitted and E vector perpendicular to the transmission axis will be absorbed. Figure 5-24 depicts E to be a randomly selected wavetrain falling on a polariser with a vertical transmission axis, then  $E_y$  (of magnitude  $E\cos\theta$ ) will be transmitted and  $E_x$  (of magnitude  $E\sin\theta$ ) will be absorbed.

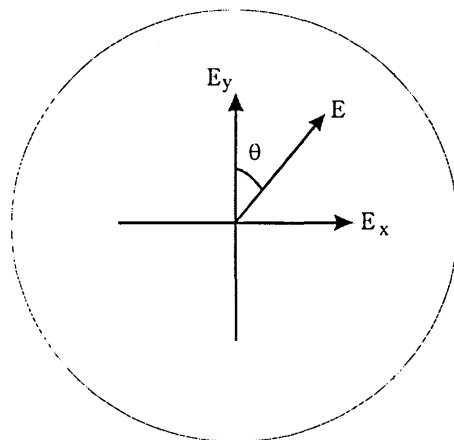


**Figure 5-24 Representation of the production of polarised light using Polaroid**

The intrinsic dichroic property of the Polaroid can be employed to examine the possibility of dichroic presence in Langmuir-Blodgett films (Liang et al 1997, Capelletti et al 1995). Plane-polarised light can be directed at the surface of the Langmuir-Blodgett films. These films can be positioned with the dipping direction parallel (transverse magnetic, TM) or perpendicular (transverse electric, TE) to the plane of polarised light. Measurements were taken by rotating the polaroid through 90° so as to change the plane of polarisation through 90°. The sample was not rotated ensuring measurements were taken at the same position on the Langmuir-Blodgett film for parallel and perpendicularly polarised light.

The ratio between absorbance of parallel and perpendicularly polarised light can be expressed as (Grieve 1995);

$$D_{\beta} = \frac{A_{\parallel}}{A_{\perp}} = \frac{A_{TM}}{A_{TE}} \quad 5.9$$

where  $D_{\beta}$  is the dichroic ratio at incident angle  $\beta$  at a given wavelength.

A material possessing a dichroic ratio of 1 exhibits the same absorption whether p-polarised light is directed parallel or perpendicular to the dipping direction. This implies that there is no preferential orientation with respect to dipping direction and the films are in-plane amorphous. However, the molecules may still have a fixed angle with respect to the normal of the substrate and display order in a direction normal to the substrate. Conversely materials with a low value of  $D_{\beta}$  display a preference in orientation with respect to dipping direction. It is possible for such molecules to determine their orientation by investigating the absorption spectra over a range of incident angles.

### 5.1.3.1 Dichroism in AmPc5

Measurement of the absorption by Langmuir-Blodgett films of AmPc5 parallel and perpendicular to the direction of dipping using p-polarised light were taken (Figure 5-25) producing the absorption spectra in Figure 5-26.

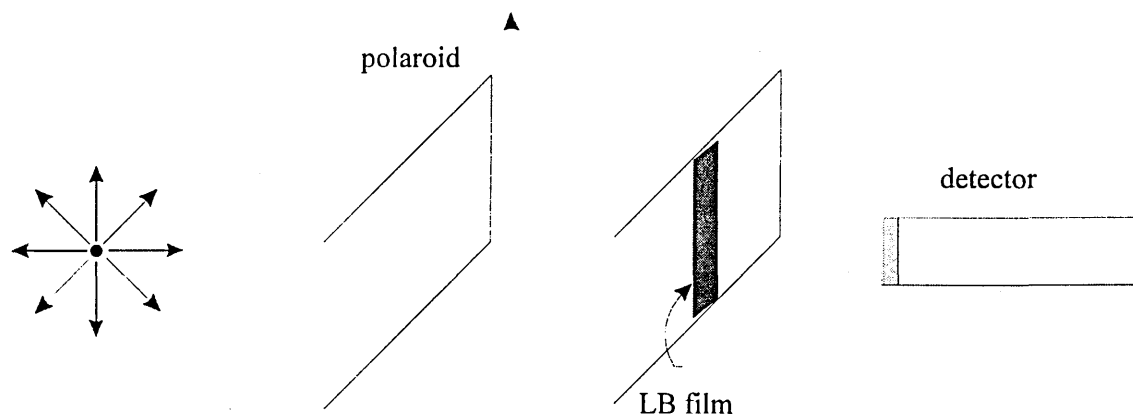


**Figure 5-25 Experimental set-up for dichroic measurements**

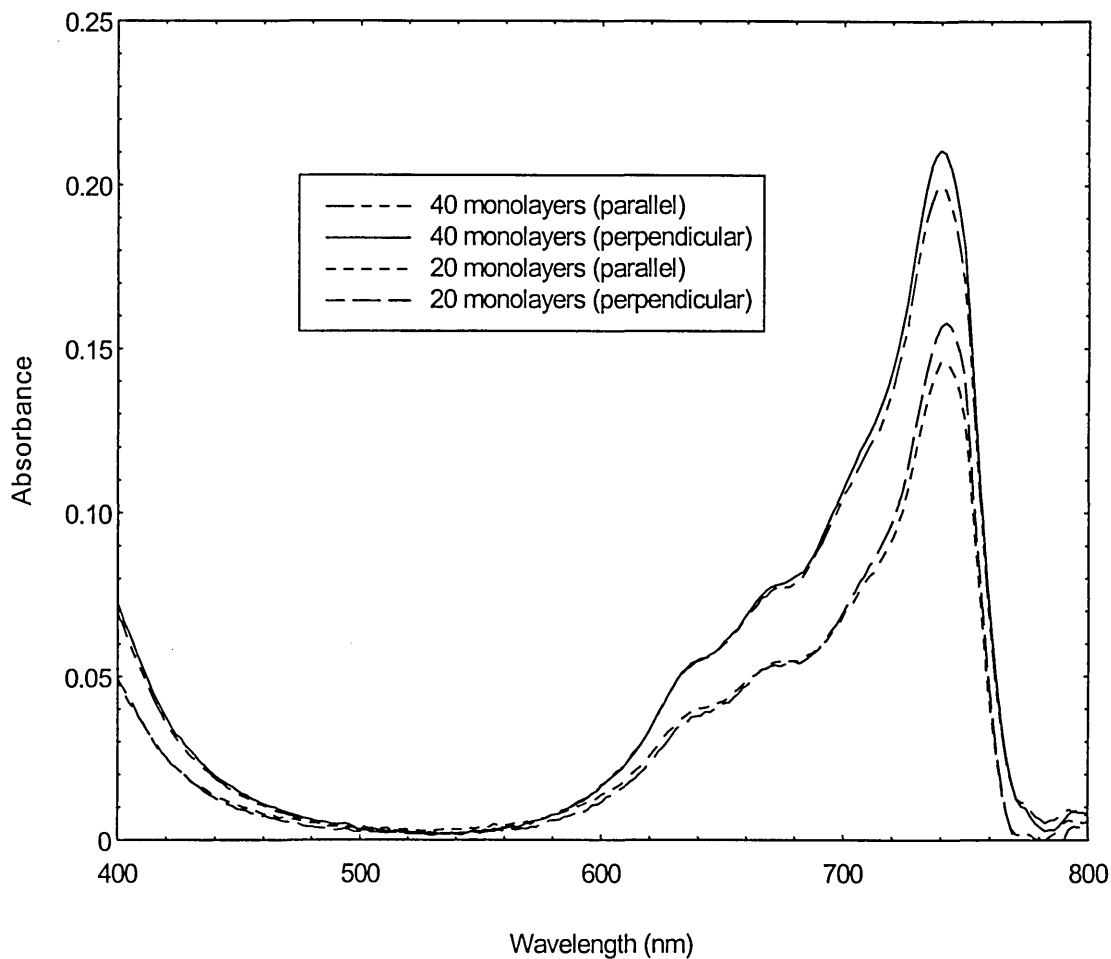


**Figure 5-26 P-polarised light absorbance spectra of AmPc5 taken at normal incidence**

The dichroic effect is apparent between the approximate wavelength range 690-760 nm for both thicknesses, implying the presence of appreciable dichroism in the  $Q_x$  band. As each absorption peak corresponds to a different electronic transition, it follows that the suppressed  $Q_y$  peak at approximately 706 nm makes a small contribution to the dichroic effect and the smaller  $Q_x$  and  $Q_y$  bands make no contribution. Values of dichroism at normal incidence are measured at the peaks in absorption of the  $Q_x$  band at 740 nm for both film thicknesses;

$$D_0 = 0.94 \text{ for 20 monolayers}$$

$$D_0 = 0.95 \text{ for 40 monolayers}$$

This suggests that in-plane order for AmPc5 does not increase with successive film depositions and that an increase in film thickness does not encourage a more highly oriented molecular planar structure. This is in contrast with the measurements performed on a differently substituted copper phthalocyanine molecule (Yoneyama et al 1986). This difference arises from the different styles of packing, in that most phthalocyanines deposit in a columnar herring-bone array, whereas AmPc5 deposits in a columnar stack style.

As the values of  $D_0$  obtained are less than 1, the value of absorption is greater when E is parallel to the dipping direction. This indicates that the phthalocyanine ring is aligned relative to the dipping direction at an angle less than  $45^\circ$ .

Polarised light absorbance measurements are also made for values of  $\beta \neq 0$  to aid calculation of molecular orientation. It is not possible to draw conclusions from these measurements alone as the E field is not polarised parallel or perpendicular to the plane of dipping direction. When the angle of incidence of light is not normal, the value of  $D_\beta$  obtained can be greater than 1.

The dichroic ratio can be expressed as (Yoneyama et al 1986 and Yan et al 1992);

$$D_\beta = [\langle \cos^2 \phi \rangle + \langle \cos^2 \theta \sin^2 \phi \rangle] \quad 5.10$$

$$[\{\langle \sin^2 \phi \rangle + \langle \cos^2 \theta \cos^2 \phi \rangle\} \cos^2 \beta + \langle \sin^2 \theta \rangle \sin^2 \beta]$$

where the angles  $\theta$ ,  $\phi$ , and  $\beta$  are defined in Figure 5-27. The use of  $\langle \rangle$  denotes a statistical average over the angles of all the molecules in the Langmuir-Blodgett film.

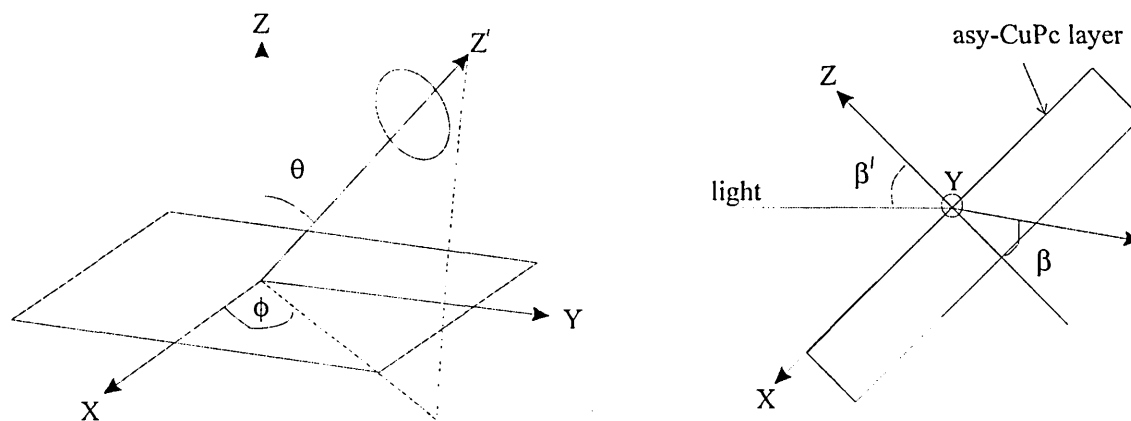


**Figure 5-27** Definitions of angles  $\theta$ ,  $\phi$  and  $\beta$

The method used to calculate orientation requires measurement of polarised light absorbance at 2 angles of incidence, yielding the orientation of the  $z'$  axis using the following equations;

$$\langle \cos^2 \theta \rangle = \frac{D_0 - (1 + D_0 \sin^2 \beta) D_\beta}{(1 - 2 \sin^2 \beta) D_\beta - (1 + D_\beta \sin^2 \beta) D_0} \quad 5.11$$

$$\langle \sin^2 \theta \cos^2 \phi \rangle = \frac{D_0 - \langle \cos^2 \theta \rangle}{1 + D_0} \quad 5.12$$

In order to calculate the orientation angles, the angle of refraction  $\beta$  must be determined.

We can consider the phthalocyanine molecule to have a ring shaped transition dipole

(Figure 5-28) with its orientation defined by the normal unit vector,  $\hat{n}$ .

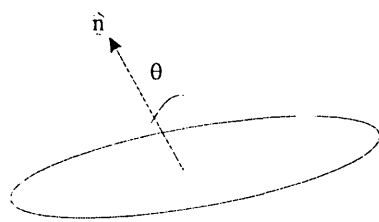


**Figure 5-28 Phthalocyanine transition dipole moment**

As the absorption of polarised light is dependant on the component of electric field in the plane of the molecule, we can define,

$\hat{E}$  = unit vector in the direction of the field

$E_0$  = magnitude

So the component of light in the direction of  $\hat{n}$  is  $(E_0 \hat{E} \cdot \hat{n})$ .

This results in the case in Figure 5-29, where  $x$  is the component of the electric field in the plane of the ring.

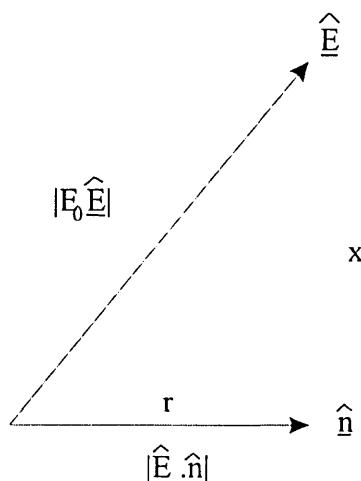


**Figure 5-29 Electric field component in the plane**

So,

$$x^2 = \left| E_0 \underline{\hat{E}} \right|^2 - \left| E_0 \underline{\hat{E}} \cdot \underline{\hat{n}} \right|^2 = E_0^2 \left| \underline{\hat{E}} \right|^2 - E_0^2 \left| \underline{\hat{E}} \cdot \underline{\hat{n}} \right|^2 \quad 5.13$$

$$x^2 = E_0^2 \left( 1 - \left| \underline{\hat{E}} \cdot \underline{\hat{n}} \right|^2 \right)$$

For ring shaped molecules. the absorption of a molecule is proportional to (Grieve 1993);

$$\frac{1}{\cos \beta} \left( 1 - \left| \underline{\hat{E}} \cdot \underline{\hat{n}} \right|^2 \right) \quad 5.14$$

The derivation yields the relation,

$$\frac{A^{TE}(\beta')}{A^{TE}(0^\circ)} = \frac{1}{\cos \beta} \quad 5.18$$

where the ratio  $\frac{A^{TE}(\beta')}{A^{TE}(0^\circ)}$  is measured experimentally.

Calculation of  $\beta$  allows determination of the refractive index at the wavelength of interrogation using Snells Law,

$$n_1 \sin \beta' = n_2 \sin \beta \quad 5.19$$

where  $n_1$  and  $n_2$  are the refractive indices of air and AmPc5 Langmuir-Blodgett films, respectively.

The calculations for the 20 and 40 monolayer Langmuir-Blodgett films at 706 and 740 nm are summarised in Table 5-3;

		Langmuir-Blodgett films			
		20 monolayers		40 monolayers	
		714 nm	740 nm	714 nm	740 nm
$\beta' = 0^\circ$	$A^{TE}$	0.088	0.158	0.131	0.211
	$A^{TM}$	0.083	0.146	0.124	0.200
	$D_0$	0.943	0.936	0.947	0.950
$\beta' = 45^\circ$	$A^{TE}$	0.082	0.139	0.125	0.192
	$A^{TM}$	0.093	0.162	0.138	0.216
	$D_{45}$	1.134	1.164	1.104	1.125
$\beta^\circ$		21.280	28.388	17.408	24.501
$\theta^\circ$		69.592	66.004	68.988	58.565
$\phi^\circ$		46.063	46.309	46.010	46.284
n		1.948	1.487	2.363	1.705

**Table 5-3 Calculated molecular orientation values for AmPc5**

The wavelength dependence of the angle of refraction  $\beta$  and hence the refractive index  $n$  is shown clearly in Table 5-3. The thickness dependence of the refractive index is only apparent in Langmuir-Blodgett films of a few monolayers and therefore does not occur in these relatively thick films. As the dichroic ratio is found to remain constant with increasing film thickness it follows that the orientation of molecules will not change with respect to monolayer increase. It is therefore possible to take an average of the molecular angles and refractive index from both thicknesses at each wavelength, as shown in Table 5-4 below;

	714 nm	740 nm
$\beta^\circ$	19.344	26.445
$\theta^\circ$	69.292	62.285
$\phi^\circ$	46.034	46.297
n	2.156	1.596

**Table 5-4 Average values for molecular orientation and refractive index at  $Q_x$  and  $Q_y$  bands**

The angle  $\theta$  corresponds to the angle between the phthalocyanine ring normal and the z-axis (Figure 5-27). A low value of  $\theta$  indicates that the phthalocyanine ring lies flat facing the substrate (Yoneyama 1986). The higher values of  $\theta$  obtained for AmPc5 imply that the molecule deposits almost perpendicular to the substrate.

The value obtained for the angle  $\phi$  suggest that the flat plane of the phthalocyanine ring does not deposit in a direction parallel to the dipping direction. From this determination it can be said that the z' axis has an azimuth of approximately  $46^\circ$  in the xy plane.

The large difference in refractive index calculated for the two wavelengths is as expected due to the obvious difference in absorbance between the  $Q_x$  and  $Q_y$  absorption bands.

#### **5.1.3.2 Dichroism in AmAz1**

The parallel and perpendicularly polarised light absorption spectra produced by a particular section of AmAz1 film with light at normal incidence are shown in Figure 5-30.

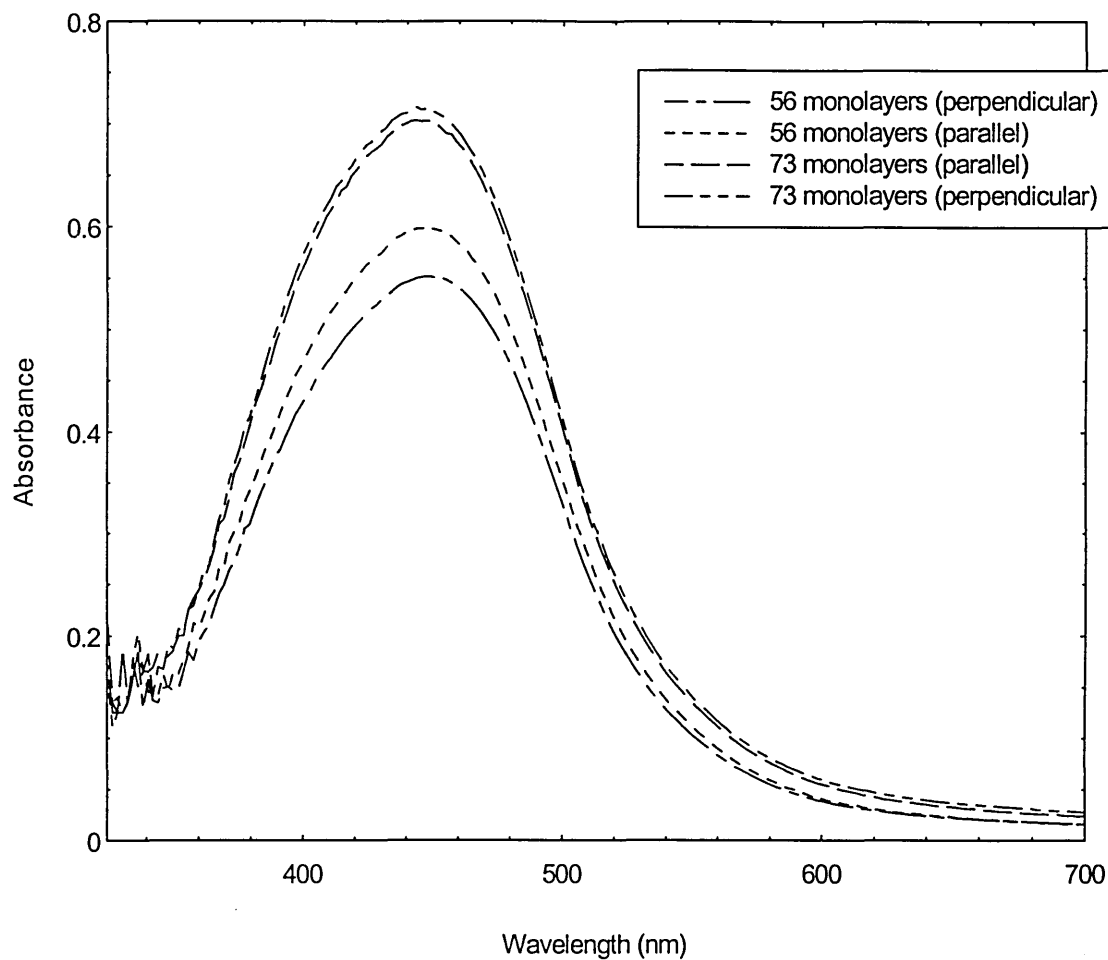


**Figure 5-30 Normally incident polarised light absorbance in Langmuir-Blodgett films of AmAz1**

These differences in dichroic ratio cannot simply be attributed to a decrease in order with increasing thickness. Thick Langmuir-Blodgett films of AmAz1 produce highly inhomogeneous monolayers when compared to thinner films. So the decrease in the difference between  $E_{\perp}$  and  $E_{\parallel}$  in the 73 monolayer film visible in Figure 5-30 may be as a result of the measurement being taken at a point of inhomogeneous deposition.

This inhomogeneity can be investigated by measuring the polarised light absorbance spectra at different positions on the same substrate of the Langmuir-Blodgett film surface, as detailed in Table 5-5.

	$\beta = 0^\circ$			$\beta = 45^\circ$		
Film thickness	$A^{TE}$	$A^{TM}$	$D_0$	$A^{TE}$	$A^{TM}$	$D_0$
56 position 1	0.551338	0.598834	1.086	0.550135	0.633745	1.152
56 position 2	0.605507	0.613134	1.013			
73 position 1	0.714208	0.702818	0.984	0.683006	0.770672	1.128
73 position 2	0.732757	0.71782	0.980			

**Table 5-5 Dichroic ratios of AmAz1 measured at 445 nm**

The dichroism in all samples is only apparent at 445 nm, arising from the  $\pi \rightarrow \pi^*$  transition in the azo group. The values of  $D_0$  calculated for the 73 monolayer sample are very similar implying that AmAz1 molecules display a preferential orientation with respect to the dipping direction at both positions of the surface. Study of the 56 monolayer sample reveals appreciably different values for  $D_0$  at both positions. This suggests that whilst dichroism is observable in AmAz1, it is variable depending upon the position of interrogation on the film surface. This points towards the film being in-plane isotropic and not showing a preference in orientation with respect to dipping direction. It is, however, possible for similar values of  $D_0$  to be observed at different position on such a film surface as the in-plane random molecular orientation at these positions can result in the same absorbance. This effect is observed in a 73 monolayer sample.

The dichroic ratios obtained for the thicker sample are less than one, whilst those obtained for the thinner sample are greater than one, implying that the molecules are angled less than and greater than  $45^\circ$  with respect to the dipping direction, respectively. One explanation for this paradox may be that the molecules display a different preference towards orientation in different thicknesses. Although, coupled with the information yielded from study at different positions on the film surface it is more likely that these results indicate the presence of an in-plane isotropic structure.

## **5.2 Surface Plasmon Resonance Measurements**

The technique of surface plasmon resonance can be used as a tool to determine the optical constants of a material and uniformity of deposition across a Langmuir-Blodgett film. Here, the complex refractive index and thickness of the materials in question have been determined.

### **5.2.1 Surface Plasmon Excitation**

In qualitative terms it can be said that surface plasmons can exist at the interface between two media with electrons behaving like an electron gas that oscillate collectively. The surface plasmons are produced by the excitation of these electrons on application of an externally applied electric field. The electromagnetic waves produced propagate along the boundary of a metal and dielectric and decay exponentially into both media with increasing distance from the interface. In a two boundary system the dielectric is usually air; in the present situation, we have a three boundary system where the dielectric is the Langmuir-Blodgett film in question. Hence, the evanescent field on the surface of the metal will decay into the Langmuir-Blodgett film changing the properties of the surface plasmon itself. It is this effect that is used in surface plasmon resonance study.

It is known that metals support TM (transverse magnetic) modes and semiconductors support TE (transverse electric) modes, so surface plasmons are TM polarised electromagnetic waves. If we consider a two boundary system, application of Maxwells Equations yields the following dispersion relation for the wavevector  $k_x$ ,

$$k_x = \frac{\omega}{c} \left( \frac{\epsilon_1 \epsilon_3}{\epsilon_1 + \epsilon_3} \right)^{1/2} \tag{5.20}$$

where  $k_x$  is the wavevector along the x-direction parallel to the surface,  $\omega/c = 2\pi/\lambda$ ,  $\epsilon_1$  and  $\epsilon_3$  are the complex dielectric constants defined as  $\epsilon_n = \epsilon_n' + \epsilon_n''$  ( $\epsilon_n'$  as the real component and  $\epsilon_n''$  as the imaginary component) with subscripts explained in Figure 5-31, for  $d_2 = 0$ .



**Figure 5-31 Surface plasmon resonance three boundary system**

At this stage it would seem that a surface wave can be excited simply by shining a light at a metal surface. Inspection of the surface wave dispersion curve shows that this is not correct (Figure 5-32).

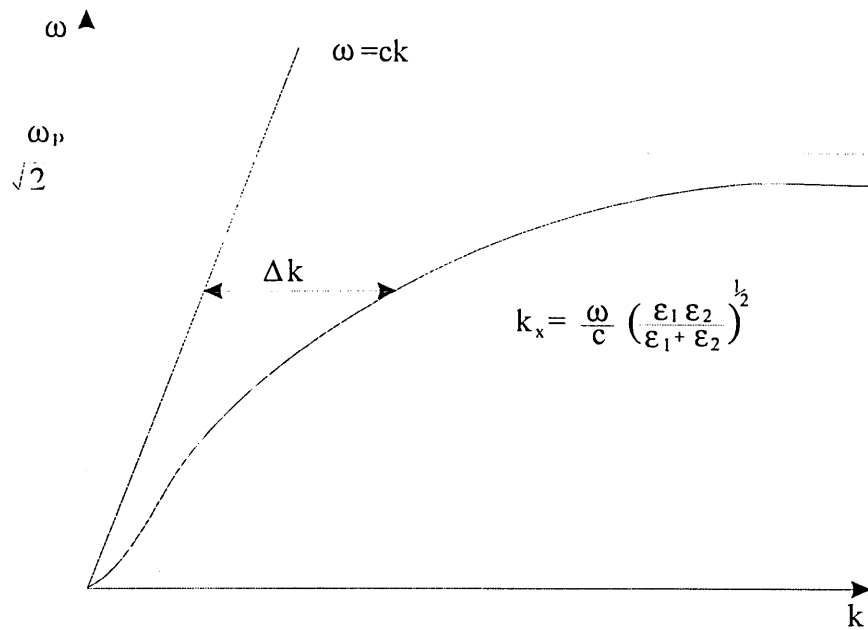


**Figure 5-32 Graphical representation of surface plasmon resonance requirements**

The light line and the dispersion curve of a surface plasmon do not coincide at any point making excitation impossible. It is necessary to increase  $k_x$  by an amount ( $\Delta k$ ), ensuring that the light line is greater than the dispersion curve.

This can be achieved by two methods; the Otto (Otto 1968) or Kretschmann (Kretschmann 1968) configurations. Both configurations use a prism in the experimental set-up, with Otto using prism/air/metal (PAM) and Kretschmann using prism/metal/air (PMA). Under conditions of total internal reflection an evanescent field is present in the air gap in the PAM configuration. By ensuring that the metal layer is close enough, the evanescent field can be used to generate surface plasmons. When using the PMA configuration the evanescent field penetrates the metal film directly, making this set-up sensitive to film thickness. This fact combined with the relative experimental ease makes the Kretschmann configuration (Figure 5-33) a more appropriate approach.

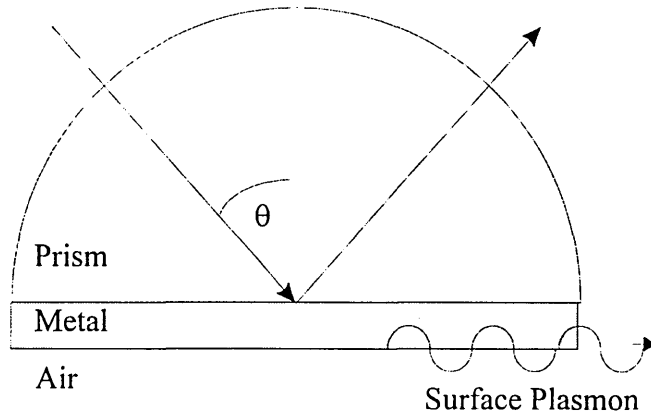


**Figure 5-33 Kretschmann configuration for surface plasmon resonance**

The evanescent wave only exists when total internal reflection occurs, hence,

$$\theta_c \leq \theta \leq 90^\circ$$

where  $\theta_c$  is the critical angle. The component of the wavevector parallel to the prism face is given by,

$$k_x = \frac{\omega}{c} n_0 \sin \theta \quad 5.21$$

where  $n_0$  is the refractive index of the prism. The range of  $k_x$  associated with the evanescent wave is,

$$\frac{\omega}{c} \leq k_x \leq \frac{\omega}{c} n_0$$

and corresponds to a region above the prism light line but below the air/vacuum light line (Figure 5-34).

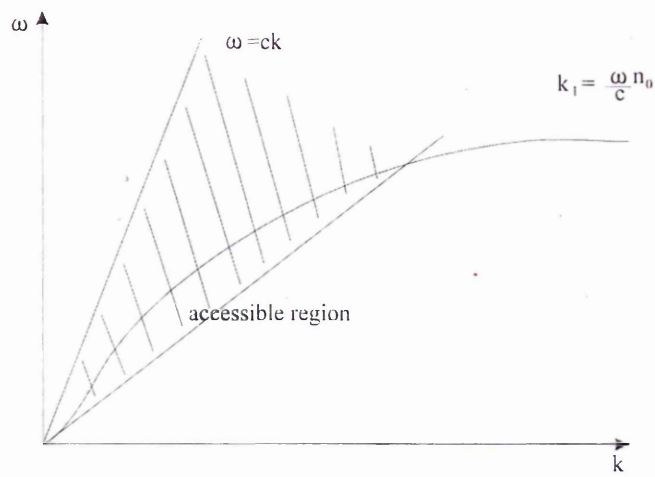


Figure 5-34 Surface plasmon resonance conditions

The phase velocity,  $v_{sp}$ , of such a wave is given by,

$$v_{sp} = \frac{c}{\sin \theta} \tag{5.22}$$

### 5.2.2 Experimental Set-up

The Kretschmann configuration has been employed in the present work with the set-up shown in Figure 5-35.

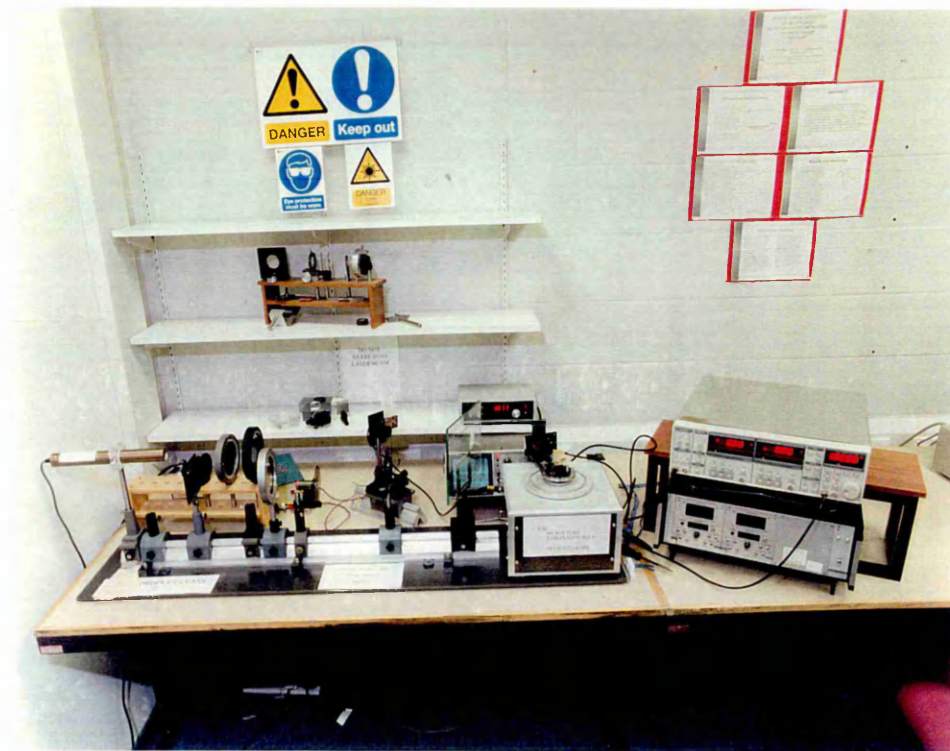


Figure 5-35 Surface plasmon resonance experimental set-up

The Langmuir-Blodgett films have been deposited onto gold and silver coated glass substrates in a step structure, whilst ensuring that an area of the metal was left bare to allow for surface plasmon resonance measurements on metal only. It was found through experience to allow approximately 1cm for each individual step, as the laser beam had a finite thickness despite focusing the lens. The glass slide is then coupled to a prism using index matching fluid and a beam of p-polarised He-Ne laser light at 632.8 nm is directed into the prism. Prior to this, the beam passes through a chopper and a glass plate where a fraction of the light is reflected onto a photodiode for intensity normalisation purposes. The reflectivity from the sample is detected using a second photodiode with the entire prism arrangement mounted on a rotating table. This allows measurement of the reflectivity across a range of angles, beginning below the critical angle and scanning past the angle at which surface plasmons are produced. The signals from both detectors are fed into a lock-in amplifier. The whole set-up is microprocessor controlled.

The first set of readings is taken using the prism alone to test for cleanliness and to allow normalisation of the metal and Langmuir-Blodgett data. Secondly, the portion of the metal slide left bare is measured showing the surface plasmon resonance angle,  $\theta_{sp}$ . The same procedure is followed for the Langmuir-Blodgett film coated portion of the sample. The curves for metal and Langmuir-Blodgett coated metal samples show an increase in reflectivity until total internal reflection is achieved. This reflectivity remains constant until the angle  $\theta_{sp}$ , at which point a sharp decrease in reflectivity is observed corresponding to resonance of the surface plasmons. The shape and position of this minimum are dependant upon the thickness and extinction of the metal. A sharp and deep minimum will yield more accurate results when analysing surface plasmon resonance curves. There are two damping mechanisms which can force broader, shallower minima; inner and radiation (or coupling) damping. Inner damping arises

from energy absorption by the metal and is given by the imaginary component,  $\epsilon_1''$ , whilst the radiation damping arises from the coupling of the incoming beam and the surface plasma and is dependant on film thickness. An upper limit for the extinction of the film is given by (Pokrowsky 1991),

$$\epsilon_1'' < \left| \epsilon_1' \right| \quad 5.23$$

and equation 5.23 has a solution only if,

$$\epsilon_1' < -1 \quad 5.24$$

This restricts the choice of metals suitable for surface plasmon resonance study. Gold and silver are popular candidates as they satisfy the above conditions. The complex dielectric constants for gold, silver and chromium are given in Table 5-6 with values of n and k for comparison purposes.

Metal	$\epsilon_1'$	$\epsilon_1''$	n	k
Silver (Sambles 1991)	-19.0	0.74	0.08	4.625
Gold (Sambles 1991)	-12.9	1.35	0.188	3.590
Chromium (Pokrowsky 1991)	-4.3	31.2	3.687	4.231

**Table 5-6 Silver, gold and chromium values for  $\epsilon_1'$  and  $\epsilon_1''$**

From this data it can be seen that 5.23 and 5.24 are not satisfied for chromium, making it unsuitable to study surface plasmon resonance effects. Silver has a higher value for  $|\epsilon_1'|$  than gold, making it theoretically more suitable as a metallic coating. A second factor when evaporating metals is that of cost, making silver a more attractive option. A practical consideration when choosing a metal is its ability to remain untarnished over a period of time. Silver has a tendency to oxidise when left in the open whereas gold remains unaffected when exposed to air. The longer a silver coated substrate is exposed

to the environment, the greater the oxidation effect. This can be seen in Figure 5-36 where surface plasmon resonance measurements have been taken for silver substrates with increasing time,

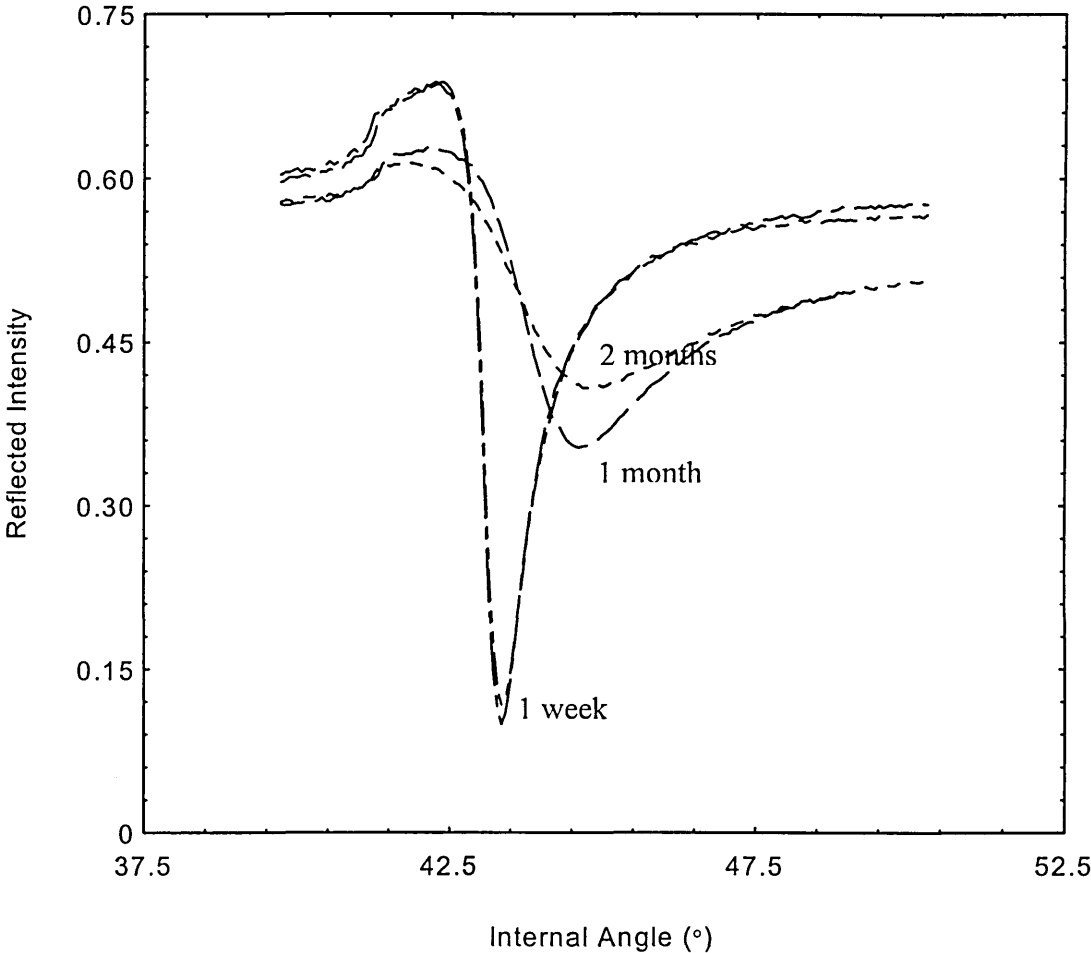


**Figure 5-36 Surface plasmon resonance curves of a silver sample taken at different times**

In order to obtain optimum resonance, the inner and radiation damping effects should be equal. For gold, this is found to occur at approximately 400 nm film thickness (Pokrowsky 1991). For thinner films the radiation damping increases and the resonance minimum becomes broader; whilst for thicker films the radiation damping decreases and the minimum reflectance increases. Hence, a gold film thickness of approximately 400 nm was selected for the surface plasmon resonance study.

### 5.2.3 Surface Plasmon Excitation in a Three Boundary System

In the present work the Langmuir-Blodgett films have been deposited onto a gold layer resulting in a three boundary system (Figure 5-31). The evanescent field on the surface of the gold will decay into the film affecting the shape of the surface plasmon resonance curve.

The dispersion relation in this case is given by (Pockrand 1978 (b)),

$$k_x^{so} = k_x^{(0)} + k_x^{(1)C} + k_x^{(1)R} + k_x^{(2)C} + k_x^{(2)R} + k_x^{(2)CR} \quad 5.25$$

where,

$$k_x^{(0)} = \frac{\omega}{c} \left( \frac{\epsilon_1 \epsilon_3}{\epsilon_1 + \epsilon_3} \right)^{1/2} \quad 5.26$$

as defined previously in equation 5.20

$$k_x^{(1)C} = \frac{\omega}{c} \left( \frac{\epsilon_2 - \epsilon_3}{\epsilon_2} \right) \left( \frac{\epsilon_1' \epsilon_3}{\epsilon_1' + \epsilon_3} \right)^2 \left( \frac{\epsilon_2 - \epsilon_1'}{\epsilon_3 - \epsilon_1'} \right) (-\epsilon_1' \epsilon_3)^{-1/2} \left( \frac{2\pi d_2}{\lambda} \right) \quad 5.27$$

$$k_x^{(1)R} = \frac{\omega}{c} r_{01} \left( \frac{2}{\epsilon_3 - \epsilon_1'} \right) \left( \frac{\epsilon_1' \epsilon_3}{\epsilon_1' + \epsilon_3} \right)^{3/2} \exp \left( -2 \frac{2\pi d_1}{\lambda} \frac{-\epsilon_1'}{(-\epsilon_1' - \epsilon_3)^{1/2}} \right) \quad 5.28$$

$$k_x^{(2)C} = k_x^{(1)C} \left[ \frac{1}{2} \frac{k_x^{(1)C}}{\text{Re}(k_x^{(0)})} \left( 2 \frac{2\epsilon_3^2 - \epsilon_2^2}{\epsilon_3(\epsilon_3 - \epsilon_2)} + \frac{\epsilon_1' + \epsilon_3}{-\epsilon_3} \right) - \frac{1}{2} i \frac{\epsilon_1''}{\epsilon_1'} \right] \quad 5.29$$

$$k_x^{(2)R} = k_x^{(1)R} \left[ \frac{1}{2} \frac{k_x^{(1)R}}{\text{Re}(k_x^{(0)})} \left( \frac{2\epsilon_1' + \epsilon_3}{-\epsilon_3} \right) - i \frac{\epsilon_1''}{\epsilon_1' - \epsilon_3} \right] \quad 5.30$$

$$k_x^{(2)CR} = \frac{k_x^{(1)R} k_x^{(1)C}}{\text{Re}(k_x^{(0)})} \left[ -\frac{\epsilon_1'}{\epsilon_3'} + \frac{2\epsilon_3}{\epsilon_3 - \epsilon_2} + \frac{\epsilon_2}{2\epsilon_3} \right] \quad 5.31$$

where  $\epsilon_2$  is the dielectric constant of the coating.

The above equations for an absorbing coating are valid for a non-absorbing coating if the term  $\epsilon_2$  is replaced by  $\epsilon_2'$ . The inner damping in this system is due to any non-vanishing imaginary part of the dielectric functions of all the layers in the system.

In a non-absorbing material the terms  $k_x^{(1)C}$  and  $k_x^{(2)C}$  give the first and second order shifts of the wavevector  $k_x^{(0)}$  as a result of the Langmuir-Blodgett coating in a metal/coating/air system. Clearly, the first order term does not contribute to the inner damping but indicates a curve shift proportional to  $d_2$  at a given wavelength. The second order term indicates an increase of the inner damping of the coating proportional to coating thickness. For an absorbing coating there is a rapid increase in inner damping with increasing film thickness due to absorbance of energy.

The  $k_x^{(1)R}$  and  $k_x^{(2)R}$  terms describe the radiation damping effects as a result of the metal layer film thickness in the glass/metal/air system. The second order term is a small correction to the first order.

$k_x^{(2)CR}$  takes into account the effect of the coating on the radiation terms.

The imbalance in damping processes arising from the  $k_x^{(1)C}$  term in absorbing films results in the resonance depth decreasing with increasing number of Langmuir-Blodgett monolayers as well as the shift observed for non-absorbing films. The shift in resonance angle of the surface plasmon resonance curves arises from the real part of  $\epsilon$ , whereas the change in half width and depth arises from the imaginary component of  $\epsilon$ .

It is possible to quantify the effect of the Langmuir-Blodgett coating on both types of damping in absorbing and non-absorbing films. For a non-absorbing film this can be written in term of two difference equations,

$$\Delta\mu_I(\text{non-abs}) \propto \text{Im}(k_x^{(0)}) - \text{Im}(k_x^{(2)C}) \quad 5.32$$

$$\Delta\mu_R \propto \text{Im}(k_x^{(1)R}) - \text{Im}(k_x^{(2)CR}) \quad 5.33$$

where  $\Delta\mu_I(\text{non-abs})$  and  $\Delta\mu_R$  are the changes in inner damping and radiation damping.

For absorbing coatings the  $\Delta\mu_I$  changes as the first order becomes significant due to the appearance of the imaginary component of the dielectric constant,  $\epsilon_2''$ . This results in a change in  $\Delta\mu_I$  which becomes,

$$\Delta\mu_I(abs) \propto \text{Im}(k_x^{(0)R}) - \text{Im}(k_x^{(2)C}) + \text{Im}(k_x^{(1)C}) \quad 5.34$$

The  $\Delta\mu_I$  term remains unchanged for an absorbing coating.

Both  $\Delta\mu_I$  and  $\Delta\mu_R$  are expected to increase almost linearly with increasing material thickness. For a non-absorbing coating both damping processes are expected to increase at the same rate, whereas for an absorbing coating the inner damping is expected to increase at a greater rate than the radiation damping.

From the surface plasma oscillation theory it is possible to deduce that for a non-absorbing coating the surface plasmon resonance curves shift in angle with little or no change in resonance minimum shape for increasing thickness. Conversely, for an absorbing coating the curves shift in angle and decrease in resonance depth for increasing thickness. It is possible to calculate the shift in angle ( $\Delta\theta$ ) of the Langmuir-Blodgett coating curves ( $\theta_{sp}$ ) relative to the metal curves ( $\theta_0$ ) using a first order approximation (Pockrand 1978 (a)),

$$\Delta\theta = \frac{2\pi d_2}{\lambda} \frac{S_m}{n_0 \cos \theta_0} \left[ \varepsilon_2' \left( 1 + \frac{\varepsilon_1'}{\varepsilon_2'^2 + \varepsilon_2''^2} \right) - \varepsilon_1' - 1 \right] \quad 5.35$$

where  $S_m$  is a scaling factor dependant upon the characteristics of the metal and is given in the form,

$$S_m = \left( \frac{1}{-\varepsilon_1'} \right)^{1/2} \left( \frac{\varepsilon_1'}{\varepsilon_1' + 1} \right)^2 \left( \frac{1}{1 - \varepsilon_1'} \right) \quad 5.36$$

and  $n_0$  is the refractive index of the prism and all other variables and constants have been previously defined.

The half width of the surface plasmon resonance curve ( $\Delta\theta_{1/2}$ ) is given by,

$$\Delta\theta_{1/2} = \frac{2\pi d_2}{\lambda} \frac{S_m}{n_0 \cos \theta_0} \left[ \varepsilon_2'' \left( 1 - \frac{\varepsilon_1'}{\varepsilon_2'^2 + \varepsilon_2''^2} \right) \right] \quad 5.37$$

#### **5.2.4 Determination of film thickness and optical constants**

The angle  $\theta_{sp}$ , the minimum value of reflectivity ( $R_{min}$ ) and the width of the resonance curve can be used to determine the thickness, refractive index and extinction coefficient of the bare metal and hence the Langmuir-Blodgett film using a fitting procedure. The program performs a least square fit of the experimental data to theoretical curves using Fresnel's theory of the absolute reflected intensity.

#### **5.2.5 Surface Plasmon Resonance in AmPc5**

Typical surface plasmon resonance curves obtained for gold and 2,4,6 and 8 monolayers of AmPc5 are shown in Figure 5-37 with the fitting results shown as data marker overlaid on each curve. The fitting curves were obtained with very low error margins as can be seen by the level of coincidence of each experimental and theoretical curve. The results were obtained in terms of the refractive index ( $n$ ) and the extinction coefficient ( $k$ ) and are shown in Table 5-7 along with the film thickness ( $d$ ).

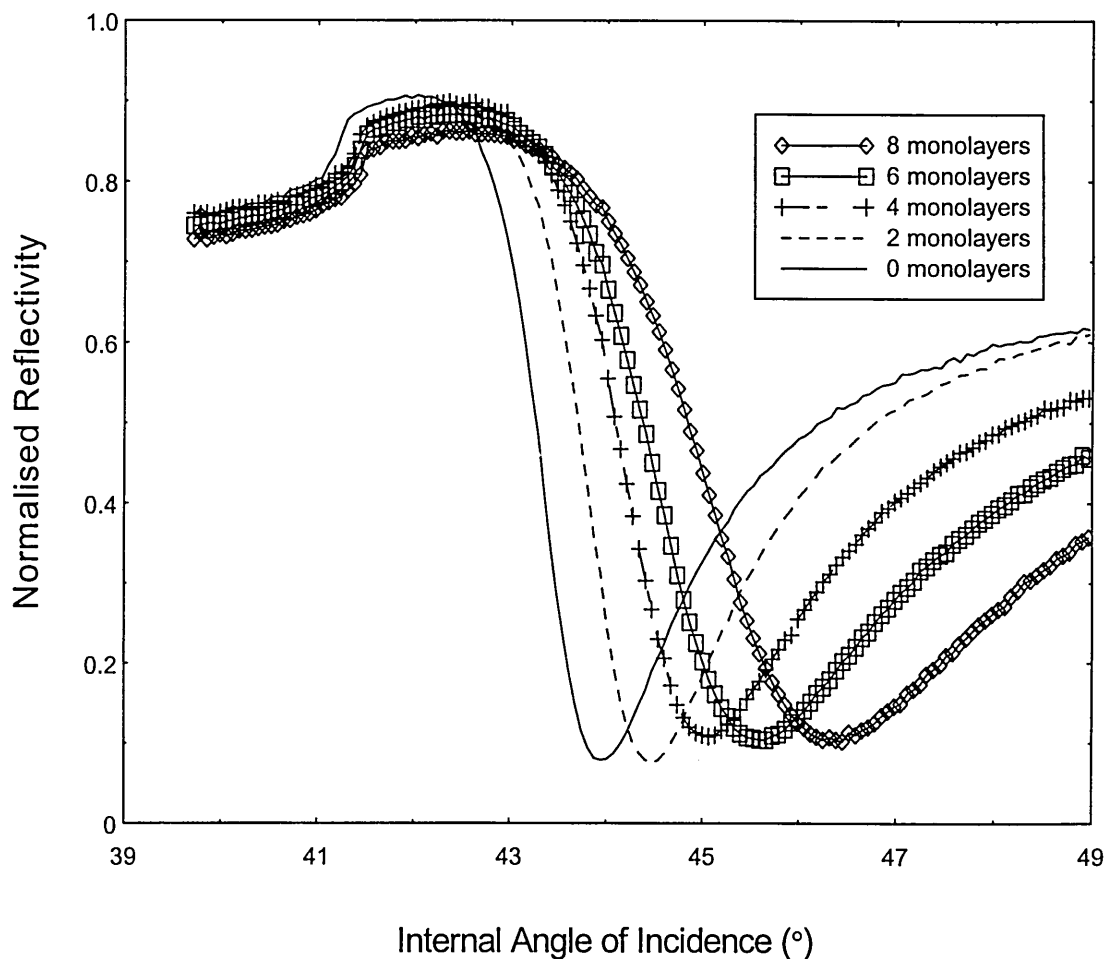


**Figure 5-37 The surface plasmon resonance curves for AmPc5 are shown with the fitting results overlaid as data markers**

Monolayer thickness	n	k	$\epsilon'$	$\epsilon''$	d (nm)
0 (bare gold)	0.385	3.446	-11.727	2.653	45.658
2	1.806	0.049	3.259	0.177	2.252
4	2.009	0.104	4.025	0.418	4.917
6	2.041	0.187	4.131	0.763	6.611
8	2.064	0.153	4.237	0.632	8.907

**Table 5-7 Refractive index, extinction coefficient and film thickness values for AmPc5 deposited in 2,4,6 and 8 Langmuir-Blodgett monolayers**

The values obtained for gold in this case can be compared with those obtained in Table 5-6. The slight variation in the values for  $n$  and  $k$  may result from different purities of the metal or the varying accuracy of fitting procedures. Also, variation from the optimum gold thickness (40 nm) results in different shaped curves, adding further to possible fitting inaccuracies.

From Table 5-7 a graph showing the increase in film thickness with number of monolayers ( $N$ ) can be plotted (Figure 5-38),

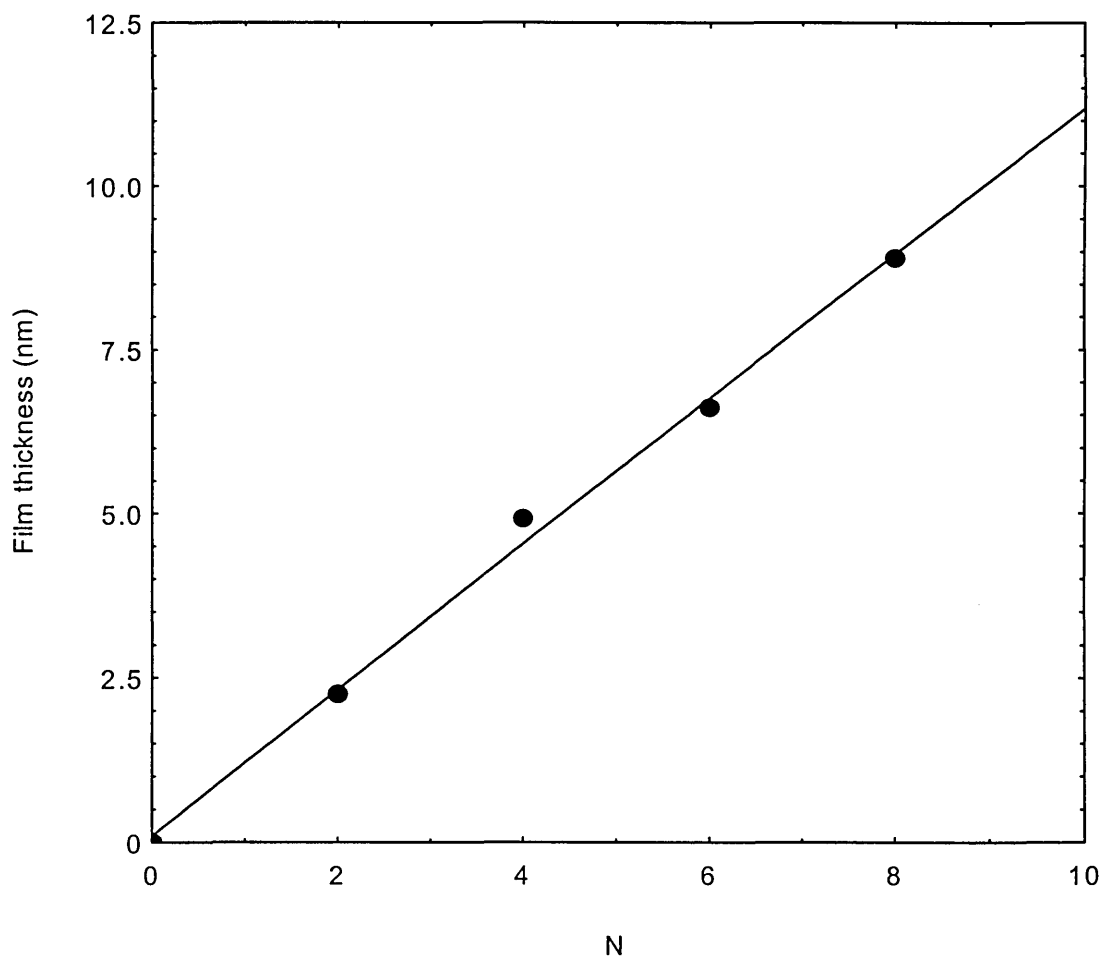


**Figure 5-38 Increase in film thickness with number of monolayers for AmPc5 obtained from surface plasmon resonance fitting data**

As this relation is linear the average monolayer thickness derived from surface plasmon resonance fitting is 1.11 nm.

From Table 5-7 it can be seen that there is a variation of  $n$  for Langmuir-Blodgett films of AmPc5 molecules with respect to the number of monolayers. This relationship can be observed in Figure 5-39 where it can be seen that for thinner films the value of  $n$  increases with increasing monolayer numbers. It then tends towards a steady value of approximately 2.0 which can be said to be close to the bulk refractive index. A similar dependence has been observed for a novel octa-substituted phthalocyanine from the same family (Ray et al 1998), reaching a steady state refractive index value of 1.6. From Figure 5-39 it can be assumed that the molecular packing and possibly the orientation relative to the substrate within the first few monolayers differs from Langmuir-Blodgett films containing many monolayers. The value of the steady state refractive index obtained is higher than obtained for phthalocyanines of the same family (Hibberd 1996, Ray et al 1998) which is consistent with the observation that the optical absorption spectra of AmPc5 are significantly different, implying a different stack structure.

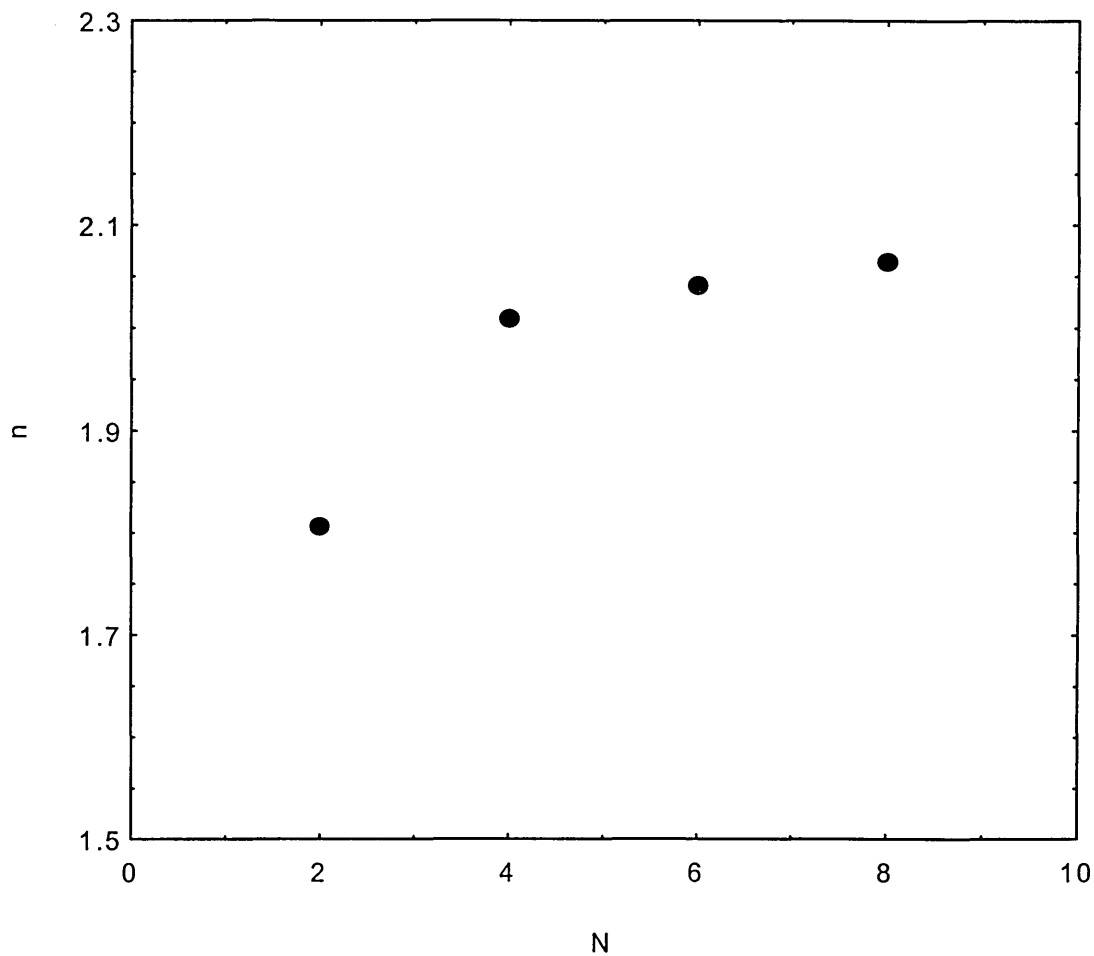


**Figure 5-39 Variation of refractive index (n) with number of monolayers (N) of AmPc5 Langmuir-Blodgett films**

The surface plasmon resonance curve obtained for bare gold in Figure 5-37 reaches an intensity minimum of 0.078 at an angle  $\theta_0$  of  $\sim 44^\circ$ . This slightly decreased reflection minimum is expected as the gold film is thicker than the optimum of 40 nm. The thicker film results in weaker coupling and an increase in the radiation damping. The half width of the curve ( $\theta_{1/2}$ ) was found to be approximately  $1.7^\circ$ . This was also expected as broader, shallower resonance minima only occur in films thinner than 400 nm. Surface plasmon resonance curves have been measured for gold films of thicknesses ranging from 20 to 75 nm (Pokrowsky 1991). For 40 nm,  $\theta_0$  was found to be at approximately

43.5° and for 50 nm at approximately 44.25°. The value of  $\theta_0$  measured in the current experiment for gold is found to agree well with this published data.

The gold substrates were prepared by evaporation in a vacuum controlled unit with a quartz crystal oscillator used as a thickness measurement device. All samples were evaporated to a thickness of 40 nm to ensure ideal experimental conditions. Upon surface plasmon resonance measurement and subsequent data fitting, the curves were found to differ significantly as shown below in Figure 5-40. Curve (a) is the curve described in Figure 5-37 and curve (b) from a different sample. Obviously curve (b) represents a thinner films as the reflection minimum is broader and shallower. The crystal monitor was found to have an error margin of  $\pm 5$  nm which was taken into consideration when performing data fitting.

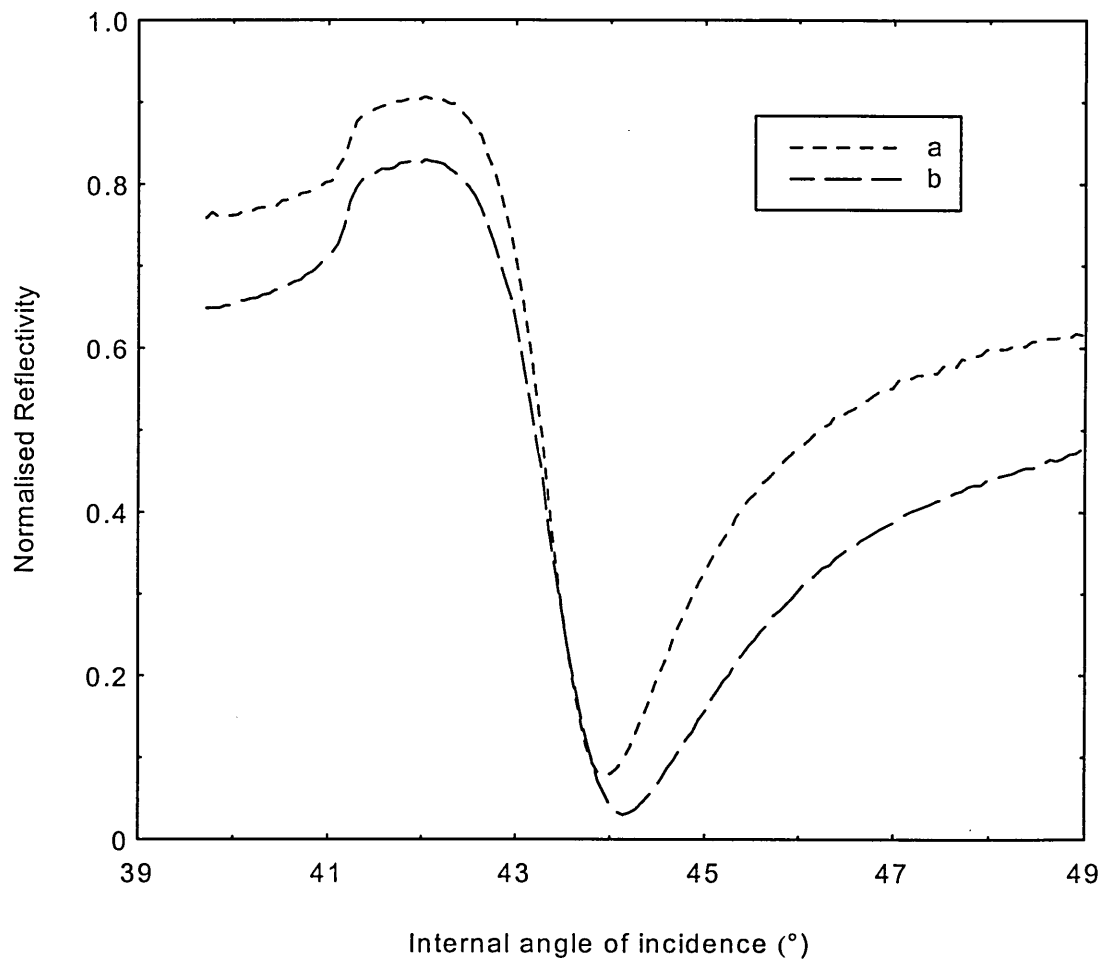


**Figure 5-40 Surface plasmon resonance curves for gold measured on sample (a) and (b)**

The quantities  $\Delta\theta$  and  $\Delta\theta_{1/2}$  defined previously in equations 5.35 and 5.37 can be measured using the surface plasmon resonance curves in Figure 5-37. This yields the results shown in Figure 5-41 and Figure 5-42 where the experimental and calculated theoretical data points are represented. It should be noted that the calculated values of  $\Delta\theta$  and  $\Delta\theta_{1/2}$  must be multiplied by a factor of 180 to enable comparison with results measured in degrees rather than radians.

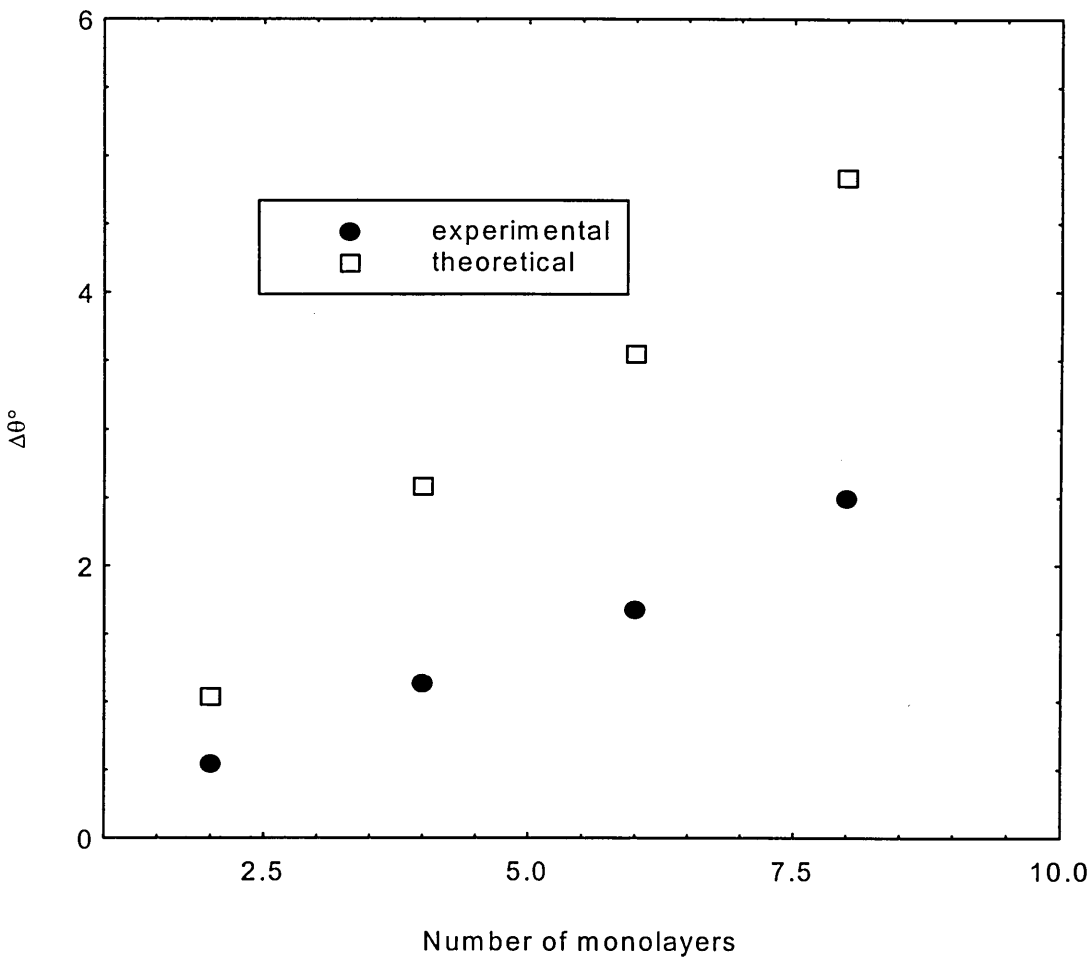


**Figure 5-41 Experimental and theoretical shifts in  $\theta$  relative to bare gold film**

The graph showing broadening of the half width can be seen in Figure 5-42. There is a small error margin between the predicted and experimental values obtained for both  $\Delta\theta$  and  $\Delta\theta_{1/2}$ . Study of the absorption spectra of AmPc5 in Figure 5-9 shows relatively low levels of absorbance at the He-Ne laser wavelength, 633 nm. The equations 5.26 to 5.31 represent the dispersion relation for absorbing materials only, whereas at 633 nm AmPc5 exhibits mild absorbance which has resulted in the slight discrepancy. Surface plasmon resonance interrogation at the peak of absorbance, 733 nm, would follow the relation more accurately. The shapes of both experimental curves have the same general shape as the theoretical curves implying that the model is applicable even at the low absorbance values.

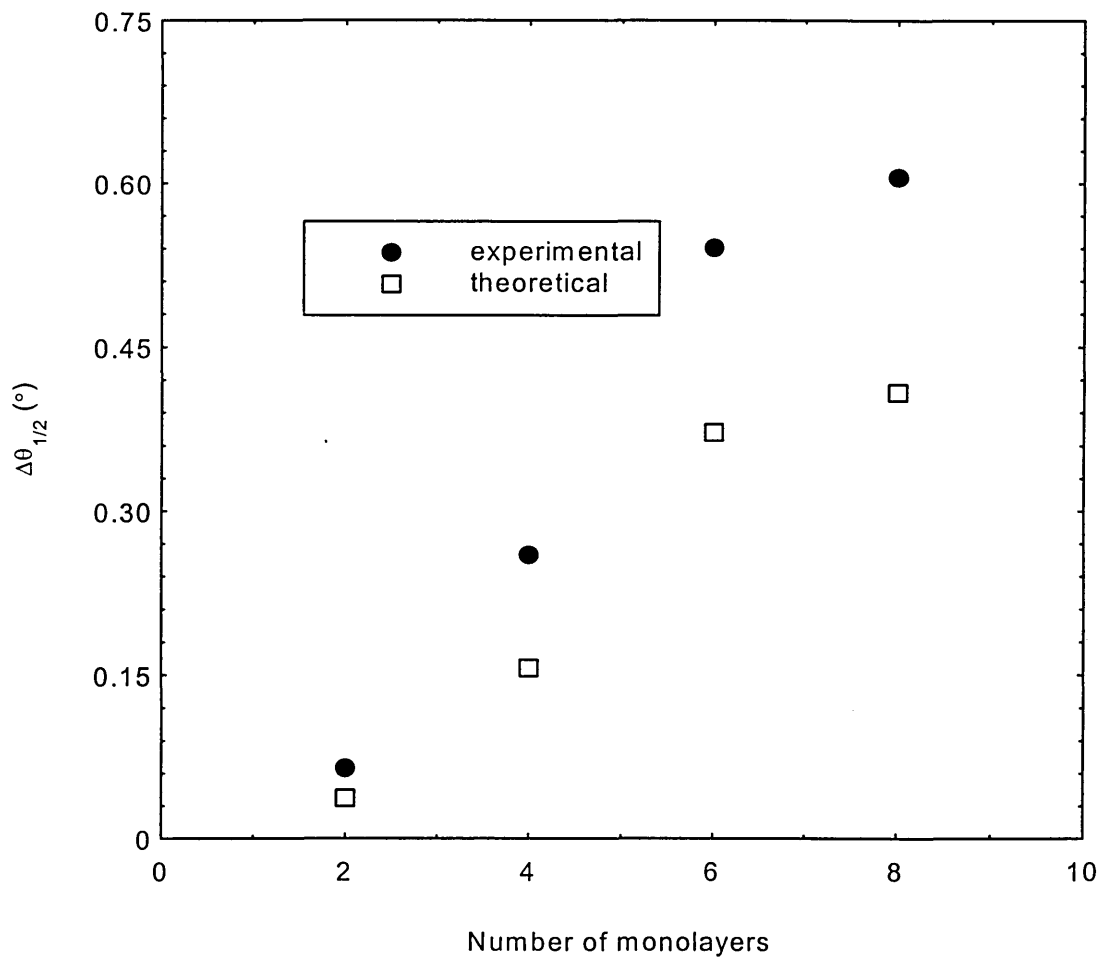


**Figure 5-42 Half width broadening in monolayers of AmPc5**

The phase velocity of the evanescent waves is given in equation 5.22 and is shown in Figure 5-43.

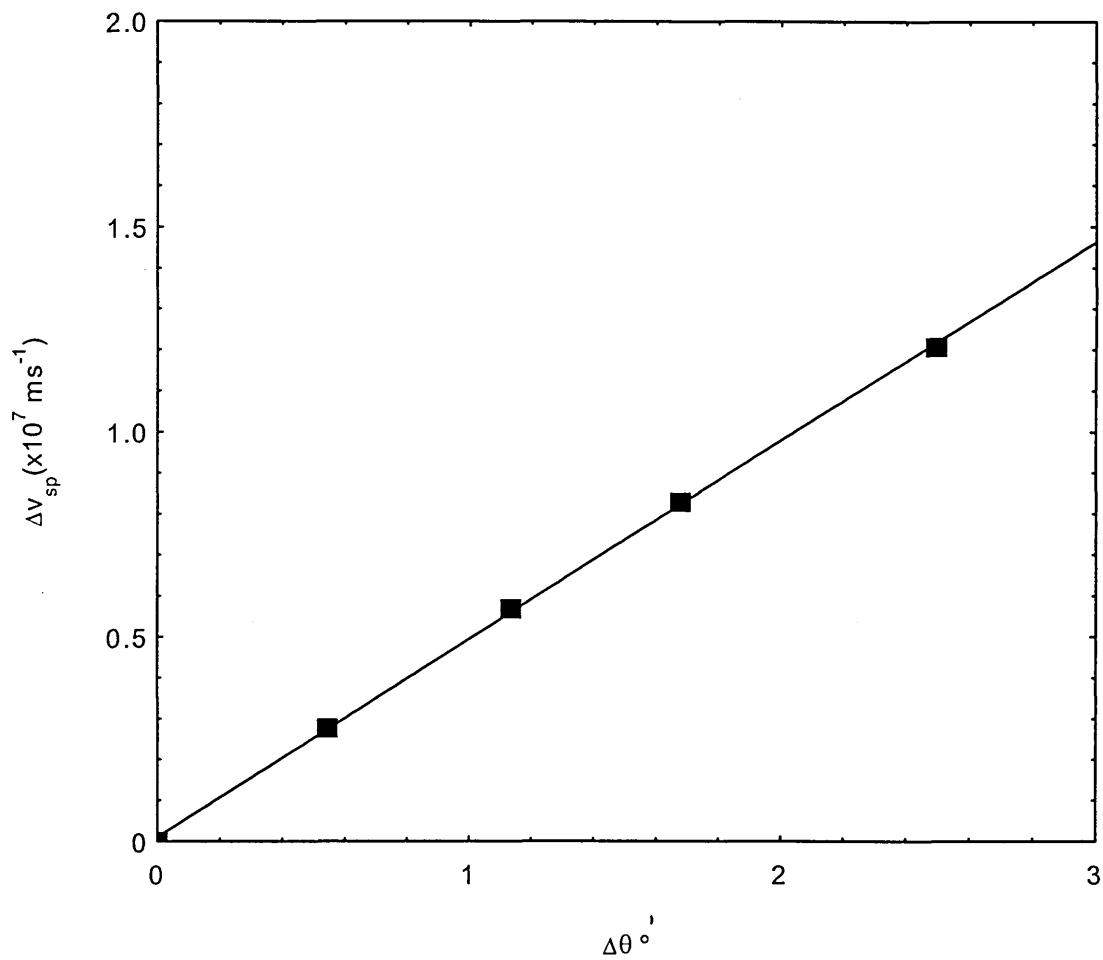


Figure 5-43 A plot of  $\Delta v_{sp}$  as a function of  $\Delta\theta$

All measured values are tabulated below in Table 5-8,

N	$\theta^\circ$	$\Delta\theta^\circ$	$\theta_{1/2}^\circ$	$\Delta\theta_{1/2}^\circ$	$v_{sp}$ ( $\times 10^7$ ms $^{-1}$ )	$\Delta v_{sp}$ ( $\times 10^7$ ms $^{-1}$ )
0	43.9456	0	1.7089	0	28.5521	0
2	44.4882	0.5426	1.7737	0.0648	28.2755	0.2766
4	45.0779	1.1323	1.9684	0.2595	27.9838	0.5683
6	45.6204	1.6748	2.2496	0.5407	27.7233	0.8288
8	46.4381	2.4925	2.3145	0.6056	27.3442	1.2079

Table 5-8 Table of measured angular values for surface plasmon resonance curves of AmPc5

The dispersion relation terms for absorbing AmPc5 have been calculated and are given below in Table 5.9. The ratios  $\Delta\mu_i$  and  $\Delta\mu_R$  are also given from equations 5.32 and 5.33 are also given. As the terms  $k_x^{(0)}$ ,  $k_x^{(1)R}$  and  $k_x^{(2)R}$  have no coating variables they are not thickness dependant and can be stated as constant for a given metal coating. Hence,

$$k_x^{(0)} = 1.0374 \times 10^7 + (1.0426 \times 10^5)i$$

$$k_x^{(1)R} = -1.637 \times 10^4 + (7.8947 \times 10^3)i$$

$$k_x^{(2)R} = -7.3561 \times 10^4 - (1.5327 \times 10^5)i$$

N	$k_x^{(1)C}$ ( $\times 10^4$ $m^{-1}$ )	$k_x^{(2)C}$ ( $\times 10^3$ $m^{-1}$ )	$k_x^{(1)CR}$ ( $\times 10^2$ $m^{-1}$ )	$\text{Im}(k_x^{(0)}) -$ $k_x^{(2)C} +$ $k_x^{(1)C}$ ( $\times 10^5$ $m^{-1}$ )	$\text{Im}(k_x^{(1)R}) -$ $k_x^{(1)CR}$ ( $\times 10^3 m^{-1}$ )
2	-0.5546 + 0.1047i	0.0443 - 0.6429i	0.9949 - 0.7150i	1.0595	7.9647
4	-1.3628 + 0.2225i	0.6420 - 1.5328i	2.6175 - 1.7460i	1.0802	8.0693
6	-1.8877 + 0.2230i	1.5356 - 1.4695i	3.775- 2.1951i	1.0796	8.1142
8	-2.5631 + 0.3555i	3.2908 - 2.1356i	5.0759 - 3.1431i	1.0995	8.2090

**Table 5-9 Dispersion relation parameters for 2, 4, 6 and 8 monolayers of AmPc5**

The two graphs produced showing the dependence of  $\mu_R$  and  $\mu_i$  on monolayer thickness are shown in Figure 5-44 and Figure 5-45.

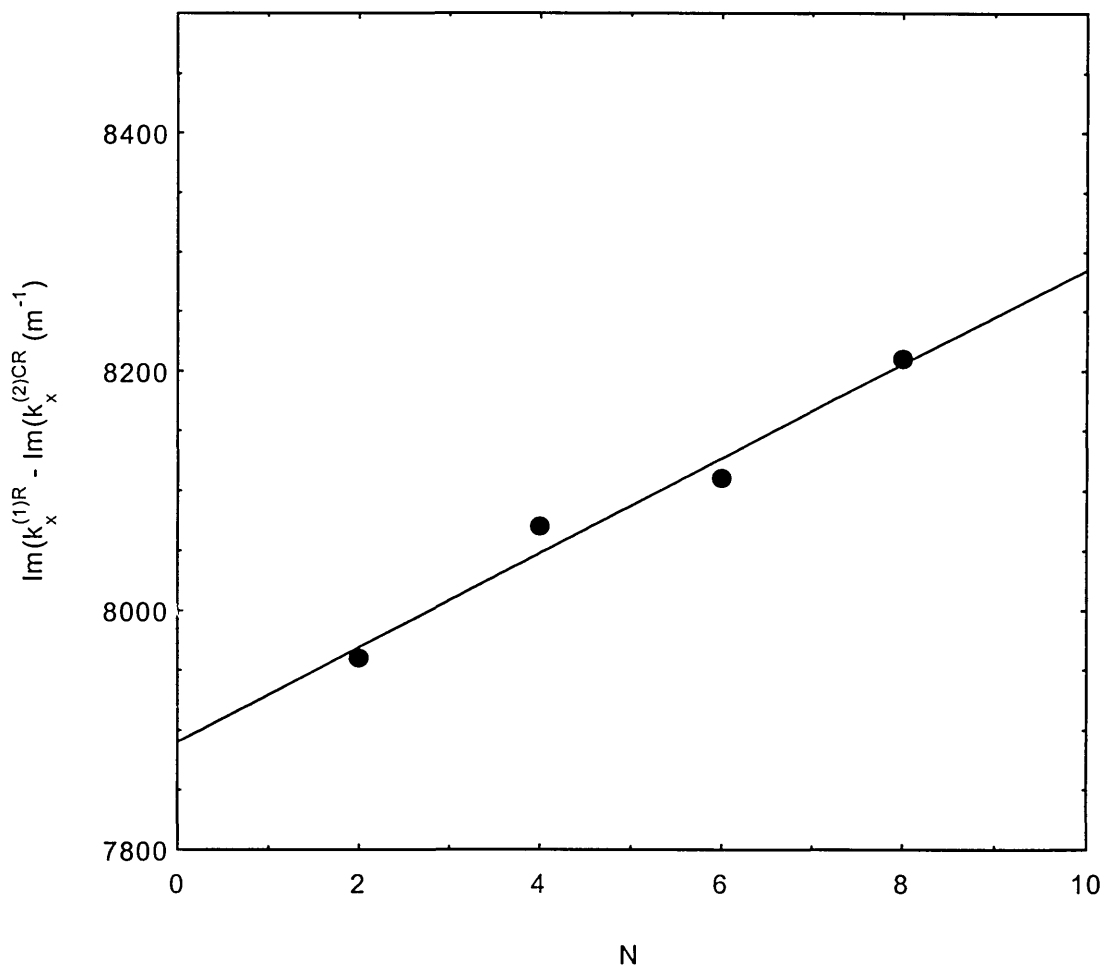


**Figure 5-44 Graph showing the changes in radiation damping due to increase in number of monolayers of AmPc5**

Both the inner and radiation damping effects are found to increase linearly with AmPc5 film thickness, as expected. The inner damping is greater than the radiation damping by one order of magnitude irrespective of the thickness, whereas the rate of increase of inner damping is approximately 15 times that of the rate of increase in radiation damping. These results are comparable with those obtained for a phthalocyanine from the same family (Ray et al 1998).  $\mu_i$  was found to be greater than  $\mu_R$  by one order of magnitude with the rate of increase roughly 18 times greater. This greater increase is due to the greater absorbance at the He-Ne laser wavelength.

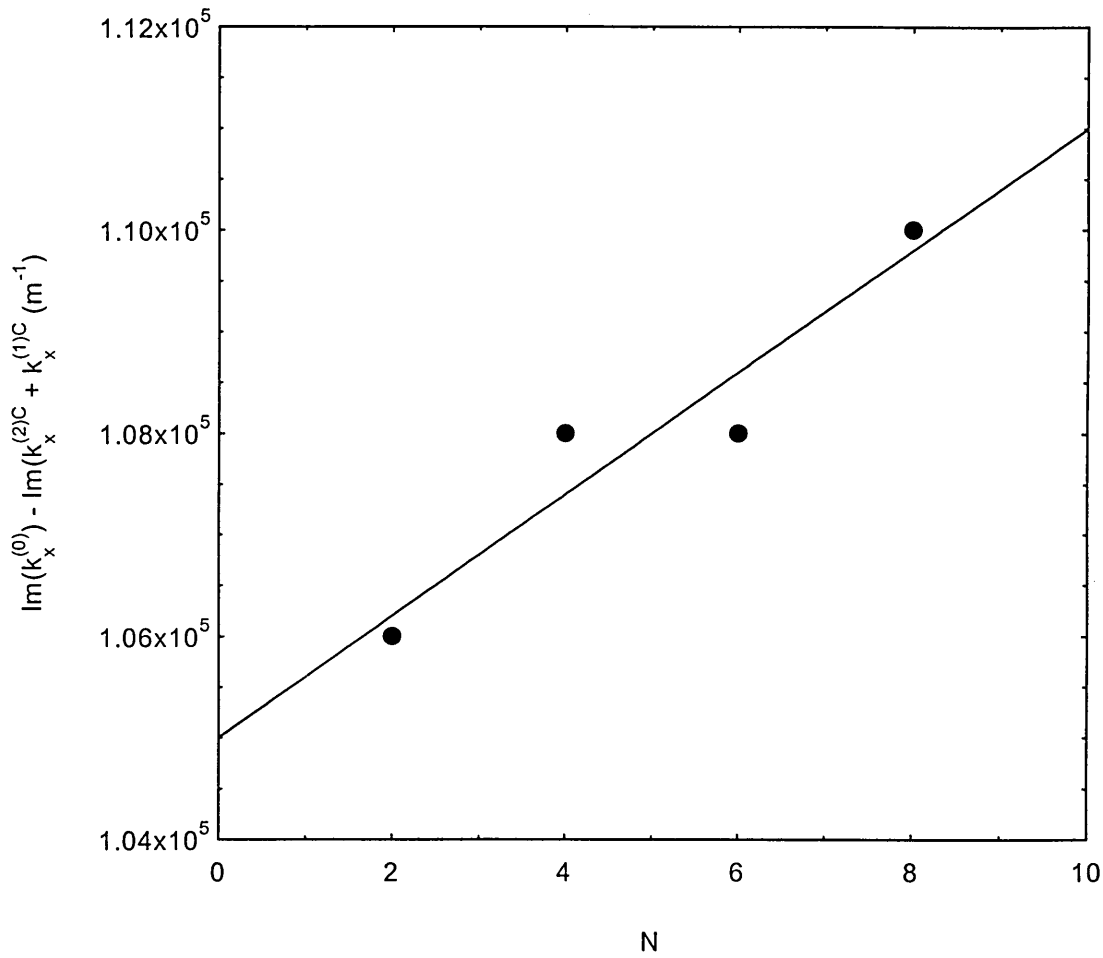


**Figure 5-45 Graph showing the changes in inner damping with respect to number of monolayers of AmPc5**

The value of  $\Delta R_{\min}$  is the difference between the reflected intensity  $R_{\min}$  for the bare gold film and that for the metal film with AmPc5 overlayers. These values are calculated and are given in Table 5-10. The ratio,  $\gamma$ , is given by the ratio of  $\mu_R$  and  $\mu_I$ ,

$$\gamma = \frac{\Delta\mu_I}{\Delta\mu_R} = \frac{\text{Im}(k_x^{(0)R}) - \text{Im}(k_x^{(2)C}) + k_x^{(1)C}}{\text{Im}(k_x^{(1)R}) - \text{Im}(k_x^{(2)CR})} \quad 5.38$$

The values for  $\gamma$  are calculated using the surface plasmon curves in Figure 5-37 and are given in Table 5-10.

N	$R_{\min}$	$\Delta R_{\min}$	$\gamma$
0	0.0765	0	
2	0.0765	0	13.3024
4	0.1072	0.0307	13.3865
6	0.1072	0.0307	13.3851
8	0.1072	0.0307	13.3938

**Table 5-10 Measured values for  $\Delta R_{\min}$  and  $\gamma$  for AmPc5 monolayers**

A plot of  $\Delta R_{\min}$  and  $\gamma$  is shown in Figure 5-46. It can be seen that the  $\Delta R_{\min}$  variation follows the same pattern as the variation in  $\gamma$ . This is an expected observation as the change in depth of resonance is dependant upon the ratio of the change in inner damping to radiation damping due to the AmPc5 coating. For an absorbing medium both  $\Delta R_{\min}$  and  $\gamma$  are expected to increase linearly with film thickness. From Figure 5-46 it is apparent that the variation does not increase linearly, but reaches a plateau after 4 monolayers. This effect arises from the low absorbance of AmPc5 at 633 nm.

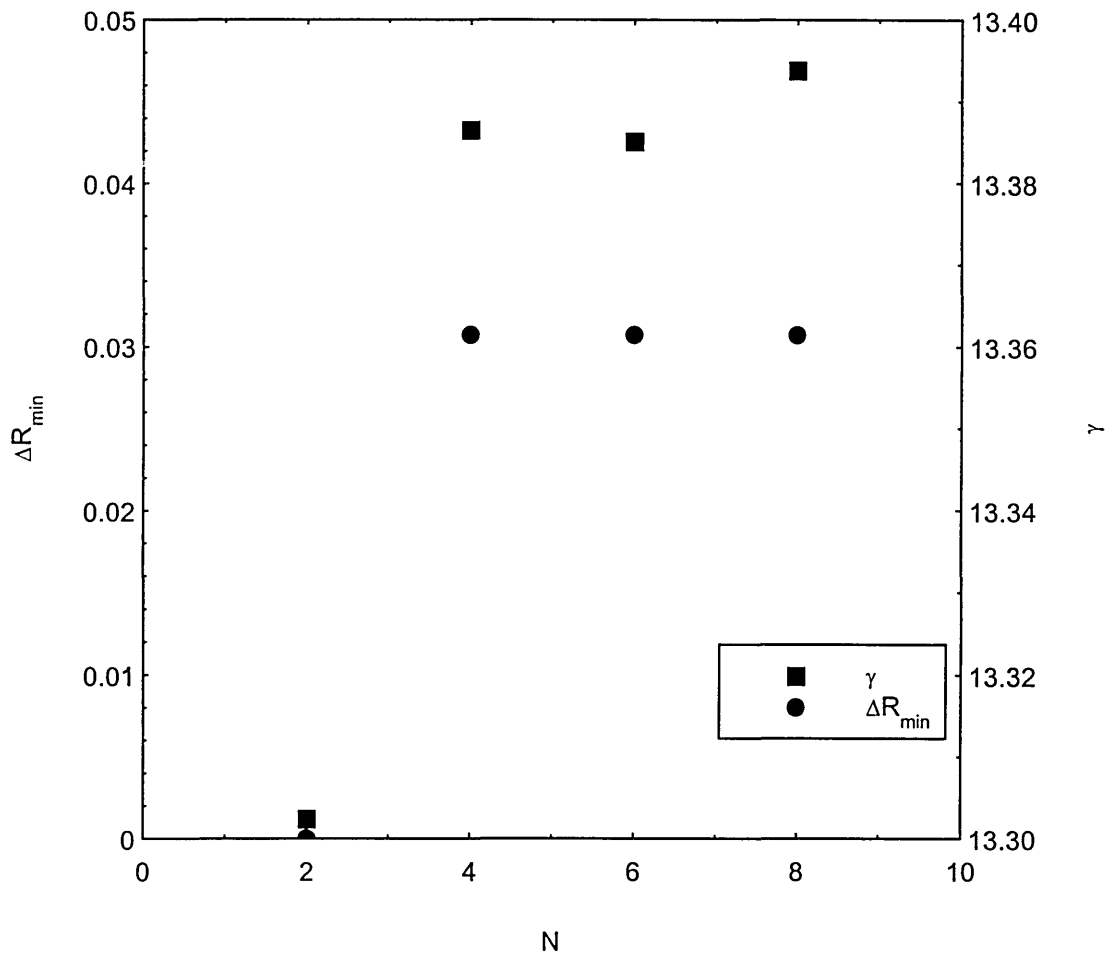


**Figure 5-46 Variation of  $\Delta R_{\min}$  and  $\gamma$  with monolayer thickness of AmPc5**

### 5.2.6 Surface plasmon resonance in AmAz1

Surface plasmon resonance curves and theoretical data of AmAz1 deposited onto gold coated glass substrates can be found in Omar et al (Omar et al 1997). In the present section surface plasmon resonance measurements of AmAz1 deposited onto silver coated substrates have been measured for comparison purposes. Typical measurements are shown in Figure 5-47 with the surface plasmon resonance fitting data overlaid as squares.

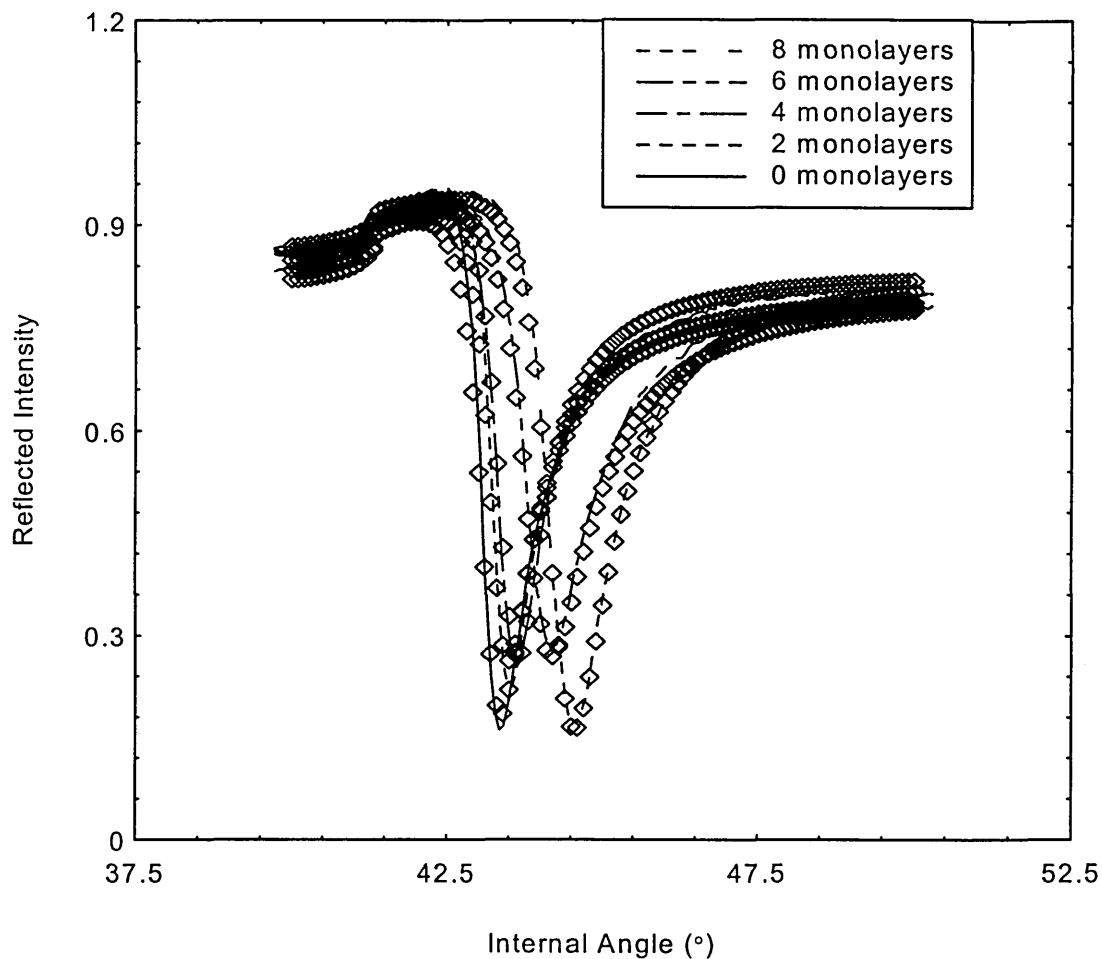


**Figure 5-47 Experimental surface plasmon resonance curves of AmAZ1 overlaid with theoretical curves obtained from the fitting procedure**

The curves display a relatively small shift in angle and minor change in curve shape with increasing film thickness. There is also a decrease in resonance minimum with thickness, although this is shown to be non-uniform. This effect arises from the variation in silver coating thickness and not from the Langmuir-Blodgett overlayer. This variation can be taken into account for each measurement within the fitting procedure.

As with AmPc5 the level of coincidence of the theoretical and experimental curves indicates a high level of accuracy in determination. The results are shown in Table 5-11 in terms of  $n$ ,  $k$  and  $d$ .

Monolayer thickness	n	k	$\epsilon'$	$\epsilon''$	d (nm)
0 (bare silver)	0.159	3.791	-14.346	1.183	50.056
2	1.356	0.002	1.839	0.004	4.072
4	1.371	0.020	1.879	0.0549	5.530
6	1.436	0.037	2.061	0.106	9.409
8	1.420	0.025	2.016	0.071	13.609

**Table 5-11 Refractive index, extinction coefficient and film thickness values for AmAz1 deposited in 2, 4, 6 and 8 Langmuir-Blodgett monolayers**

The complex refractive index value obtained for bare silver differs from those in the literature (Table 5-12) which can be attributed to tarnishing of the silver surface due to environmental conditions.

Author	n	k	d (nm)
Sambles 1991	0.08	4.652	24.5
Pockrand 1978 (b)	0.088	4.184	60.0

**Table 5-12 N, k and d values of silver**

The increase in thickness with the number of monolayers (N) determined from the surface plasmon fitting data is shown in Figure 5-48. This linear relationship allows the average monolayer thickness for AmAz1 1.63 nm, to be found. This is in excellent agreement with the 1.60 nm monolayer thickness value obtained from surface plasmon resonance data for AmAz1 Langmuir-Blodgett films deposited on gold (Omar et al 1997).

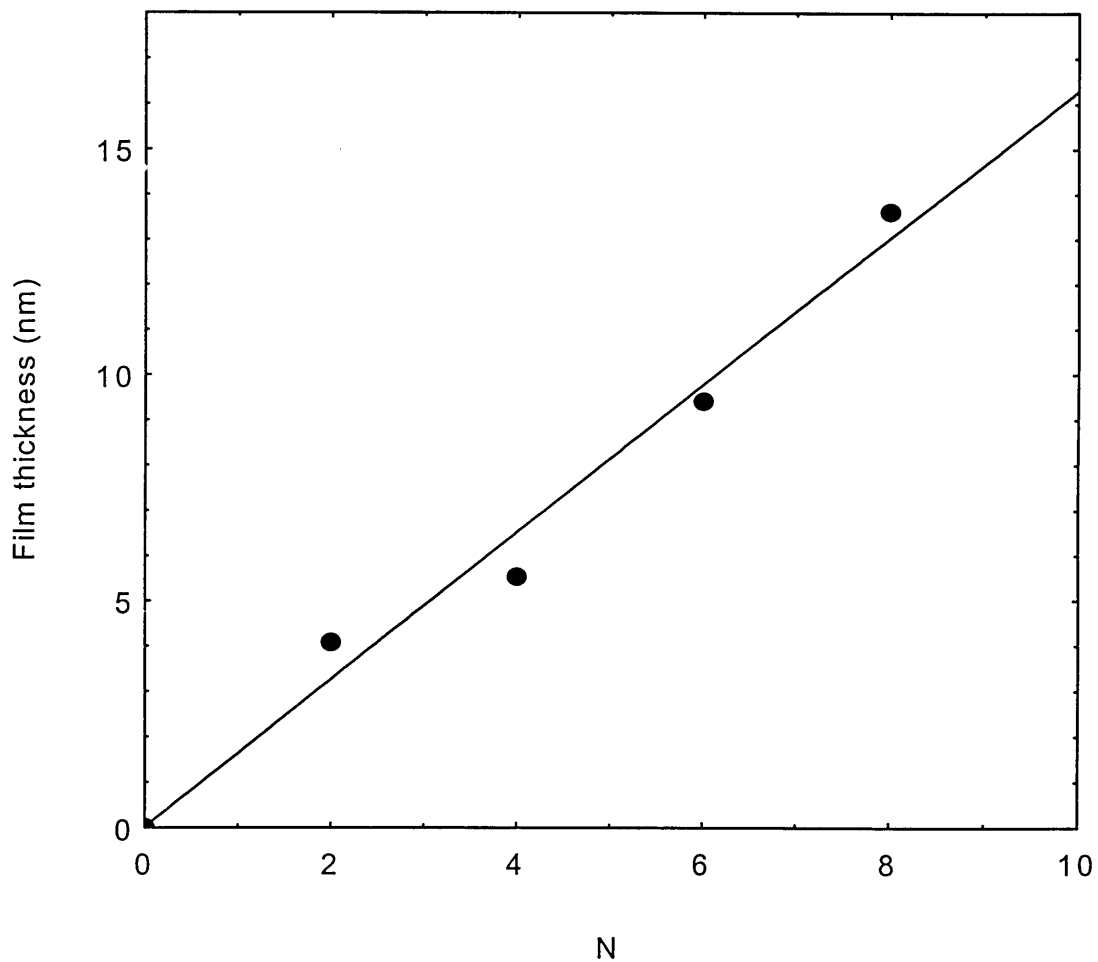


**Figure 5-48 Increase in film thickness of AmAz1 with monolayers deposited determined using surface plasmon resonance data**

As with AmPc5 there is a variation in refractive index with number of monolayers, which is shown in Figure 5-49. The refractive index increases with fewer monolayers and reaches a steady state value of approximately 1.43. Similarly, this implies that the packing in the thinner films of AmAz1 differs from that in thicker films. The packing also varies when considering different substrates. The Langmuir-Blodgett films of AmAz1 on gold coated substrates (Omar et al 1997) have a refractive index of 1.35, which implies an alternative type of structure.

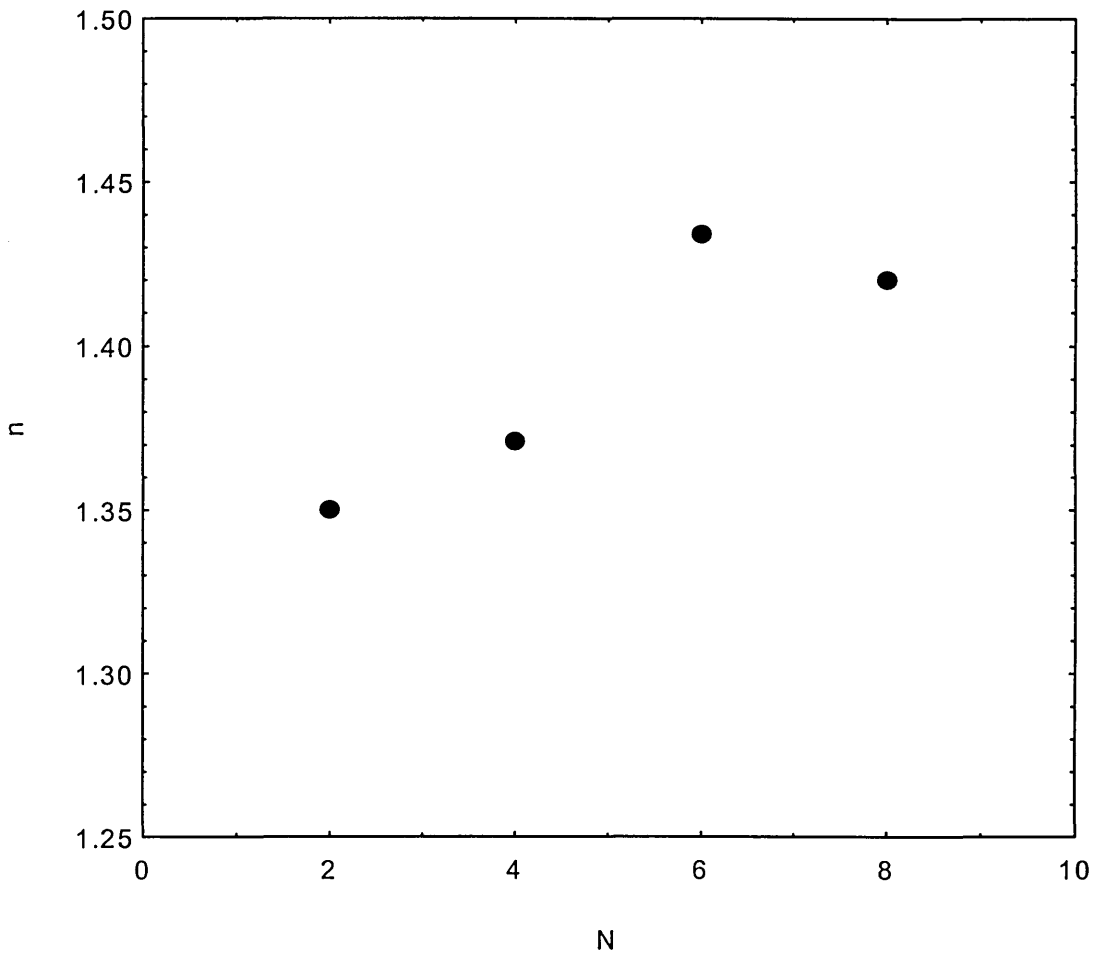


**Figure 5-49 Refractive index variation with increasing number of Langmuir-Blodgett monolayers of AmAz1**

The surface plasmon resonance curve measured from pure silver shown in Figure 5-47 reaches an intensity minimum of 0.165 at  $43.365^\circ$ . The deviation of the intensity minimum value from zero indicates a thinner silver coating than the optimum for surface plasmon resonance. The half width of the curve is estimated at  $0.9^\circ$  which indicates significant broadening as compared to curves obtained for silver by Pockrand (Pockrand 1978 (b)), with a  $\theta_{1/2}$  value of  $0.43^\circ$ . This broadening of the curve is attributable to the oxidation of the silver and adsorption of environmental pollutants into the coating.

The silver coated substrates were prepared in a similar manner to the gold coated substrates in section 5.2.4.

As with AmPc5, the quantities  $\Delta\theta$  and  $\Delta\theta_{\lambda}$  of AmAz1 can be measured using the surface plasmon resonance curves in Figure 5-47, as shown in Figure 5-50 and Figure 5-51.

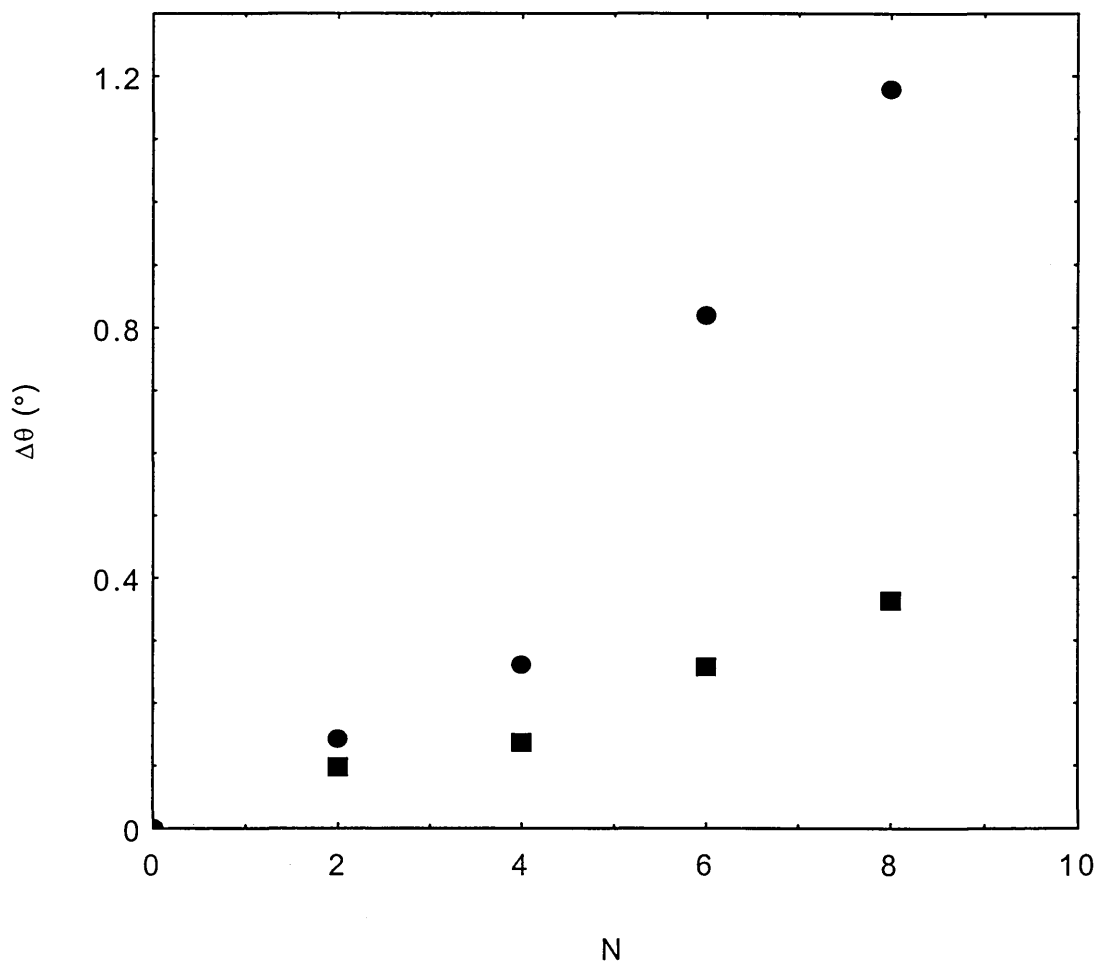
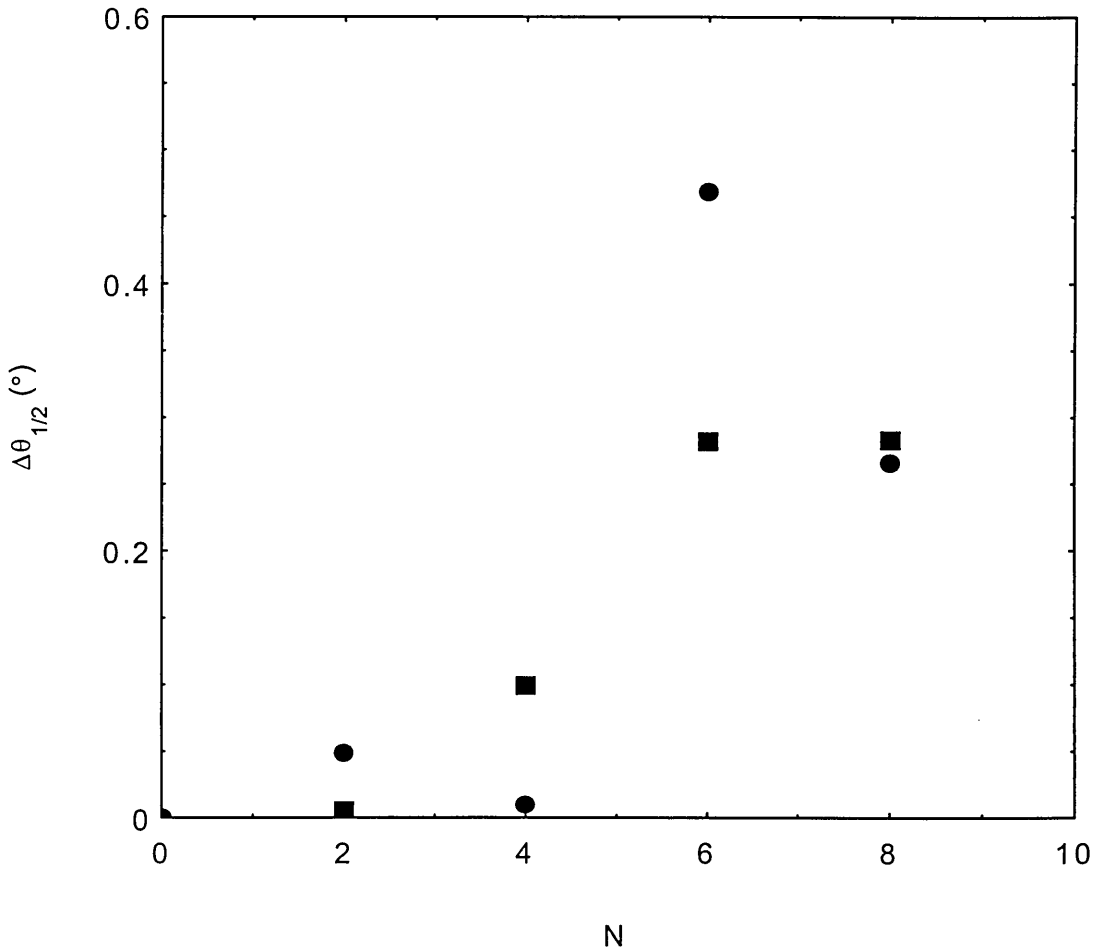


Figure 5-50 Experimental (●) and theoretical (■) shifts in  $\theta$  for AmAz1 relative to bare silver film

Both experimental and theoretical values of  $\Delta\theta$  are found to increase with thickness, although the experimental values increase more rapidly than the theoretical. The theoretical values calculated using the model for non-absorbing materials follow the behaviour of such films at lower thicknesses (Pockrand 1978 (b)).

The experimentally obtained data follow the general theoretical curve shape with influences from the absorbing model. Study of the absorbance spectra in Figure 5-14 reveals slight absorbance at a wavelength of 633 nm, resulting in the contribution from the absorbing surface plasmon resonance model.



**Figure 5-51 Experimental (●) and theoretical (■) half width broadening in Langmuir-Blodgett films of AmAz1**

The theoretical half width broadening curve for AmAz1 follows the general pattern for non-absorbing coatings, although the broadening takes place at much lower film thicknesses due to the influence of absorbance. The experimental values appear to follow the pattern for non-absorbing coatings more closely than the theoretical (Pockrand 1978 (b)).

The increase in phase velocity of the evanescent waves from equation 5.22 is given below in Figure 5-52, and is shown to be linear for a given shift in surface plasmon resonance angle.

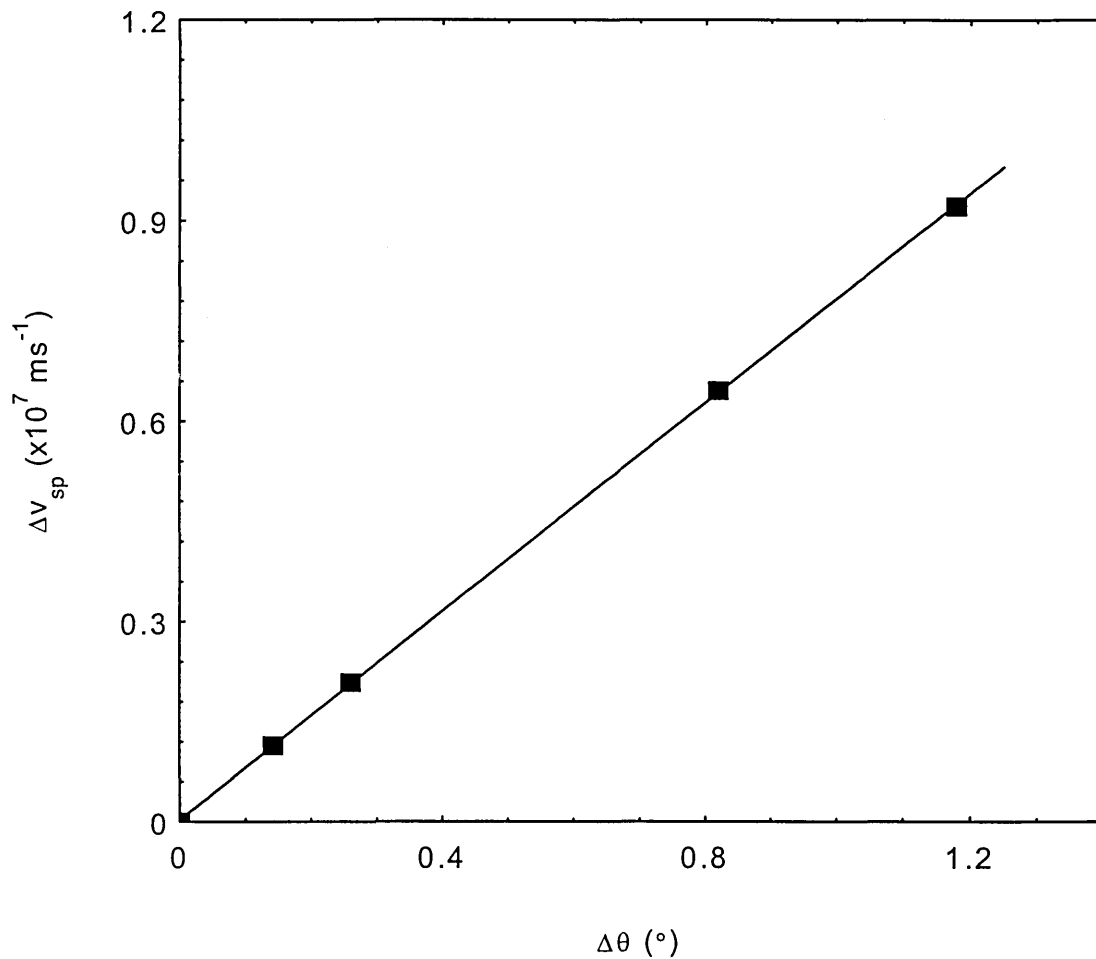


**Figure 5-52 Phase velocity increase as a function of  $\Delta\theta$  for AmAz1**

The experimentally obtained values are tabulated below in Table 5-13.

N	$\theta^\circ$	$\Delta\theta^\circ$	$\theta_{1/2}^\circ$	$\Delta\theta_{1/2}^\circ$	$v_{sp}$ ( $\times 10^7$ $\text{ms}^{-1}$ )	$\Delta v_{sp}$ ( $\times 10^7$ $\text{ms}^{-1}$ )
0	43.3761	0	0.9198	0	43.6516	0
2	43.5182	0.1421	1.1514	0.2514	43.5375	0.1141
4	43.6365	0.2604	1.2095	0.3095	43.4431	0.2085
6	44.1952	0.8191	1.6682	0.7680	43.0053	0.6463
8	44.5550	1.1789	1.4655	0.5650	42.7302	0.9214

**Table 5-13 Tabulated measured angular values for surface plasmon resonance curves of AmAz1**

The coating thickness dependant dispersion relation terms for non-absorbing AmAz1 have been calculated and are given below in Table 5-14. The thickness independent terms, constant for a given metal coating are given below,

$$k_x^{(0)} = 1.0308 \times 10^7 + (3.1801 \times 10^4)i$$

$$k_x^{(1)R} = -6.3953 \times 10^3 + (3.8037 \times 10^3)i$$

$$k_x^{(2)R} = -1.8542 \times 10^4 - (3.1300 \times 10^4)i$$

N	$k_x^{(1)C}$ ( $\times 10^4$ $m^{-1}$ )	$k_x^{(2)C}$ ( $\times 10^3$ $m^{-1}$ )	$k_x^{(1)CR}$ ( $\times 10^2$ $m^{-1}$ )	$\text{Im}(k_x^{(0)} -$ $k_x^{(2)C})$ ( $\times 10^4$ $m^{-1}$ )	$\text{Im}(k_x^{(1)R} -$ $k_x^{(1)CR})$ ( $\times 10^3 m^{-1}$ )
2	-1.0089 + 0.0803i	0.0430 - 0.4279i	0.7616 - 0.5379i	3.2229	3.8575
4	-2.0090 + 0.091i	0.2731 - 0.8460i	1.5785 - 1.0085i	3.2647	3.9045
6	-2.6465 + 0.0716i	0.5777 - 1.0767i	2.1896 - 1.3290i	3.2878	3.9366
8	-3.0435 + 0.1308i	0.7257 - 1.2827i	2.4652 - 1.5674i	3.3084	3.9604

**Table 5-14 Dispersion relation parameters for 2,4,6 and 8 monolayers of AmAz1**

The dependence of  $\mu_R$  and  $\mu_I$  on film thickness is shown in Figure 5-53 and Figure 5-54.

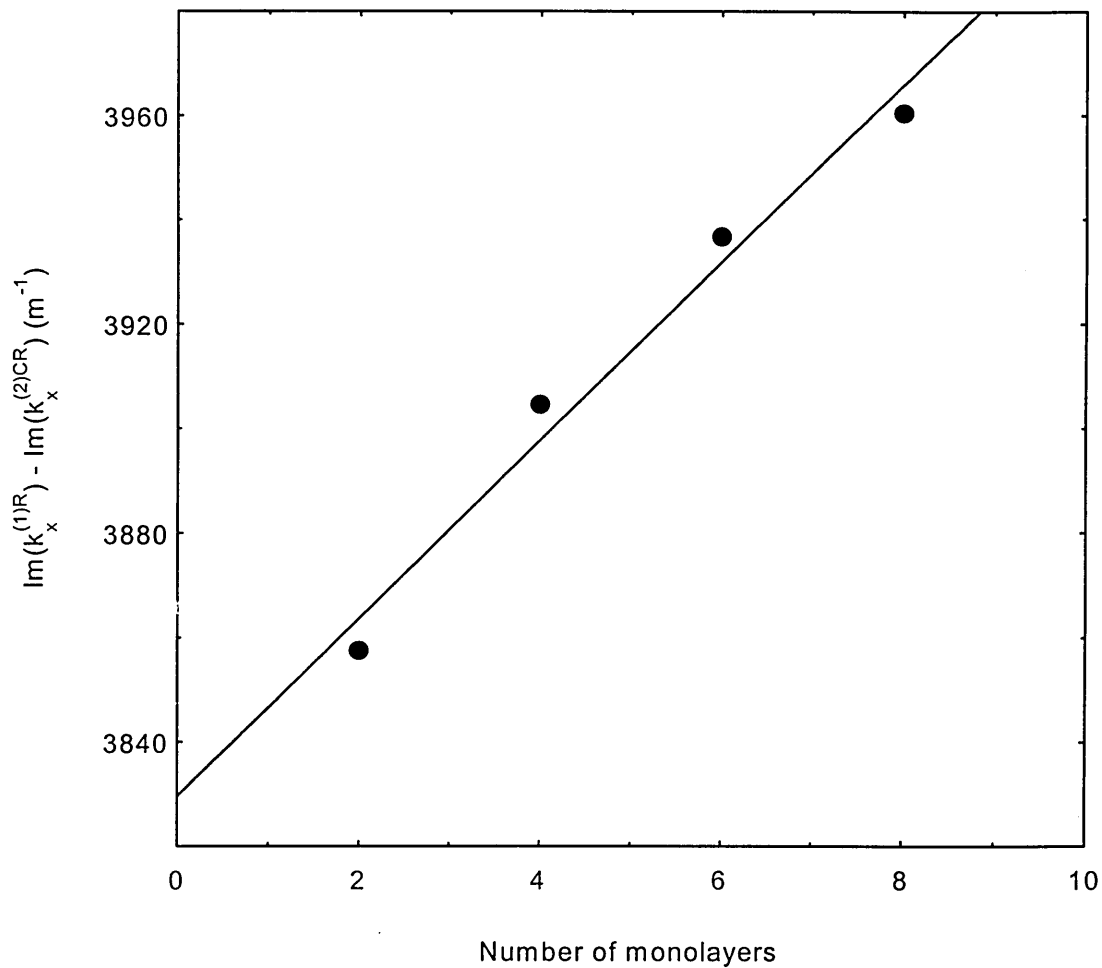


**Figure 5-53 Graph showing the changes in radiation damping due to increase in number of monolayers of AmAz1**

The inner and radiation damping processes are found to increase linearly with film thickness with the radiation damping being approximately ten times greater than the inner damping. The rate of increase of inner damping equals the rate of increase of radiation damping, where this behaviour follows the theoretical model of non-absorbing materials. The inner and radiation damping are altered by the same amount due to the Langmuir-Blodgett coating.

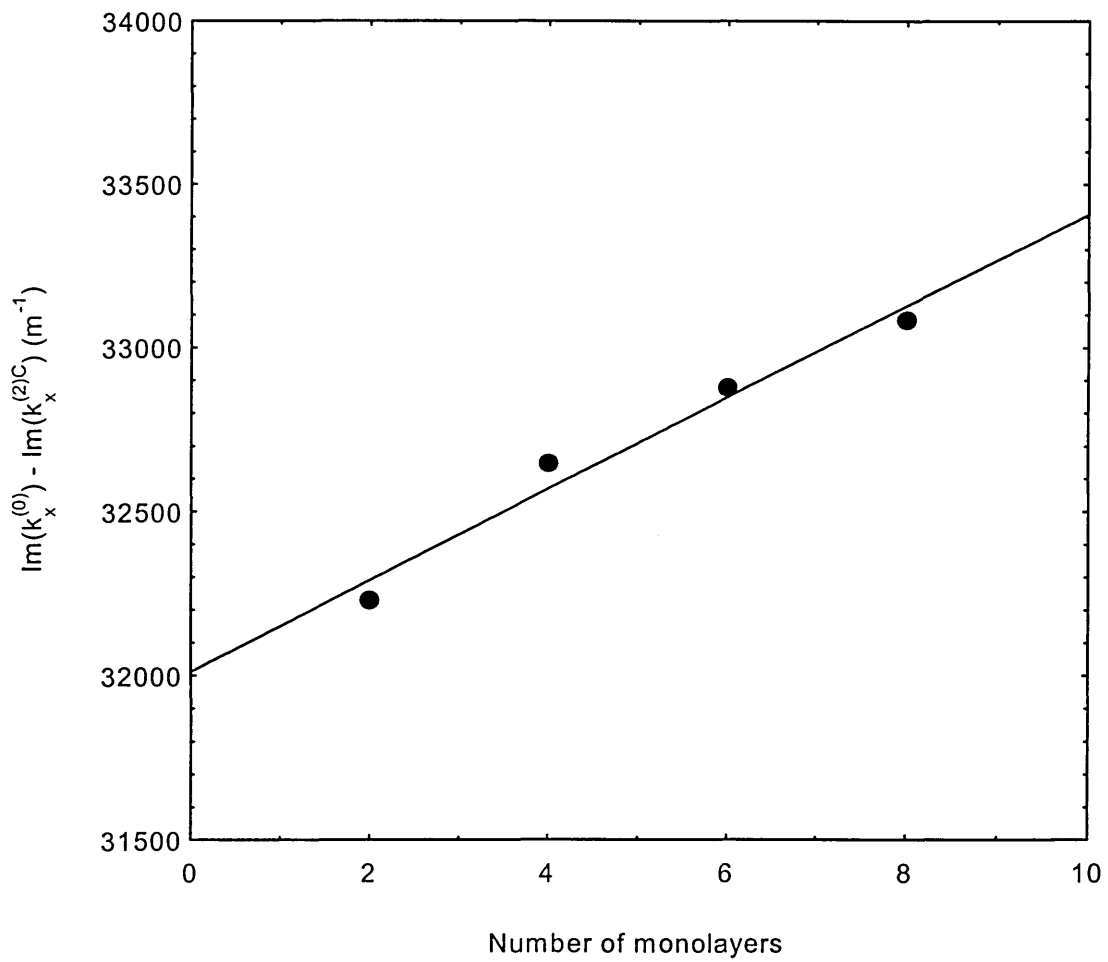


**Figure 5-54 Graph showing the changes in inner damping with respect to the number of monolayers of AmAz1**

The values of  $\Delta R_{\min}$  and  $\gamma$  (defined in equation 5.38) are given in Table 5-15.

N	$R_{\min}$	$\Delta R_{\min}$	$\gamma$
0	0.1623	0	
2	0.2218	0.0595	8.3549
4	0.2564	0.0941	8.3614
6	0.2827	0.1204	8.3519
8	0.1664	0.0041	8.3537

**Table 5-15 Measured values for  $\Delta R_{\min}$  and  $\gamma$  for AmAz1 monolayers**

$\Delta R_{\min}$  and  $\gamma$  are shown in Figure 5-55 as a function of film thickness. In contrast to  $\Delta R_{\min}$  and  $\gamma$  values for AmPc5 shown in Figure 5-46, the two curves for AmAz1 do not follow the same pattern. The values of  $\gamma$  are shown to form a straight line with a constant value for increasing film thickness, due to the non-absorbing nature of the material. The uncharacteristic change in  $\Delta R_{\min}$  with monolayer thickness for AmAz1 originates in the non-uniform silver coating and is not due to absorbance in the Langmuir-Blodgett coating.

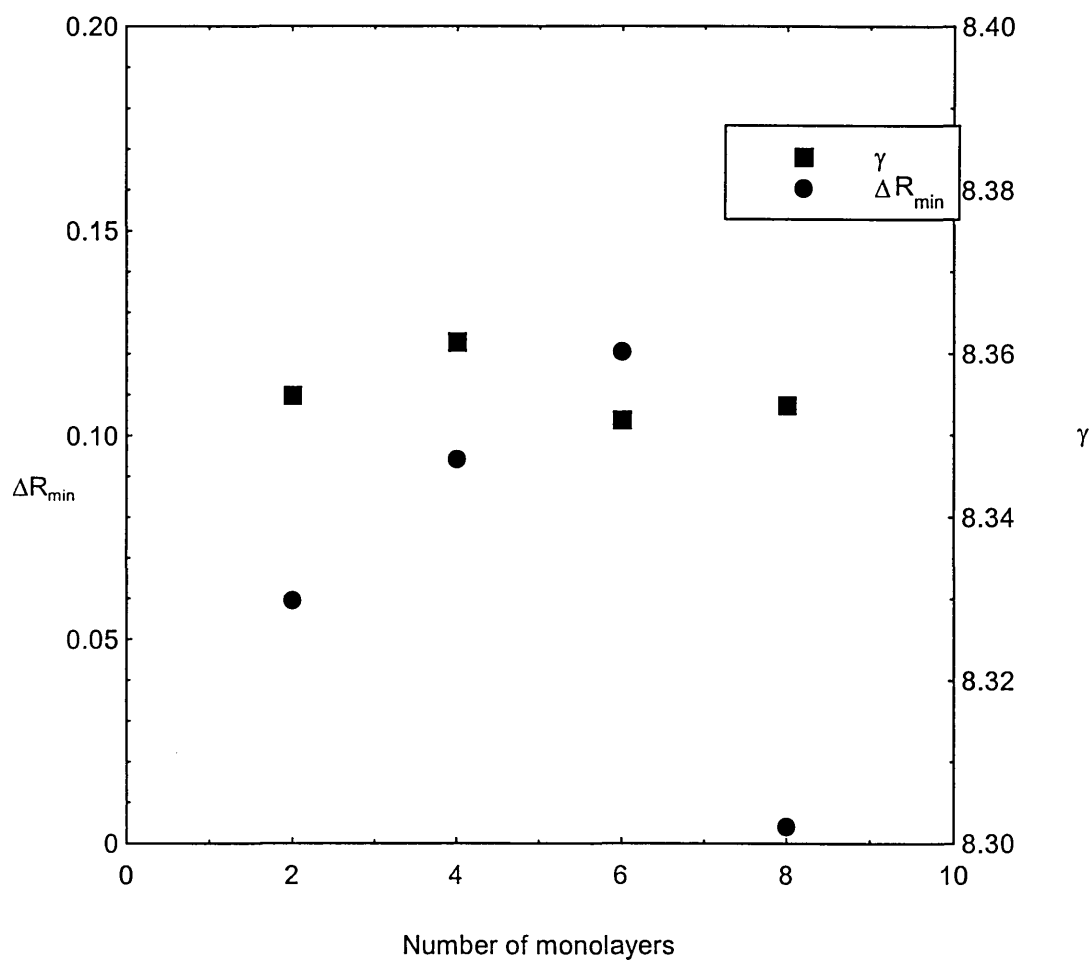


**Figure 5-55** Variation of  $\Delta R_{\min}$  and  $\gamma$  with monolayer thickness of AmAz1

### 5.3 Alternate Layer Structure

The alternate layer structure shown schematically in Figure 4.4 (d) was achieved using AmAz1 and  $\omega$ -tricosenoic acid (TA), with AmAz1 deposited on the down stroke and TA deposited on the up stroke. TA was selected as a spacer layer for AmAz1 due to its ease of deposition and transparency in the IR and UV sections of the spectrum.

#### 5.3.1 X-Ray Diffraction Analysis

Study of the transfer ratios of both AmAz1 and TA during Langmuir-Blodgett film deposition indicate successful deposition by both materials, although this can not be confirmed by measurement of absorption spectra due to the transparency of TA in the visible region of the spectrum. Analysis of the X-ray diffraction pattern was undertaken at the University of Manchester in order to demonstrate the presence of an alternate layer structure. The studies were carried out using a Philips PW1380 horizontal diffractometer fitted with a graphite crystal monochromator and using the  $\text{CuK}\alpha$  line at wavelength 0.1542 nm. The x-ray diffraction pattern of 20 bilayers of AmAz1 and TA on glass showed a Bragg peak at a value of  $2\theta$  of  $1.936^\circ$ . This gives a bilayer spacing of 4.56 nm using Bragg's Law in equation 5.39 (Stout et al 1989).

$$l\lambda = 2d \sin\theta \quad 5.39$$

where  $l$  is an integer equal to 1 in this case,  $d$  is the bilayer spacing and  $\lambda$  is the  $\text{CuK}\alpha$  wavelength at an incident angle of  $\theta$ .

The monolayer thickness of TA is given as 2.65 nm (Wang et al 1994), resulting in an AmAz1 monolayer thickness of 1.91 nm in this alternate layer structure. This value can be compared with the bilayer spacing of 3.18 nm obtained from x-ray diffraction studies of AmAz1 single material Langmuir-Blodgett films (Omar et al 1997). Molecular models show that the fully extended molecule is 2.24 nm long, indicating tilting or interdigitation of the sidechains, although to a lesser degree than with pure AmAz1

films. The bilayer spacing of TA, AmAz1 alternating layers (4.56 nm) is less than that of the fully extended molecules ( $2.24 + 2.65 = 4.89$  nm), indicating interdigitation within these films.

### 5.3.2 Second Harmonic Generation Measurements

Essentially all materials exhibit non-linear optical phenomena to a degree, depending on the power of the optical field required to observe the effects. The intensity of such a field is dictated by the electronic structure and geometrical arrangement of the molecular constituents of the medium. The polarisation,  $P$ , of the medium is given by (Agrawal 1989),

$$P = \chi^{(1)}E + \chi^{(2)}E^2 + \chi^{(3)}E^3 + \dots \quad 5.40$$

where  $\chi^{(1)}$  = first order susceptibility

$\chi^{(2)}$  = second order susceptibility

$\chi^{(3)}$  = third order susceptibility

$E$  = electric field strength

The higher order terms are extremely difficult to observe and usually terms beyond the third order are omitted from discussion.

If we consider the electric field as a sinusoidal oscillation with amplitude  $E_0$ , oscillation frequency  $\omega$ , time  $t$ , wave vector  $k$  travelling in the  $z$  direction, then the polarisation can be given by,

$$P = \chi^{(1)}E_0 \cos(\omega t - kz) + \chi^{(2)}E_0^2 \cos(\omega t - kz) + \chi^{(3)}E_0^3 \cos(\omega t - kz) \quad 5.41$$

This equation yields the following expression for the second order polarisation term,

$$P = \frac{1}{2} \chi^{(2)} E_0^2 [1 + \cos(2\omega t - 2kz)] \quad 5.42$$

$$P = \frac{1}{2} \chi^{(2)} E_0^2 [1 + \cos(2\omega t - 2kz)]$$

In general, second order optical effects can be visualised as a three-wave mixing process and categorised according to the frequency, intensity and phases of the field components (Prasad 1991) and can be written as,

$$\chi_{ijk}^{(2)}(-\omega_3; \omega_2, \omega_1) \quad 5.43$$

where  $\omega_3 = \omega_2 \pm \omega_1$  and  $i, j$  and  $k$  represent the Cartesian components of the interacting fields and polarisation waves.

In the case where  $\omega_3 = 2\omega$  and  $\omega_1 = \omega_2 = \omega$  we can write,

$$\chi_{zxx}^{(2)}(-2\omega; \omega, \omega) \quad 5.44$$

which indicates a process where the second harmonic frequency is generated in the z direction as a result of field components in the x direction. The negative sign indicates conservation of momentum. It should be noted that the above expression (5.44) is equivalent to,

$$\chi_{xxz}^{(2)}(-2\omega; \omega, \omega) \quad 5.45$$

due to symmetry conditions.

The second order polarisation term in equation 5.44 contains a  $2\omega$  term derived from  $\chi^{(2)}$  which oscillates at twice the frequency of the fundamental wave.

A second order non-linear polarised medium can be said to consist of an array of oscillating dipoles where the phase of the radiating dipole is determined by the relative phases of two waves at differing frequencies. The oscillating dipole produces radiation at the harmonic and second harmonic frequencies

The harmonic polarisation propagates with the velocity of the fundamental wave and will constructively interfere in the forward direction, whereas the opportunity for dephasing of the second harmonic radiation in the forward direction is appreciable. As a result, the second harmonic radiation is subject to destructive interference at the molecular level in an amorphous material. If the medium possesses a centrosymmetric

structure, the radiation patterns generated by two individual dipoles related by inversion symmetry will be  $\pi/2$  out of phase. The subsequent destructive interference means that second harmonic generation can not be observed in a centrosymmetric medium.

Langmuir-Blodgett film deposition of one material in a z or x type structure or deposition of two different materials in an alternating layer structure forms a non-centrosymmetric structure, permitting constructive interference of second harmonic radiation waves.

The ability of a medium to produce second harmonic radiation is dependent on the macroscopic structure of the material, and the microscopic behaviour of the individual molecules. This can be visualised as the ability of a radiation field to create an induced dipole in the molecules. A molecule that contains a conjugated electron system contains highly deformable delocalised  $\pi$ -electrons, leading to optical nonlinearities.

AmAz1 contains such an electron system around the nitrogen groups, which results in the second harmonic signal.

The second order non-linear coefficient ( $\chi^{(2)}$ ) in Langmuir-Blodgett films is known to be proportional to the number of bilayers (or monolayers in a z or x type structure), and hence the second harmonic signal intensity ( $I_{2\omega}$ ) is expected to vary as the square of the number of monolayers ( $N^2$ ) (Prasad 1991),

$$\frac{I_{2\omega(LB)}}{I_{2\omega(ref)}} \propto N^2 \quad 5.46$$

where  $\frac{I_{2\omega(LB)}}{I_{2\omega(REF)}}$  represents the normalised second harmonic intensity. Deviation from

this quadratic dependence on N is usually taken as an indication of changing structural factors, whether they be electronic or geometric in nature within the multilayer film.

The second harmonic generation measurements were carried out at Cranfield University using the apparatus schematically shown in Appendix VI (Ashwell et al 1990).

The films were irradiated with light from a Q-switched Nd:YAG laser (1064 nm) with a p-polarised beam incident to the substrate at  $45^\circ$ . Measurements of 3, 4, 5, 6 and 10 bilayers were taken across each sample width using a quartz plate as reference, with 1 and 2 bilayer samples showing no second harmonic response. The average signal value from each individual sample was adjusted by a factor of 150 to account for the lens correction factor.

The measured signals as a function of the number of bilayers is shown in Figure 5-56.

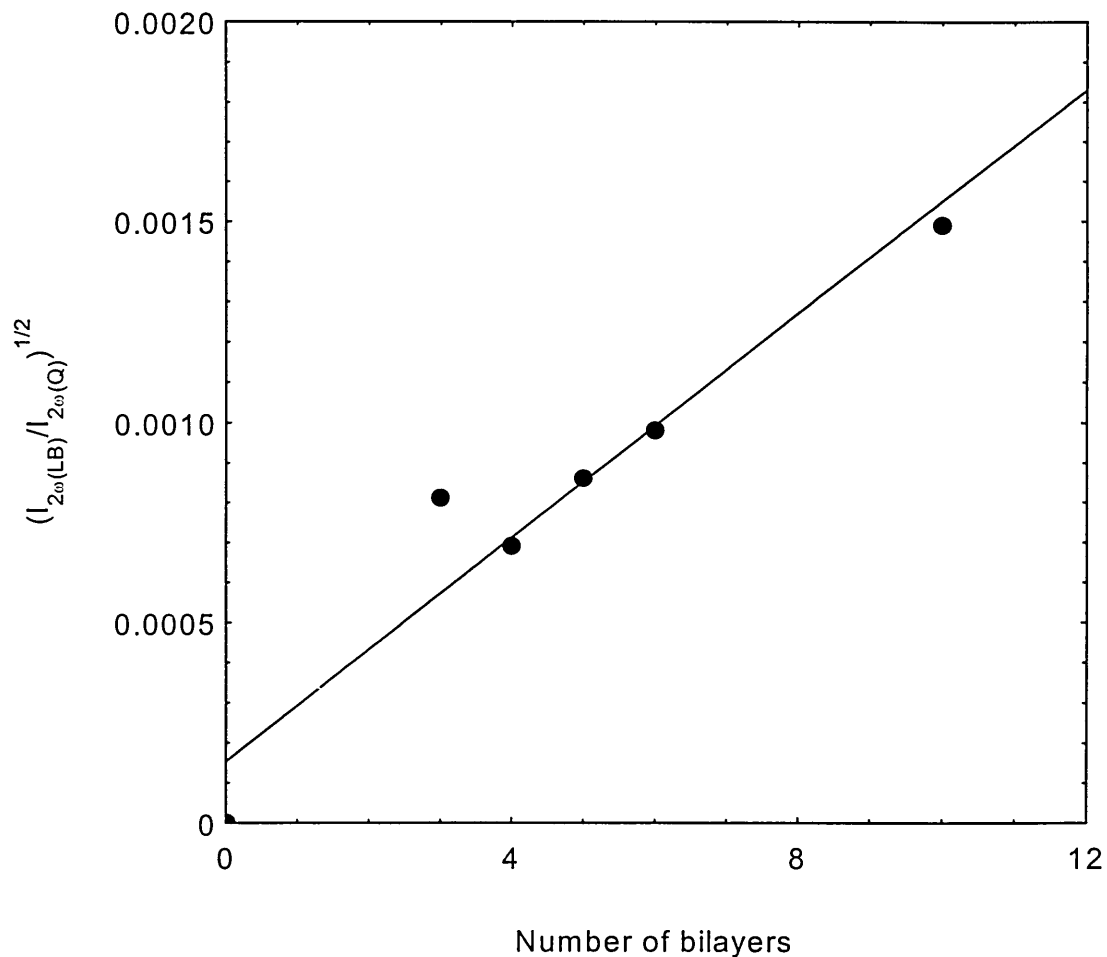


**Figure 5-56 Normalised second harmonic intensity with increasing number of AmAz1/TA Langmuir-Blodgett bilayers**

The linear relationship in which the second harmonic intensity increases quadratically with the number of bilayers is consistent with theory. This follows the pattern for other materials deposited in alternate layers (Ashwell et al 1990) and in a z-type structure (Ashwell et al 1990).

#### 5.4 Scanning Electron Microscopy

Scanning electron microscopy study provides information about the surface morphology and edge definition of Langmuir-Blodgett films. Phthalocyanine compounds have been investigated as materials in optical data storage applications due to their thermal and light stability (Gu et al 1995 and Tao et al 1994). However, the formation of aggregates and defects on the surface can affect the device suitability of the material (Dutta et al

1996 and Kim et al 1994). A scanning electron microscopy image of a 40 monolayer Langmuir-Blodgett film (Figure 5-57) shows the surface to be relatively homogeneous with only minor defects, whilst inspection of a 200 monolayer section (Figure 5-58) reveals a rougher, more grainy structure. This can be as a result of amplification of monolayer deformities within the Langmuir-Blodgett film structure.



Figure 5-57 Scanning electron microscope image of 40 monolayers of AmPc5



Figure 5-58 Scanning electron microscope image of 200 monolayers of AmPc5

The relatively smooth surface of both film thicknesses indicates the suitability of AmPc5 as an optical data storage media.

## Chapter 6 Conclusion and Suggestions for Further Work

The optical and structural analyses of AmPc5 and AmAz1 are presented in this thesis, with the materials studied in the solid monolayer, floating monolayer and monomer form. In this concluding chapter the properties and behaviour of both molecules are compared. The data for both materials are centralised and discussed.

In Chapter 3, the properties and applications of both AmAz1 and AmPc5 are discussed. The molecules possess very different structures, although they may both be used in gas sensing (Travis et al 1995, Dickert et al 1997) and applications in non-linear optics (Nalwa et al 1995, Morley et al 1997). Adsorption of NO<sub>x</sub> in between phthalocyanine molecules is found to be dependant upon the central metal atom, where cobalt > lead > metal-free > copper (Kim et al 1997). Calixarenes form complexes with the host molecules utilising the central cavity in both the solid and solution state (Diamond et al 1996).

One of the most attractive features of calixarenes is the ease of chemical modification, making possible changes to ion complexing selectivity, for example, very simple. Comparison of calixarene synthesis (Omar et al 1997) to a material such as a TCNQ adduct (Ray et al 1998) where synthesis takes about two weeks clearly illustrates the advantage.

Study of the pressure-area isotherms produced by floating monolayers of AmPc5 and AmAz1 revealed the presence of hysteresis during compression for both molecules (see Figures 4.3 and 4.5). Hysteresis was apparent to a much greater degree for AmAz1 (Figure 4.3) and was shown to decrease to a lesser degree after monolayer training when compared to AmPc5. The tetrapodal structure of AmAz1 provided flexibility to the molecule and hence to the monolayer. Upon monolayer compression the hydrocarbon and azo side chains were compressed and upon decompression were allowed to relax.

Monolayer training reduced hysteresis, but did not completely eliminate the effect. The disc-like, rigid structure of AmPc5 was illustrated by the minimal hysteresis apparent in the pressure-area isotherm, which was further reduced by monolayer training (Figure 3.5).

Both materials produced consistent transfer ratios implying a Y-type deposition onto the substrates, with deposition at varying speeds depending upon the substrate used.

The Langmuir-Blodgett deposition parameters for both materials are summarised in Table 6-1.

Material	AmPc5	AmAz1
Solvent	TCE	Chloroform
Concentration (mg/ml)	0.1	0.5
Additions to solution	None	ethanol (10%)
Optimum solution spreading quantity ( $\mu\text{l}$ )	500-600	50-100
Solvent evaporation time (minutes)	30	5-10
Critical pressure, $\pi_c$ (mN/m)	28	30
Stability test pressure (mN/m)	25	25
Area/molecule on water surface ( $\text{nm}^2$ )	1.61	1.86
Dipper speed for glass substrates (mm/min)	20	20
Substrate type	Hydrophobic	Hydrophobic
Deposition type	Y	Y

**Table 6-1 Langmuir-Blodgett parameters for AmPc5 and AmAz1**

Comparison of the absorbance spectra of both materials highlighted the contrast in shape and position of absorption peaks. The absorption bands in both materials arose

from  $\pi \rightarrow \pi^*$  transitions; AmPc5 from conjugation of the phthalocyanine ring and AmAz1 from conjugation in the azobenzene side chains. The calixarene basket is transparent in the visible region of the spectrum, so the orange colour of the material arose from absorption in the azobenene side chains. The solution and film form spectra for AmPc5 displayed the phthalocyanine characteristic Q absorption band split which contrasted with the AmAz1 featureless spectrum.

Absorption spectra of floating monolayers of AmPc5 indicated formation of the two-dimensional solid phase very soon after the spread of solution. This phenomenon is characteristic of rigid molecules that induce order in floating monolayer form.

Close analysis of the AmPc5 pressure-area diagram revealed a hump at about 25mN/m. This may have been an indication of the lack of formation of a monolayer and a possible rearrangement of the bilayer on the surface at this pressure. Analysis of the floating monolayer absorbance spectra (Figure 5.12) showed a large increase in absorbance between spectra measured at 18mN/m and 20mN/m. This suggested the formation of a bilayer between these pressures.

Determination of the AmPc5 extinction coefficient across the visible spectral range revealed a pattern similar to the absorption spectra of the material. The k values were shown to increase linearly with monolayer thickness. In contrast, the k values across the same wavelength range and monolayer thicknesses for AmAz1 followed the pattern of the absorption spectrum, but did not increase linearly with film thickness. Instead, the AmAz1 extinction coefficient values tended towards a steady value of approximately 1.5 with film thickness.

The refractive index values for both materials were shown initially to increase with film thickness, then approach a steady value; 2.1 for AmPc5 and 2.0 for AmAz1. These values were compared with those obtained from surface plasmon resonance measurements (Table 6-2). These values can be said to be close to the bulk refractive

index. Comparison between the AmAz1 refractive index obtained via spectroscopic and surface plasmon resonance methods showed a difference in values. This suggested a different type of packing structure for AmAz1 on gold coating glass and glass substrates and a similar packing type for AmPc5.

n	Absorbance	SPR
AmPc5	1.90	2.00
AmAz1	1.48	1.43

**Table 6-2 Refractive index values obtained through spectroscopic and surface plasmon resonance data**

Measurement of absorption spectra using polarised light showed that AmPc5 Langmuir-Blodgett films exhibited a dichroic effect, whereas spectra for AmAz1 indicated Langmuir-Blodgett deposition formed in-plane isotropic films. The preference of orientation with respect to dipping direction displayed by AmPc5 may have been as a result of the rigid nature of the floating monolayer. The flexible nature of the AmAz1 molecule resulted in the lack of preference of orientation with dipping direction. The expected increase of AmPc5 in-plane order was not apparent. The columnar stack style of deposition exhibited by AmPc5 is one possible reason, as most phthalocyanine deposit in the columnar herring-bone array.

The monolayer behaviour and Langmuir-Blodgett film forming properties of alkyl phthalocyanine belonging to the same family as AmPc5 have been reported, with the molecular packing probed by visible region spectroscopy and x-ray diffraction methods (Cook et al 1994). The material behaviour as a function of attached chain length for alkoxy and alkyl amphiphiles was studied. The results indicated a variation in behaviour according to the length of the attached chains and whether or not the chains were

branched. The alkyl amphiphiles synthesised possessed a structure as shown in Figure 1.1, where the carbon chain length (R) varied from 6 to 10. The floating monolayer characteristics for this family indicated that the molecules were oriented with their planes approximately perpendicular to the surface of the water. A tendency for the molecular chains to tilt and/or interdigitate into adjacent layers was observed from x-ray diffraction studies.

The visible absorption spectra of the molecules with alkyl chain length  $C_7$  to  $C_{10}$  displayed red and blue shifted absorptions relative to the solution phase spectrum. Spectra obtained from Langmuir-Blodgett films of alkyl chain length  $C_6$  gave a sharper main band that replaced the split band for chain length  $C_7$  to  $C_{10}$ . The behaviour of the  $C_6$  derivative is similar to that of the molecule in the current research, which possess the same structure with a  $C_5$  alkyl chain length. The paper highlighted the difference in behaviour of the  $C_6$  molecule to the rest of the family, which coupled with the effects reported here of the  $C_5$  chain length phthalocyanine derivative showed that for hydrophobic chain lengths of 6 and under, the molecular packing changed from the herring-bone structure to an offset columnar stack.

Visual inspection of scanning electron micrographs of a 40 and 200 monolayer sample illustrated the differences in structure between a thin and thick sample. The relatively inhomogeneous surface of the thick sample may have been as a result of amplification of monolayer deformities with the Langmuir-Blodgett film structure.

When performing surface plasmon resonance studies gold was selected over silver as the material of preference. Despite the economical advantage of using silver, gold did not oxidise as readily when left in the air and hence provided a more stable substrate. The data presented in Chapter 5 for AmAz1 illustrates surface plasmon resonance measurements performed on silver coated glass substrates for comparison purposes. Figures 5.16 and 5.26 differ in shape partially due to the coating materials, but primarily

due to the different substrate metals. The AmAz1 curves show much sharper minima as a result of the nature of silver. For AmPc5, the half width of the surface plasmon resonance curve was approximately 1.7°, whereas Azo was found to be 0.9°. Fitting of both data demonstrated the stability of gold over silver. The n and k values for gold differ substantially less than those for silver (Table 5.6).

The refractive index values obtained from surface plasmon resonance measurements taken on gold and silver and those calculated from spectroscopic analysis are summarised below in Table 6-3.

Substrate (used for AmAz1 deposition)	Refractive index
Gold coated glass (Omar et al 1997)	1.35
Silver coated glass	1.43
Glass	1.48

**Table 6-3 Refractive index values for AmAz1**

The difference in values between gold and silver implies a different type of deposition on gold from one on silver. The difference in n value for both silver and gold to glass can be explained partly by a different packing style and also by the difference in experimental methods (Arndt et al 1984).

Both materials displayed a linear increase in film thickness with number of monolayers using both spectroscopic and surface plasmon resonance methods.

The surface plasmon resonance data was analysed in terms of absorbing and non-absorbing materials. Study of the absorbance spectra of both AmAz1 and AmPc5 at the surface plasmon resonance wavelength of interrogation, 633 nm, revealed a relatively low level of absorbance for AmPc5 and less for AmAz1. Hence AmPc5 was studied as an absorbing material and AmAz1 as a non-absorbing one. The first indication of the

differences in the absorbing properties between the two materials was observed in the shift in angle and change in shape of the surface plasmon resonance curves. For a non-absorbing coating the theory predicts a shift in angle with little change in resonance minimum for increasing thickness, whereas for an absorbing coating a shift in angle and decrease in resonance minimum is predicted. The theoretical values were calculated for both materials using the respective absorbing and non-absorbing models, and then the data was compared to the experimentally obtained values. AmPc5 behaved as an absorbing material with higher experimental values when compared with theory due to the contribution from the non-absorbing term. Similarly, for AmAz1 contributions from the absorbing term resulted in the different values of each theoretical to experimental point. In both cases, the shape of the experimental curves matched the theoretical suggesting that both models were applicable even in areas not entirely inside or outside the absorbance bands.

In addition, the resonance curve halfwidth ( $\Delta\theta_{1/2}^\circ$ ) for the two materials was observed to increase along with the theoretical predictions with increasing film thickness. The broadening of surface plasmon resonance curves arises from the damping mechanisms: inner and radiation damping. Inner damping arises from energy absorption by the metal (given by  $\epsilon_1''$ ) and radiation damping from the coupling of the incoming beam and the surface plasma and is dependant upon film thickness. Both types of damping were shown to increase linearly with increasing film thickness in accordance with damping mechanism theory for both materials. For non-absorbing AmAz1 the damping processes were expected to increase at the same rate, whereas for absorbing AmPc5 the inner damping was expected to increase at a greater rate. AmAz1 damping mechanisms behaved according to theory, however the inner damping in AmPc5 was shown to increase at a greater rate initially but reach a plateau region after 4 monolayers. This effect arose from the low absorbance of AmPc5 at 633 nm.

The second harmonic generation properties of AmAz1 were investigated by deposition of the material in alternating AmAz1/Tricosenoic acid Langmuir-Blodgett layers. The alternate layer structure was confirmed by X-ray diffraction studies which indicated interdigitation of the molecular sidechains, although to a lesser degree than with pure AmAz1 films. The conjugated  $\pi$ -electron system around the nitrogen groups on the AmAz1 sidechains gave rise to the optical non-linearities observed in the film. The second harmonic signal is known to be proportional to the square of the number of bilayers and hence the second harmonic signal of increasing numbers of monolayers was measured. The results illustrated a quadratic increase of second harmonic intensity consistent with theory.

The study of AmPc5 presented provides an understanding of the optical effects of this novel material. The shorter carbon chain length of this molecule as compared to phthalocyanines of the same family demonstrates the uncharacteristic behaviour of the material in Langmuir-Blodgett films.

The research conducted into the optical behaviour of AmAz1 has enabled the determination of certain optical constants and the study of a non-linear optical response.

In conclusion the Langmuir-Blodgett film deposition parameters onto glass and metallic substrates have been presented with study of the floating monolayer and molecular orientation on the water surface. The complex refractive indices for both materials in film form have been determined by visible absorbance spectroscopy and surface plasmon resonance. The indices at the He-Ne laser wavelength have been compared and are shown to agree well. Surface plasmon resonance data has provided a method for studying the surface plasma damping mechanisms at work in each material. Dichroic measurements of AmPc5 have enabled calculation of molecular orientation within Langmuir-Blodgett films. Alternate layer films of AmAz1 and tricosenoic acid have

provided a means of measuring second harmonic generation from AmAz1 molecules. These optical parameters provide a foundation for the development of these materials in both device application and further research into optical effects. The effects investigated for both materials are summarised below in Table 6-4

Effects	Am	Am
	Pc5	Az1
Floating monolayer isotherm	✓	✓
Solution spectra	✓	✓
Film spectra	✓	✓
Floating monolayer spectra	✓	✓
Polarised light spectra	✓	✓
Surface plasmon resonance	✓	✓
X-ray diffraction		✓
Second harmonic generation		✓
Scanning electron microscopy	✓	

**Table 6-4 Summary of effects studied for AmPc5 and AmAz1**

### 6.1 Suggestions for Further Work

All the surface plasmon resonance studies were performed using a He-Ne laser (635 nm) and neither AmPc5 or AmAz1 absorb strongly at this wavelength. Further surface plasmon resonance studies may also be performed at the materials absorbance peaks. Interrogation at the peak wavelengths of 733 nm for AmPc5 and 454 nm for AmAz1

will require application of the absorbing model and yield improved agreement between experimental and theoretical data.

Further to the current research,  $\chi^{(2)}$  of AmAz1/TA alternating layers can be determined.

This study will require the determination of the refractive index of AmAz1 at  $\omega$  and  $2\omega$  (1064 nm and 532 nm). Determination of the refractive index of tricosenoic acid is not necessary as it is transparent at 532 nm. This makes it an ideal candidate for second harmonic measurements.

In addition, measurements of the long term stability of the alternating films can be determined by re-measuring the second harmonic signal over a period of many months. Alternating films have a tendency to rearrange over extended periods of time, reducing the second harmonic signal as a result.

## References

### A

- Abdelghani A, Chovelon JM, Jaffrezic-Renault N, Ronot-Trioli C, Veillas C, Gagnaire H, Surface plasmon resonance fibre-optic sensor for gas detection, *Sensors and Actuators B*, 1997, Vol.39, No.1-3, pp.407- 410
- Adams H, Davis F, Stirling CJM, Selective adsorption in gold-thiol monolayers of calix-4-resorcinarenes, *Journal of the Chemical Society: Chemical Communications* 1994, No.21, pp.2527-2529
- Agrawal, GP, Nonlinear Fiber Optics, Academic Press, 1989, Chapter 1
- Ahlers M, Blankenburg R, Grainger DW, Meller P, Ingsdorf H, Salesse C, Specific recognition and formation of two-dimensional streptavidin domains in monolayers: Applications to molecular devices, *Thin Solid Films*, 1989, Vol.180, pp.93-99
- Aktsipetrov OA, Fedyanin AA, Melnikov AV, Mishina ED, Murzina TV, Second harmonic generation as a nondestructive readout of optical (photo(electro)chromic and magnetic) memories, *Japanese Journal of Applied Physics Part 1-Regular Papers Short Notes and Review Papers*, 1998, Vol.37, No.1, pp.122-127
- Allen CM, Weber JM, Vanlier JE, Sulfophthalocyanines for photodynamic inactivation of viruses in blood products - Effect of structural modifications, *Photochemistry and Photobiology*, 1995, Vol.62, No.1, pp.184-189
- Araya K, Mukoh A, Narahara T, Shirakawa H, Synthesis of highly oriented polyacetylene film in a liquid crystal solvent, *Synthetic Metals*, 1986, Vol.14, No.3, pp.199-206
- Archibald F, RoyArcand L, The use of ozone to decolourize residual direct paper dyes in kraft paper machine whitewater, *Ozone - Science and Engineering*, 1997, Vol.19, No.6, pp.549-565

Arnaud-Neu F, Schwing-Weill MJ, Calixarenes, new selective molecular receptors, *Synthetic Metals*, 1997, Vol.90, No.3, pp.157-164

Arndt DP, Azzam RMA, Bennett JM, Borgogno JP, Carniglia CK, Case WE, Dobrowolski JA, Gibson UJ, Hart TT, Ho FC, Odgkin VA, Klapp WP, Macleod HA, Pelletier E, Purvis MK, Quinn DM, Strome DH, Swenson R, Temple PA, Thonn TF, Multiple determination of the optical constants of thin-film coating materials, *Applied Optics*, 1984, Vol.23, No.20, pp.3571-3596

Ashwell GJ, Dawnay EJC, Kuczynski AP, Martin PJ, Highest observed second harmonic intensity from a multilayered Langmuir-Blodgett film structure, *SPIE*, 1991, Vol.1361, No.1., pp.589-598

Ashwell GJ, Dawnay EJC, Kuczynski AP, Szablewski M, Sandy IM, Bryce MR, Grainger AM, Hasan M, Langmuir-Blodgett alignment of zwitterionic optically non-linear D- $\pi$ -A materials, *Journal of the Chemical Society Faraday Transactions*, 1990, Vol.86, No.7, pp.1117-1121

Ashwell GJ, Handa T, Leeson P, Skjonnemand K, Jefferies G, Green A (c), Second harmonic generation from Langmuir-Blodgett films of centrosymmetric squarines with heterocyclic donor groups, *Journal of Materials Chemistry*, 1998, Vol.8, No.2, pp.377-382

Ashwell GJ, Handa T, Ranjan R (b), Improved second harmonic generation from homomolecular Langmuir-Blodgett films of a transparent dye, *Journal of the Optical Society of America B-Optical Physics*, 1998, Vol.15, No.1, pp.466-470

Ashwell GJ, Hargreaves RC, Baldwin CE, Bahra GS, Brown CR, Improved second harmonic generation from Langmuir-Blodgett films of hemicyanine dyes, *Nature*, 1992, Vol.357, No.6377, pp.393-395

Ashwell GJ, Leeson P, Bahra GS, Brown CR (a), Aggregation-induced second harmonic generation, *Journal of the Optical Society of America B-Optical Physics*, 1998, Vol.15, No.1, pp.484-488

## **B**

Baker S, Petty MC, Roberts GG, Twigg MV (a), The preparation and properties of stable metal free phthalocyanine Langmuir-Blodgett films, *Thin Solid Films*, 1983, Vol.99, No.1-3, pp.53-59

Baker, S, Roberts, GG, Petty, MC (b), *Proceedings of the IEEE Part 1*, Vol 130, 1983

Baran J, Marchewka MK, Ratajczak H, Borovikov AY, Byckov VN, Naumovets AG, Podzelinsky AV, Puchkovskaya GA, Styopkin VI, Investigation of stearic acid and manganese stearate films obtained by Langmuir-Blodgett and vacuum deposition methods, *Thin Solid Films*, 1995, Vol.254, No.1-2, pp.229-239

Barker PS, Petty MC, Monkman AP, McMurdo J, Cook MJ, Pride R, A hybrid phthalocyanine/silicon field-effect transistor for NO<sub>2</sub>, *Thin Solid Films* 1996, Vol.285, pp.94-97

Barraud A, Leloup J, Maire P, Ruau delteixier A, Microdefect decoration and visualisation in Langmuir-Blodgett films, *Thin Solid Films*, 1985, Vol.133, No.1-4, pp.133-139

Bjornholm T, Geisler T, Larsen J, Jorgensen M, Brunfeldt K, Schaumburg K, Bechgaard K (a), Donor-acceptor interfaces in Langmuir-Blodgett films. Structural and optical features related to nonlinear optical properties, *Synthetic Metals*, 1993, Vol.57, No.1, pp.3813-3818

Bjornholm T, Larsen NB, Christensen FE, Sommerlarsen P, Skettrup T, Jorgensen M (b), Structural and optical properties of Langmuir-Blodgett films of the electron acceptor 2-octadecylthio-1,4-benzoquinone, *Synthetic Metals*, 1993, Vol.57, No.1, pp.3807-3812

Bliznyuk VN, Kirstein S, Mohwald H, Structural control of optical spectra of two-dimensional mixed dye crystals, *Journal of Physical Chemistry*, 1993, Vol.97, No.3, pp.569-574

Blodgett, KB, *Journal of the American Chemical Society*, 1935, Vol 57

Born M., Wolf E., Principles of Optics, Pergamon Press, 1970, pp 613

Bown SG, Photodynamic therapy in gastroenterology - Current status and future prospects, *Endoscopy*, 1993, Vol.25, No.9, pp.683-685

Brecht A, Gauglitz G, Recent developments in optical transducers for chemical or biochemical applications, *Sensors and Actuators B*, 1997, Vol.38, No.1-3, pp.1-7

Brouyere E, Persoons A, Bredas JL, Geometric structure and second order non-linear optical response of substituted calix(4)arene molecules: A theoretical study, *Journal of Physical Chemistry*, 1997, Vol.101, No.22, pp.4142- 4148

Bryant GC, Cook MJ, Ruggiero C, Ryan TG, Thorne AJ, Haslam SD, Richardson RM, Structural study of spin-coated and Langmuir-Blodgett films of monomeric and oligomeric phthalocyanines, *Thin Solid Films*, 1994, Vol.243, No.1-2, pp.316-324

## C

Capelletti R, Fontana MP, Nicolae CA, Paradiso R, Bonnett R, Wilkins RF, Characterization of phthalocyanine Langmuir-Blodgett films by optical dichroism and resonance raman scattering, *Molecular Crystals and Liquid Crystals*, 1995, Vol.266, pp.35-45

Chen Q, Gu D, Gan F, Optical recording using copper phthalocyanine thin films, *Solid State Electronics*, 1994, Vol 37, pp1768-1770

Cook MJ, Mcmurdo J, Miles DA, Poynter RH, Simmons JM, Haslam SD, Richardson RM, Welford K, Monolayer behaviour and Langmuir-Blodgett film forming properties of some amphiphilic phthalocyanines: Factors influencing molecular organisation

within the film assembly, *Journal of Material Chemistry*, 1994, Vol.4, No.8, pp.1205-1213

Cook MJ, 1.4.8.11,15,18,22,25 - octasubstituted phthalocyanines - The contrasting effects of alkyl and alkoxy substituents on molecular self assembly, *Journal of Material Science - Materials in Electronics*, 1994, Vol.5, No.2, pp.117-128

Cook MJ, Optical and Infrared Spectroscopy of Phthalocyanine Molecular Assemblies, *Spectroscopy of New Materials*, Wiley, 1993

Cook MJ, Thin film formulations of substituted phthalocyanines, *Journal of Material Chemistry*, 1996, Vol.6, No.5, pp.677-689

## D

Dasaradhi L, Stark PC, Huber VJ, Smith PH, Jarvinen GD, Gopalan AS, 4-tert-Butylcalix(4)arene tetrahydroxamate chelators for the selective extraction of actinide ions: synthesis and preliminary metal ion extraction studies, *Journal of the Chemical Society, Perkin Transactions 2*, 1997, No.6, pp.1187-1192

Davies J, Surface plasmon resonance - the technique and its applications to biomaterial processes, *Nanobiology*, 1994, Vol 3, pp 5-16

Davis F, Gerber M, Cowlam N, Stirling CJM (b), Morphology and binding of spontaneously assembled multilayers of calix-4-resorcinarenes, *Thin Solid Films* 1996, Vol.285, pp.678-682

Davis F, OToole L, Short R, Stirling CJM (c), Selective ion-binding by Langmuir-Blodgett films of calix(8)arenes, *Langmuir*, 1996, Vol.12, No.7, pp.1892-1894

Davis F, Stirling CJM (a), Calix-4-resorcinarene monolayers and multilayers - Formation, structure and differential adsorption, *Langmuir*, 1996, Vol.12, No.22, pp.5365-5374

Davis F, Stirling CJM, Spontaneous multilayering of calix-4-resorcinarenes, *Journal of the American Chemical Society*, 1995, Vol.117, No.41, pp.10385-10386

Davydov AS, Theory of molecular excitons, *McGraw-Hill*, 1962

Diamond D, McKervey MA, Calixarene based sensing agents, *Chemical Society Reviews*, 1996, Vol.25, No.1, p.15

DiazGarcia MA, Cabrera JM, AgulloLopez F, Duro JA, delaTorre G, Torres T, FernandezLazaro F, Delhaes P, Mingotaud C, Third order nonlinear optical susceptibilities of the Langmuir-Blodgett films of octa-substituted metallophthalocyanines, *Applied Physics Letters*, 1996, Vol.69, No.10, p.1495

Dickert FL, Baumler UPA, Stathopoulos H, Mass sensitive solvent vapour detection with calix(4)resorcinarenes: Tuning sensitivity and predicting sensor effects, *Analytical Chemistry*, 1997, Vol.69, No.6, pp.1000-1005

Dutta AK, Misra TN, Pal AJ, A spectroscopic study of nonamphiphilic pyrene assembled in Langmuir-Blodgett films: formation of aggregates, *Langmuir*, 1996, Vol.12, No.2, pp.459-465

Dutta AK, Aggregation-induced reabsorption of *p*-terphenyl in Langmuir-Blodgett films: A spectral study, *Journal of Physical Chemistry*, 1995, Vol.99, No.40, pp.14758-14763

## **E**

Eckhardt CJ, Peachey NM, Takacs JM, Uphaus RA, Crystal engineering in two-dimensions - Control of planar packing by design of new amphiphiles, *Thin Solid Films*, 1994, Vol.242, No.1-2, pp.67-73

Era M, Adachi C, Tsutsui T, Saito S, Organic electroluminescent device with cyanine dye Langmuir-Blodgett films as an emitter, *Thin Solid Films*, 1992, Vol.210, No.1-2, pp.468-470

## F

Franklin B, Of the filling of waves by means of oil (extract of a letter fro Dr Brownrigg to Dr Franklin, *Philosophical Transactions of the Royal Society of London*, 1774, Vol 64, pp 445

Fu YS, Forman M, Leznoff C C, Lever A B P, Effect of stearic-acid on molecular-orientation in metal-free 2,9,16,23-tetra-tert-butyltetrabenzotriazaporphine Langmuir-Blodgett films, *Journal Of Physical Chemistry*, 1994, Vol.98, No.36, pp.8985-8991

Fuchs H, Ohst H, Prass W, Ultrathin organic films: molecular architectures for advanced optical, electronic and bio-related systems, *Advanced Materials*, 1991, Vol.3, No.1, pp.10-18

Fujita J, Ohnishi Y, Ochiai Y, Matsui S, Ultrahigh resolution of calixarene negative resist in electron beam lithography, *Applied Physics Letters*, 1996, Vol.68, No.9, pp.1297-1299

## G

Garland NL, Lambrakos SG, Barger WR, Trzaskoma-Paulette PP, Structure of a Langmuir film based on the construction of a system response function for the analysis of second harmonic signals, *Surface and Interface Analysis*, 1997, Vol.25, No.9, pp.715-724

Garland PB, Optical evanescent wave methods for the study of biomolecular interactions, *Quarterly Reviews of Biophysics*, 1996, Vol.29, No.1, pp.91-117

Geddes NJ, Martin AS, Caruso F, Urquhart RS, Furlong DN, Sambles JR, Than KA, Edgar JA, Immobilisation of IgG onto gold surfaces and its interaction with anti-igG studied by surface plasmon resonance, *Journal of Immunological Methods*, 1994, Vol.175, No.2, pp.149- 160

Geddes NJ, Sambles JR, Martin AS, Organic molecular rectifiers, *Advanced Materials for Optics and Electronics*, 1995, Vol.5, No.6, pp.305-320

Gilmartin MAT, Hart JP, Patton DT, Prototype, solid phase, glucose biosensor, *Analyst*, 1995, Vol.120, No.7, pp.1973-1981

Gizeli E, Lowe CR, Immunosensors, *Current Opinion in Biotechnology*, 1996, Vol.7, No.1, pp.66-71

Gould RD, Structure and electrical conduction properties of phthalocyanine thin films, *Coordination Chemistry Reviews*, 1996, Vol.156, pp.237-274

Grady T, Butler T, MacCraith D, Diamond D, McKervey MA, Optical sensor for gaseous ammonia with tuneable sensitivity, *Analyst*, 1997, Vol.122, No.8, pp.803-806

Granito C, Goldenberg LM, Bryce MR, Monkman AP, Troisi L, Pasimeni L, Petty MC, Optical and electrochemical properties of metallophthalocyanine derivative Langmuir-Blodgett films, *Langmuir*, 1996, Vol.12, No.2, pp.472-476

Grieve M, An optical investigation of porphyrin derivatives in Langmuir and Langmuir-Blodgett films, PhD Thesis Sheffield University, 1995

Grunfeld F, A modular multifunctional Langmuir-Blodgett trough, *Review of Scientific Instruments*, 1993, Vol.64, No.2, pp.548-555

Gu DH, Chen QY, Shu JP, Tang XD, Gan FX, Shen SY, Liu K, Xu HJ, Optical recording performance of thin films of phthalocyanine compounds, *Thin Solid Films*, 1995, Vol.257, No.1, pp.88-93

Gutsche CD, Calixarenes, The Royal Society of Chemistry, 1989, Chapters 1-2

## H

Halliday D, Resnick R, Fundamentals of Physics, John Wiley and Sons, 1988, Chapter

38

Hayashi S, Kozaru K, Yamamoto K, Enhancement of photoelectric conversion efficiency by surface plasmon excitation: A test with an organic solar cell, *Solid State Communications*, 1991, Vol.79, No.9, pp.763-767

Heavens OS, Measurements of optical constants of thin films, *Physics of Thin Films, Advances in Research and Development*, Academic Press, 1964, Chapter 6

Herold M, Schmid W, Vogtmann T, Fischer R, Haarer D, Schwoerer M, Electro-optic Pockels and Kerr effects for the determination of  $\chi^{(2)}$  and  $\chi^{(3)}$ : thin films of side-chain polymers containing dimethylaminonitrostilbene and of the polydiacetylene poly-(butoxycarbonylmethyleneurethane), *Applied Optics*, 1995, Vol.34, No.6, pp.996-1002

Hibberd AJ, Investigation of the optoelectronic behaviour of novel phthalocyanine Langmuir-Blodgett films, Sheffield Hallam University Thesis, Jan 1996

Ho ZZ, Ju CY, Hetherington III WM, Third harmonic generation in phthalocyanines, *Journal of Applied Physics*, 1987, Vol 62, pp 716-718

Homola J, Ctyroky J, Skalsky M, Hradilova J, Kolarova P, A surface plasmon resonance based integrated optical sensor, *Sensors and Actuators B*, 1997, Vol.39, No.1-3, pp.286- 290

Hutchinson AM, Characterization of glycoprotein oligosaccharide using surface plasmon resonance, *Analytical Biochemistry*, 1994, Vol.220, No.2, pp.303-307

## I

Imanishi Y, Hattori S, Hamada T, Ishihara S, Kakuta A, Numata S, Fabrications and optical properties of phthalocyanine multi-layered films, *Molecular Crystals and Liquid Crystals Science And Technology Section A-Molecular Crystals And Liquid Crystals*, 1994, Vol.255, pp.35-44

Ivarsson B, Bioanalysis with surface plasmon resonance: principles, *Proceedings 3rd International Meeting on Chemical Sensors*, 1990, Vol 23, pp 445

## J

Jakusch M, Mizaikoff B, Kellner R, Towards a remote IR fibre-optic sensor system for the determination of chlorinated hydrocarbons in water, *Sensors and Actuators B-Chemical*, 1997, Vol.38, No.1-3, pp.83-87

James SA, Ray AK, Silver J, Dielectric and optical studies of sublimed MoOPc films, *Physica Status Solidi A-Applied Research*, 1992, Vol.129, No.2, pp.435-441

Janietz D, Hofmann D, Reiche J, Molecular organization of amphiphilic disc-shaped penta-alkynes in LB monolayers and multilayers, *Thin Solid Films*, 1994, Vol.244, No.1-2, pp.794-798

Jones RW, Fundamental principles of sol-gel technology, The Institute of Metals, 1989

## K

Kasha M, *Spectroscopy of the Excited State*, NATO Advance Studies Serial B, Physics, Plenum Press, 1976

Kawaura H, Sakamoto T, Baba T, Ochiai Y, Fujita J, Matsui S, Sone J, Transistor operation of 30 nm gate length EJ-MOSFETs, *IEEE Electron Device Letters*, 1998, Vol.19, No.3, pp.74-76

Kazantseva ZI, Lavrik NV, Nabok AV, Dimitriev OP, Nesterenko BA, Kalchenko VI, Vysotsky SV, Markovskiy LN, Marchenko AA, Structure and electronic properties of Langmuir-Blodgett films of calixarene/fullerene composites, *Supramolecular Science*, 1997, Vol.4, No.3-4, pp.341-347

Kelderman E, Heesink GJT, Derhaeg L, Verbiest T, Klaase PTA, Verboom W, Engbersen JFJ, Vanhulst NF, Clays K, Persoons A, Reinhoudt DN, Highly ordered films of neat calix(4)arenes for second order non-linear optics, *Advanced Materials*, 1993, Vol.5, No.12, pp.925-930

Kim SR, Kim JD, Choi KH, Chang YH, NO<sub>2</sub> sensing properties of octa(2-ethylhexyloxy)metallophthalocyanine Langmuir-Blodgett films using quartz crystal microbalance, *Sensors and Actuators B - Chemical*, 1997, Vol.40, No.1, pp.39-45

Kim YK, Sohn BC, Kim JH, Kim DS, Jeong SW, Yoo DS, Kang DY, Surface characterisation of ultra-thin polyimide films formed by using Langmuir-Blodgett method, *Molecular Crystals and Liquid Crystals Science And Technology Section A- Molecular Crystals And Liquid Crystals*, 1994, Vol.247, pp.243-250

Kopecek J, Kopeckova P, Konak C, Biorecognizable polymers: Design, structure and bioactivity, *Journal of Macromolecular Science - Pure and Applied Chemistry*, 1997, Vol.A34, No.10, pp.2103-2117

Kretschmann E, Raether H, Radiative decay of non-radiative surface plasmons excited by light, *Zeitschrift fur Naturforschung*, 1968, Vol 23a, pp 2135-2136

Kuder JE, Organic materials for optical data storage media - an overview, *Journal of Imaging Technology*, 1986, Vol.12, No.3, pp.140-143

Kudrevich S, Brasseur N, LaMadeleine C, Gilbert S, vanLier JE, Synthesis and photodynamic activities of novel trisulfonated zinc phthalocyanine derivatives, *Journal of Medicinal Chemistry*, 1997, Vol.40, No.24, pp.3897- 3904

Kuhn H, Functionalized monolayer assembly manipulation, *Thin Solid Films*, 1983, Vol.99, No.1-3, pp.1-16

## L

Labarthe FL, Sourisseau C, Raman study of the photoisomerisation and angular reorientation of azobenzene molecules in a DR1-doped polymer matrix, *Journal of Raman Spectroscopy*, 1996, Vol.27, No.6, pp.491-498

Lamuraglia GM, Adili F, Schmitzrixen T, Michaud NA, Flotte TJ, Photodynamic therapy inhibits experimental allograft rejection: A novel approach for the development of vascular bioprotheses, *Circulation*, 1995, Vol.92, No.7, pp.1919-1926

Langmuir, I, *Transactions of the Faraday Society*, 1920, Vol 15, pp 62

Lavrik NV, DeRossi D, Kazantseva ZI, Nabok AV, Nesterenko BA, Piletsky SA, Kalchenko VI, Shivaniuk AN, Markovskiy LN, Composite polyaniline/calixarene Langmuir-Blodgett films for gas sensing, *Nanotechnology*, 1996, Vol.7, No.4, pp.315-319

Law KY, Organic photoconductive materials: Recent trends and developments, *Chemical Reviews*, 1993, Vol.93, No.1, pp.449-486

Lefevre D, Porteu F, Balog P, Roulliay M, Zalczer G, Palacin S, Chemical reactivity in organized mediums: Building up a two-dimensional polymer, *Langmuir*, 1993, Vol.9, No.1, pp.150-161

Lehmann F, Mohr GJ, Grummt UW, Synthesis and structure-property relationships of amphiphilic acidochromic hydroxystilbazolium dyes, *Sensors and Actuators B - Chemical*, 1997, Vol.39, No.1-3, pp.229-234

Lenferink ATM, Kooyman RPH, Greve J, An improved optical method for surface plasmon resonance experiments, *Sensors and Actuators B - Chemical*, 1991, Vol.3, No.4, pp.261-265

Lenz P, Nonlinear optical effects in PDT, *Journal De Physique IV*, 1994, Vol.4, No.C4, pp.237-240

Liang BJ, Yuan CW, Wei Y, Determination of the molecular orientation of rare-earth bisphthalocyanine derivative Langmuir-Blodgett films by polarized ultraviolet-visible spectra, *Spectrochimica Acta Part A - Molecular And Biomolecular Spectroscopy*, 1997, Vol.53, No.4, pp.531-535

Liu YQ, Xu Y, Zhu DB (b), Preparation and electronic properties of Schottky devices utilizing an asymmetrically substituted metal-free phthalocyanine Langmuir-Blodgett film as barrier layers, *Synthetic Metals*, 1995, Vol.71, No.1-3, pp.2249-2250

Liu YQ, Xu Y, Zhu DB, Wada T, Sasabe H, Zhao XS, Xie XM (a), Optical second harmonic generation from Langmuir-Blodgett films of an asymmetrically substituted phthalocyanine, *Journal of Physical Chemistry*, 1995, Vol.99, No.18, pp.6957-6960

Liu YQ, Xu Y, Zhu DB, Zhao XS, Second harmonic generation in Langmuir-Blodgett films of an asymmetrically substituted metallophthalocyanine, *Thin Solid Films*, 1996, Vol.289, No.1-2, pp.300-305

Lofas S, Malmqvist M, Ronnberg I, Stenberg E, Liedberg B, Lundstrom I, Bionalysis with surface plasmon resonance, *Sensors and Actuators B - Chemical*, 1991, Vol.5, No.1-4, pp.79-84

Lucklum R, Rosler S, Hartmann J, Hauptmann P, On line detection of organic pollutants in water by thickness shear mode resistance, *Sensors and Actuators B-Chemical*, 1996, Vol.35, No.1-3, pp.103- 111

## M

Maack J, Ahuja RC, Mobius D, Tachibana H, Matsumoto M, Molecular cis-trans switching in amphiphilic monolayers containing azobenzene moities, *Thin Solid Films*, 1994, Vol.242, No.1-2, pp.122-126

Manno D, Rella R, Troisi L, Valli L, Langmuir-Blodgett films of Cu(II)-tetrakis(3,3-dimethylbutoxycarbonyl) phthalocyanine : a spectrophotometric and TEM analysis of their structure and morphology, *Thin Solid Films*, 1996, Vol.280, No.1-2, pp.249-255

McCartney CM, Richardson T, Greenwood MB, Cowlam N, Davis F, Stirling CJM, The effect of pendant chain structure on the pyroelectric behaviour of calix(8)arene Langmuir-Blodgett films, *Supramolecular Science*, 1997, Vol.4, No.3-4, pp.385-390

Melendez J, Carr R, Bartholomew D, Taneja H, Yee S, Jung C, Furlong C, Development of a surface plasmon resonance sensor for commercial applications, *Sensors and Actuators B - Chemical*, 1997, Vol.39, No.1-3, pp.375- 379

Melendez J, Carr R, Bartholomew DU, Kukanskis K, Elkind J, Yee S, Furlong C, Woodbury R, A commercial solution for surface plasmon sensing, *Sensors and Actuators B - Chemical*, 1996, Vol.35, No.1-3, pp.212- 216

Merle HJ, Alberti B, Schwendler M, Peterson IR, Surface plasmon observation of striations in Langmuir-Blodgett films, *Journal of Physics D: Applied Physics*, 1992, Vol.25, No.10, pp.1556-1558

Miyamoto Y, Kaifu K, Koyano T, Saito M, Kato M, Kawamura K, Molecular rearrangement in heat-treated Langmuir-Blodgett films of mixtures of N-acyl-p-nitroaniline and fatty acid monitored by second harmonic generation, *Thin Solid Films*, 1992, Vol.208, No.1, pp.62-66

Morgan H, Taylor DM, Surface plasmon resonance microscopy: Reconstructing a three-dimensional image, *Applied Physics Letters*, 1994, Vol.64, No.11, pp.1330-1331

Morley JO, Naji M, Evaluation of optical nonlinearities in calixarenes, *Journal of Physical Chemistry A*, 1997, Vol.101, No.14, pp.2681- 2685

## N

Nabok AV, Lavrik NV, Kazantseva ZI, Nesterenko BA, Markovskiy LN, Kalchenko VI, Shivaniuk AN, Complexing properties of calix(4)resorcinolarene Langmuir-Blodgett films, *Thin Solid Films*, 1995, Vol.259, No.2, pp.244-247

Nabok AV, Ray AK, Hassan AK, Omar O, Taylor R, Richardson T, Pavier M, Inclusion phenomena in mixed floating layers containing phthalocyanines, *Thin Solid Films*, 1998, Vol.329, pp.104-108

Nabok AV, Ray AK, Hassan AK, Travis JR, Cook MJ, Further optical studies on Langmuir-Blodgett films of octa-substituted metal-free phthalocyanines, *Supramolecular Science*, 1997, Vol.4, No.3-4, pp.407-411

Nakayama T, Haga K, Haba O, Ueda M, A negative-working alkaline developable photoresist based on calix(4)resorcinarene, a cross-linker, and a photoacid generator, *Chemistry Letters*, 1997, No.3, pp.265-266

Nalwa HS, Kakuta A, Third order nonlinear optical properties of donor- and acceptor-substituted metallophthalocyanines, *Thin Solid Films*, 1995, Vol.254, No.1-2, pp.218-223

Nilsson P, Persson B, Uhlen M, Nygren PA, Real-time monitoring of DNA manipulations using biosensor technology, *Analytical Biochemistry*, 1995, Vol.224, No.1, pp.400-408

## O

Ogawa K, Kinoshita S, Yonehara H, Nakahara H, Fukuda K, Highly ordered monolayer assemblies of phthalocyanine derivatives, *Journal of the Chemical Society - Chemical Communications*, 1989, No.8, pp.477-479

Ohki S, Ohki C B, Monolayers at the oil/water interface as a proper model for bilayer membranes, *Journal of Theoretical Biology*, 1976, Vol 62, pp 389-407

Omar O, Ray AK, Hassan AK, Davis F, Resorcinol calixarenes (resorcarenes); Langmuir-Blodgett films and optical properties, *Journal of Supramolecular Science*, Vol.4, No.3-4, pp.417-421

Omar O, Ray AK, Hassan, AK, Ghasemlooy Z, Cook MJ, Optical characterisation of amphiphilic, metal-free, non-peripheral phthalocyanine in Langmuir-Blodgett films, *SPIE*, 1996, Vol 2852, pp 81-88

Orti E, Bredas JL, Clarisse C, Electronic structure of phthalocyanines: Theoretical investigation of the optical properties of phthalocyanine monomers, dimers and crystals, *Journal of Chemical Physics*, 1990, Vol.92, No.2, pp.1228-1235

Ott, A. Excitation of nonradiative surface plasma waves in silver by the method of frustrated total reflection, *Zeitschrift fur Physik*, 1968, Vol 216, pp 398-410

## **P**

Pasimeni L, Rella R, Troisi L, Valli L, Spectroscopic characterization of a substituted phthalocyanine thin film deposited by the Langmuir-Blodgett technique, *Materials Science Forum*, 1996, Vol.203, pp.297-301

Petty M C, Langmuir-Blodgett Films; An Introduction, Cambridge University Press, 1996, Chapter 1

Petty MC, Molecular engineering using the Langmuir-Blodgett technique, *Polymer Surfaces and Interfaces*, John Wiley & Sons, 1987, Chapter 6

Pichler K, Friend RH, Burn PL, Holmes AB, Chain alignment in poly(p-phenylene vinylene) on oriented substrates, *Synthetic Metals*, 1993, Vol.55, No.1, pp.454-459

Pockels A, On the relative contamination of the water surface by equal quantities of different substances, *Nature*, 1892, Vol 46, pp 419-419

Pockrand I (b), Surface plasma oscillations at silver surfaces with thin transparent and absorbing coatings, *Surface Science*, 1978, Vol 72, pp 577-588

Pockrand I, Swalen J D (a), Anomalous dispersion of surface plasma oscillations, *Journal of the Optical Society of America*, 1978, Vol 68, pp 1147-1151

Podgorsek RP, Sterkenburgh T, Wolters J, Ehrenreich T, Nischwitz S, Franke H, Optical gas sensing by evaluating ATR leaky mode spectra, *Sensors and Actuators B - Chemical*, 1997, Vol.39, No.1-3, pp.349- 352

Pokrowsky P, Optical methods for thickness measurements on thin metal films, *Applied Optics*, 1991, Vol.30, No.22, pp.3228-3232

Pope M and Swenberg C, *Electronic Processes in Organic Crystals*, Clarendon Press, 1982, pp 327

Poynter RH, Cook MJ, Chesters MA, Slater DA, Mcmurdo J, Welford K, Chain length dependence of molecular ordering in LB films of amphotropic phthalocyanines, *Thin Solid Films*, 1994, Vol.243, No.1-2, pp.346-350

Prasad PN, Williams DJ, *Introduction to Nonlinear Optical Effects in Molecules and Polymers*, John Wiley and Sons, 1991, Chapter 5

## R

Ray AK, Hogarth CA, The use of organic materials including macromolecules in active electronic devices, *International Journal of Electronics*, 1992, Vol.73, No.5, pp.1027-1037

Ray AK, Nabok AV, Hassan AK, Omar O, Taylor R, Cook MJ, An interpretation of the structure of Langmuir-Blodgett films of octa-substituted metal-free phthalocyanine molecules from optical spectra, *Philosophical Magazine B - Physics Of Condensed Matter Statistical Mechanics Electronic Optical And Magnetic Properties*, 1998, Vol.78, No.1, pp.53-64

Rayleigh, Lord, On the tension of recently formed liquid surfaces, *Proceedings of the Royal Society of London*, Vol 47, 1890

Rella R, Serra A, Siciliano A, Tepore A, Valli L, Zocco A (a), Applications in gas sensing devices of a new macrocyclic copper complex, *Sensors and Actuators B - Chemical*, 1997, Vol.42, No.1, pp.53-58

Rella R, Serra A, Siciliano P, Tepore A, Valli L, Zocco A (c), Langmuir-Blodgett multilayers based on copper phthalocyanine as gas sensor materials: Active layer gas

interaction model on conductivity modulation, *Langmuir*, 1997, Vol.13, No.24, pp.6562-6567

Rella R, Serra A, Siciliano P, Tepore A, Valli L, Zocco A (d), NO<sub>2</sub> gas detection by Langmuir-Blodgett films of copper phthalocyanine multilayer structures, *Supramolecular Science*, 1997, Vol.4, No.3-4, pp.461-464

Rella R, Serra A, Siciliano P, Tepore A, Valli L, Zocco A, Effects of NO<sub>2</sub> oxidizing gas on a novel phthalocyanine Langmuir-Blodgett thin film, *Thin Solid Films*, 1996, Vol.286, No.1-2, pp.256-258

Rella R, Siciliano P, Manno D, Serra A, Taurino A, Tepore A, Valli L, Zocco A (b), Gas sensing properties of multilayers of two new macrocyclic copper complexes, *Sensors and Actuators B - Chemical*, 1997, Vol.44, No.1-3, pp.585- 589

Richardson T, Greenwood MB, Davis F, Stirling CJM, Pyroelectric molecular baskets: Temperature dependant polarization from substituted calix(8)arene Langmuir-Blodgett films, *Langmuir*, 1995, Vol.11, No.12, pp.4623-4625

Richardson T, Majid WHA, Cochrane ECA, Holder S, Lacey D, Langmuir-Blodgett films of linear polysiloxanes incorporating aromatic side chains - Structure - property relationships, *Thin Solid Films*, 1994, Vol.242, No.1-2, pp.61-66

Richardson T, Smith VC, Topacli A, Jiang J, Huang CH, In situ visible spectroscopy of a gadolinium bisphthalocyanine Langmuir-Blodgett film exposed to chlorine gas, *Supramolecular Science*, 1997, Vol.4, No.3-4, pp.465-470

Roberts GG, Langmuir-Blodgett films, *Contemporary Physics*, 1984, Vol.25, No.2, pp.109-128

Rosenthal I, Phthalocyanines - Properties and applications, VCH Publishers, 1989, Chapter 4

Ruadel-Teixier A, Supermolecular architecture in Langmuir-Blodgett films: Control and chemistry, *Heterogeneous Chemistry Reviews*, 1996, Vol.3, No.1, pp.1-15

## S

- Sakaguchi H, Nagamura T, Penner TL, Whitten DG, Ultrafast optical modulation of quadratic non-linearity from Ru(II)-bipyridine complex in Langmuir-Blodgett assemblies, *Thin Solid Films*, 1994, Vol.244, No.1-2, pp.947-950
- Salamon Z, Wang Y, Tollin G, Macleod HA, Assembly and molecular organization of self-assembled lipid bilayers on solid substrates monitored by surface plasmon resonance spectroscopy, *Biochimica et Biophysica Acta - Biomembranes*, 1994, Vol.1195, No.2,
- Sambles JR, Bradbery GW, Yang FZ, Optical excitation of surface plasmons: an introduction, *Contemporary Physics*, 1991, Vol.32, No.3, pp.173-183
- Schuster SC, Swanson RV, Alex LA, Bourret RB, Simon MI, Assembly and function of quaternary signal transduction complex monitored by surface plasmon resonance, *Nature*, 1993, Vol.365, No.6444, pp.343-347
- Schwiegk S, Vahlenkamp T, Wegner G, Xu Y, On the origin of main chain orientation of rigid-rod macromolecules during the Langmuir-Blodgett process, *Thin Solid Films*, 1992, Vol.210, No.1-2, pp.6-8
- Scott K, Sudiwala RV, Donovan KJ, Wilson EG, Clark TR, Control of electron transfer in a nanostructure assembled from organic molecules, *Thin Solid Films*, 1994, Vol.242, No.1-2, pp.187-190
- Separovic D, He J, Oleinick NL, Ceramide generation in response to photodynamic treatment of L5178Y mouse lymphoma cells, *Cancer Research*, 1997, Vol.57, No.9, pp.1717-1721
- Seto J, Nagai T, Ishimoto C, Watanabe H, Frictional properties of magnetic media coated with Langmuir-Blodgett films, *Thin Solid Films*, 1985, Vol.134, No.1-3, pp.101-108

Smilowitz L, Jia QX, Yang X, Li DQ, McBranch D, Buelow SJ, Robinson JM, Imaging nanometre thick patterned self assembled monolayers via second harmonic generation microscopy. *Journal of Applied Physics*, 1997, Vol.81, No.5, pp.2051-2054

Stout GH and Jensen LH, X-Ray Structure Determination, John Wiley and Sons, 1989, pp 24

Swalen JD, Optical properties of Langmuir-Blodgett films, *Journal of Molecular Electronics*, 1986, Vol 2, pp 155-181

## T

Tabor D, Babylonian legacy: An ancient text on the spreading of oil on water, *Journal of Colloid and Interface Science*, 1980, Vol 240, No 1, pp 240-245

Tao L, Fuxi G, Optical behaviour of tetra-neopentoxy phthalocyanine zinc Langmuir-Blodgett film, *Applied Optics*, 1994, Vol.33, No.17, pp.3760-3763

Thuery P, Nierlich M, Lamare V, Dozol JF, Asfari Z, Vicens J, Potassium and sodium complexes of 1,3-calix(4)-bis-crown-6: Crystal and molecular structures, H-1-NMR investigation and molecular dynamics simulation, *Supramolecular Chemistry* 1997, Vol.8, No.4, pp.319-332

Travis J, Ray AK, Thorpe SC, Cook MJ, James SA, Langmuir-Blodgett films of copper tetra-4-tert-butyl phthalocyanine molecules as NO<sub>2</sub> gas sensors, *Measurement Science and Technology*, 1995, Vol.6, No.7, pp.988-994

Tredgold RH, Hodge P, Aliadib Z, Evans SD, Surface potentials of Langmuir-Blodgett alternating layer structures, *Thin Solid Films*, 1992, Vol.210, No.1-2, pp.4-5

Truong KD, Bandrauk AD, Tranthi TH, Grenier P, Houde D, Palacin S, Time resolved third order nonlinear optical susceptibility of Langmuir-Blodgett films of mixed dimers ZnP(N<sup>+</sup>C<sub>22</sub>)<sub>4</sub>/H<sub>2</sub>P<sub>c</sub>TS<sup>4-</sup> by femtosecond laser spectroscopy, *Thin Solid Films*, 1994, Vol.244, No.1-2, pp.981-984

## U

Ueda M, Fukushima N, Kudo K, Ichimura K, Photocontrolled dispersability of colloidal silica by surface adsorption of a calix(4)resorcinarene having azobenzene groups,

*Journal of Materials Chemistry*, 1997, Vol.7, No.4, pp.641-645

Ulman A, In Introduction to Organic Thin Films, Academic Press Ltd, 1991, Chapter 2

Ungaro R, Arduini A, Casnati A, Pochini A, Ugozzoli F, New synthetic receptors based on calix(4)arenes for the selective recognition of ions and neutral molecules, *Pure And Applied Chemistry*, Vol.68, No.6, pp.1213-1218, 1996

## V

Vandevyver M, Bourgoïn JP, Barraud A, Perez X, Veber M, Jallabert C, Strezelecka H, In plane anisotropy of tetracyanoquinodimethane in Langmuir-Blodgett films, *Journal of Applied Physics D, Applied Physics*, 1992, Vol.25, No.2, pp.284-287

Vukusic PS, Sambles JR, Wright JD, Surface plasmon resonance characterization of spin-deposited phthalocyanine films, *Journal of Material Chemistry*, 1992, Vol.2, No.10, pp.1105-1106

## W

Wang J, Caffrey M, Bedzyk MJ, Penner TL, Structure changes in model membranes monitored by variable period x-ray standing waves - effect of Langmuir-Blodgett film thickness on thermal behaviour, *Journal Physical Chemistry*, 1994, Vol.98, No.42, pp.10957- 10968

Wang Y, Zhou YQ, Wang XP, Chen WQ, Xi SQ, Determination of the molecular orientation of a phthalocyanine derivative in a Langmuir-Blodgett film by polarised UV-VIS spectra, *Journal of the Chemical Society, Chemical Communications*, 1992, No.12, pp.873-875

Williams D, Fleming I, Spectroscopic Methods in Organic Chemistry, McGraw Hill Publishing Company, 1966, Chapter 2

Willock DJ, The need for realistic electrostatic models to predict the crystal structures of non-linear optic molecules, *Proceedings of the Third International Symposium on Organic Materials for Non-linear Optics*, Royal Society of Chemistry, Vol 137, 1993

Witjes MJH, Mank AJG, Speelman OC, Posthumus R, Nooren CAAM, Nauta JM, Roodenburg JLN, Star WM, Distribution of aluminium phthalocyanine disulfonate in an oral squamous cell carcinoma model. In vivo fluorescence imaging compared with ex vivo analytical methods, *Photochemistry and Photobiology*, 1997, Vol.65, No.4, pp.685-693

## X

Xu JH, Lu XZ, Han K, Zhou GP, Zhang ZM, Photoinduced molecular reorientation in optical nonlinear Langmuir-Blodgett films, *Langmuir*, 1997, Vol.13, No.12, pp.3187-3190

## Y

Yokoyama S, Nakahama T, Mashiko S, Functional dendritic macromolecules: Preparation and optical properties, *Molecular Crystals and Liquid Crystals Science and Technology Section A-Molecular Crystals and Liquid Crystals*, 1997, Vol.294, pp.19-22

Yoneyama M, Sugi M, Saito M, Ikegami K, Kuroda S, Iizima S, Photoelectric properties of copper phthalocyanine Langmuir-Blodgett film, *Japanese Journal of Applied Physics 1-Regular Papers Short Notes & Review Papers*, 1986, Vol.25, No.7, pp.961-965

## Z

Zhao XS, Xie XM, Xia XH, Wang KZ, Huang CH, Li TK, Xu LG, Effect of gas environment on second harmonic generation of Langmuir-Blodgett films, *Thin Solid Films*, 1995, Vol.263, No.1, pp.13-15

Zhou DJ, Ashwell GJ, Huang CH (b), Improved second harmonic generation from Langmuir-Blodgett monolayers of an ionically combined bis-chromophore zinc complex, *Chemistry Letters*, 1997, No.1, pp.7-8

Zhou DJ, Gan LB, Luo CP, Huang CH, Wu Y (a), A new 4-acetalphenyl C-60-pyrrolidine derivative and its Langmuir-Blodgett film study, *Solid State Communications*, 1997, Vol.102, No.12, pp.891-894

# Optical characterisation of amphiphilic, metal-free, non-peripheral Phthalocyanine in Langmuir-Blodgett films

Ozma Omar<sup>1</sup>, Asim K. Ray<sup>1</sup>, Aseel K. Hassan<sup>1</sup>, Zabih Ghassemlooy<sup>1</sup> and Mike J. Cook<sup>2</sup>

<sup>1</sup> Electronics and Communications Engineering Research Group, School of Engineering, Sheffield Hallam University, Sheffield, England.

<sup>2</sup> School of Chemical Sciences, University of East Anglia, Norwich, England

## ABSTRACT

Langmuir-Blodgett (LB) films of the amphiphilic, metal free, phthalocyanine 1,4-di(4-hydroxybutyl)-8,11,15,18,22,25-isopentylphthalocyanine (A40iso5H<sub>2</sub>) have been deposited onto a hydrophobically treated glass slide. Extrapolation of the pressure-area isotherm shows the area per molecule to be approximately 161Å<sup>2</sup>, which is consistent with similar phthalocyanines. The relationship between absorption and film thickness was studied by measuring the absorption spectra of increasing numbers of monolayers. A mathematical program was used to fit the absorption peaks and hence allow calculation of the phthalocyanine molecule angle on the substrate surface in the characteristic herringbone structure. Measurement of the diffuse reflectance spectra enabled a calculation of the refractive index and extinction coefficient to be made across a range of wavelengths. The step structure of the films was analysed using a scanning electron microscope to investigate film homogeneity at the boundary and across the film surface.

The films were deposited onto a layer of gold in order to excite surface plasmons with a 632.8nm He-Ne laser. The optical constants of the LB films were determined at this wavelength from the surface plasmon curves using a fitting procedure. The results obtained at 632.8nm were compared with the values calculated from spectroscopic data, and found to be in good agreement.

**Keywords:** Phthalocyanine, Langmuir-Blodgett, spectra, surface plasmon

## 1. INTRODUCTION

The LB method of organic film deposition has been used extensively as a technique for obtaining precise film thickness, for applications ranging from fibre optic filters to fabrication of Schottky devices.<sup>1,2</sup> The deposition process of LB films make them suitable for second order non-linearity experiments as a non-centrosymmetric structure can be formed, achieving a macroscopic non-linearity. In view of the possible device applications it is important to be able to optically characterise the organic material in question. Many techniques can be used to lay down the material, although the exactness and reproducibility of LB film deposition makes it an ideal candidate.

The organic materials are easily processible and structurally diverse whilst possessing the ability to be adjusted at a molecular level. These properties have lead to much interest in the applications of molecular electronics.<sup>2,3</sup> The phthalocyanine molecule is a 2-dimensional,  $\pi$ -conjugated system that has been used as a commercial dye and exhibits interesting photoconductive, electrical and optical properties.<sup>4</sup> It can incorporate as many as 70 different metal atoms into the central ring, as well as allowing substitutions at the peripheral sites. The synthesis of metal-free phthalocyanines suitable for LB deposition has been reported in literature<sup>5</sup>.

In this paper we describe the LB and optical properties of a substituted phthalocyanine (Figure 1) specially designed for LB deposition.

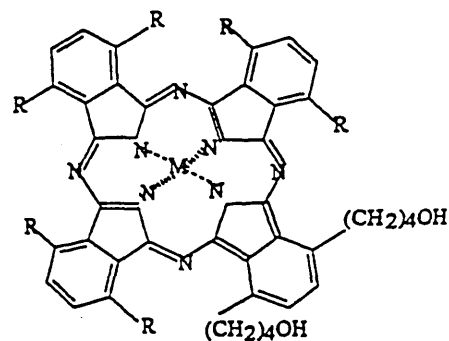


Figure 1 Chemical structure of A40iso5H<sub>2</sub> where M=H<sub>2</sub>

## 2. LANGMUIR-BLODGETT MONOLAYER STUDY AND FILM DEPOSITION

### 2.1 Experimental procedure

The phthalocyanine was ultrasonically dissolved in very high purity 1,1,1-trichloroethane to make a solution of approximately 0.1mg/ml concentration as a spreading solution. The Millipore water subphase remained at a pH of approximately 5.5 at room temperature during all experiments. A computer controlled Nima 622 trough was used to compress the monolayer whilst the pressure was monitored using a microbalance with Wilhelmy plate. Monolayer stability was assessed by maintaining a particular surface pressure for a given time.

### 2.2 Langmuir-Blodgett monolayer study

The monolayer was compressed approximately 30 minutes after spreading to allow complete evaporation of solvent. Repeated compression and decompression were performed in order to reduce hysteresis and in effect, 'train' the monolayer. The pressure-area isotherm produced shows a marked decrease in hysteresis (Figure 2) and film collapse take place above 25 mN/m (Figure 3). Extrapolation of the linear region of the diagram (Figure 3) shows the area occupied per molecule on the water surface to be approximately  $161\text{\AA}^2$ . This is consistent with similar phthalocyanines synthesised by M. Cook et al.<sup>6</sup>

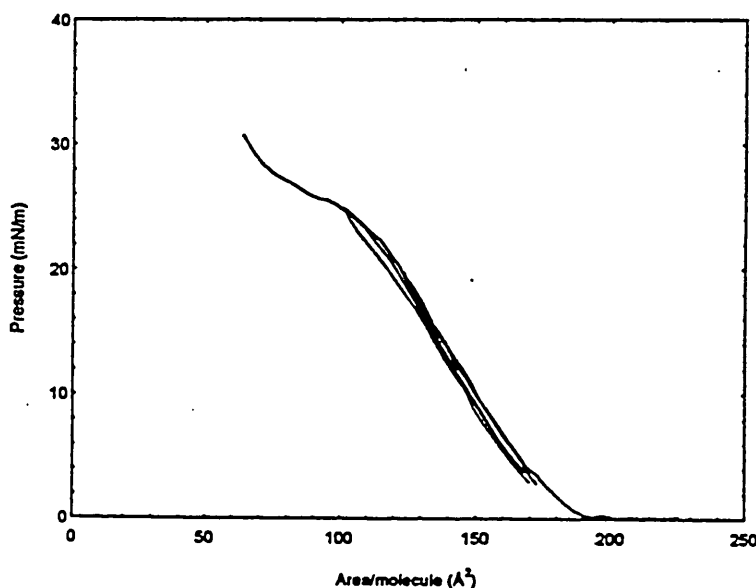


Figure 2 Pressure area diagram showing hysteresis effect in A40iso5H<sub>2</sub>.

### 2.3 LB film deposition

Ultrasonically cleaned, hydrophobically treated microscope glass slides were used as substrates for deposition resulting in films suitable for spectroscopic analysis. LB films deposited onto gold coated slides enabled surface plasmon resonance experiments to be conducted. Both substrate types produced Y-type multilayers with a dipping speed of 20 mm/min, for both up and down strokes, at a constant surface pressure of 25 mN/m.

The films were deposited in a 'step' structure on the glass enabling a relation between monolayer thickness and absorption to be made. A similar step structure was formed on gold substrates enabling a more accurate determination of optical constant from the surface plasmon resonance data.

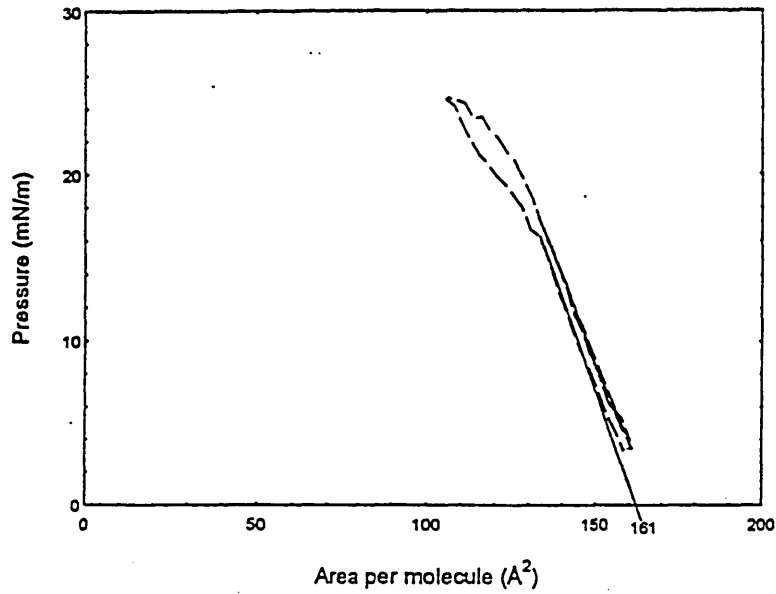


Figure 3 Pressure area diagram of A40iso5H<sub>2</sub>

### 3. SPECTRAL ANALYSIS

The visible absorption and reflectance spectra were obtained using an ATI Unicam UV-VIS spectrophotometer and integrating sphere on a Hitachi U-2000 double beam spectrophotometer with light at normal incidence to the substrate surface and reference sample. The solution spectra was measured in aristar grade 1,1,1-trichloroethane of concentration 0.1 mg/ml. Figure 4 shows the linear relation between the absorbance and number of monolayer. The value of absorbance was measured at its maximum obtained at wavelength of 749nm for greater accuracy.

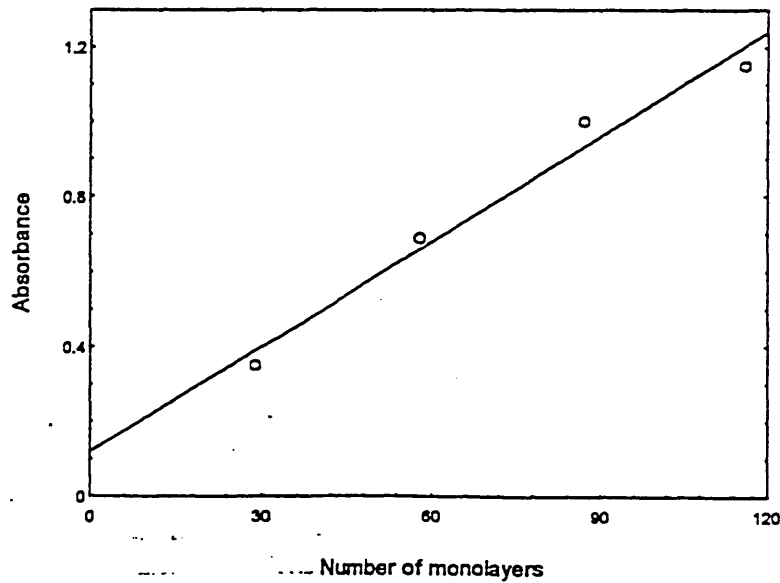


Figure 4 Relation between absorbance of A40iso5H<sub>2</sub> and increasing monolayer thickness at  $\lambda_{max}=749nm$

The spectra of the solution and the material in thin film form were compared (Figure 5) revealing pronounced differences caused by the degrees of freedom of movement available to the molecule. Both spectra show the two characteristic peaks of

this material. The optical absorption spectra shows absorption in the Q-band which is split into  $Q_x$  and  $Q_y$  bands due to the decrease in symmetry when compared with the metal phthalocyanines. The lower intensity 'shoulders' to the blue side of the  $Q_x$  and  $Q_y$  are of a vibrational nature. The Q-band absorption arises from  $\pi \rightarrow \pi^*$  transitions where the  $Q_x$  band corresponds to the  $4_{au} \rightarrow 6b_{2g}$  transition and the  $Q_y$  to  $4_{au} \rightarrow 6b_{3g}$ . The LB film absorption spectra (Figure 5) shows the  $Q_x$  and  $Q_y$  bands slightly broadened and shifted symmetrically to the 'red' and 'blue' side when compared to solution. Although, it should be noted that the  $Q_y$  band of the LB film spectra has a considerably reduced intensity when compared with similar materials.<sup>6</sup> This spectral shifting behaviour can be explained by the formation of physical dimers in the herring-bone structure of the LB films. The close proximity of the phthalocyanine rings leads to coupling between their electronic states and exciton band splitting of the dimer. The energy is shifted symmetrically to the red and blue sides of the  $Q_x$  and  $Q_y$  bands.

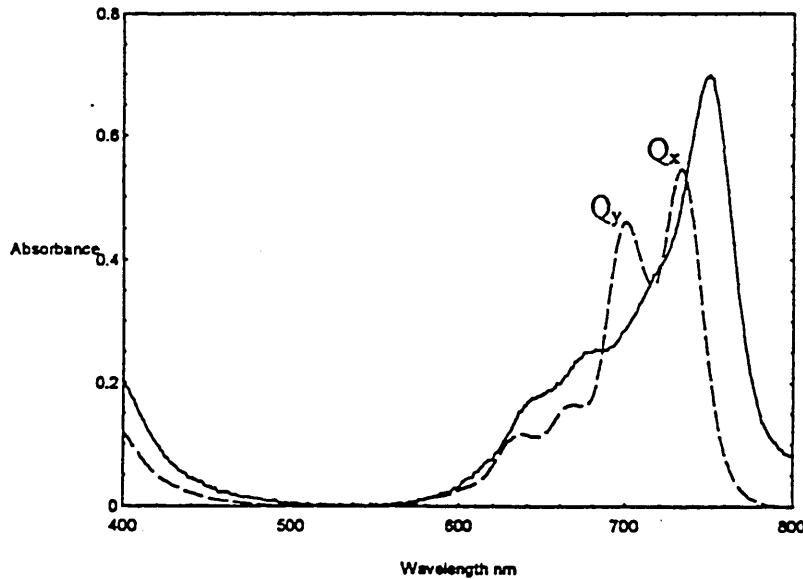


Figure 5 Optical absorbance profile for LB films (solid line) and solution 0.1mg/ml in trichloroethane (dashed line)

### 3.1 Refractive index and extinction coefficient calculation

The absorption and reflectance spectra enabled a calculation of the refractive index and extinction coefficient profiles to be made (Figure 6) using<sup>7</sup>;

$$R = \frac{(n-1)^2 + k^2}{(n+1)^2 + k^2} \quad (1)$$

where  $R$  = reflectance,  $n$  = refractive index and  $k$  = extinction coefficient.

With reference to Figure 6 the maximum and minimum values of refractive index and extinction coefficient, as well as those at 632.8nm for SPR comparison are shown below in Table 1 for a monolayer thickness of 17Å;

Wavelength nm	Refractive index	Wavelength nm	Extinction coefficient
$\lambda_{max} = 775$	4.24	$\lambda_{max} = 750$	0.92
$\lambda_{min} = 624$	1.65	$\lambda_{min} = 105-147$	0
$\lambda = 633$	1.68	$\lambda = 633$	0.16

Table 1 Values of refractive index and extinction coefficient at  $\lambda_{max}$ ,  $\lambda_{min}$ , and at 632.8nm.

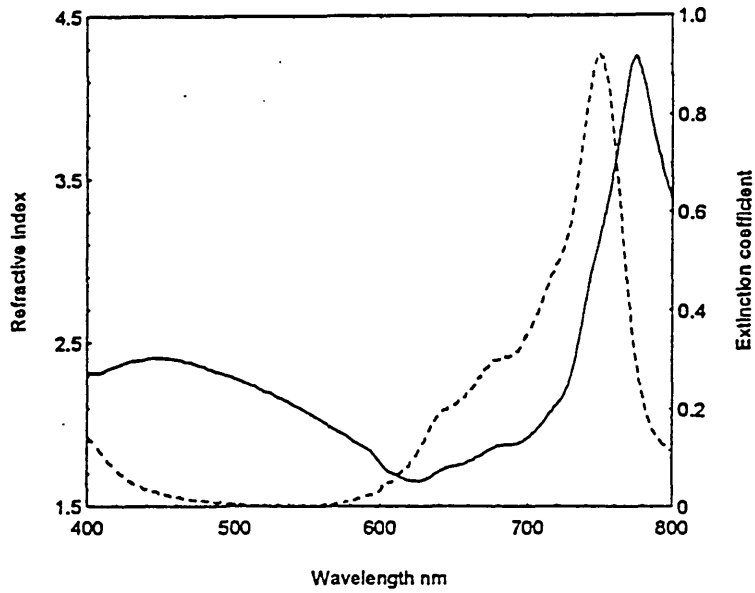
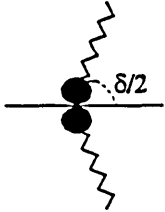


Figure 6 Refractive index (solid line) and extinction coefficient (dashed line) profile

### 3.2 Gaussian analysis

The visible spectra (Figure 5) for LB films was decomposed into Gaussian peaks enabling calculation of the angle ( $\delta$ ) between phthalocyanine molecules in the herring-bone structure of deposited LB films (Figure 7).



It was found that the spectra from 500nm to 800nm decomposed into four peaks, where each peak corresponded to a characteristic electronic transition (Figure 8). The peaks could not be accurately described as simple Gaussian functions, but as a mixture of Gaussian and Lorentzian approximations. The function parameters are given in the table 2;

Figure 7 Angle between LB film phthalocyanine molecules

Centre	Amplitude	Width	% Gaussian	Area
15738.8	0.38192	3142.41	87.9485	1350.75
14055.2	0.989438	1130.96	35.6589	1555.7
17419.9	0.0959587	1479.87	100	151.161
15046.1	0.114717	809.409	99.5203	99.0645

Table 2 Function parameters corresponding to Gaussian/Lorentzian approximations of Figure 8

The angle  $\delta$  can be calculated using the following equation<sup>8</sup>;

$$\tan^2 \frac{\delta}{2} = \frac{f_{||}}{f_{\perp}} \quad (2)$$

where  $f_{//}$  = oscillator strength component parallel to stack axis,  $f_{\perp}$  = oscillator strength component perpendicular to stack axis.

Assuming that  $f_{//}$  and  $f_{\perp}$  correspond to the blue and red shifted bands of the molecular dimer, respectively and that the oscillator strength is proportional to the integral of the absorption intensity through the corresponding band<sup>9</sup>, equation (2) can be written as;

$$\tan^2 \frac{\delta}{2} = \frac{\int J_{//}(\nu) d\nu}{\int J_{\perp}(\nu) d\nu} \quad (3)$$

where  $\int J_{//}(\nu) d\nu$  = integral of absorption intensity through the blue shifted band,  $\int J_{\perp}(\nu) d\nu$  = integral of absorption intensity through the red shifted band.

Substituting values of areas of the integral intensity into equation 3 yields a value of 94.04 for  $\delta$ . This value is in good agreement with previous studies performed on similar phthalocyanines<sup>10</sup> showing the characteristic herring-bone structure.

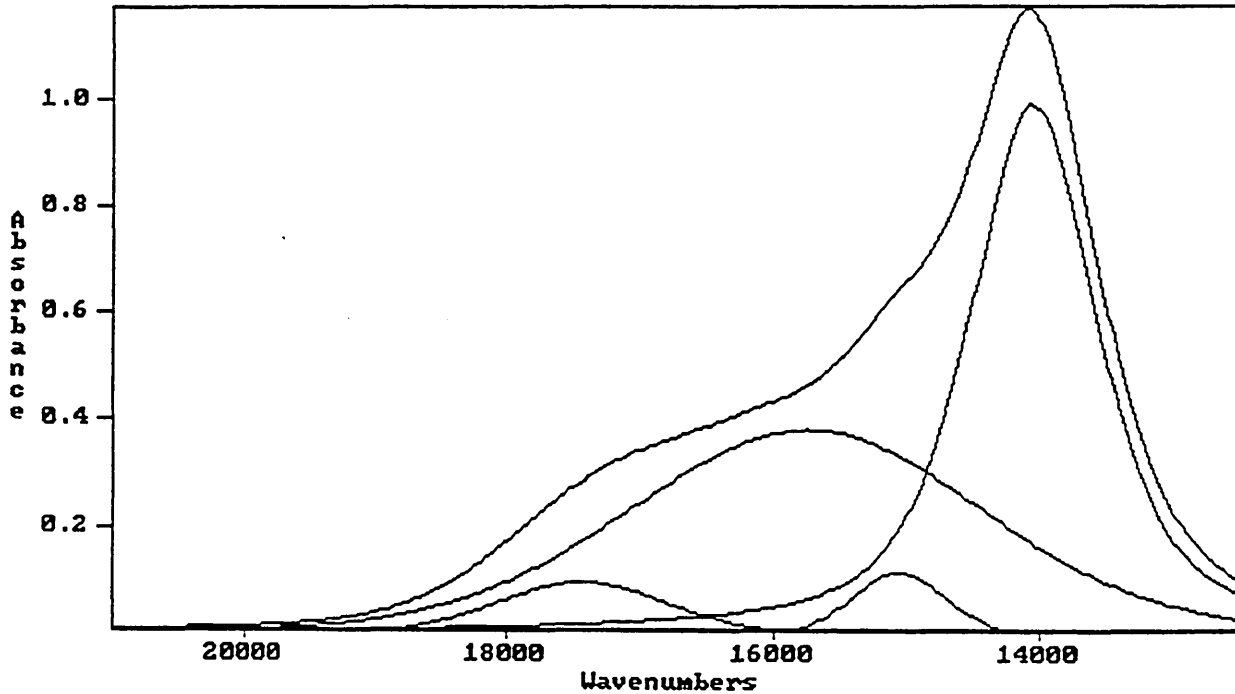


Figure 8 Decomposition of phthalocyanine absorption spectra into Gaussian/Lorentzian peaks

#### 4. SURFACE PLASMON RESONANCE STUDY

The Kretschmann configuration of apparatus was used to excite surface plasmons with He-Ne laser light at a wavelength of 632.8nm incident on the LB film/gold/glass structure. A gold layer of 435Å was evaporated onto an ultrasonically cleaned glass slide and stored under vacuum until use. An LB film step structure of 2 and 4 monolayers was deposited onto a section of this substrate enabling surface plasmon resonance (SPR) study (Figure 9). The normalised reflectance curves were used to fit the experimental data to theoretical values, enabling determination of refractive index, extinction coefficient and monolayer thickness.

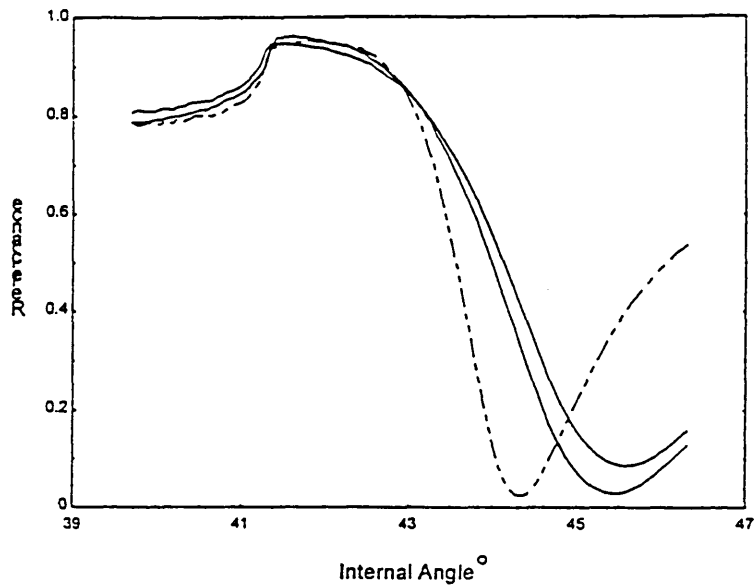


Figure 9 Normalised SPR curves for 435 Å gold layer only (dashed line) and 2 and 4 monolayers of A40iso5H<sub>2</sub> (solid lines)

The data fitting yielded results to a reasonable accuracy;

Refractive index	$1.6 \pm 0.1$
Extinction coefficient	$0.35 \pm 0.1$
Monolayer thickness Å	$16.25 \pm 1.25$

### 5. SCANNING ELECTRON MICROSCOPY

Scanning electron microscopy (SEM) study reveals valuable information about the surface morphology and edge definition of the LB films. The possible formation of aggregates and defects on the surface can affect the device suitability of the material<sup>11,12</sup>. The SEM image of the 40 monolayer LB film (Figure 10) shows the surface to be relatively homogeneous with only minor defects, whilst inspection of the 200 monolayer section (Figure 11) reveals a rougher, more grainy structure.

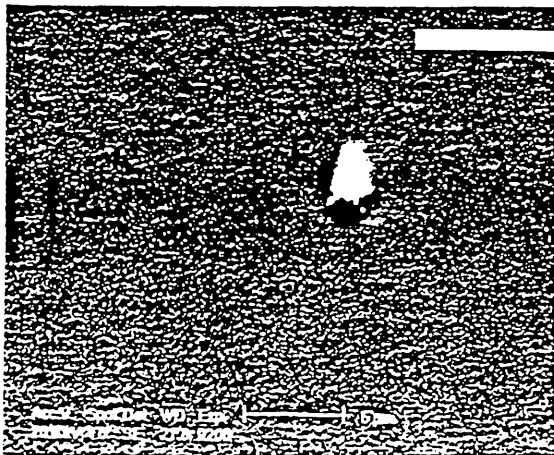


Figure 10 SEM image of 40 monolayers of A40iso5H<sub>2</sub>

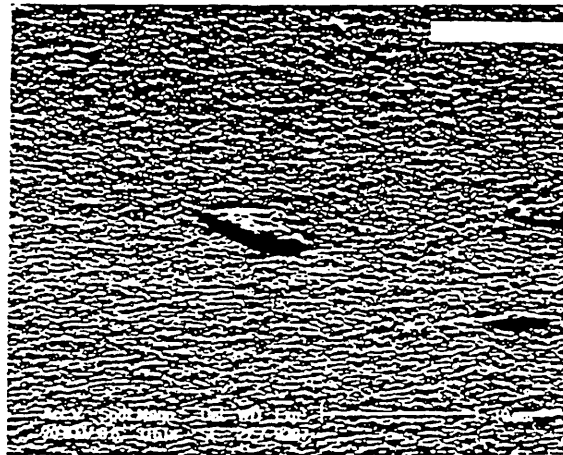


Figure 11 SEM image of 200 monolayers of A40iso5H<sub>2</sub>

## 6. CONCLUSIONS

The Langmuir-Blodgett monolayer and film deposition properties of the material A40iso5H<sub>2</sub> have been studied revealing its suitability for use as a LB material. The technique of SPR and measurements of visible spectra performed on LB films have enabled an estimation of the values of refractive index, extinction coefficient and monolayer thickness to be made. The value of refractive index and extinction coefficient obtained were found to agree well. The solution absorption spectra clearly shows two main absorption peaks corresponding to the Q<sub>x</sub> and Q<sub>y</sub> bands which shift symmetrically to the 'red' and 'blue' due to the formation of physical dimers in the LB films. Decomposition of the spectra into Gaussian/Lorentzian peaks yields a molecular angle of 94.04° indicating the characteristic herring-bone structure of phthalocyanine molecules.

## REFERENCES

1. R. B. Charters, A. P. Kuczynski, S. E. Staines, R. P. Tatam and G. J. Ashwell, "In-line fibre optic channel dropping filter using Langmuir-Blodgett films," *Electronic Letters*, Vol. 30 No. 7, pp. 594-595, 1994.
2. Y. Q. Liu, Y. Xu and D. B. Zhu, "Preparation and electronic properties of Schottky devices utilising an asymmetrically substituted metal-free phthalocyanine Langmuir-Blodgett film as barrier layers," *Synthetic Metals*, Vol. 71, pp. 2249-2250, 1995.
3. J. Tsibouklis, M. Petty, Y. Song, R. Richardson, J. Yarwood, M. C. Petty and W. J. Feast, "Docosanoyl itaconate/1-docosylamine alternate-layer Langmuir-Blodgett films: polymerisation, pyroelectric properties and infrared spectroscopic studies," *Journal of Material Chemistry*, Vol. 1 No. 5, pp. 819-826, 1991.
4. K. Law, "Organic photoconductive materials: recent trends and developments," *Chemical Reviews*, Vol. 93, pp. 449-486, 1993.
5. R. H. Poynter, M. J. Cook, M. A. Chesters, D. A. Slater and J. McMurdo, "Chain length dependence of molecular ordering in LB films of amphotropic phthalocyanines," *Thin Solid Films*, Vol. 243, pp. 346-350, 1994.
6. M. J. Cook, Personal communication, 1995.
7. A. Abass, A.K. Hassan and R.H. Misho, "Investigation of optically allowed transitions of alpha-sulfur thin- films.", *Journal Of Applied Physics*, Vol. 58(4), pp. 1640-1642, 1985
8. S. Kirstein and H. Mohwald, "Structure and optical properties of a monolayer single crystal of a cyanine dye," *Chemical Physics Letters*, Vol 189, pp. 408-413, 1992.
9. M. Pope and C. E. Swenberg, "Electronic processes in organic crystals," Clarendon Press, 1982
10. M. J. Cook, J. McDurdo, D. A. Miles, R. H. Poynter, J. M. Simmons, S. D. Haslam, R. M. Richardson and K. Welford, "Monolayer behaviour and Langmuir-Blodgett film properties of some amphiphilic phthalocyanines: Factors influencing molecular organisation within the film assembly," Vol 4, pp. 1205-1213, 1994.
11. A. K. Dutta, T. N. Misra and A. J. Pal, "A spectroscopic study of nonamphiphilic pyrene assembled in Langmuir-Blodgett films: formation of aggregates", *Langmuir*, Vol 12, pp. 459-465, 1996.
12. Y. K. Kim, B. C. Sohn, J. H. Kim, D. S. Kim, S. Jeong, D. Yoo and D. Kang, "Surface characterisation of ultra-thin polyimide films formed by using Langmuir-Blodgett method", *Molecular Crystals and Liquid Crystals*, Vol 247, pp. 243-250, 1994.

# Resorcinol calixarenes (resorcarenes): Langmuir-Blodgett films and optical properties

O. Omar, A. K. Ray\* and A. K. Hassan

*Physical Electronics and Fibre-optics Laboratories, School of Engineering, Sheffield Hallam University, Pond Street, Sheffield S1 1WB, UK*

and F. Davis

*Department of Chemistry, Sheffield University, Brook Hill, Sheffield S3 7HF, UK  
(Received 6 September 1996; revised 6 December 1996)*

Specially synthesized amphiphilic resorcinol calixarene (resorcarenene 2) molecules have been deposited as Langmuir-Blodgett (LB) films on a variety of substrates including hydrophobically treated glass slides, silicon and gold-coated glass slides. A value of  $1.9\text{nm}^2$  is obtained for the area per molecule from measurements of pressure/area isotherms of the floating layer. Optical absorption studies within the ultraviolet-visible frequency region have been performed on these molecules in both LB films and in solution of resorcarenene 2 in chloroform, containing 10% ethanol. Molecular aggregation in the form of dimerization is believed to take place during film formation. Further analysis has been carried out for Langmuir-Blodgett films of resorcarenene 2 by using Fourier transform infra-red spectroscopy, low-angle X-ray diffraction and surface plasmon resonance (SPR) techniques. The monolayer thickness of 1.6 nm found from SPR measurements is consistent with that from other experimental observations. © 1997 Elsevier Science Ltd. All rights reserved.

(Keywords: calixarene; Langmuir-Blodgett films; optical characterization)

## INTRODUCTION

Calixarenes and resorcarenes are known as molecular baskets owing to their ability to form complexes with a range of chemical species<sup>1</sup>. These compounds form a series of well-defined cyclic oligomers, allowing variations of the cavity size according to the requirements of different guest molecules. Films of *p*-tert-butyl calixarene molecules adhere well to the gate oxide layer of a field-effect transistor for application as a chemical sensor in liquid media<sup>2</sup>. Substituted resorcin[4]arenes can be deposited in the form of a self-assembled monolayer on a quartz crystal<sup>3</sup>. Calixarenes were shown to form stable monolayers when spread over a water subphase and their films deposited by the Langmuir-Blodgett (LB) technique are quite homogeneous<sup>4</sup>. Such films have great potential for chemical sensing applications, where they are capable of complexing with neutral compounds such as aromatic compounds and hydrocarbons<sup>5</sup>. Where carboxyl and amino groups have been included into the calix(8)arene rings two materials have been produced

whose alternate-layer LB films have displayed a pyroelectric effect<sup>6</sup>. Highly ordered structures have also been produced by immobilizing resorcarenes in gold-thiol monolayers, a technique known as self-assembly film deposition<sup>7</sup>. Resorcarenes have also been reported to rapidly form a multilayered structure from a bulk solution onto such an ordered film by van der Waals' interdigitation-hydrogen-bonding alternations<sup>8</sup>.

This paper reports the results of optical characterization of the azobenzene derivative, resorcarenene 2 molecules. These molecules have been deposited as LB films on a variety of solid substrates. The LB technique allows the layer-by-layer transfer of molecules from the subphase onto a solid substrate, enabling an ordered molecular structure to be obtained. Optical methods include Fourier transform infra-red spectroscopy (FTIR) and surface plasmon resonance (SPR). SPR is a very sensitive optical probe of the optical properties of metal surfaces. The technique can be used to determine the optical parameters of thin dielectric layers such as LB films deposited on a metal surface<sup>9</sup>. It has been widely exploited as an optical technique for chemical and bio sensing.

\* To whom correspondence should be addressed

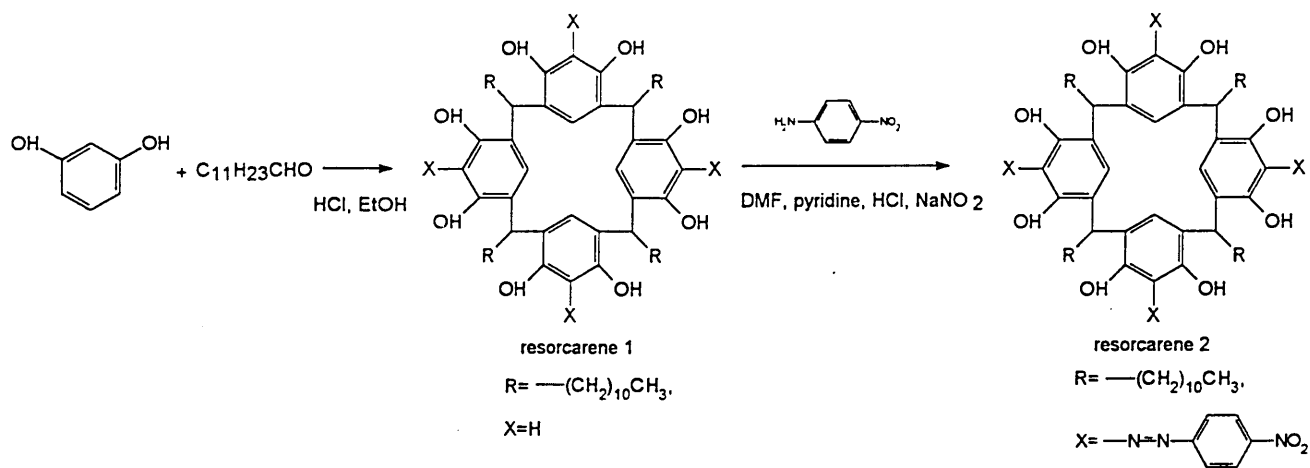


Figure 1 Synthesis of resorcarenes

## EXPERIMENTAL

### Material synthesis

The tetra-undecyl substituted resorcarene **1** (Figure 1) was synthesized by the acid-catalysed condensation of dodecanal and resorcinol as previously published<sup>10</sup>, and its purity verified by nuclear magnetic resonance spectroscopy (NMR), infra-red spectroscopy (IR) and elemental analysis. It was then coupled with *p*-nitroaniline under similar conditions to those described by Manabe *et al.*<sup>11</sup>. Dimethyl formamide (DMF) (20 ml), HCl (1.3 ml) and *p*-nitroaniline (0.69 g) were combined and cooled in an ice bath. Sodium nitrite (0.38 g) in 10 ml DMF was added dropwise whilst stirring. Resorcarene **1** (1.1 g) was then added and the mixture kept refrigerated overnight. The mixture turned a very deep wine red in colour. The resorcarene **2** was isolated by precipitation into water and recrystallization to constant NMR from EtOH. The yield was 1.66 g (97%), and one peak was obtained by high-performance liquid chromatography. <sup>1</sup>H NMR showed loss of the calix proton and formation of the diazo compound [loss of singlets at 7.1 and 6.5 ppm, appearance of peaks at 7.25 (s, 1H, *para* proton of resorcinol unit), 15.5, 15.0 (s, 1H, -OH), 7.50 (d, 1H), 7.7 (d, 1H), 8.3 (t, 2H), all N Ar-NO<sub>2</sub> protons]. Analysis: C, 67.3%; H, 7.3%; N, 9.6% (calc.: C, 67.7%; H, 7.3%; N, 9.9%). Ultraviolet (UV) spectrophotometry (CHCl<sub>3</sub>): 451 nm, = 110 000 cm<sup>2</sup> mol<sup>-1</sup>.

### LB deposition

Experiments were performed on a NIMA 622 dual-compartment trough containing deionized water with a nominal pH of 5.5 at room temperature. The compound was spread from 0.5 mg ml<sup>-1</sup> concentration in chloroform (10% ethanol) on the subphase, enabling monolayer study following complete evaporation of the solvent (5–10 min). Under

compression, the resorcarene **2** monolayer exhibited fairly stable behaviour with little decrease in surface area. Upon sonification glass substrates were rendered hydrophobic by treatment with dimethyldichlorosilane for 30 min. The LB films were transferred onto these glass slides at a constant surface pressure of 25 mN m<sup>-1</sup> for optical absorption experiments. Gold-coated glass slides and silicon substrates were used for SPR measurements and FTIR analysis, respectively. Different deposition parameters were employed for different types of substrate and these are summarized in Table 1.

### Film characterization

X-ray diffraction studies were carried out with a Philips PW1380 horizontal diffractometer fitted with a graphite crystal monochromator and using the Cu K<sub>α</sub> line (wavelength 0.1542 nm). FTIR spectra were measured in reflection and transmission on a Perkin-Elmer 1725X spectrometer with a Harrick reflection accessory and an MCT detector.

UV-visible (UV-vis.) absorption spectra have been taken for 72 monolayers deposited onto glass microscopic slides. The spectra were measured with a UNICAM UV-VIS spectrophotometer in the wavelength range 300–800 nm.

Surface plasmon resonance measurements have been

Table 1 Parameters showing Langmuir-Blodgett deposition

Substrate	Transfer ratios for strokes		Dipping speed (mm min <sup>-1</sup> )	Waiting time between two successive dips (s)
	Up	Down		
Glass	1	0.6	10	300
Silicon	1	0.5	10	300
Gold-coated glass	1	0.3	10	300

performed by using the Kretschmann<sup>12</sup> configuration, where a gold (Au)-coated slide was brought in contact with a 90° glass prism with index-matching fluid. p-Polarised monochromatic light from a He-Ne laser source ( $\lambda=632.8\text{ nm}$ ) has been used to excite the surface plasmons on an Au layer of about 36 nm in thickness. LB films of resorcarene **2** were deposited onto a section of the gold film and the shifted reflectance curves obtained were fitted to the theoretical curves by using Fresnel reflection theory, enabling determination of the refractive index, extinction coefficient and monolayer thickness.

## RESULTS AND DISCUSSION

Figure 2 shows a pressure/area ( $\pi/A$ ) isotherm of the resorcarene **2** on compression. The isotherm exhibited some hysteresis during the first compression run, but after the monolayer was trained by performing a few compression-relaxation processes it became more stable and reproducible. The area per molecule ( $A$ ) was derived from the  $\pi/A$  isotherm by extrapolating the linear section of the graph to  $\pi=0$ , and a value of about  $1.9\text{ nm}^2$  was obtained.

X-ray diffraction studies of 40 monolayers of resorcarene **2** on Si showed one Bragg peak, giving a spacing of 3.18 nm. CPK models of resorcarene **2** indicate that the fully extended molecule is 2.24 nm long. It appears therefore that there must be tilting of the side chains or interdigitation, as was found in the crystal structure of resorcarene **1**<sup>6</sup>. Interdigitation of the head groups is also a possibility from CPK modelling.

The FTIR spectra of resorcarene **2** deposited onto Si, in both reflection and transmission modes, are shown in Figure 3. Most noticeable are the variations

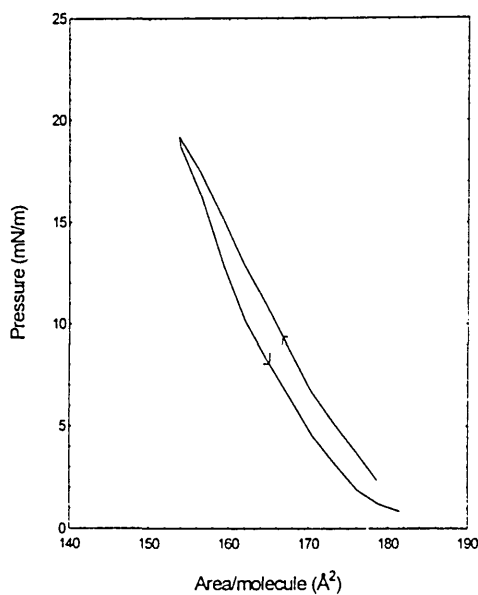


Figure 2 Pressure area isotherm of resorcarene **2**

in intensity of the N-O asymmetric and symmetric stretches at  $1524$  and  $1343\text{ cm}^{-1}$ , respectively. From CPK models, the azo groups are at about 60° to the substrate (assuming that resorcarene **2** stands perpendicular to the surface) which would have this orientation effect on the IR spectra. The C-H asymmetric stretch is at  $2927\text{ cm}^{-1}$ , which indicates that the side chains are mobile and have a liquid-like structure.

The UV-vis. absorption spectrum of the 72-monolayer LB film of resorcarene **2** deposited on glass substrate is shown in Figure 4 superposed on a similar spectrum of the same compound as a solution in chloroform. The LB film spectrum shows a single absorption peak within the spectral range of study, centred at about 454 nm. This absorption is slightly red-shifted (6 nm) and broadened relative to the spectrum of the chloroform solution. The shift in the absorption band of the LB film may be the result of some kind of molecular aggregation which takes place during film formation, such as dimerization<sup>13</sup>.

Reflectance versus the angle of incidence SPR curves of Au and Au/LB films are shown in Figure 5. The presence of two and four monolayers of resorcarene **2** LB films on Au has obviously resulted in a shift of SPR position to a greater angle of incidence and a slightly broader reflectance curve with increasing film thickness. The data for the Au and Au/LB films (four monolayers of resorcarene **2**) curves have been fitted to Fresnel reflection formula to determine the optical parameters of both films (Table 2). Results for the Au film are in reasonable agreement with the literature<sup>14</sup> while the optical parameters for resorcarene **2** are found to compare well with those obtained for similar resorcarenes<sup>5</sup>. From Table 2, a thickness of about 6.0 nm for four monolayers was obtained for resorcarene **2**, implying a thickness per monolayer of about 1.6 nm and hence a value of 3.2 nm for bilayer thickness. This is in excellent agreement with the X-ray diffraction measurements undertaken in this study.

## CONCLUSION

Resorcarene **2** has been synthesized and deposited as LB films on glass slides, gold-coated glass slides and silicon substrates. The films have been characterized optically by means of X-ray diffraction, FTIR, UV-vis. spectroscopy and surface plasmon resonance. By comparing the X-ray results with CPK analysis it appears that tilting of the side chains of the molecules or interdigitation, as was found in the crystal structure of resorcarene **1**, is taking place. This may account for the smaller bilayer thickness of LB films of resorcarene **2** when compared with twice the length of the resorcarene **2** molecule on its

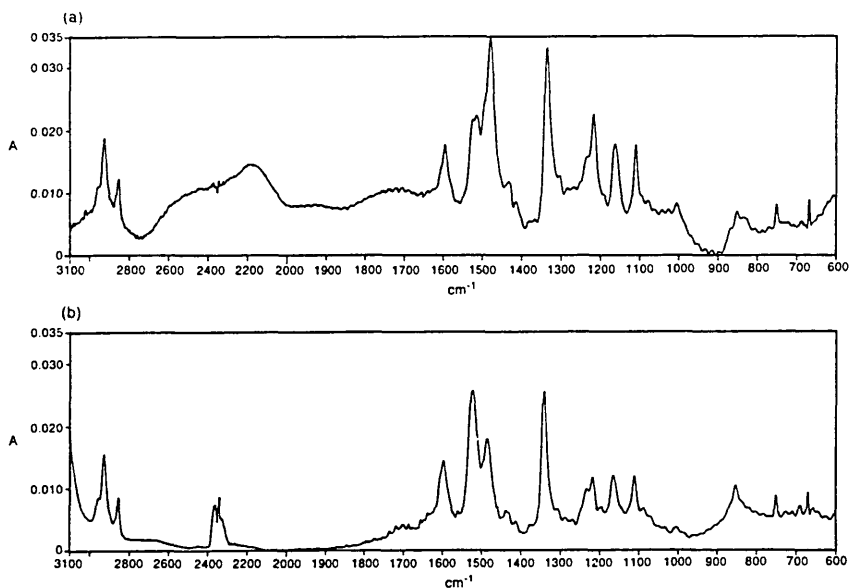


Figure 3 FTIR spectra of resorcarene 2: (a) transmission of 40 LB monolayers on Si; (b) grazing-angle spectrum of 20 LB monolayers on gold-glass

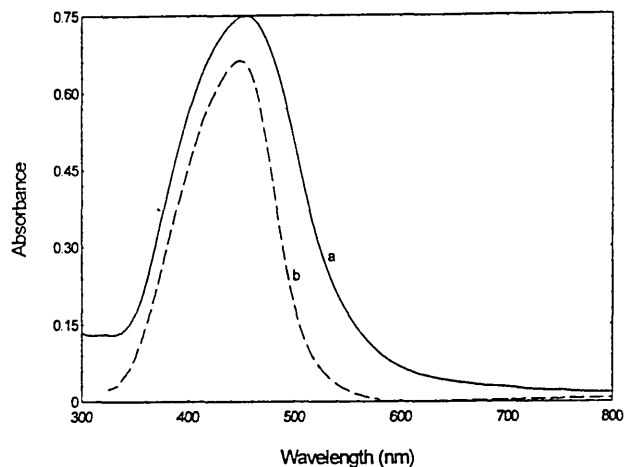


Figure 4 Absorption spectra of resorcarene 2: (a) 72 LB monolayers; (b) in solution (chloroform)

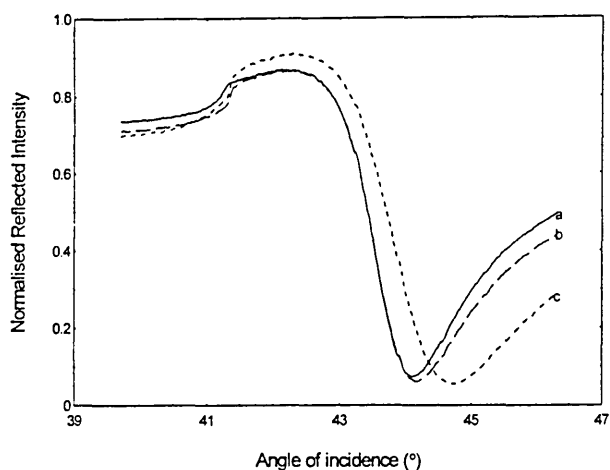


Figure 5 SPR reflectance curves for gold (a) and for resorcarene 2 LB films of two monolayers (b) and four monolayers (c) deposited on gold

Table 2 Values of optical constants of gold and resorcarene 2 LB films

Materials	Refractive index ( $n$ )	Extinction coefficient ( $k$ )	Thickness of the film (nm)
Gold film	$0.224 \pm 0.067$	$3.460 \pm 0.525$	$36 \pm 1$
LB films of resorcarene 2 molecules	$1.35 \pm 0.20$	$0.063 \pm 0.026$	$6.0 \pm 0.5$

full extension. Monolayer thickness derived from SPR reflectance curve fitting is in good agreement with the above findings, and optical parameters obtained compare very well with those found in the literature.

## ACKNOWLEDGEMENTS

The authors acknowledge the assistance of Dr Z. Ali-Adib of the University of Manchester for X-ray diffraction measurements and Professor J. R. Sambles of the University of Exeter for the provision of a theoretical fitting program.

## REFERENCES

- Gutsche, C. D., in *Calixarenes*. Monographs in Supramolecular Chemistry. Royal Society of Chemistry, London, 1989.
- Ben chaabane, R., Gamoudi, M., Guillaud, G., Jouve, C., Lamartine, R., Bouazizi, A. and Maaref, H., *Sensors and Actuators B*, 1996, **31**, 41.
- Ricket, J., Weiss, T. and Gopel, W., *Sensors and Actuators B*, 1996, **31**, 45.
- Kudhara, K., Ohto, K., Tanaka, Y., Aoyama, Y. and Kunitake, T., *J. Am. Chem. Soc.*, 1991, **113**, 444.
- Nabok, A. V., Lavrik, N. V., Kazantseva, Z. I., Nesterenko, B. A.,

- Markovskiy, L. N., Kalchenko, V. I. and Shivaniuk, A. N., *Thin Solid Films*, 1995, **259**, 244.
6. Adams, H., Davis F. and Stirling, C. J. M., *J. Chem. Soc., Chem. Commun.*, 1994, 2527.
  7. Richardson, T., Greenwood, M. B., Davis, F. and Stirling, C. J. M., *Langmuir*, 1995, **11**, 4623.
  8. Davis, F. and Stirling, C. J. M., *J. Am. Chem. Soc.*, 1995, **117**, 10385.
  9. Gordon, J. G. and Swalen, J. D., *Optics Commun.*, 1977, **22**, 374.
  10. Aoyama, Y., Tanaka, Y., Toi, H. and Ogoshi, H., *J. Am. Chem. Soc.*, 1988, **110**, 634.
  11. Manabe, O., Asakura, K., Nishi, T. and Shinkai, S., *Chem. ELT*, 1990, **7**, 1219.
  12. Kretschmann, E., *Z. Phys.*, 1971, **241**, 313.
  13. Pope, M. and Swenberg, C. E., in *Electronic Processes in Organic Crystals*. Clarendon Press, Oxford, 1982.
  14. Vukusic, P. S., Sambles, J. R. and Wright, J. D., *J. Mater. Chem.*, 1992, **2**, 1105.

## Appendix III

### Langmuir-Blodgett Trough Cleaning Procedure

- a) empty the trough of its contents and remove pressure sensor
- b) initially swab out the trough with deionised water
- c) clean the trough using Analar grade Chloroform
- d) clean the trough using Analar grade Propan-2-ol
- e) clean the trough using Aristar grade Chloroform
- f) clean the trough using Aristar grade Propan-2-ol
- g) swab out the trough using deionised water

All of the above procedures are carried out using dust free tissues whilst wearing dust free gloves as recommended by the Health and Safety Executive, Sheffield. This cleaning procedure was repeated at least every other day and each time the deposition material was changed.

### Langmuir-Blodgett Substrate Cleaning Procedure

- a) Wash slides in deionised water and treat in ultra-sonic bath for 5 minutes
- b) Soak in Analar grade Dichloromethane and treat in ultra-sonic bath for 5 minutes
- c) Soak in Analar grade Propan-2-ol and treat in ultra-sonic bath for 5 minutes
- d) Soak in Aristar grade Propan-2-ol and treat in ultra-sonic bath for 5 minutes
- e) Wash with deionised water

The substrates were then dried and left in a sealed container to ensure minimal contact with the environment. The flasks were thoroughly dried and kept sealed until use.

# Inclusion phenomenon in mixed floating layers containing phthalocyanines

A.V. Nabok<sup>a,\*</sup>, A.K. Ray<sup>a</sup>, A.K. Hassan<sup>a</sup>, O. Omar<sup>a</sup>, R. Taylor<sup>a</sup>, T. Richardson<sup>b</sup>, M. Pavier<sup>b</sup>

<sup>a</sup>Physical Electronics and Fibre Optics Research Laboratories, School of Engineering, Sheffield Hallam University, City Campus Pond Street, Sheffield S1 1WB, UK

<sup>b</sup>The University of Sheffield, Centre for Molecular Materials and Department of Physics, Hicks Building, Hounsfield Road, Sheffield S3 7RH, UK

## Abstract

UV-vis absorption spectra of floating layers of octa-substituted metal-free phthalocyanines (AmPc) mixed with stearic acid or calix(4)-resorcinarene derivatives (CA) were studied during monolayer compression. Most of the mixed floating layers, as well as those of the pure AmPc compounds, show characteristic spectra typically attributed to the AmPc condensed state, even at zero surface pressure. These results indicate the formation of aggregates of AmPc molecules on the water surface immediately after spreading. However mixed AmPc/CA floating layers with the molar ratios less than 1:2 show some spectral transformation at high values of surface pressure, which can be interpreted in terms of molecular rearrangement. Isolated AmPc molecules are thought to have formed due to their inclusion within the CA matrix. © 1998 Elsevier Science S.A. All rights reserved

**Keywords:** Phthalocyanines; Calixarenes; Floating layers; Langmuir films; Molecular aggregation; Molecular inclusion

## 1. Introduction

The formation of thin organic films from molecules having various functions is one of the main directions in molecular engineering [1]. Methods of producing thin films of organic composite materials include Langmuir–Blodgett (LB) deposition [2] and the self-assembly polyelectrolyte technique [3]. However, these techniques facilitate the formation of alternate layers of different components. Mixing different molecules in the same layer and producing homogeneous mixed films seem to be more complicated because of the difference in the physico/chemical properties of the components, such as their amphiphility. Molecular aggregation and phase separation also restrict the formation of homogeneous mixed organic films. As an example, mixing of non-amphiphilic fullerenes with straight chain amphiphilic molecules, like fatty acids, yields very inhomogeneous LB films with pronounced phase segregation [4]. LB films of amphiphilic calixarene derivatives (CA), having nanoporous and very flexible structure [5], is a more suitable matrix for the incorporation of other organic molecules.

Several attempts to produce homogeneous mixed LB films containing fullerene [6], polyaniline [7], and even CdS nanoparticles [8], have been successfully done using calix(4)resorcinarene as a matrix.

The main goal of the present work is to study floating layers of amphiphilic metal-free phthalocyanines (AmPc), mixed with other amphiphilic molecules, in particular, calix(4)resorcinarene. Well known spectroscopic properties of AmPc molecules and their aggregates [9–11] allow the investigation of transformations of molecular arrangement in floating layers on the water subphase during compression. Mixing AmPc with CA derivatives is hoped to break down AmPc molecular aggregates, which are usually observed in LB films [9–11].

## 2. Experimental details

Two amphiphilic octa-substituted metal free phthalocyanines (AmPc) [9] with long ( $C_{10}H_{21}$ ) and short ( $isoC_5H_{11}$ ) chains, referred throughout the text to as AmPc10 and AmPc5, respectively, were used to form mixed monolayers, either with amphiphilic calix(4)resorcinarene (CA), having  $C_7H_{15}$  alkyl chains, or stearic acid (SA), for comparison. Chemical structure of these compounds are shown in

\* Corresponding author. Tel: +44 114 2533512; fax: +44 114 2533306; e-mail: a.nabok@shu.ac.uk

Fig. 1. Solutions (0.5 mg/ml) of each compound in trichloroethene (TCE) were mixed at certain molar ratios just before spreading onto an Elga UHP water subphase with nominal pH of 5.5.  $\pi$ -A isotherms of the monolayers were measured using 601 Nima LB trough equipped with transparent window in the centre. UV-vis absorption spectra of floating layers during compression were measured in transmission through this window using two optical fibre waveguides connected to the light source and photodetector (MCPD-100 PHOTAL Otsuka Electronics multichannel spectrometer).

### 3. Results and discussion

$\pi$ -A isotherms of the mixed AmPc5/C(4)RA monolayers and the pure AmPc5 are shown in Fig. 2a as an example. The area per AmPc5 molecule is determined as a total monolayer area divided by the number of AmPc5 molecules. So, the shift of  $\pi$ -A isotherms to larger areas is caused by addition of the area of calixarene molecules. Besides, decreasing of the molar ratio AmPc5/CA causes some changes in isotherm shape, in particular, the plateau appears at surface pressures higher than 30 mN/m in the case of 1:3 and 1:5 mixtures.

For more detailed analysis, the values of the area per AmPc5 molecules in condensed state, obtained by extrap-

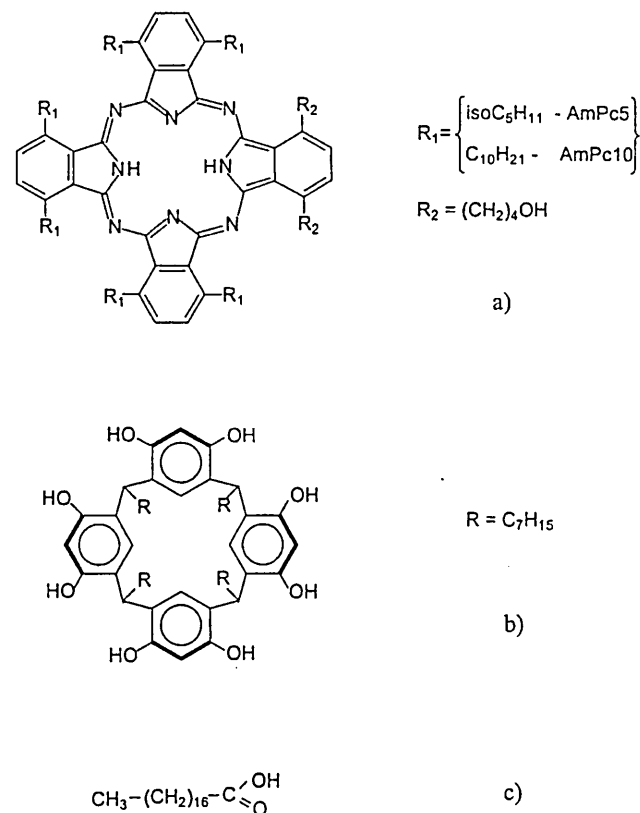


Fig. 1. Chemical structure of the compounds used: (a) AmPc5, AmPc10, (b) CA, (c) SA.

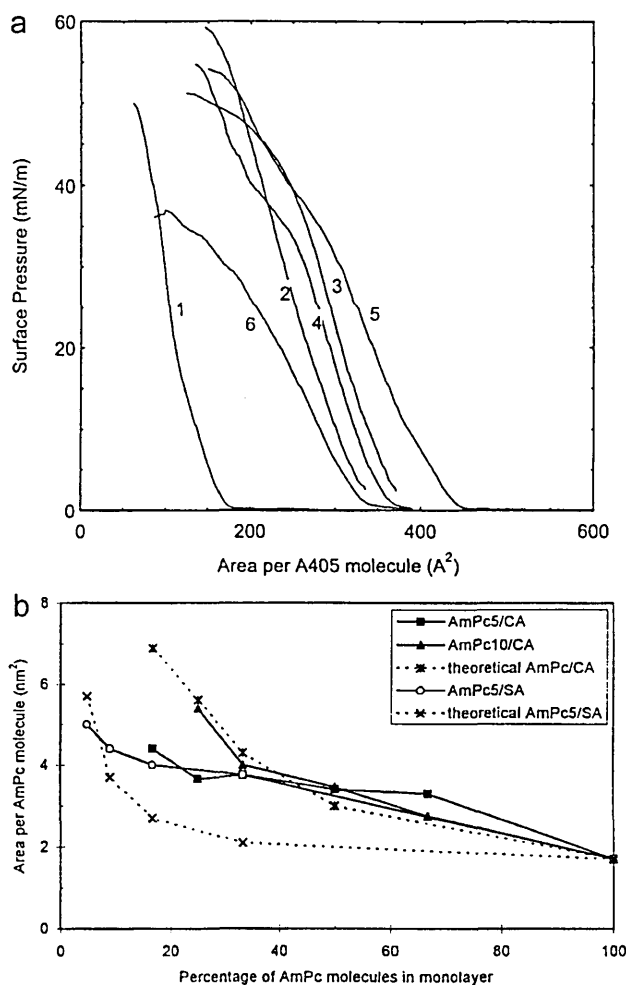


Fig. 2. (a)  $\pi$ -A isotherms of floating layers of (1) AmPc5 pure compound mixed with CA at various molar ratios, (2) 1:1, (3) 1:2, (4) 1:3, (5) 1:5, (6) 2:1. (b) The dependence of area per molecule in condensed state on the percentage of AmPc compound in mixed floating layers.

lation of the linear part of isotherms (Fig. 2a), are plotted against the percentage of AmPc5 in the mixture and shown in Fig. 2b. The same procedure was done for mixtures AmPc10/CA and AmPc5/SA, and the results are also presented in Fig. 2b. Theoretical curves for ideal AmPc/CA and AmPc/SA mixed monolayers were obtained by simple addition of the area of calix(4)resorcinarene ( $1.3 \text{ nm}^2$ ) [5] or stearic acid ( $0.2 \text{ nm}^2$ ) [2], respectively. AmPc10/CA mixed layers shows a similar behaviour to that of an ideal mixture, while the values of area for AmPc5/CA mixtures are less than expected at low molar percentages. This can be explained by 3D aggregation of both CA and, most likely, AmPc5 components. In contrast, mixed floating layers of AmPc5/SA gives the area per molecule higher than predicted, which is more difficult to explain. We could only suppose some molecular rearrangement and formation of AmPc5 molecular stacks consisting of more inclined molecules yielding a larger area.

The series of spectra of pure AmPc5 and AmPc10 monolayers measured at various surface pressures is shown in

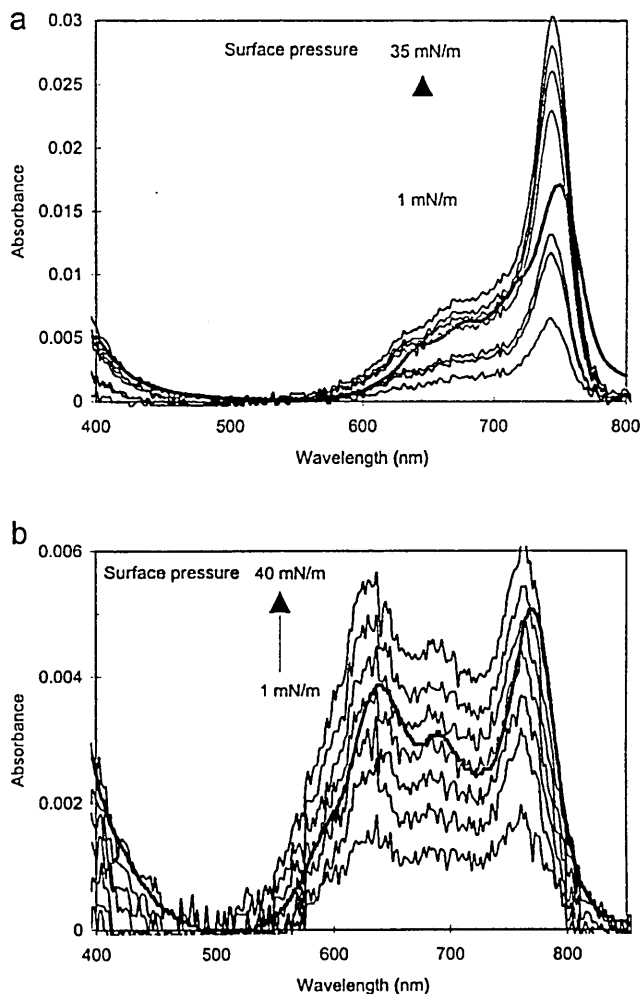


Fig. 3. UV-vis spectra of floating layers of pure (a) AmPc5 and (b) AmPc10 compounds measured at various surface pressures. Spectra of respective LB films are shown as darker solid lines.

Fig. 3a,b, respectively. The shape of the spectra are very similar to characteristic spectra of corresponding LB films. Therefore, this indicates a similar molecular arrangement in floating layers and LB films. In particular, a single band at 740 nm with a wide shoulder on the short wavelength side of the AmPc5 layer corresponds to formation of molecular J-stacks [9–11]. The Davydov doublet at 620 and 770 nm in the spectra of AmPc10 layers is typically attributed to herring-bone molecular arrangement [9–11]. It should also be noticed that the shape of the spectra does not change with the surface pressure, which means that molecular aggregates are formed in the floating layers even at very low surface pressures.

Using the data from  $\pi$ - $A$  isotherms and values of maximum absorption intensity ( $A_{MAX}$ ) from the UV-vis spectra, the values of the molecular surface concentration ( $C$ ) and specific absorption coefficient  $\alpha_M$  can be calculated as follows:

$$C = \frac{10^{16}}{A[\text{\AA}^2]} [cm^{-2}], \quad \alpha_M = \frac{\alpha}{C} = \frac{2.303 A_{MAX}}{C d} [cm] \quad (1)$$

where  $\alpha$  is the absorption coefficient and  $d$  is the thickness of the floating layer. Fig. 4a, curve 1, shows the dependence  $\alpha_M$  on  $C$  for the pure AmPc5 floating layer. The value of  $\alpha_M$  in an ideal 2D monolayer should be constant, as actually observed in the low concentration range. At higher concentrations,  $\alpha_M$  increases sharply, this can be explained by the formation of 3D aggregates due to monolayer collapse.

Measurements of UV-vis absorption spectra of AmPc5/CA and AmPc10/CA mixed monolayers with molar ratios of 2:1, 1:1 and 1:2 as well as of AmPc/SA mixed monolayers with molar ratios of 1:2, 1:5, 1:10 and 1:20 do not show any substantial spectral differences as compared with the spectra of pure AmPc5 and AmPc10 compounds, respectively. This allows us to conclude that AmPc molecular aggregates are also formed in mixed monolayers, and these monolayers contain separate segregated phases of

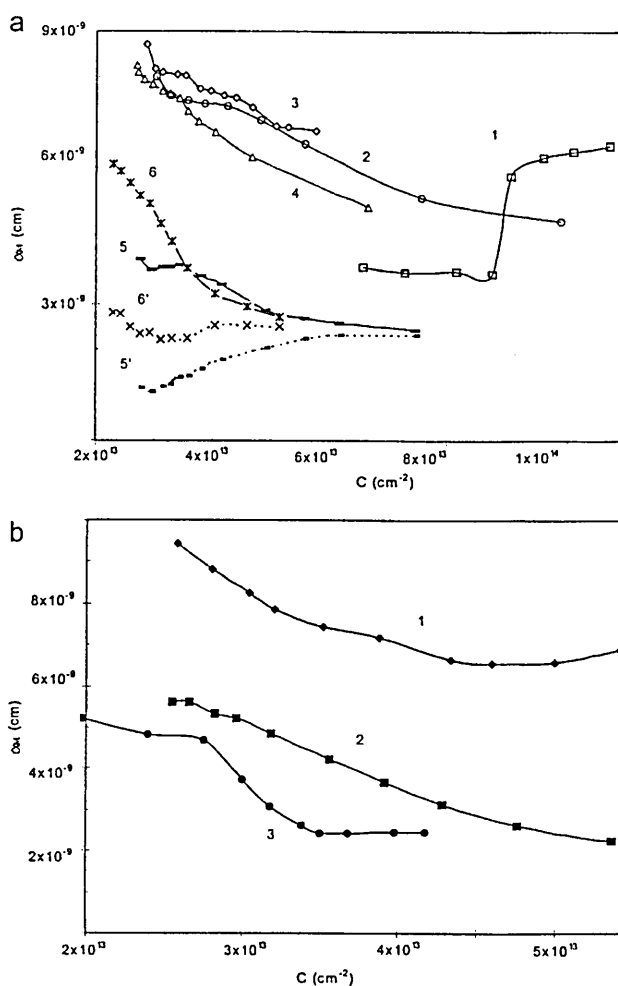


Fig. 4. (a) The dependence of specific absorption coefficient on the surface concentration of AmPc5 molecules in (1) pure floating layer and mixed layers with CA at various molar ratios, (2) 2:1, (3) 1:1, (4) 1:2, (5,5') 1:3, (6,6') 1:5 (all curves correspond to absorption at 740 nm except curves 5' and 6' which were measured at 700 nm). (b) The dependence of specific absorption coefficient on the surface concentration of AmPc5/SA floating layers mixed at molar ratios: (1) 1:2, (2) 1:10 and (3) 1:20.

both chromophore (AmPc5 or AmPc10) and matrix (CA or SA) components. Obviously, the maximum absorption intensity of these mixed floating layers decrease with the molar ratio due to the decreasing number of AmPc chromophores.

The dependencies of the specific absorption coefficient ( $\alpha_M$ ) on the surface molecular concentration ( $C$ ) are also shown in Fig. 4a,b for AmPc5/CA and AmPc5/SA mixed floating layers, respectively. All these curves demonstrate completely different behaviour from that of a pure AmPc5 (Fig. 4a, curve 1). A monotonic decrease of  $\alpha_M$  is observed for all mixed floating layers of AmPc5/CA (Fig. 4a, curves 2–6). Initial values of  $\alpha_M$  are mostly higher than that for a layer of pure AmPc5, which indicates the formation of 3D aggregates of AmPc5 just after spreading of the mixed solutions. Further compression of floating layers leads to some disaggregation, which is thought to relate to the incorporation of AmPc5 molecules into the CA matrix. A similar behaviour is observed in the case of AmPc5/SA mixed layers. It should be noted that results, presented in Fig. 4, clearly demonstrate qualitative trends. Some inconsistency of absolute values of the experimental data may have, how-

ever, been caused by changes of the instrumental baseline as well as noisy experimental spectra, where measurements were taken near the lower sensitivity limit of the spectrometer.

Further decrease of the molar ratio of AmPc5/CA mixtures (1:3 and 1:5) causes a very unusual change of the absorption spectra. For the case of floating layers of AmPc5/CA (1:3), which is shown in Fig. 5a, the band at 740 nm shifts to shorter wavelengths, and another band at 700 nm appears at surface pressures higher than of 30 mN/m. The spectra at 50–55 mN/m become similar to those observed for AmPc5 solution [9–11]. These transformations suggest that the monolayer under higher surface pressure contains isolated AmPc5 molecules. The same effect was also observed in AmPc5/CA (1:5) mixed floating layers. Curves 5' and 6' in Fig. 4a, corresponding to absorption at 700 nm, show an increase of the specific absorption coefficient. It is interesting to see that both  $\alpha_M$  at 740 and 700 nm become the same and nearly constant over the final stage of compression (see Fig. 4a, curves 5, 5', 6 and 6') indicating the formation of an ideal non-aggregative monolayer.

The following explanation of the phenomenon observed seems to be quite reasonable. The behaviour of the AmPc5/CA (1:3) and (1:5) mixed floating layers at surface pressures up to 30 mN/m is similar to those of the other mixed monolayers. The monolayers consist of separate islands (2D aggregates) of AmPc5 and CA molecules. Further increase of the surface pressure causes collapse of the monolayer which leads to overlapping of AmPc5 and CA islands. This molecular rearrangement is clearly seen from the plateau in the  $\pi$ - $A$  isotherms of AmPc5/CA (1:3) and (1:5) mixed layer (Fig. 2a, curves 4 and 5) observed at 30–35 mN/m. The overlapping can be accompanied by the inclusion of AmPc5 molecules into CA matrix. This inclusion may take place in the cavity of CA molecules or, most likely, between CA molecules.

Although less pronounced, similar changes of the spectra of AmPc10/CA mixed floating layers with molar ratios less than 1:2, were observed at higher surface pressures, as shown in Fig. 5b. The band at 760 nm shifts to 750 nm, and the band at 630 nm falls in intensity while another band at 670 nm emerges. The spectra again become closer to that of the isolated AmPc10 molecules in solution due to the inclusion of AmPc10 molecules into CA matrix. Some AmPc10 molecules remain in the aggregative state which causes broadening of the spectral lines. It can be understood that the inclusion of AmPc10 molecules, having long  $C_{10}H_{21}$  alkyl chains, seems to be more difficult as compared to AmPc5 with shorter  $isoC_5H_{11}$  chains.

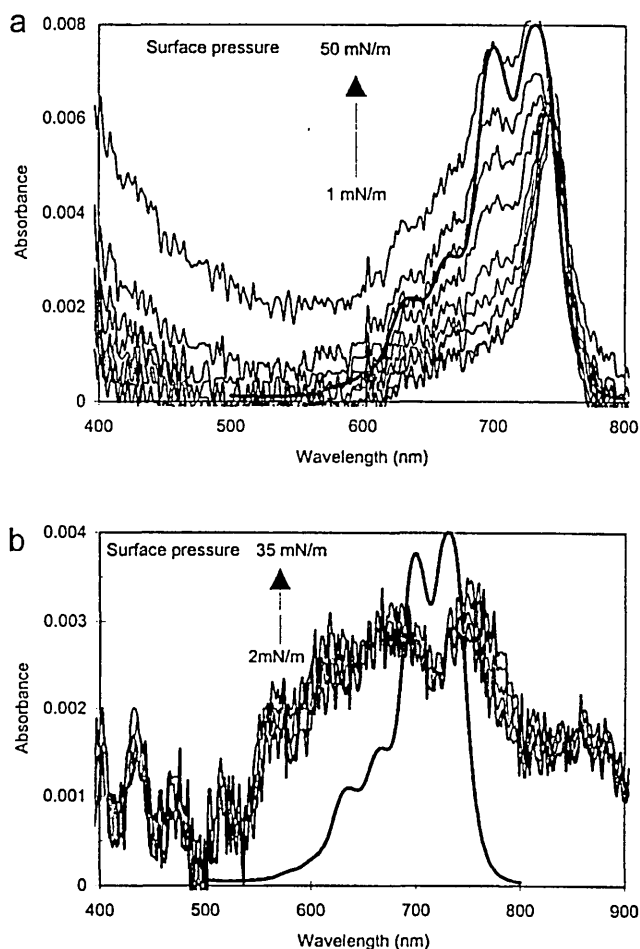


Fig. 5. UV-vis spectra of mixed floating layers of (a) AmPc5/CA (1:3) and (b) AmPc10/CA (1:3) measured at various surface pressures. Spectra of 0.5 mg/ml solutions of the respective compounds in TCE are shown as darker solid lines.

#### 4. Conclusions

Floating layers of amphiphilic metal-free phthalocyanine

derivatives were studied during compression using both  $\pi$ -A isotherms and UV-vis absorption spectra. It was shown that typical AmPc molecular aggregates, similar to those characteristic of LB films, are formed on the water surface immediately after spreading. Mixing of AmPc with stearic acid as well as with calix(4)resorcinarenes at molar ratios 2:1, 1:1 and 1:2 does not substantially affect the aggregation process in floating layers. Detailed analysis of absorption intensities shows some disaggregation in mixed monolayers during compression.

However, AmPc/CA mixed floating layers at molar ratio 1:3 or less, reveals dramatic changes of the absorption spectra, which can be interpreted in terms of the formation of isolated AmPc molecules. Overlapping of 2D aggregates of AmPc and CA at high surface pressures and inclusion of phthalocyanine molecules into the calixarene matrix is the most reasonable explanation of the phenomenon observed.

### Acknowledgements

The authors would like to acknowledge financial support by TQ Environmental Ltd, Wakefield, UK.

### References

- [1] J.H. Fendler, F.C. Meldrum, *Adv. Mater.* 7 (1995) 607.
- [2] T. Richardson in M. Petty, M.R. Bryce, D. Bloor (eds.), *An Introduction to Molecular Electronics*, Edward Arnold, London, 1995, p. 220.
- [3] Y. Lvov, H. Haas, G. Decher, H. Mohwald, A. Kalachev, *J. Phys. Chem.* 97 (1993) 12835.
- [4] Y.S. Obeng, A.J. Bard, *J. Am. Chem. Soc.* 113 (1991) 6279.
- [5] A.V. Nabok, N.V. Lavrik, Z.I. Kazantseva, B.A. Nesterenko, L.N. Markovskiy, V.I. Kalchenko, A.N. Shivanyuk, *Thin Solid Films* 259 (1995) 244.
- [6] Z.I. Kazantseva, N.V. Lavrik, A.V. Nabok, et al., *Supramol. Sci.* 4 (3–4) (1997) 341.
- [7] N.V. Lavrik, D. DeRossi, Z.I. Kazantseva, et al., *Nanotechnology* 7 (1996) 1.
- [8] A.V. Nabok, T. Richardson, F. Davis, C.J.M. Stirling, *Langmuir* 13 (1997) 3198.
- [9] M.J. Cook, J. McMurdo, D.A. Miles, R.H. Poynter, J.M. Simmons, S.D. Haslam, R.M. Richardson, K. Welford, *J. Mater. Chem* 4 (8) (1994) 1205.
- [10] R.H. Poynter, M.J. Cook, M.A. Chester, D.A. Stater, J. McMurdo, K. Welford, *Thin Solid Films* 243 (1994) 346.
- [11] A. Nabok, A.K. Ray, A. Hassan, J.R. Travis, M.J. Cook, *Supramol. Sci.* 4 (3–4) (1997) 407.

## An interpretation of the structure of Langmuir-Blodgett films of octa-substituted metal-free phthalocyanine molecules from optical spectra

By A. K. RAY, A. V. NABOK, A. K. HASSAN, O. OMAR, R. TAYLOR

Physical Electronics and Fibre Optics Research Laboratories,  
School of Engineering City Campus, Sheffield Hallam University,  
Sheffield S1 1WB, England

and M. J. COOK

School of Chemical Sciences, University of East Anglia, Norwich NR4 7TJ,  
England

[Received 8 July 1997 and accepted 6 January 1998]

### ABSTRACT

Ultraviolet-visible absorption spectra of Langmuir-Blodgett (LB) films of octa-substituted metal-free phthalocyanine molecules are decomposed into Gaussian-Lorentzian components in order to compare the in-plane molecular arrangements of the two groups of the compounds with short and long alkyl chains. LB films of long-chain molecules represent the Davydov splitting of the Q band, which corresponds to the 'herringbone' molecular structure and the angle between the molecules is estimated to be  $75^\circ$ . For short-chain molecules, the largely broadened 'blue' component of the Davydov doublets is suppressed and this can be explained by the domination of an anisotropic stack-like molecular arrangement in LB films.

### §1. INTRODUCTION

Phthalocyanines (Pcs) exhibit several interesting properties for applications in electronics. This has stimulated interest in research on these compounds in the thin film form. Roberts and his group are the first to deposit thin films of Pc molecules using Langmuir-Blodgett (LB) technique (Baker *et al.* 1983). The study of molecular packing in LB films has since received much attention (Orthmann and Wegner 1986, Barger *et al.* 1988). The synthesis of a series of structurally related amphiphilic octa-substituted Pc derivatives has been reported in the literature (Cook *et al.* 1994). The high solubility of these compounds in organic solvents, their isomeric purity, a reasonable balance between hydrophobic and hydrophilic parts and the ability to self-assemble in molecular stacks facilitate the deposition of highly ordered LB films for applications in gas sensing (Cole *et al.* 1994, Barker *et al.* 1996). X-ray diffraction and Fourier transform infrared (FTIR) spectral study of amphiphilic phthalocyanine (AmPc) LB films have shown that the films have a Y-type layer-by-layer structure. Each monolayer consists of AmPc molecules oriented almost vertically and packed in stacks (Bryant *et al.* 1994). Ultraviolet (UV)-visible optical spectra also give information about molecular arrangement in LB films.

For the present investigation, four metal-free compounds have been chosen from the series of octa-substituted AmPc derivatives. As shown in figure 1, their chemical

structures consist of four different substituents of iso-C<sub>5</sub>H<sub>11</sub>, C<sub>6</sub>H<sub>13</sub>, C<sub>8</sub>H<sub>17</sub> and C<sub>10</sub>H<sub>21</sub> alkyl chains and, for further references in this article, these molecules can be identified as AmPc5, AmPc6, AmPc8 and AmPc10 respectively. For Pc monomers in solution, the main  $Q$  bands which corresponds to the  $\pi$ - $\pi^*$  electron transition from the top ground state  $a_{1u}$  to the lowest excited  $e_g$  is split into two broad bands  $Q_x$  and  $Q_y$ . This is because a metal-free Pc molecule possesses a  $D_{2h}$  symmetry which is lower than the  $D_{4h}$  symmetry of metal substituted Pcs (Simon and Andre 1984). The  $Q$  band for the LB films, on the other hand, displays different characteristic features depending upon the length of chains.

In comparison with the monomer band in solution, the two bands  $Q_x$  and  $Q_y$  for the LB films of AmPcB and AmPc10 molecules are shifted symmetrically to the 'red' and 'blue' side. Moreover, the intensity of these two bands is changed alternately depending upon whether the polarized light is incident with its  $\mathbf{E}$  vector parallel or perpendicular to the dipping direction of the sample (Poynter *et al.* 1994). This behaviour has been successfully explained in terms of the Davydov splitting for the 'herringbone' molecular structure which consists of two non-equivalent molecules per unit cell.

In contrast with the previous case, absorption spectra of short-chain compounds (AmPc5 and AmPc6) show a single well pronounced 'red' band. The 'blue' band is relatively suppressed in height with the diminished splitting value and appears as a shoulder. Measurements with polarized light show azimuthal dichroism of LB films along the dipping direction (Cook 1996). It has been assumed that these films consist of separate molecular stacks oriented along the dipping direction by molecular flow during LB deposition. A Soret band observed at 350 nm resulting from the  $\pi$ - $\pi^*$  electron transition from a deeper state  $a_{2u}$  to the excited state  $e_g$  is the same for both types of molecule irrespective of the fact whether they are in solution or in LB films (Cook 1994).

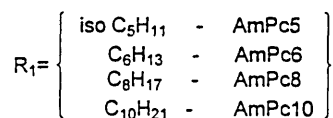
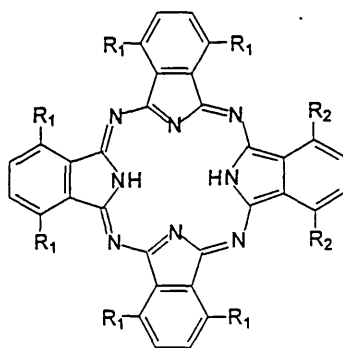


Figure 1. Chemical structure of octa-substituted metal-free AmPcs.

The origin of noticeable changes in the absorption spectra of LB films caused by small changes in alkyl length ( $C_6 - C_{10}$ ) has not been fully explored. It should be noted that spectra of solutions of all four molecules are the same because the length of substituting alkyl chains does not affect the main electron transitions of monomer Pc moieties. Further work on optical absorption spectra has been undertaken on the basis of the decomposition of visible spectra into an appropriate number of Lorentz-Gaussian distributions. The purpose of this article is to present information on the molecular arrangements in LB films of octa-substituted metal-free Pcs with different alkyl chains obtained from this analysis. Experimental evidence based upon previously reported X-ray diffraction, polarized UV-visible and FTIR spectral measurements is discussed in support of the proposed model.

## §2. EXPERIMENTAL DETAILS

The computer-controlled NIMA 622 trough was used for the LB deposition of the molecules on hydrophobic glass slides. The substrate preparation procedure was outlined in an earlier publication (Crouch *et al.* 1994). To prepare a monolayer, a 0.1% solution of the materials in 1,1,1-trichloroethane was used as a spreading solution on the subphase of pure Millipore water of resistivity of about 18 M $\Omega$  cm. The pH value of the subphase is nominally maintained at 5.6. After measurements of  $\Pi$ - $A$  isotherms, the floating monolayer was found to be stable at the surface pressure of 25–30 mN m<sup>-1</sup> for a period of  $\frac{1}{2}$  h and this pressure was chosen for LB deposition. Vertical dipping was performed at a constant surface pressure lying between 25 and 30 mN m<sup>-1</sup> with a speed of 10 mm min<sup>-1</sup> for both the down and up strokes. The sample was dried after each up stroke. The resulting films consist of Y-type multilayers (even numbers of dips). UV and visible absorption spectra of LB films on glass slides were obtained at normal incidence with a double-beam Unicam UV2 spectrometer. Visible spectra for LB films ten layers thick were decomposed into an appropriate number of the Gaussian peaks to be used for correct calculation of Davydov splitting.

## §3. RESULTS AND DISCUSSION

UV-visible absorption spectra were obtained for a large number of samples containing LB films of different thickness for all four substituted Pc molecules. The characteristic features were reproducible. Figure 2 shows typical absorption spectra of LB films of AmPc8 and AmPc10 molecules while the spectra for short-chain AmPc5 and AmPc6 molecules are given in figure 3. It is apparent that all spectra display the characteristic features as discussed before. Because of the lower symmetry than metal Pcs, the  $Q$  band of the monomer in solution degenerates into two narrow bands  $Q_x$  and  $Q_y$ . This composite  $Q_x$ - $Q_y$  band in LB films transforms into two broadened and shifted respectively to the 'blue' and 'red'-side  $Q_x$ - $Q_y$  bands.

As shown in figure 4, the decomposition of the  $Q$  band of optical absorption in the LB film of AmPc10 molecules into several Gaussian components has been undertaken in order to find a correlation between electron transitions and the type of molecular aggregate in LB films. It should be noted that it is not possible to describe individual bands by simple Gaussian functions, and the best fit can be achieved by using a mixture of Gaussian and Lorentzian approximations. A similar decomposition procedure was performed for the remaining three molecules. The error functions of the fitting lie in the range  $10^{-5}$ . All spectra consist of four bands, each representing a characteristic electronic transition. Results of these fitting procedures are shown in

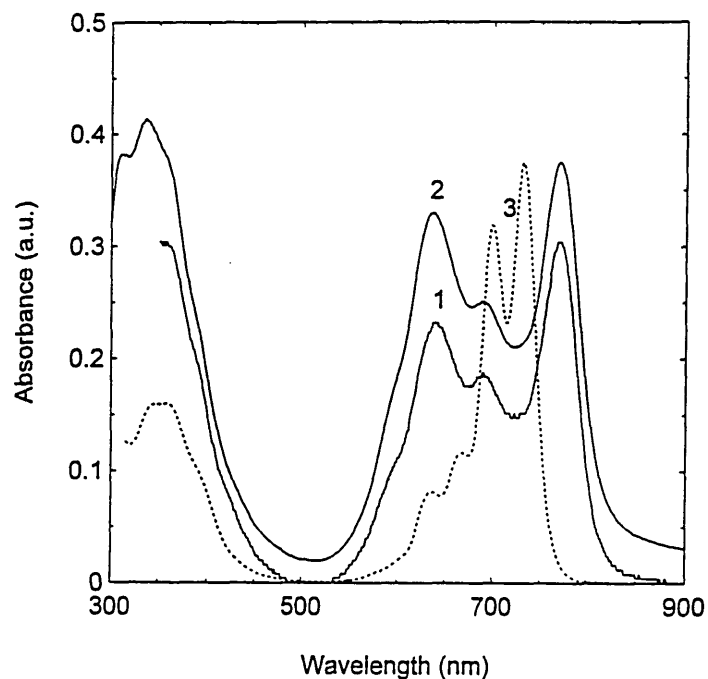


Figure 2. UV-vis absorption spectra of LB films of AmPc10 (curve 1) and AmPc8 (curve 2) compounds (a.u., arbitrary units). The spectrum of AmPcB monomers in 0.1% solution of the materials in 1,1,1-trichloroethane is shown by the broken curve 3.

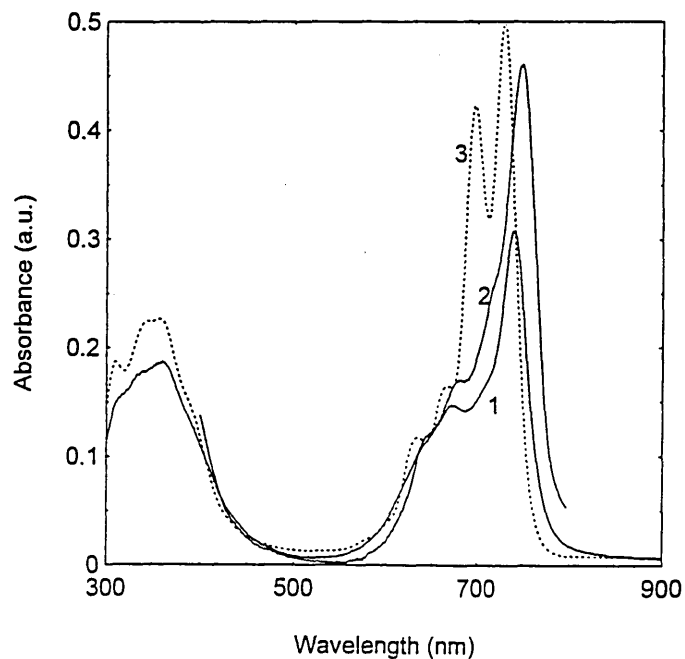


Figure 3. UV-vis absorption spectra of LB films of AmPc6 (curve 1) and AmPc5 (curve 2) compounds (a.u., arbitrary units). The spectrum of AmPc5 monomers in 0.1% solution of the materials in 1,1,1-trichloroethane is shown by the broken curve 3.

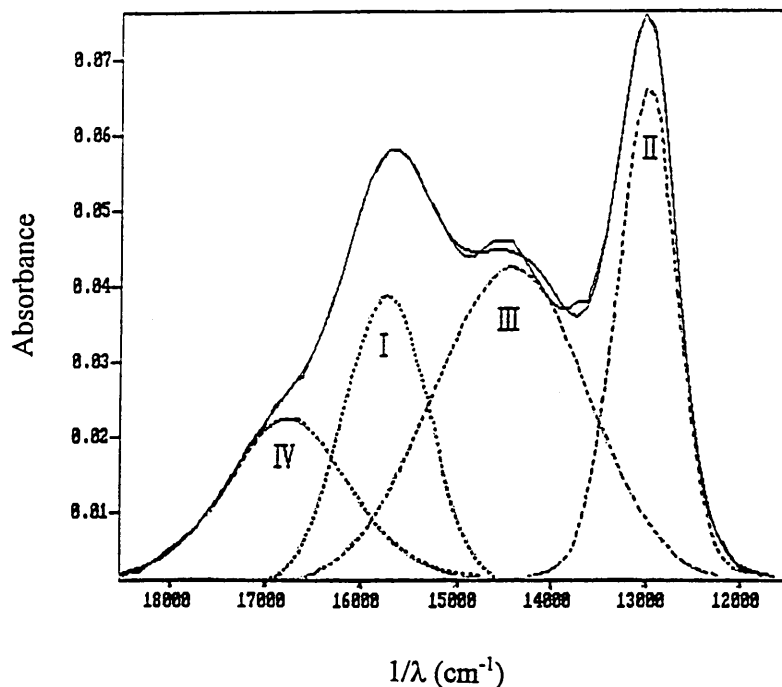


Figure 4. Results of fitting the *Q*-band shape of the AmPc10 LB film made by approximation with Gaussian-Lorentzian bands. The parameters of these bands are summarized in the table below.

Band number	Peak position (cm <sup>-1</sup> )	Peak amplitude	Area under the peak (cm <sup>-2</sup> )
I	15 721	0.9388	43.82
II	12 969	0.0667	58.08
III	14 414	0.0424	87.49
IV	16 751	0.0222	42.25

figures 5–7. For implementation of the software used, the abscissa are given in terms of the wavenumbers. Values of the fitting parameters of these bands are summarized in tabular form in the captions for each figure.

The Davydov splitting of the monomer exciton band can be explained in the context of the 'herringbone' molecular arrangement having two molecules per unit cell. Figure 8(a) shows a schematic diagram. The stack axis is taken to be perpendicular to the distance  $r_h$  between the centres of two molecules in the unit cell. The angle  $\alpha$  between two Pc molecules in a unit cell may be calculated using the following expression (Kirstein and Mohwald 1992):

$$\tan^2\left(\frac{\alpha}{2}\right) = \frac{f_+}{f_-} \quad (1)$$

where  $f_+$  and  $f_-$  are the oscillator strength components parallel and perpendicular to the stack axis and correspond to the 'blue' and 'red' bands respectively of the Davydov doublet.

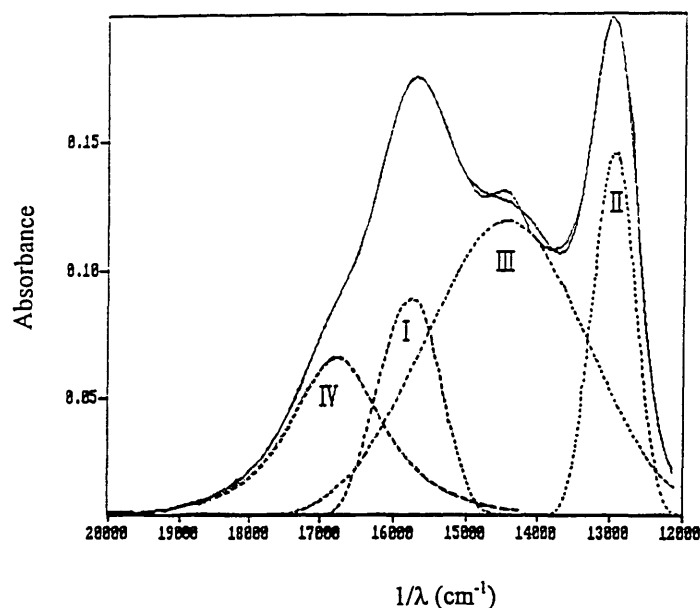


Figure 5. Results of fitting the  $Q$ -band shape of the AmPc8 LB film made by approximation with Gaussian-Lorentzian bands. The parameters of these bands are summarized in the table below.

Band number	Peak position ( $\text{cm}^{-1}$ )	Peak amplitude	Area under the peak ( $\text{cm}^{-2}$ )
I	15 776	0.0891	100.58
II	12 941	0.1472	112.95
III	14 450	0.1196	350.75
IV	16 796	0.0659	162.79

According to the model for molecular dimers proposed by Kasha *et al.* (1965), bands I, IV and II, III of decomposed spectra correspond to the 'blue  $Q_x-Q_y$ ' and 'red  $Q_x-Q_y$ ' components respectively of the Davydov doublet. This assumption is more reasonable for symmetrically split  $Q$  bands of LB films of long-chain molecules (figures 4 and 5) than for asymmetrical spectra of short-chain molecules (figures 6 and 7). Taking into account that the oscillator strength is proportional to the integral of absorption intensity through the corresponding band (Bliznyuk *et al.* 1993), equation (1) can be modified in the form

$$\tan^2\left(\frac{\alpha}{2}\right) = \frac{A_I + A_{IV}}{A_{II} + A_{III}} \quad (2)$$

where  $A_I$ ,  $A_{II}$ ,  $A_{III}$  and  $A_{IV}$  are the integral intensities of the respective bands. Using the numerical values of the respective area enclosed between the curve and the abscissa, values of  $\alpha$  are evaluated for the first three molecules. The angle  $\theta$  between the molecule and the molecular distance  $r_h$  is also calculated given that  $\theta = (\pi - \alpha)/2$ . Knowing that  $\Delta E = hc \Delta k$ , the exciton splitting energy  $\Delta E$  for  $Q_x$  and  $Q_y$  bands can be obtained from the distance  $\Delta k$  between the positions of the

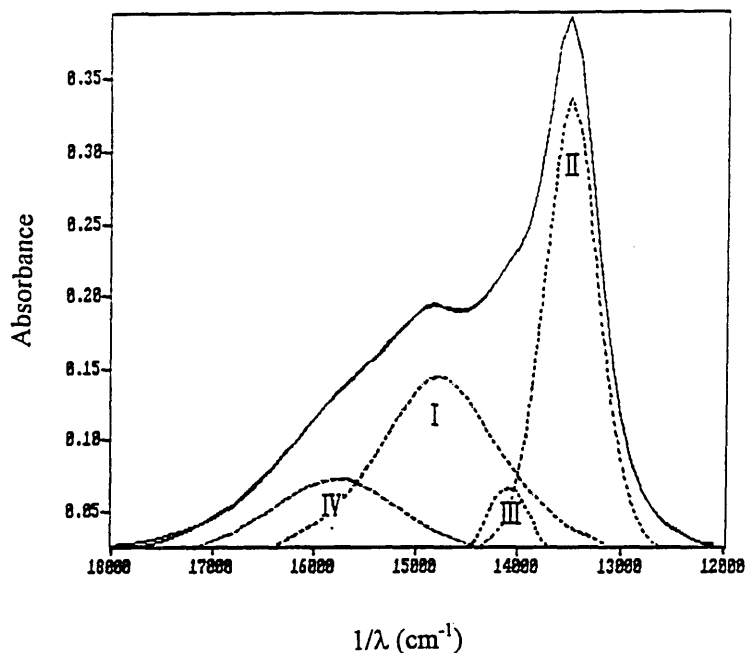


Figure 6. Results of fitting the  $Q$ -band shape of the AmPc6 LB film made by approximation with Gaussian-Lorentzian bands. The parameters of these bands are summarized in the table below.

Band number	Peak position (cm <sup>-1</sup> )	Peak amplitude	Area under the peak (cm <sup>-2</sup> )
I	14 776	0.1442	351.23
II	13 492	0.3376	288.76
III	14 083	0.0676	43.54
IV	15 779	0.0726	223.9

respective peaks of two decomposed spectral components. Values of the angles  $\alpha$ ,  $\theta$  and  $\Delta E$  for both  $Q_X$  and  $Q_Y$  components for LB films of the first three molecules are given in table 1.

Using the model for dimers, given by Kasha *et al.* (1965), the exciton splitting energy  $\Delta E$  can be written in the form

$$\Delta E = \frac{2|M|^2}{r_h^3} (1 + \cos^2 \theta). \quad (3)$$

where  $M$  is the dipole moment for the singlet-singlet transition of the monomers.

The dipole moment  $M$  is assumed to be the same for all four monomers since they contain the same chromophores. It is therefore possible to make a relative estimate of  $r_h$  for AmPc molecules from equation (3). Values of  $\theta$  and  $\Delta E$  are nearly equal for both AmPc8 and AmPc10 molecules, implying that the molecular distance  $r_h$  is the same for both compounds. It can therefore be concluded that LB films of both AmPc10 and AmPc8 molecules have the same molecular herringbone in-plane arrangement with the angle between molecular planes being about 75°. LB films of

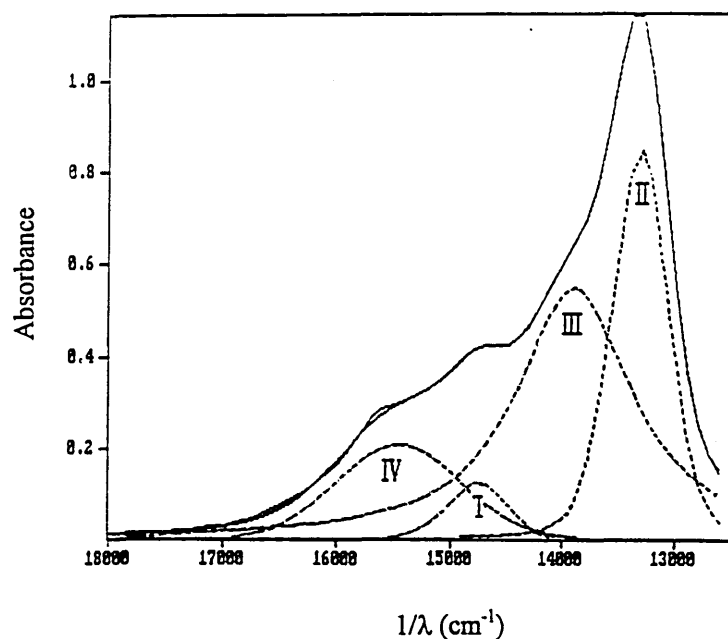


Figure 7. Results of fitting the  $Q$ -band shape of the AmPc5 LB film made by approximation with Gaussian-Lorentzian bands. The parameters of these bands are summarized in the table below.

Band number	Peak position (cm <sup>-1</sup> )	Peak amplitude	Area under the peak (cm <sup>-2</sup> )
I	14 760	0.1267	98.55
II	13 317	0.8555	594.82
III	13 904	0.5486	1064.14
IV	15 446	0.2087	303.88

AmPc6 molecules which have alkyl chains shorter than those of AmPc10 and AmPc8 molecules exhibit increases in both the angle between molecules and the exciton splitting energy. The mean value of  $r_h$  in this case is found to be 1.4 times larger than that for AmPc8 and AmPc10 molecules. This indicates a different in-plane molecular structure for AmPc6 molecules.

It can be seen from figures 4 and 5 that the 'blue' part (bands I and IV) of the Davydov doublet is suppressed and broadened in comparison with the 'red' part (bands II and III). This difference can be understood by considering the interaction of two dipoles in a unit cell with other dipoles in the herringbone structure. These dipoles are not permanent but induced by an external electromagnetic field (light). It is believed that the interaction of this type gives rise to a damping effect on electron vibrations in a preferential direction. It can be assumed for this case that the interaction between the molecules in the stack enhances electron vibrations along the stack axis but depresses them in the perpendicular direction.

The 'red' absorption band ( $A_- = A_I + A_{IV}$ ) corresponding to vibrations along the stack is expected to be more pronounced than the 'blue' band ( $A_+ = A_{II} + A_{III}$ ) corresponding to vibrations across the stack. As shown in figure 6, the 'blue' bands of AmPc6 molecules are more diminished in the intensity and more broadened than

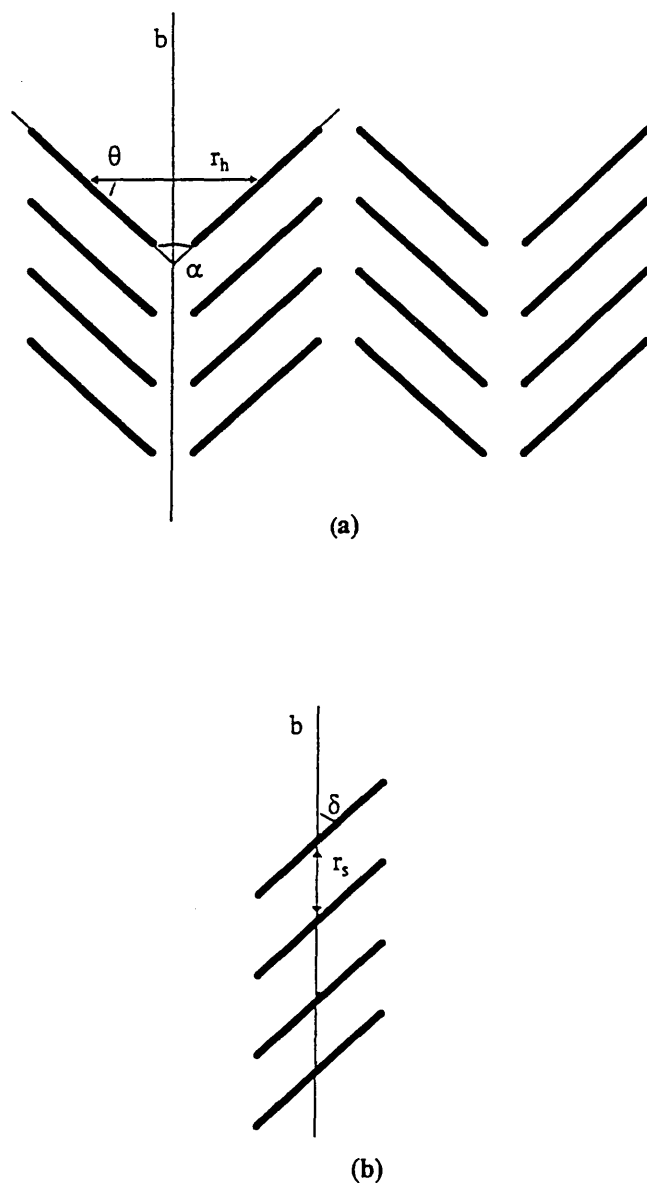


Figure 8. Schematic diagram of in-plane molecular arrangements in AmPc LB films: (a) herring-bone structure; (b) molecular stack.

Table 1. Values of the angle between molecules and energy for exciton splitting calculated by the Davydov splitting theory

Compound	$\alpha$ (degrees)	$\theta$ (degrees)	$\Delta E$ (eV)	
			$Q_v$	$Q_r$
AmPc10	75.0	52.5	0.341	0.290
AmPc8	74.4	52.8	0.352	0.291
AmPc6	105.5	37.3	0.159	0.210

those observed for compounds AmPc8 and AmPc10 (see figures 4 and 5). This can be interpreted as an increasing tendency for the molecules with shorter chain length to form molecular stacks.

In the case of LB films of AmPc5 molecules, the value of  $\alpha$  is found to be  $55^\circ$  from equation (2). This value is not consistent with those obtained for other compounds (see table 1). As shown in figure 7, 'red-shifted' bands in the spectrum are very pronounced. 'Blue' bands become more suppressed than those for AmPc6 molecules presumably due to a weak interaction between neighbouring molecular stacks. Moreover, the redistribution of intensities is seen to be taking place among all spectral components. It can be postulated that further shortening of alkyl chains leads to the stack-like arrangement of the LB film in-plane structure. Equation (1) is no longer applicable in this case. The energy shift  $\Delta E$  of the exciton line of molecules in the stack-like arrangement is given in the form (Pope and Swenberg 1982)

$$\Delta E = \frac{N}{N-1} \frac{|M|^2}{r_s^3} (1 - 3 \cos^2 \delta), \quad (4)$$

where the angle  $\delta$  is between molecular plane and the stack axis and  $N$  is the number of the molecules in the stack. As shown in figure 8(b), the symbol  $r_s$ , represents the distance between the centres of the molecules in the stack. The energy shift is  $\Delta E = E_S - E_M$  where  $E_S$  and  $E_M$  are the positions of exciton lines in the stack and monomer respectively.  $M$  has the same meaning as in equation (3). According to equation (4), the condition that  $\Delta E = 0$  for no shift yields a value of about  $54^\circ$  for  $\delta$ . The molecules which are inclined to the stack axis at angle  $\delta > 54^\circ$  give the 'blue' shift of the spectral line, while the condition that  $\delta < 54^\circ$  leads to the 'red' shift. As seen from the experimental spectra in figure 3, the 'red' shift of the main absorption band for LB films of AmPc5 molecules from the band of monomer in solution gives a value of  $\Delta E = -0.04$  eV. This negative value can only be achieved if  $\delta$  is less than  $54^\circ$ .

#### §4. CONCLUDING REMARKS

The analysis of UV-visible absorption spectra of LB films of octa-substituted metal-free AmPcs based upon the decomposition of experimental spectra onto several Gaussian-Lorentzian components can be used for the study of in-plane molecular arrangements. The results show that the in-plane molecular arrangement of LB films of metal-free Pc molecules depends on the length of alkyl substituting chains. The origin of the type of stacking depends upon the competition between the face-to-face and the edge-to-edge molecular interactions and this effect can be greatly influenced by the chain length of the substituents.

The Davydov splitting of the  $Q$  band for LB films with 'long'-chain ( $C_{10}H_{21}$  and  $C_8H_{17}$ ) molecules implies the presence of the 'herringbone' structure with an angle between molecules of about  $75^\circ$ . The decrease in the chain length down to  $C_6H_{13}$  causes broadening with a smaller peak of the 'blue' component of the Davydov doublet. This is believed to be due to the domination of the face-to-face over edge-to-edge interaction with the greater possibility of the formation separate molecular stacks. Both the angle and the distance between molecules are increased as a result. Further shortening of the chain (iso- $C_5H_{11}$ ) makes edge-to-edge interaction much weaker, and the stack-like arrangement becomes predominant. Therefore, the absorption spectra cannot be described by the Davydov splitting theory in this case.

LB films of the Pc molecules with a  $C_6H_{13}$  chain represent an intermediate case of the structure combining both a herringbone and a stack arrangement.

The present model of molecular arrangement is consistent with the published results of the structural study of LB films of these AmPc molecules. A herring-bone molecular arrangement is typical of Pcs in the condensed phase, and X-ray diffraction patterns of LB films have shown that AmPc molecules form a similar structure (Cook 1993). FTIR spectral measurements have been performed on AmPc LB films at both normal and grazing angles. The presence of the spectral line corresponding to out-of-plane molecular vibrations in the transmission mode and its absence in the reflection mode indicate vertical orientation of Pc moieties to the substrate plane (Ray *et al.* 1997).

UV-visible spectra have been obtained for LB films of all four AmPc molecules at normal incidence using polarized light with the electrical vector parallel and perpendicular to the dipping direction. All spectra show dichroism but the dichroic ratio  $\gamma$  for long-chain molecules is characteristically different from that for short-chain molecules. For long-chain AmPc derivatives,  $\gamma > 1$  for the 'blue' band while  $\gamma < 1$  for the 'red' band. This behaviour is generally attributed to the Davydov splitting owing to the presence of transitionally non-equivalent molecules within the unit cell of a herringbone molecular arrangement. In contrast with that, LB films of short-chain AmPc derivatives show  $\gamma > 1$  over the whole spectrum. This can be explained in terms of preferential orientation of stacks of AmPc molecules along the dipping direction (Cook 1996). An alternative model has been proposed to explain the origin of the Davydov splitting in Pc polysiloxane LB films due to rotation of neighbouring Pc moieties (Kalvoda *et al.* 1994). However, this model is not suitable for the present investigation. It has been shown that these substituted AmPc molecules in the floating monolayer are situated on their edges almost vertically to the air-water interface and this molecular arrangement is retained even after the monolayers have been transferred onto the solid substrate (Ray *et al.* 1997).

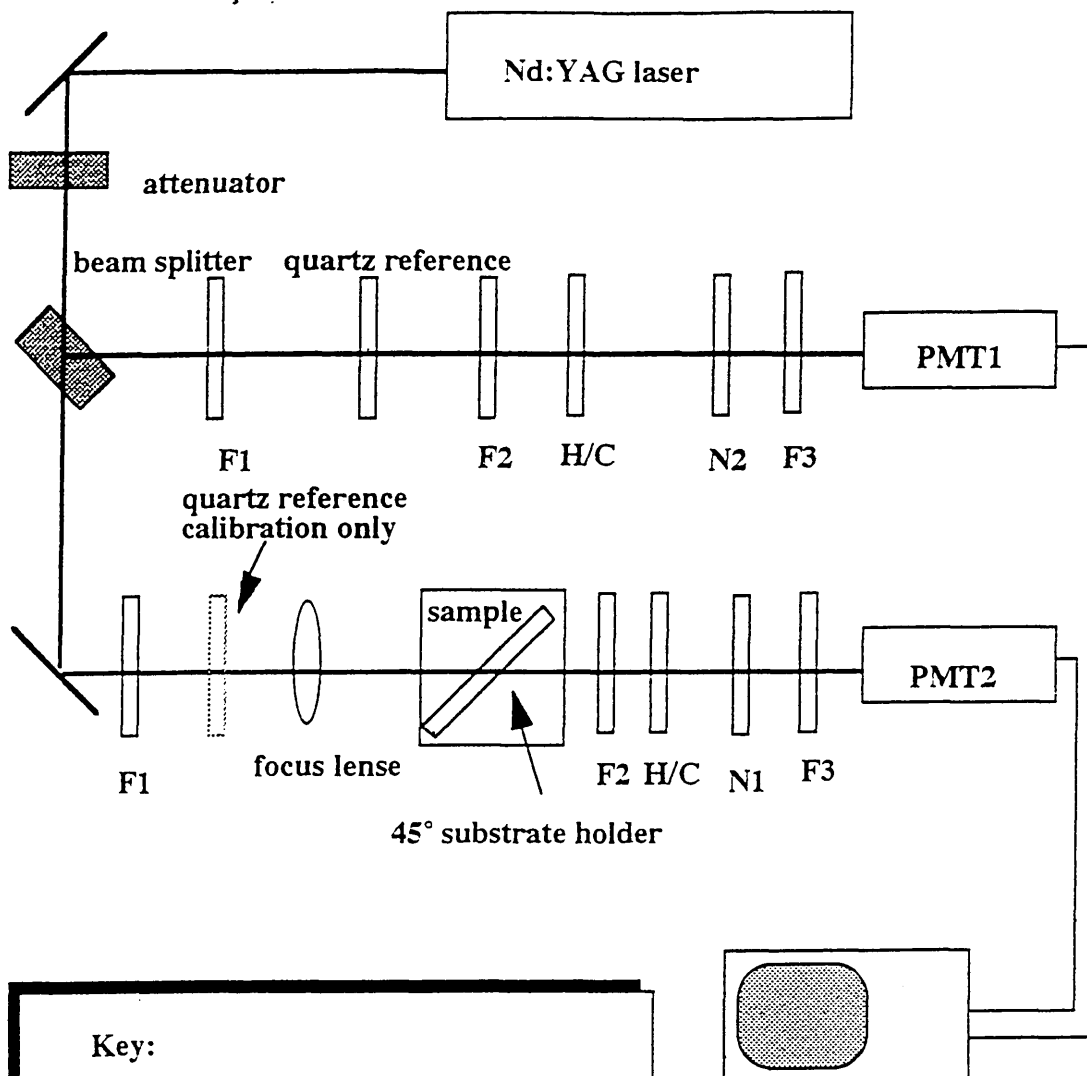
#### ACKNOWLEDGEMENT

The authors are grateful to the INTAS, Brussels, for financial support for this work.

#### REFERENCES

- BAKER, S., PETTY, M. C., ROBERTS, G. G., and TWIGG, M. V., 1983, *Thin Solid Films*, **99**, 53.  
BARGER, W., DOTE, J., KLUSTY, R., MOWERY, R., PRICE, R., and SNOW, A., 1988, *Thin Solid Films*, **159**, 369.  
BARKER, P. S., PETTR, M. C., MONKMAN, A. P., MCMURDO, J., COOK, M. J., and PRIDE, R., 1996, *Thin Solid Films*, **285-285**, 94.  
BLIZNYUK, V. N., KIRSTEIR, S., and MOHWALD, H., 1993, *J. phys. Chem.*, **97**, 569.  
BRYANT, G. C., COOK, M. J., RUGGIERO, C., RYAN, T. G., THORNE, A. J., HASLAM, S. D., and RICHARDSON, R. M., 1994, *Thin Solid Films*, **243**, 316.  
COLE, A., MCILROY, R. J., THORPE, S. C., COOK, M. J., MCMURDO, J., and RAY, A. K., 1993, *Sens. Actuators B*, **13-14**, 416.  
COOK, M. J., 1993, *Spectroscopy of New Materials*, edited by R. J. H. Clark and R. E. Hester (London: Wiley) pp. 87-149; 1994, *J. mater. Sci. Mater. Electron.*, **5**, 117; 1996, *Mater. Chem.*, **6**, 677.  
COOK, M. J., MCMURDO, J., MILES, D. A., POYNTER, R. H., SIMMONS, J. M., HASLAM, S. D., RICHARDSON, R. M., and WELFORD, K., 1994, *J. Mater. Chem.*, **4**, 1205.  
CROUCH, D., THORPE, S. C., COOK, M. J., CHAMBIER, I., and RAY, A. K., 1994, *Sens. Actuators B*, **18-19**, 411.

- KASHA, M., RAWLS, H. R., and EL-BAYOUMI, M. A., 1965. *Pure appl. Chem.*, **11**, 371-392.
- KIRSTEIN, S., and MOHWALD, H., 1992. *Chem. Phys. Letter.*, **189**, 408.
- KALVODA, L., BACK, R., FERENCZ, A., NEHER, D., and WEGNER, G., 1994. *Molec. Crystals liq. Crystals*, **252**, 223.
- ORTHMANN, É., and WEGNER, G., 1986. *Angew. Chem., Int. Edn. Engl.*, **25**, 1105.
- POPE, M., and SWENBERG, C. E., 1982. *Electronic Processes in Organic Crystals* (Oxford: Clarendon), p. 45.
- POYNTER, R. H., CROOK, M. J., CHESTERS, M. A., SLATER, D. A., MCMURDO, J., and WELFORD, K., 1994. *Thin Solid Films*, **243**, 346.
- SIMON, J., and ANDRE, J. J., 1984. *Molecular Semiconductors* (Springer: Berlin), pp. 86-94.
- RAY, A. K., NABOK, A. V., HASSAN, A. K., TRAVIS, J. R., and COOK, M. J., 1997. *Superamolec. Sci.*, **4**, 65.



**Key:**

- F1 = 532 nm notch filter
- F2 = 1064 notch filter
- H/C = hot/cold mirror
- N1 = neutral density filter
- N2 = neutral density filter
- F3 = 532 nm bandpass filter
- PMT1 = photomultiplier tube
- PMT2 = photomultiplier tube

**digital storage scope**